University of Strathclyde
Department of Chemical & Process Engineering

REMOVAL OF ORGANIC CONTAMINANTS FROM AQUEOUS SYSTEMS

Goh Sher Leen

A thesis submitted to the Department of Chemical and Process Engineering, University of Strathclyde in fulfilment of the requirements for the degree of Doctor of Philosophy

2015

This thesis is the result of the author’s original research. It has been composed by the author and has not been previously submitted for examination which has led to the award of a degree.

Sign:
Date:

ACKNOWLEDGEMENT

First of all, I would like to express my sincere gratitude to my supervisor, Dr. Ashleigh Fletcher, for providing supervision and support, her wisdom, patience and continuous motivation leading to my completion of this study. Secondly, I would like to thank Faculty of Engineering, University of Strathclyde, for funding my study; also, many thanks to the departmental administration and technical staffs for giving their support in these three years.

Also, thanks to Dr. Siddharth Patwardhan, for giving me advice and guidance. I would like to thank all the Postdoc and PhD students in the department for keeping me company and motivation throughout these periods. To Jun Yi, thanks for the care and encouragement during these periods; I have to say with your support, I have the courage to pursue this study.

Lastly, I would like to extend my gratitude to my family – grandparents, parents, uncles and aunties – for the love, care and encouragement that have been given to me throughout my study. To my late grandfather, I would like to tell you that I have fulfil your wish as I have now completed my study. I am sure you will be very proud of my achievement.

ABSTRACT

This research investigates the removal of aromatic organic contaminants (nitrobenzene (NB), aniline (AN), paracetamol (PCT) and hydroquinone (HQ)) from aqueous systems. For NB, this study focusses on removal via both iron reduction and adsorption, while removal of the other three compounds is focussed purely on adsorption. The results demonstrate NB degradation using iron powder produces AN, with the rate decreasing under basic conditions, due to corrosive effects; it is established that the iron surface is essential to the degradation process. Initial NB concentration influences degradation, and pseudo-first order kinetics are observed for all systems studied. For the adsorption studies on all four species, non-functionalised Macronet MN200, acidic functionalised hyper-cross-linked polymeric resins MN500 and S957, and Granular Activated Carbon (GAC) were tested as sorbents. The results show the kinetics of adsorption, for all contaminants, follow pseudo-second order models with rates controlled by particle diffusion. For adsorption of NB, PCT and HQ, the equilibrium uptake capacities increase with decreasing acidic functionalisation of the sorbent surface; while the opposite trend was obtained for AN removal. The adsorption rate decreased as sorbent acidic capacity increased, for all sorbents, due to the inherent surface chemistry and smaller surface area of the acidic functionalised sorbents used. For equilibria study, the Freundlich equation fits the data most appropriately and adsorption of all contaminants onto the selected sorbents is a physical process. Adsorption of NB, AN, and PCT onto the studied sorbents is favourable, while it is moderately favourable for HQ. Leaching tendencies showed < 40% of all contaminants were leached from the sorbents with the higher leaching rates for the macroporous sorbents. Overall, the results obtained suggest polymeric resins as viable candidates for the removal of targeted aromatic substances from aqueous systems.

TABLE OF CONTENTS

LIST OF FIGURES

LIST OF TABLES

CHAPTER 1

1.0 INTRODUCTION

This chapter provides the background to this study, which focusses on the discussion of limited water supplies and sources of water contamination. Here, four types of organic pollutants (nitroaromatics, aromatic amines, emerging organic pollutants and phenolic compounds) are discussed in detail, including the associated health risks. A target contaminant is selected from each group and their physical and chemical properties are given.

1.1 Water Pollution

On Earth, 97.3% of water is salt water while only 2.7% is fresh water. Additionally, only 0.027% of freshwater can be used, with the remaining quantities held in glaciers, polar ice caps, rivers, lakes and soils, and the distribution of water on Earth shown in Table 1[1].

Table 1 Distribution of water on Earth (Source: Adapted from [1])

Site	Percentage (%)
Ocean (salt water)	97.3
Water vapour (air)	0.001
Glaciers and ice caps	2.14
Groundwater (depth < 4000 m)	0.61
Fresh water lakes	0.009
Saline lakes and inland seas	0.008
Under soil	0.005
Rivers	0.0001

Due to the limited amount of water available for consumption, the increase in human global population has caused a shortage of freshwater supplies [2]. Furthermore, disposal routes from human activities such as agricultural, pharmaceutical, industrial, household and municipal sewage treatment plants into surface waters Figure 1, has contributed to adverse environmental and health impacts [3, 4].

Figure 1 Water contamination by human activities (Source: Adapted from [5], reproduced under permission QA, International, 2014 [6])

Any substance, present in an aqueous system, not in the form of molecular water is considered a *contaminant*, and the water sample termed impure. Water quality *criteria* and *standards* are vital to ensure post-consumption water discharges into seas, rivers, and lakes meet standards regulated by legislation. A water quality *criterion* is a limit on the concentration of a contaminant, where exceedance of the limit may cause toxic effects in specific living species. Water quality *standards*, on the other hand, are quasi-legal limits of the concentration of contaminants, which depend on the toxic severity of the contaminant [7].

The toxicity of a contaminant can be divided into two categories: *acute* and *chronic*; the former generates a reaction more quickly after ingestion, and the effects are easier to detect compared to the latter. In contrast, the rate of absorption is lower for chronic toxic compounds, producing irreversible and cumulative long term health effects. The permissible levels of toxic compounds are conveyed as the maximum acceptable concentrations for quality standards [8].

The U.S. Environmental Protection Agency (USEPA) reported that up to 762,000 t of industrial waste were released into the environment and at least 100,000 t of chemicals were emitted into surface waters, in 2001 [4]. In addition, the European Environment Agency (EEA) reported that nearly 3 million sites are polluted and different types of contaminants, such as aromatics, heavy metals, dissolved nutrients and chlorinated compounds are detected in soils, sediments and ground and surface waters [9]. These contaminants can be categorised in different groups and representative substances for each group are shown in Table 2. Furthermore, information pertaining to types of contaminants, CAS numbers and laws for regulation, are stated in the USEPA Register of Lists [7], and 126 contaminants are categorised in the Priority Pollutant List. Numeric limits for the contaminants shown in Table 3 have been set and any water streams exceeding these limits are required to undergo treatment.

Although different types of contaminants have been detected in water streams; this study focuses on the removal of aromatic organic substances due to their toxicity and the negative effects on flora and fauna. Here, four types of targeted organic pollutants (nitrobenzene, aniline, paracetamol and hydroquinone) are discussed in detail including their physical and chemical properties and their related hazards to provide a better understanding of each contaminant.

Table 2 Categories of contaminants (Source: Adapted from [7])

Category	Subcategory	Group	Examples
Dissolved compound	Organic	Aromatic	Benzene
		Chlorinated hydrocarbons	Chlorophenol, dichlorobromomethane, chloroform, chloropropane, trihalomethane
		Total organic carbon (TOC)	Chloroethanol, trichlorophenol, chloroacetic acid, chloroacetone
	Inorganic	Anion	Bicarbonate, chloride, carbonate, nitrate, nitrite, sulphate
		Cation	Copper , lead, mercury, nickel
Particle	Biological	Bacteria	Pathogenic, nonpathogenic
		Fungi	Cladosporium, penicillium, aspergillus, alternaria
		Protozoa cyst	Cryptosporidium parvum, entamoeba histolytica, giardia lamblia
		Plankton	Blue-green algae, green algae, diatoms
		Viruses	Pathogenic (ECHO, hepatitis, coxsackie, poliomyelitis), nonpathogenic
		Invertebrates	Crustaceans, ciliates, rotifers, nematodes
	Mineral	Asbestos	Amphibole, chrysotile
		Clays	Kaolinite, montmorillonite

Table 3 List of Priority Pollutants issued by EPA (Source: Adapted from [10])

Acenaphthene	Acrolein	Acrylonitrile
Benzene	Benzidine	Carbon tetrachloride
Chlorobenzene	1,2,4-trichlorobenzene	Hexachlorobenzene
1,2-dichloroethane	1,1,1-trichloreothane	Hexachloroethane
1,1-dichloroethane	1,1,2-trichloroethane	1,1,2,2-tetrachloroethane
Chloroethane	Bis(2-chloroethyl) ether	2-chloroethyl vinyl ethers
2-chloronaphthalene	2,4,6-trichlorophenol	Parachlorometa cresol
Chloroform	2-chlorophenol	1,2-dichlorobenzene
1,3-dichlorobenznene	1,4-dichlorobenzene	3,3-dichlorobenzidine
1,1,-dichloroethylene	1,2-trans-dichloroethylene	2,4-dichlorophenol
1,2-dichloropropane	1,3-dichlropropylene	2,4-dimethylphenol
2,4-dinitrotoluene	2,6-dinitrotoluene	1,2-diphenylhydrazine
Ethylbenzene	Fluoranthene	4-chlorophenyl phenyl ether
4-bromophenyl phenyl ether	Bis(2-chloroisopropyl) ether	Bis(2-chloroethoxy) methane
Methylene chloride	Methyl chloride	Methyl bromide
Bromoform	Dichlorobromomethane	Chlorodibromomethane
Hexachlorobutadiene	Hexachlorocyclopentadiene	Isophorone
Naphthalene	Nitrobenzene	2-nitrophenol
4-nitrophenol	2,4-dinitrophenol	4,6-dinitro-o-cresol
N-nitrosodimethylamine	N-nitrosodiphenylamine	N-nitrosodi-n-propylamine
Pentachlorophenol	Phenol	Bis(2-ethylhexyl) phthalate
Butyl benzyl phthalate	Di-N-Butyl Phthalate	Di-n-octyl phthalate
Diethyl Phthalate	Dimethyl phthalate	benzo(a) anthracene
Benzo(a)pyrene	Benzo(b) fluoranthene	Benzo(k) fluoranthene
Chrysene	Acenaphthylene	Anthracene
Benzo(ghi) perylene	Fluorene	Phenanthrene
Dibenzo(,h) anthracene	Indeno (1,2,3-cd) pyrene	Pyrene

Tetrachloroethylene	Toluene	Trichloroethylene
Vinyl chloride	Aldrin	Dieldrin
Chlordane	4,4-DDT[§]	4,4-DDE[§]
4,4-DDD[§]	Alpha-endosulphan	Beta-endosulphan
Endosulphan sulphate	Endrin	Endrin aldehyde
Heptachlor	Heptachlor epoxide	Alpha-BHC[§]
Beta-BHC[§]	Gamma-BHC[§]	Delta-BHC[§]
PCB–1242 (Arochlor 1242)[§]	PCB–1254 (Arochlor 1254)[§]	PCB–1221 (Arochlor 1221)[§]
PCB–1232 (Arochlor 1232)[§]	PCB–1248 (Arochlor 1248)[§]	PCB–1260 (Arochlor 1260)[§]
PCB–1016 (Arochlor 1016)[§]	Toxaphene	Antimony
Arsenic	Asbestos	Beryllium
Cadmium	Chromium	Copper
Cyanide	Lead	Mercury
Nickel	Selenium	Silver
Thallium	Zinc	2,3,7,8-TCDD[§]

[§] Where DDT is dichlorodiphenyltrichloroethane, DDD is dichlorodiphenyldichloroethane, DDE is dichlorodiphenyldichloroethylene, BHC is benzene hexachloride, PCB is polychlorinated biphenyl and TCDD is 2,3,7,8-Tetrachlorodibenzo-p-dioxin.

1.2 Nitroaromatic Compounds

Nitroaromatic compounds are organic compounds with at least one nitro group attached to one or more benzene rings; examples of nitroaromatic substances are shown in Figure 2. Most nitroaromatic compounds are used industrially to manufacture insecticides, dyes, herbicides, solvents, explosives and polyurethane foams; while only a few are generated via metabolism by microorganisms, e.g. 4-nitroanisole and 4-nitrobenzoate are produced by fungal and bacterial degradation of chloramphenicol, respectively [11, 12]. These compounds are difficult to degrade or remove via biological treatments, and only a few microorganisms use them as a source of energy, carbon or nitrogen. Moreover, nitroaromatic substances are usually toxic, carcinogenic and mutagenic toward living species; hence, they are listed as contaminants [11]. Nitroaromatics have not only been detected in water streams, such as wastewaters and rivers, they have also been detected in airs and soils [12].

Nitrated Polycyclic Aromatic Hydrocarbons (NPAHs) are contaminants released from automotive, plus other additives, coal and oil stoves via pyrolysis of organic compounds [13]. Previously, these compounds have been detected in soils [14, 15] and airs [16, 17]; however, they have also recently been found in aqueous systems. Previous studies have reported that nitroanthracene (482.18 ng L^{-1}), 6-nitrobenzo[*a*]pyrene (50.54 ng L^{-1}) and nitropyrene (49.45 ng L^{-1}) have been detected in the water stream in Japan. NPAHs are mutagenic and carcinogenic; 2-nitrofluorene is listed in the International Agency of Research of Cancer’s (IARC’s) Group B (possibly carcinogenic toward humans) while 6-nitrochrysene and nitropyrene are listed in IARC’s Group 2A (probably carcinogenic towards humans) [18], hence, the release of NPAHs has contributed to adverse environmental and health impacts; exposure to 2-nitrofluorene may cause damage to DNA, lungs and liver, as well as skin and eye irritation [19].

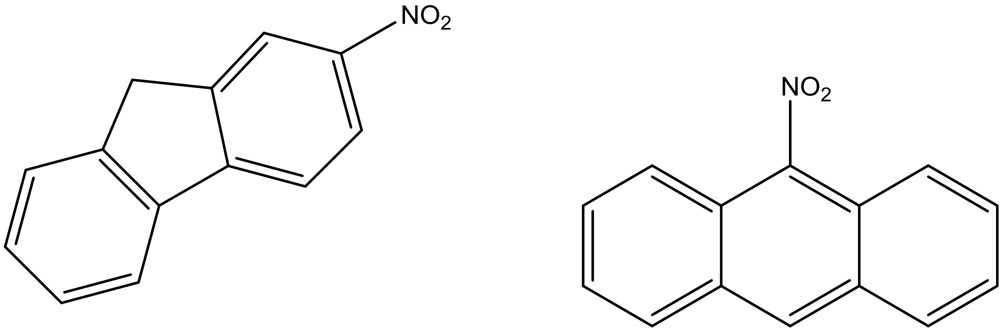

Nitrofluorene Nitroanthracene

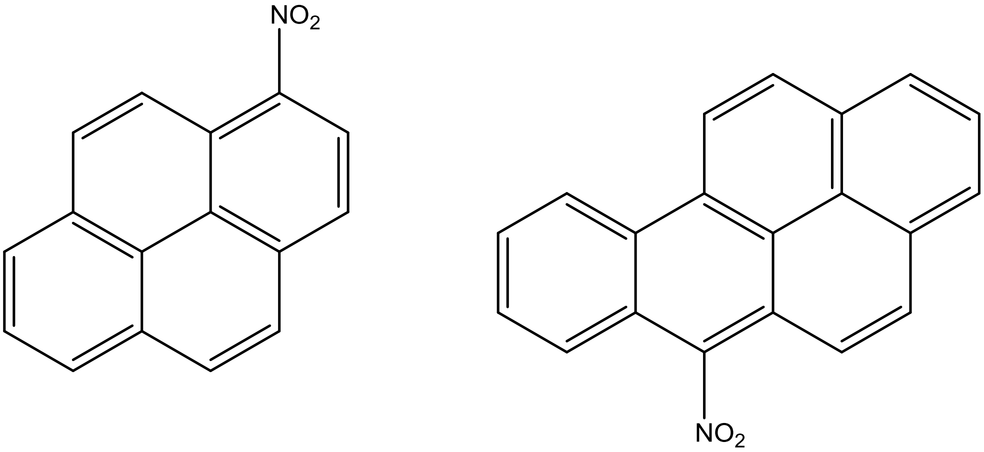

Nitropyrene 6-Nitrobenzo[*a*]pyrene

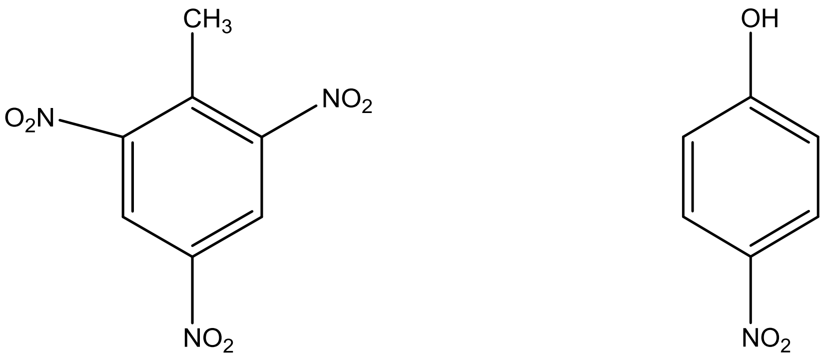

2,4,6-trinitrotoluene (TNT) p-nitrophenol (PNP)

Figure 2 Chemical structures of nitroaromatic compounds

In addition, nitrophenols, nitrotoluenes, nitrobenzoates and nitrobenzene are widely used in industrial applications as pharmaceuticals, dyes, explosives, polymers, pesticides and precursors in chemicals production; and most of these compounds have negative effects on the ecosystem. Nitrotoluenes such as 2,4-dinitrotoluene (2,4-DNT), 1,3-dinitrobenzene and 2,4,6-trinitrotoluene (TNT) are toxic to microorganisms such as yeasts, fungi and bacteria and exposure to these compounds may cause anaemia and hepatitis in humans [12]. TNT is a common contaminant widely used in industry to manufacture explosives, hence, TNT is detected in industrial wastewaters and groundwaters, close to military training areas [20-22] with one study reporting that up to 100 industrial and military sites are contaminated by TNT due to its persistence and stability [20]. TNT is toxic, mutagenic and a suspected carcinogen, hence, the presence of TNT in aqueous systems threatens human health and ecological systems [20-22]; exposure to TNT will damage blood, liver, reproductive and immune systems [23].

p-Nitrophenol (PNP) is another nitroaromatic compound widely used in industry to produce medicines, synthetic dyes, pesticides and explosives [24, 25]. PNP is detected in industrial wastewater streams due to its large consumption [26] and up to 33.2 mg L^{-1} of PNP was found in the wastewater of industry [27]. Moreover, PNP is also found in groundwaters, especially in developing countries due to extensive usage of pesticides (i.e. parathion and methyl parathion) and herbicides (i.e. dinitrocresol). Hydrolysis of these compounds causes PNP to be emitted into soil and leached into contaminated groundwaters [28]. PNP is listed as a priority pollutant by USEPA [10]; it is toxic and mutagenic, with negative impacts on public health and the environment [25, 26]; exposure to PNP may cause kidney and liver failure, anaemia, methaemoglobin, skin and eye irritation [25].

For nitroaromatics, nitrobenzene (NB) is selected as the targeted contaminant to be investigated in this study; hence, NB is discussed in detail compared to other nitroaromatic compounds. NB is an organic compound with a nitro group attached to a benzene ring; it is a flammable and oily liquid with a bitter almond-like smell [29]. NB is widely used in industry to manufacture dyes [30], pesticides, explosives [31], aniline (AN), and as a solvent in polishes [32], with at least 95% of NB used to generate AN [33]. Previous studies reported that up to 1.7 x 10^{-6} t of NB is consumed per annum over the world [33]. To produce NB, benzene undergoes nitration with nitric acid in the presence of sulphuric acid at 50 - 55 °C. The reaction is complete when the temperature is increased from 80 to 90 °C [33]; the simplified reaction of NB production is shown in Figure 3.

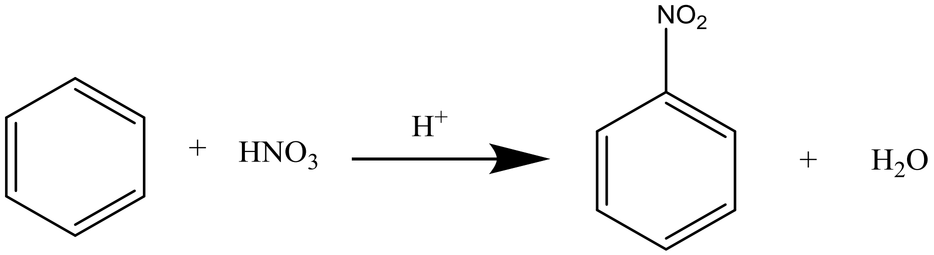

Figure 3 Formation of NB via nitration of benzene (Source: Adapted from [33])

NB is highly toxic in nature and a suspected carcinogen [34], contributing to adverse human health and environmental impacts [35], even at low concentrations [32]. Due to the large consumption of NB, significant amounts of NB are often released into surface and ground-water streams from industry, including discharges from poorly performing industrial wastewater treatment systems [34, 36]; with levels previously reaching as high as 100 mg L^{-1} (ppm) [37], while the EPA recommend levels below 19.8 mg L^{-1} to protect human health with NB visually and gustatorily detected at concentrations in excess of 30 µg L^{-1} [38].

The nitro-substituted aromaticity of nitrobenzene makes it an extremely stable pollutant [35], and populations close to contaminated and industrial sites risk exposure through inhalation, ingestion and contact with skin, causing, amongst other symptoms, nausea, cyanosis, headache, hyperalgesia and methaemoglobinemia [39]. In 2003, an explosion at a petrochemical plant in China saw 100 t of aromatic chemicals, including NB, aniline and benzene, released in to the Songhua River, resulting in restricted water supplies and requiring more than 1000 t of activated carbon to remove the contaminants [40]. The chemical and physical properties of NB are summarised in Table 4.

Nitroaromatic compounds are present in several water system forms; not only toxic towards humans, they are also hazardous towards flora and fauna. Most nitroaromatics are mutagenic and carcinogenic with many more and have listed as possible carcinogens by USEPA or IARC, hence, the removal of these pollutants from aqueous systems is vital to reduce anthropogenic and environmental impact.

Table 4 Physical and chemical properties of NB (Source: Adapted from [41])

Molecular structure	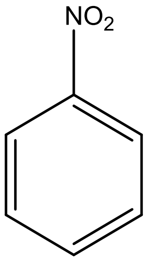
Molecular formula	$C_6H_5NO_2$
Synonyms	Nitrobenzol; mirbane oil
Molecular weight	123.11 g mol^{-1}
Physical state	Liquid
Appearance	Yellow
Solubility in water	Slightly soluble
Melting point	5 – 6 °C / 278 - 279 K
Boiling point	210 – 211 °C / 483 – 484 K
Flash Point	88 °C / 361 K
Carcinogenicity	Category 2 (Group 2B - Possible carcinogenic toward human)

1.3 Aromatic amines

Aromatic amines are organic substances with one or more amino substituent attached to at least an aromatic ring with examples shown in Figure 4. Aromatic amines are widely used for industrial processes, such as the manufacture of dyes, synthetic polymers, pesticides, explosives, oil refinery, drugs and rubbers. In addition, aromatic amines are also found in automobile exhausts, hair dyes and tobacco smoke [42, 43], and are also released into the environment via degradation of pesticides, other industrial activities and bacterial conversion of azo compounds [44]. These substances are usually very toxic, mutagenic and carcinogenic [44], hence, the presence of aromatic amine compounds in aqueous systems has adverse effects on anthropological and aquatic life.

4-chloroaniline (*p*-chloroaniline) p-nitroaniline (PNA)

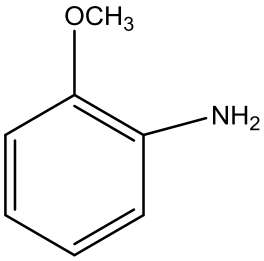

2-methoxyaniline (*o*-anisidine)

Figure 4 Chemical structures of aromatic amine compounds

4-chloroaniline (*p*-chloroaniline) is a chemical intermediate formed via the manufacture of synthetic polymers and organic chemicals such as azo dyes, pesticides, medicines, rubber, varnishes, polyurethanes and herbicides [45, 46]. About 45 - 450 t of 4-chloroaniline is generated annually in the US; it is usually released into environment as effluent from dye manufacture industries and degradation of herbicides i.e. phenylurea and acylanilinde, and fungicides i.e. nitroaniline [47]. 4-chloroaniline is toxic and carcinogenic [42] and is categorised in Group 2B (possibly carcinogenic to humans) by IARC [47]. 4-chloroaniline is readily absorbed into body via skin absorption, ingestion and inhalation of vapour, which may be fatal [48, 49].

p-Nitroaniline (PNA) is an aniline derivative, used as a precursor to manufacture fuel additives, pesticides, azo dyes, antioxidants, pharmaceuticals and corrosion inhibitors [50, 51]. PNA is highly toxic, mutagenic and carcinogenic and is a listed priority pollutant in many countries e.g. China, in term of its splenotoxicity, nephrotoxicity, hematoxicity and hepatoxicity [51-53]. Exposure to PNA (even at low concentration) may cause severe damage toward organs, and the cardiovascular and central nervous systems [50, 54].

A further example is 2-methoxyaniline (*o*-anisidine); widely used as an intermediate in the production of naphthol pigments and azo dyes for printing, textile and paper purpose [55, 56], most releases occur from textiles and dyes manufacturing; it also a constituent of tobacco smoke [56]. A carcinogenic compound, it is known to cause growth of tumours in the bladder of both genders of rats and mice, and kidney cancer in male rats [57]. Hence, *o*-anisidine is classified in Group 2B (possibly carcinogenic toward human) by IARC [58]; long term exposure may cause vertigo, headaches, methaemoglobin and sulphaemoglobin [59]. In 1993, an incident at a chemical plant in Frankfurt, Germany caused the release of azo and chlorinated species, including *o*-anisidine, resulting in environmental contamination [56, 60].

For aromatic amine compounds, aniline (AN) is selected as the targeted contaminant to be investigated in this study; hence, AN is discussed in detailed in terms of its physical and chemical properties and hazards. AN is widely used in industry to manufacture rubber [61], dyes, pesticides, polymers, cosmetics and shoe polishes [62]. 537,000 t of AN is manufactured annually in China and US, combined [63]. In the laboratory, AN can be generated via nitration of benzene in the presence of nitric and sulphuric acids to form NB, followed by the reduction of NB, by either catalytic hydrogenation, or using iron fillings and concentrated HCl, which acts as a reducing agent (Figure 5) [64].

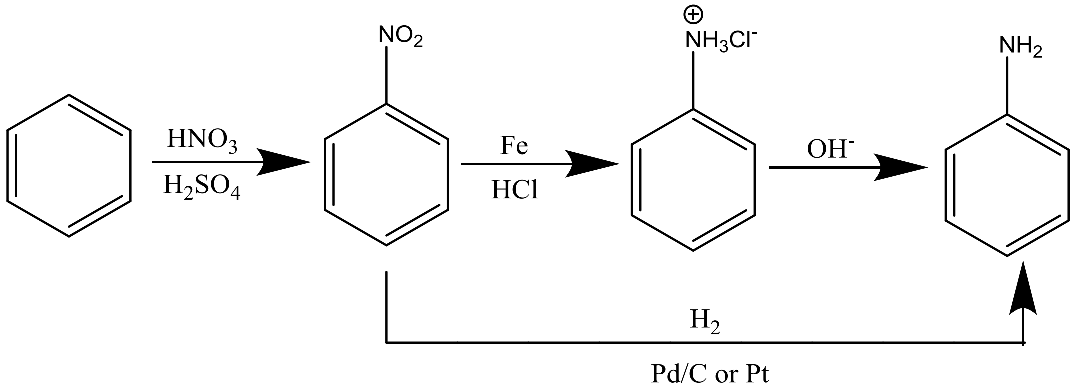

Figure 5 Formation of AN via nitration of benzene and reduction of NB (Source: Adapted from [64])

AN can be discharged directly from industry into wastewaters, as industrial residue, or indirectly, as the by-product of pesticides production, which both contribute to adverse environmental and health impacts [65, 66]. Toxic and harmful to aquatic life, even at low concentrations in aqueous systems [66]; AN is a suspected anthropogenic carcinogen and is readily absorbed via skin absorption, inhalation and ingestion. Short, or long term exposure to AN affects the lungs and blood by converting haemoglobin to methaemoglobin, causing cyanosis [61, 67]. Despite these adverse effects, AN is not legislating regulated; however, the US Environmental Protection Agency (USEPA) suggest a maximum limit in water of <

0.262 mg L^{-1} to protect human health [68]. The chemical and physical and chemical properties of NB are summarised in Table 5.

In short, exposure to aromatic amines especially AN may cause severe health impact to humans and has negative effects on environments; majority of these substances have been listed in Group 2B (possibly carcinogen to humans) by IARC. Therefore, the removal of AN is essential to protect the ecosystem.

Table 5 Physical and chemical properties of AN (Source: Adapted from [69])

Molecular structure	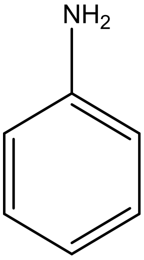
Molecular formula	$C_6H_5NH_2$
Synonyms	Phenylamine; aminobenzene
Molecular weight	93.13 g mol^{-1}
Physical state	Liquid
Appearance	Light yellow
Solubility in water	36 g L^{-1} (20 ˚C)
Melting point	-6.2 °C / 266.8 K
Boiling point	181 - 185°C / 454 – 458 K
Flash Point	76°C / 349 K

1.4 Emerging organic pollutant (EOP)

Synthetic organic substances are widely used in industry to manufacture food preservatives and pharmaceutical products. The release of these ‘micro-organic pollutants’ into environment, especially groundwater, has elicited interest among scientists due to their potential toxicity [70]. Although the concentrations of these substances, in aquatic systems, are relatively low, long term exposure may harm terrestrial and aquatic organisms. Hence, they are classified as emerging contaminants [71].

'Emerging Organic Pollutants' (EOPs), which include compounds newly discover or developed, and substances that are recently listed as pollutants, contain a wide range of compounds, such as pesticides, personal care products (PCPs), food additives, healthcare products and tailor-made nano-sized materials [70]. These compounds are released into environment via several pathways including the effluents of hospital [72] and industrial sites, agricultural land and household waste [73], as shown in Figure 6.

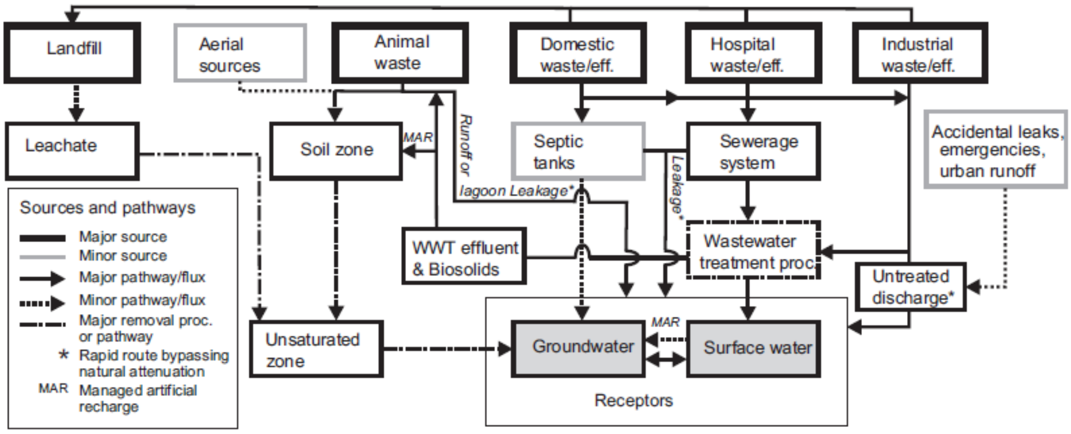

Figure 6 Source and pathway of 'EOP' contamination (Source: Adapted from [70])

The different EOPs detected in groundwaters are listed in Table 6; among these compounds, pharmaceuticals were reported to be of highest concentration in aquatic systems [74]. Up to 1000 t of pharmaceuticals are manufactured annually, and are often released to aquatic systems due to incomplete removal in treatment processes. These substances are detected in drinking water, sewage treatment plant effluents (STPs), and ground and surface waters, at concentrations of ng L^{-1} to µg L^{-1} [75]. Examples of EOP are shown in Figure 7.

Table 6 ‘EOP’ detected in groundwater via different pathways (Source: Adapted from [70])

Source	Compounds
Pharmaceuticals	Paracetamol, Carbamazepine, Ibuprofen, Primidone, Clofibric acid, Ketoprofen, Triclosan, Lopamidol, Diclofenac, Phenazone, Sulphamethoxazole, Lincomycin, Propyphenazone, Sulphamethazine
Hormones	Estrone, 17b-estradiol
Industry	Nonylphenol, Galoxalide, Bisphenol A, TCEP
Life-style	Caffeine, Cotinine

Carbamazepine (CBZ) is used in pharmaceuticals to treat neuralgia, psychiatric disorders, diabetes, insipidus and seizure disorders [76, 77]; up to 1014 t of CBZ is consumed per annum worldwide, and it is second largest antiepileptic medicine used in China [77]. CBZ has not only been detected in ground and surface waters, wastewater and sludge; it has also been found in sediments and soils [78, 79]. Previous studies reported that 0.1 – 1.68 µg L^{-1} and 1.64 – 99,194 ng L^{-1} of CBZ were detected in wastewater and ground water, respectively [70, 71]. CBZ is toxic to aquatic life such as algae, bacteria, fishes and invertebrates, occurs abundantly and is persistent [77, 78]; exposure of CBZ may cause eye, skin and respiratory tract irritation [80]. Associated with this, primidone is another anti-convulsant; applied to the treatment of movement disorders i.e. tremors, it is metabolised in the liver to phenobarbital before excretion via urine [81] with 0.11 to 12 μg L^{-1} of primidone detected in groundwater [70]. Primidone is a suspected carcinogen and exposure to this substance causes vomiting, nausea, anorexia, drowsiness, fatigue and ataxia [82].

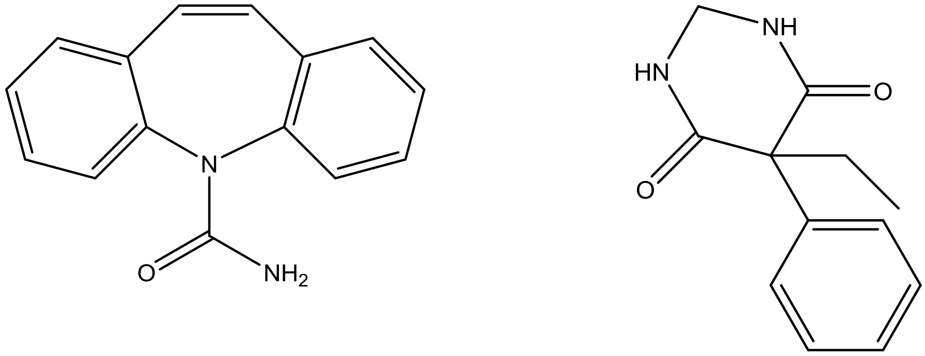

Carbamazepine (CBZ)

Primidone

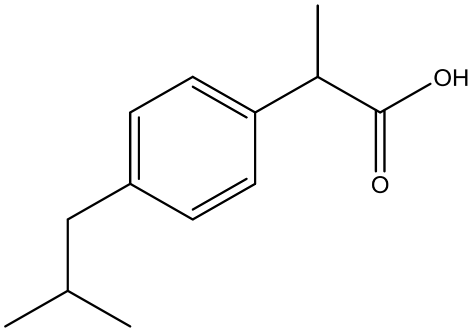

Ibuprofen

Figure 7 Chemical structures of example EOP

Ibuprofen (2-(4-isobutylphenyl) propionic acid) is a non-steroidal anti-inflammatory drug (NSAID) used to treat rheumatoid inflammation. It is also used for pain and fever relief [83], and is one of the most consumed drugs globally [84]. As a result, ibuprofen has been detected in the effluent of treatment plants and surface waters in several countries (Table 7). Ibuprofen is environmentally toxic due to its properties, such as high mobility in aquatic systems [85], and its hydrophobic crystal structure [86]. The release of ibuprofen has raised public concern since it is harmful to human health, causing heart disease and gastrointestinal bleeding [87], and ecological systems, where the reproduction of living species has been observed to change in the presence of ibuprofen [86].

Table 7 Concentration of ibuprofen detected in different countries

Country	Source	Concentration detected
UK (South Wale)	Surface water	0.1µg/L [88]
UK	River	27.3µg/L [89]
Sweden	Sewage treatment plant effluent	7.11µg/L [90]
Canada	Sewage treatment plant effluent	6.71 µg/L [91]

Paracetamol is selected as a target EOP in this study and detailed information is provided. Paracetamol (acetaminophen), also known as N-acetyl-para-aminophenol or para-acetyl-amino-phenol [92], is widely used as an antipyretic analgesic [93] to reduce fever, relieve joint aches and headaches [94].

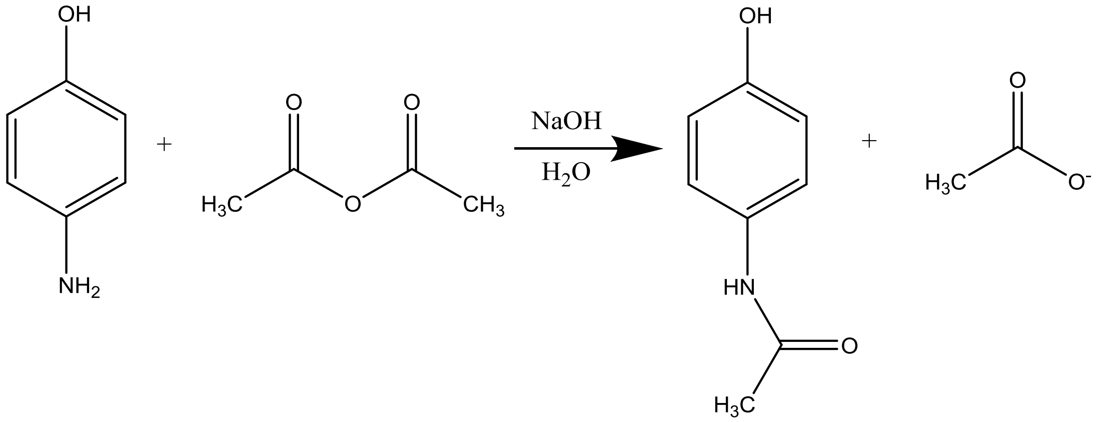

Figure 8 Formation of PCT using p-hydroxyaniline and acetic anhydride (Source: Adapted from [95])

PCT is synthesized from p-hydroxyaniline and acetic anhydride. The $–NH_2$ group of p-hydroxyaniline acts as a nucleophile, reacting with acetic anhydride to produce PCT [95], as shown Figure 8. Up to 403 t of PCT are consumed annually in the UK [96], and it has been detected in effluents and surface waters (Table 8).

Table 8 Global PCT concentrations detected in rivers, surface waters and waste streams

Country	Source	Concentration detected
UK (Howden WTW)	River	0.069 µg/L [89]
UK (South Wale)	Surface water	2.382 µg/L [88]
Spain	Surface water	0.04 µg/L [97]
Spain	Waste water treatment plant effluent	0.058 µg/L [97]
France	Surface water	0.071 µg/L [98]
Korea	Surface water	0.033 µg/L [99]
Korea	Waste water treatment plant effluent	0.0095 µg/L [99]

PCT is haematologically toxic causing methaemoglobinemia, anaemia and haemostasis. Furthermore, it is also adversely affects the thyroid and salivary glands [100]. The chemical and physical and chemical properties of PCT are summarised in Table 9.

Table 9 Physical and chemical properties of PCT [101]

Molecular structure	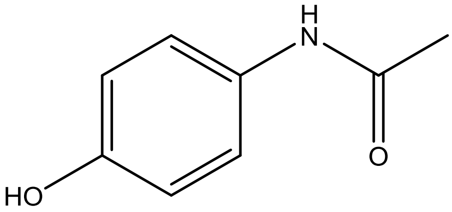
Molecular formula	$C_8H_9NO_2$
Synonyms	4-Acetamidophenol; 4’-hydroxyacetanilide; APAP; N-acetyl-4-aminophenol
Molecular weight	151.16 g mol^{-1}
Physical state	Powder
Appearance	White
Melting point	168 - 172 °C / 441 – 445 K

Although the majority of EOP have not been regulated by legislation, it is recognised that long term exposure to these substances will contribute to adverse environmental and health effects, thereby, supporting the development of technologies to remediate EOPs.

1.5 Phenolic compounds

Phenol and its derivatives are organic compounds with one or more *OH* groups attached to an aromatic ring; acting as intermediates in the production of synthetic resins, flavours, pesticides and disinfectors [102]. Phenol and its derivatives are readily adsorbed into the body via inhalation, ingestion and absorption via the skin; they are toxic, mutagenic, teratogenic and carcinogen. Hence, the presence of phenol and its derivatives in water harms human health, including effects on the liver, central nervous system and nephridium, and aquatic life [102, 103]. They are usually detected in industrial wastewaters from petroleum refineries, and cosmetics, textiles and plastics industries [104]; their presence in water creates an unpleasant smell [105]. Examples of phenolic compounds are shown in Figure 9.

Phenol

Catechol

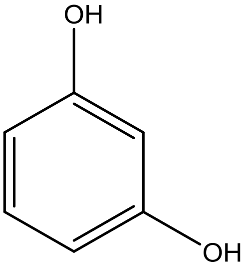

Resorcinol

Figure 9 Chemical structures of phenol and its derivatives

Phenol is used as a raw material in industry to manufacture medicines, plastics, petrochemicals and insecticides, with ~7.8 million t of phenol generated worldwide in 2001 [106]. Phenol has been detected in industrial wastewater to levels of a few thousand mg L^{-1}; while USEPA have regulated that the concentration must be < 1 mg L^{-1} [107]. Phenol is toxic, hence, it is listed as a priority pollutant by USEPA [10], and long term exposure of phenol, via ingestion and inhalation may cause vertigo, diarrhoea, anorexia, salivation and weight loss; it also affects the liver and blood [108].

Catechol is used as an industrial precursor in the generation of various chemicals [109], and is an intermediate formed in the biodegradation of aromatic compounds [110]. Detected in industrial wastewaters from industrial processes for the manufacture of drugs, dyes, plastic, resins, textiles, cosmetics and chemicals manufacturers, up to 5500 mg L^{-1} of catechol has been found in effluent streams [110, 111]. Catechol is toxic towards animals such as rabbits, rats, fish and cats; it also harmful to human health, causing damage in proteins and DNA [112].

Resorcinol is widely used to manufacture plastics, synthetic fibres and dyes [113]. Previous studies have reported that up to 250 mg L^{-1} of resorcinol is detected in industrial effluents [110]. Less toxic than catechol, resorcinol exposure, via ingestion, can still result in diarrhoea, vomiting, tachypnea, pulmonary oedema and nausea, and may cause hepatic injury and methaemoglobinemia.

For phenolic compounds, hydroquinone (HQ) is selected as the target contaminant for this study, and the physical and chemical properties are discussed in detailed. HQ is a phenolic compound with two *OH* groups attached to an aromatic ring in the *para* position. HQ is widely used in industry to manufacture pesticides, rubber, medicine and is also used in skin whitening. Up to 43,000 t of HQ is manufactured per annum worldwide, via phenol hydroxylation, as shown in Figure 10. In brief, phenol undergoes hydroxylation in the presence of a catalyst (strong mineral acid, cobalt (II) or iron (II) salt) and hydrogen peroxide to produce hydroquinone and catechol. Finally, these products are separated via solvent-stripping and extractions [114]. HQ can be absorbed into the body via inhalation, ingestion and absorption via skin, and it is a suspected carcinogen [115]. HQ is toxic to the kidneys and stomach, it can cause vomiting, nausea and tinnitus [104, 116]. The physical and chemical properties of HQ are shown in Table 10.

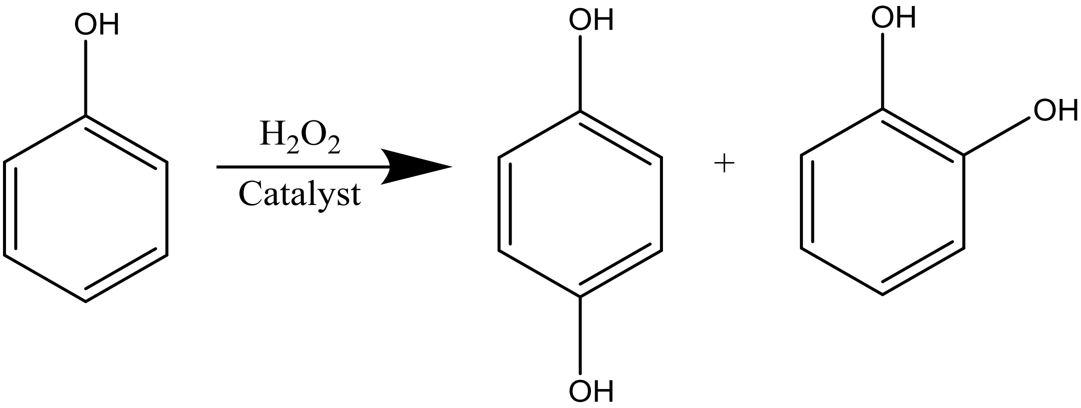

Figure 10 Formation of HQ via hydroxylation of phenol (Source: Adapted from [114])

Most phenolic compounds, especially phenol and HQ, have been proven to be hazardous to human health, flora and fauna; hence, they are listed as priority pollutants and are suspected carcinogens. It is, therefore, essential that methods are developed to remove phenolic compounds from aqueous systems.

Table 10 Physical and chemical properties of HQ (Source: Adapted from [115])

Molecular structure	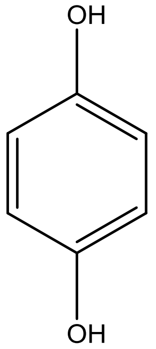
Molecular formula	$C_6H_6O_2$
Synonyms	1,4-Benzenediol; 1,4-Dihydroxybenzene
Molecular weight	110.11 g mol^{-1}
Physical state	Solid (Form: crystalline)
Appearance	Colourless
Solubility in water	50 g L^{-1}
Melting point	172 - 175 °C / 445 K – 448 K
Boiling point	285 °C / 558 K
Flash Point	165 °C/ 438 K

CHAPTER 2

2.0 WATER REMEDIATION TECHNOLOGIES

This chapter discusses different types of water remediation technologies including general operating costs involved. Contaminants removal mechanisms for advanced oxidation processes, iron reduction and adsorption, especially in aromatics uptake, are also given with detailed equations and schematic diagrams. The removal of nitrobenzene, aniline, paracetamol and hydroquinone, via various techniques, is also discussed.

2.1 Water remediation technologies

In the previous chapter, different types of contaminants, especially organic compounds were discussed in detailed. The presence of these substances usually contributes to adverse environmental and health impacts; hence, various methods of remediation techniques are adopted to remove these toxic pollutants from aqueous systems. Here, various remediation technologies, including pump and treat, ultraviolet oxidation treatment, air sparging and reactive/passive treatment walls, for removal of organic species from water streams are discussed.

2.1.1 Pump and treat

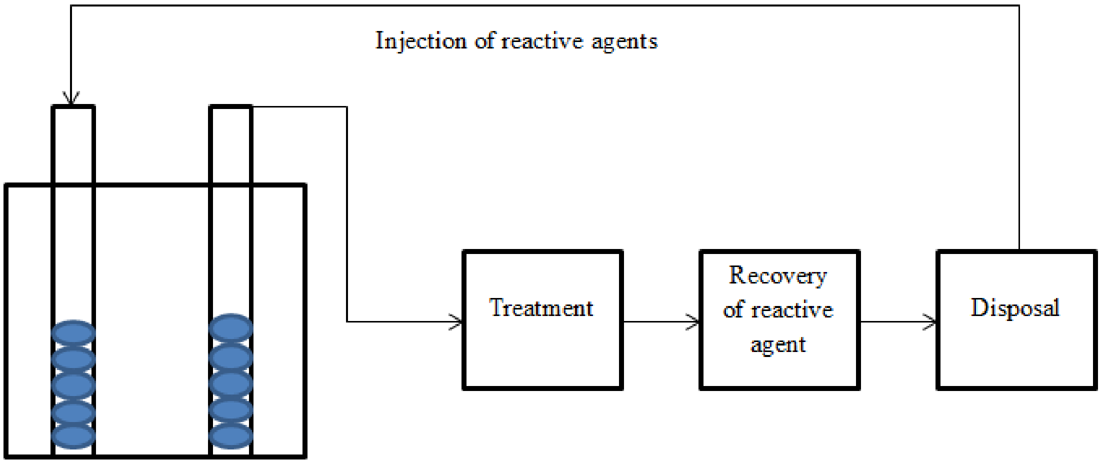

Figure 11 Diagram of chemical enhancement pump and treat technology. The reactive agent can usually be regenerated and reused. For this treatment the reactive agent is used to transform contaminants into harmless substances via oxidation or reduction (Source: Adapted from [117])

Pump and treat is the most common remediation technology used to remove organic contaminants, such as fuels and Volatile Organic Compounds (VOCs); the contaminated water is pumped to the surface via extraction wells where it is subsequently treated. The remediated water is either discharged into surface waters such as sewage plants and rivers, or re-inject into water aquifers [118]. The remediation technologies employed are usually granular activated carbon (GAC), advanced oxidation processes, and air stripping [119] with a diagram pump and treat shown in Figure 11.

The type of contaminants and the site influence the design of the pumping systems, extraction wells and treatment techniques adopted; the effectiveness of the extraction system is monitored, hence, the system can be adjusted according to the condition of the subsurface [120]. Capital and operation costs vary and are also dependent on the type of contaminants and site characteristics; the design and installation costs of a 100 gal min^{-1} system are $200,000 USD, with operation costs in the range US$1 to $100 per 1000 gal of water [118]. The advantages [118] and disadvantages [118, 120] of this type of technology are summarised in Table 11.

Table 11 Advantages and disadvantages of pump and treat technologies (Source: Adapted from [118, 120])

Advantages	Disadvantages
Successfully treats all dissolved pollutants	Incurs high capital and operating costs
Equipment is readily available	Does not meet drinking water standards
Requires small area for installation	Not applicable for removal compounds adsorbed to soils
Design is simple and easy to operate	Time consuming
Fast implementation	Ineffective
Can be used in conjunction with other remediation systems, e.g. air stripping	

2.1.2 Chemical oxidation

In aqueous systems, organic compounds can be degraded to water and carbon dioxide, or nontoxic species, in the presence of oxidants such as oxygen, air, ozone (O_3), high valency metals or hydrogen peroxide. Figure 12 shows contaminants remediation via ozonation, which can be enhanced if UV (Ultraviolet) light is applied, causing hydroxyl radicals to be produced and any contaminants in the water to be degraded [121].

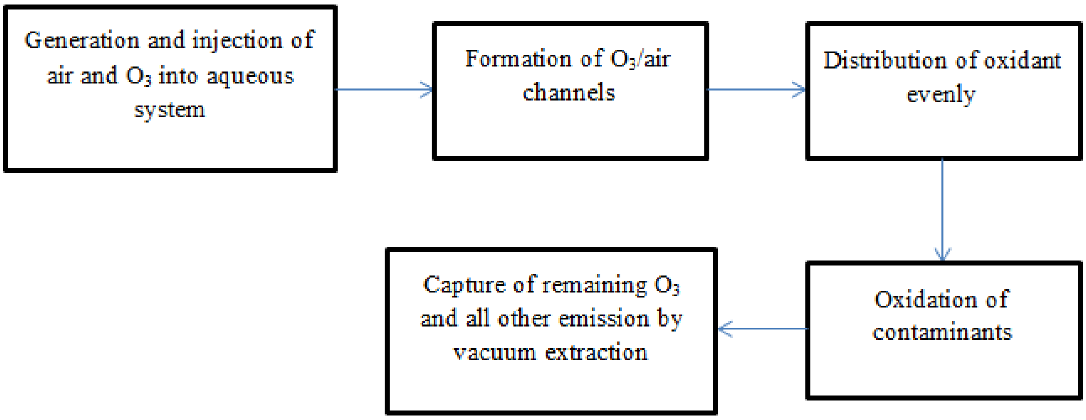

Figure 12 Schematic diagram for ozonation of contaminants in aqueous systems (Source: Adapted from [122]).

In such processes, UV bulbs are used as the light source, located in the reactor and the oxidants produced are allowed to come into contact with the contaminated water [118, 123]. UV oxidation has shown promise in the degradation of aromatics, pesticides, VOCs, dioxins and all types of petroleum products [118]. Despite its effectiveness, UV oxidation does experiences disadvantages, such as high capital and operating costs and can only be applied for the removal of organics at low concentrations [124]. In addition, the presence of suspended solids in contaminated waters will affect the transmission of light and may cause fouling on the surface of quartz used to construct the reactor vessel, with additional treatment required to minimise cleaning [121]. Moreover, this method of remediation is ineffective at high wavelengths, if hydrogen peroxide is used, the presence of free radical scavengers may also affect the reactions that occur, and oxidants used in these processes need to be stored and handled carefully. Hence, there are numerous factors that influence the capital and operating costs of chemical oxidation processes, such as flow rate, the pre- and post - treatments involved, types and concentrations of contaminants, and the degree to which contaminants need to be destroyed. The estimated associated costs incurred to treat 1000 gal of contaminated water using such technologies is between $10 to $50 USD [118].

2.1.3 Air sparging

Air sparging is widely used to remove dissolved VOCs and semi volatilised compounds (SVOC), including gasoline and chlorinated solvents, from water systems; the process of remediation involves air injection into a saturated zone under pressure, whereby the water contaminants are volatilised (Figure 13). The subsurface oxygen concentration also increases in this zone, hence, enhanced biodegradation occurs [118, 125]. This technology involves several remediation mechanisms; the contaminants are initially stripped by the channels created by the injected air, before contaminants volatilisation, and finally, aerobic biodegradation. The cost ranges from $20 to $50 USD per cubic yard of soil for the remediation of fuel contaminated water or soil [118]. Air sparging is limited by high capital costs ($5,000 to $25,000 for air injection pump) [121] and cannot be used for systems containing heavier constituents such as kerosene and diesel [125]. Moreover, the efficiency of such systems for remediation of non-biodegradable and non-strippable compounds is poor [126].

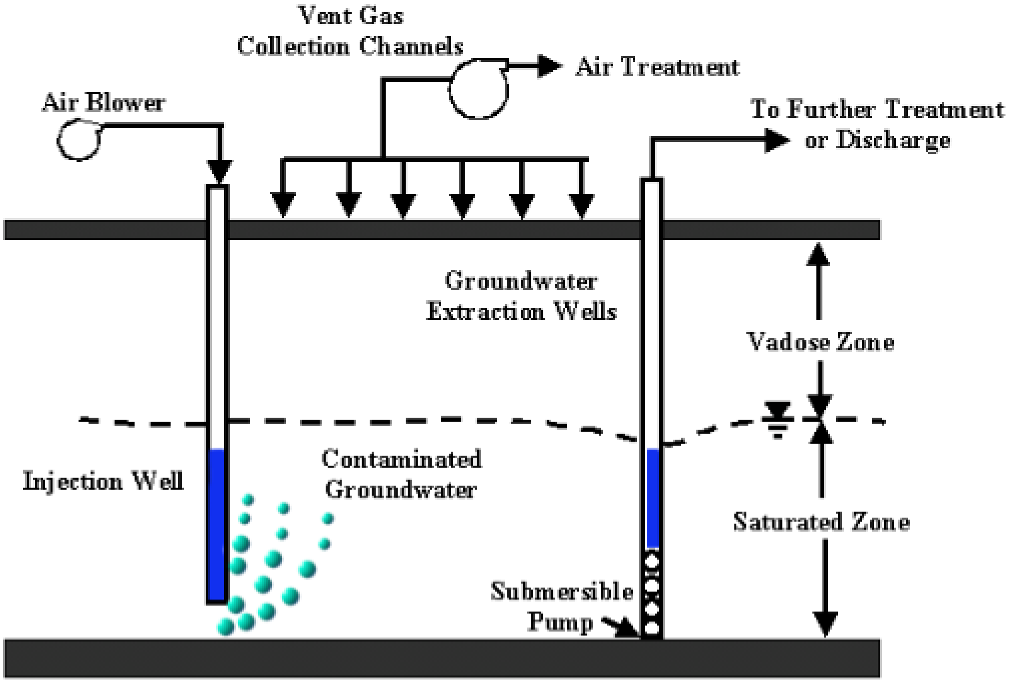

Figure 13 Diagram of air sparging technology where air is injected and transported via channels into the water system volatilising the contaminants. The contaminants travel with the bubbles to the unsaturated zone where vapour extraction is applied, simultaneously with air sparging, to remove the volatilised contaminants (Source: Adapted from [127]) (reproduce under permission [128])

2.1.4 Reactive and passive treatment walls

A reactive, or passive, treatment wall (Figure 14) is a water remediation technology recently developed and adopted to treat inorganics, SVOCs and VOCs; treatment walls are built underground at contaminated waste areas [118, 129] with the contaminants passing through the treatment walls via the natural movement of water, where they are converted into harmless compounds and emitted from, or trapped in, the walls, by the reactive fillings [118, 130]. This technology is the most successfully adopted technique due to the low overall costs, high remediation efficiency and ease of application [129].

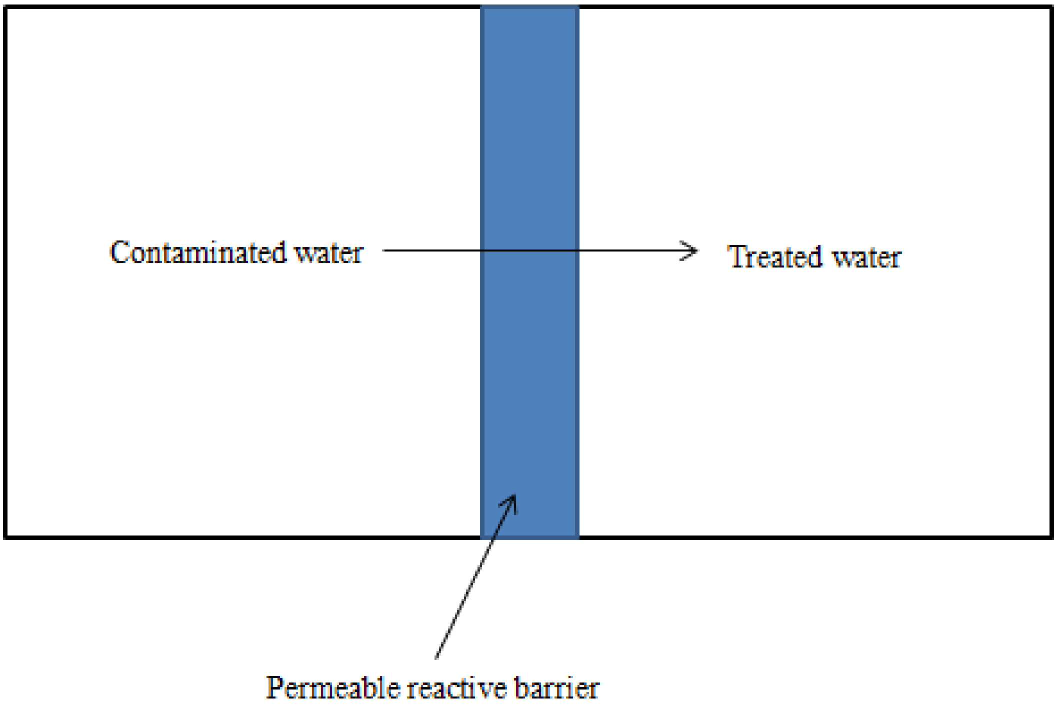

Figure 14 Diagram of contaminated plume treated using reactive or passive treatment walls (Source: Adapted from [131])

Two types of treatment walls are used, permeable reactive trench, and funnel and gate systems [129] (Figure 15), and the design for the former is simpler compared to the latter. For permeable reactive trenches, a trench is built across the width of plume filled with permeable materials; the contaminants are subsequently removed by adsorption or air stripping. If the contaminant plumes are too deep or too wide, a funnel and gate system is usually applied, where the contaminants are funnelled into a small reactive wall where they are treated by a series of low permeability cut-off walls. The funnel serves to force the contaminated water through the gates; while the gate controls the flow of the contaminated plume through the reactive wall [118].

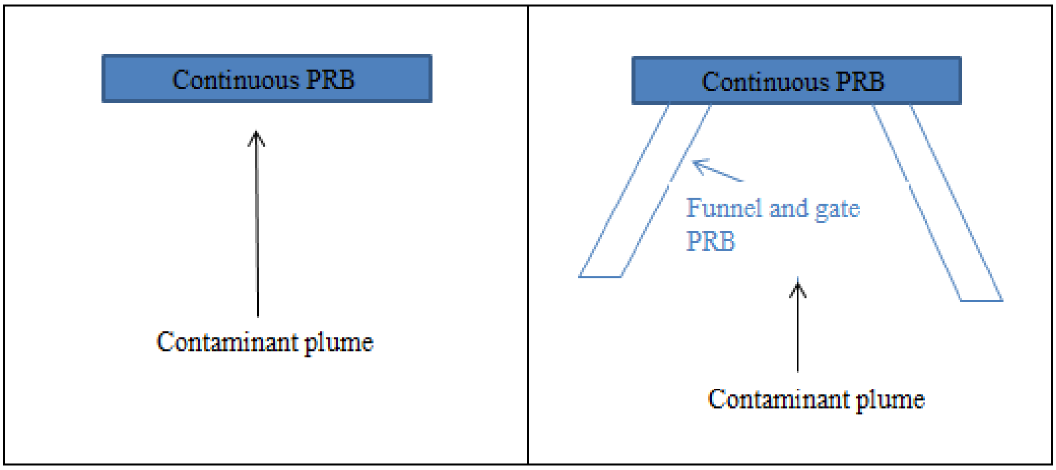

a) Permeable reactive trench

b) Funnel and gate system

Figure 15 Diagrams of treatment walls adopted in passive or reactive treatment walls (Source: Adapted from [131])

Three different remediation processes can be used, which are precipitate, degradation and sorption barriers. For precipitate barriers, dissolved contaminants react with the fillings of precipitate wall and precipitate out as they pass through the barriers; these precipitates will be trapped in the walls and the treated water emitted into the aqueous system. The fillings of the degradation barriers will interact and degrade the contaminants into environmentally friendly compounds, and are usually composed of iron granules for reduction processes or a mixture of oxygen and nutrients for the biodegradation of contaminants. Sorption barrier fillings physically remove contaminants; toxic substances are trapped in the walls, and Granular Activated Carbon (GAC) and zeolite are usually used as the fillings [130]. Diagrams for precipitation, degradation and sorption treatment walls are shown in Figure 16.

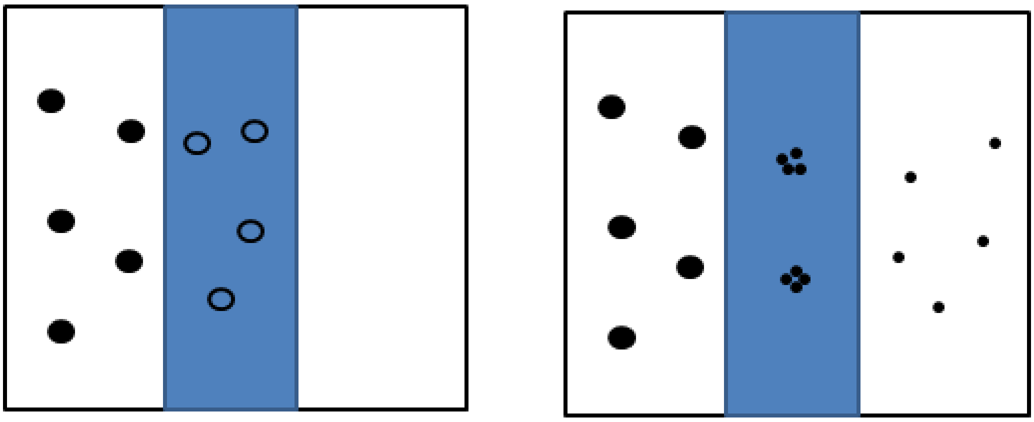

a) Precipitation: Dissolved contaminants precipitated out and remain in walls

b) Degradation: Contaminants are transformed into harmless compounds

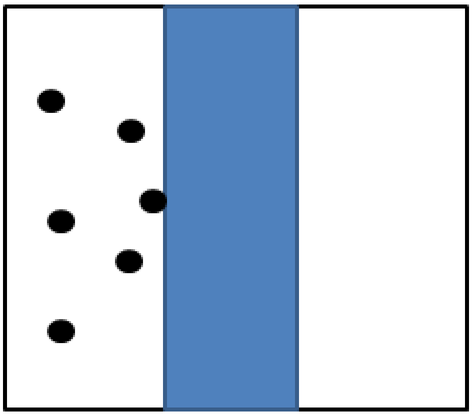

c) Sorption: Contaminants are trapped by the fillings in the treatment walls

Figure 16 Remediation processes of passive and reactive treatment walls (Source: Adapted from [130])

There are no available costs for this technology as it depends on contaminant concentrations and the types of reactive media used [118]; however, the cost to remediate a pound of weight of contaminants, via adsorption, can be estimated at $20 to $50 USD [121].

2.2 Advanced oxidation process

Advanced Oxidation Processes (AOPs) are aqueous phase oxidation processes that have been widely adopted in water treatment to remove toxic substances, which can be applied in conjunction with biological oxidation to enhance the biodegradability of hazardous compounds or reduce the Total Organic Content (TOC) of water [132, 133]. Highly reactive species such as hydroxyl radicals (*OH), are generated via mixture of oxidants, including hydrogen peroxide and O_3, or an oxidant in the presence of UV irradiation, to destroy the targeted organic and inorganic contaminants [132-134].

Numerous AOP systems have been adopted for water treatment, such as hydrogen peroxide (H_2O_2), O_3, $H_2O_2 + O_3$, photo-oxidation, photo-catalysis, Fenton or photo-Fenton oxidation, sonolysis and electron beam irradiation [135]. Here, Fenton and photo-Fenton oxidation are discussed in detailed. At high concentrations of contaminants, H_2O_2 exhibited a low efficiency for contaminant oxidation due to low reaction rates; while the stronger oxidant *OH, which also degrades the contaminants, can be generated by activating H_2O_2 in presence of O_3 (Equation 1), UV radiation (Equation 2) or transition metal salts (Equation 3), such as iron salts, as below:

$$H_2O_2 + O_3 \longrightarrow {}^*OH + O_2 + HO_2{}^* \qquad \text{Equation 1}$$

$$H_2O_2 + UV \longrightarrow 2{}^*OH \qquad \text{Equation 2}$$

$$H_2O_2 + Fe^{2+} \longrightarrow {}^*OH + Fe^{3+} + OH^- \qquad \text{Equation 3}$$

The oxidation process involving activation of H_2O_2 using iron salts (Equation 3) is known as Fenton oxidation, and it is referred to as photo-Fenton oxidation if UV radiation is also used [135, 136]. The mixture of H_2O_2 and ferrous iron (Fe^{2+}), known as Fenton's reagent, was discovered in the 1900s but was only applied to destroy hazardous organic substances in the late 1960s [136, 137]. Fenton oxidation has shown promising results in water remediation, especially for the degradation of organic compounds by converting them into non-toxic products, including inorganic salts, water and carbon dioxide. Fenton oxidation is initiated and catalysed by Fe^{2+}, causing the dissociation of H_2O_2 to produce *OH and ferric iron (Fe^{3+}) as shown in Equation 3. Fe^{2+} can be regenerated via the reduction of Fe^{3+} by H_2O_2; Fe^{3+} may also catalyse the decomposition of H_2O_2 into oxygen and water (Equations 5 to 9) [136, 138].

$$*OH + Fe^{2+} \longrightarrow Fe^{3+} + OH^- \qquad \text{Equation 4}$$

$$H_2O_2 + Fe^{3+} \longrightarrow FeOOH^{2+} + H^+ \qquad \text{Equation 5}$$

$$FeOOH^{2+} \longrightarrow Fe^{2+} + *O_2H \qquad \text{Equation 6}$$

$$Fe^{2+} + *O_2H \longrightarrow Fe^{3+} + HO_2^- \qquad \text{Equation 7}$$

$$Fe^{3+} + *O_2H \longrightarrow Fe^{2+} + H^+ + O_2 \qquad \text{Equation 8}$$

$$*OH + H_2O_2 \longrightarrow H_2O + *O_2H \qquad \text{Equation 9}$$

$$RH + *OH \longrightarrow H_2O + *R \qquad \text{Equation 10}$$

Highly reactive organic radicals (*R) are formed via oxidation of organic compounds (RH) in the presence of *OH via proton abstraction, with further oxidation as per Equation 10. The toxic organic substances can be degraded into carbon dioxide, water and inorganic salts within a continuous treatment system if the concentrations of H_2O_2 and Fe^{2+} are sufficient. The overall equation for Fenton oxidation can be simplified to:

$2Fe^{2+} + H_2O_2 + 2H^+ \longrightarrow 2Fe^{3+} + 2H_2O$ Equation 11

Fenton oxidation requires acidic conditions (pH ~3) to generate sufficient *OH by decomposition of H_2O_2 in the presence of hydrogen cations (H^+); *OH can be added directly to the unsaturated bonds of alkenes, alkynes or the aromatic ring of RH. Furthermore, hydrogen atom abstraction by *OH can generate *R which undergoes dimerization, reduction by Fe^{2+} or oxidation by Fe^{3+} (Equation 12 to Equation 14) [139, 140].

$2{*R} \longrightarrow R - R$ (dimerization) Equation 12

${*R} + Fe^{2+} \longrightarrow Fe^{3+} + R^-$ Equation 13

${*R} + Fe^{3+} \longrightarrow Fe^{2+} + R^+$ Equation 14

The Fenton reaction (Equation 3, rate constant = 70 $M^{-1}s^{-1}$) [141] is faster than the partial destruction of H_2O_2 (Equation 5, rate constant = 0.001 – 0.01 $M^{-1}s^{-1}$) [142], indicating that the regeneration of Fe^{2+} is slower than its consumption; this causes the formation of ferric hydroxide sludge, which may require secondary treatment and separation processes, hence, several techniques such as electro-Fenton and photo-electro-Fenton have been adopted to overcome this problem. In electro-

Fenton, the regeneration of *OH (Equation 15) is enhanced in the presence of cathodic electricity; while the regeneration of Fe^{2+} can be promoted, generating more *OH via photoreduction (Equation 16), for photo-electro-Fenton [138, 143].

$$Fe^{3+} + e^{-} \longrightarrow Fe^{2+} \qquad \text{Equation 15}$$

$$Fe(OH)^{2+} + hv \longrightarrow Fe^{2+} + {}^{*}OH \qquad \text{Equation 16}$$

AOP techniques are employed to degrade various types of contaminants discharged from industrial activities, such as pesticides, petrochemicals dyes, pulp and paper; additionally, such technologies have been applied to remove endocrine - disrupting pharmaceutical substances released from hospital effluents, and the remediation of heavy metals such as arsenic has also been studied [133]. Although AOP has proven to be effective for the degradation of various contaminants [144, 145], it has high associated operating costs due to significant H_2O_2 and electrical power consumptions for complete pollutant mineralisation [146].

2.3 Iron reduction

On the Earth's surface, iron is found in three valence states: ferrous iron (Fe^{2+}), ferric iron (Fe^{3+}) and elemental or zero valent iron (Fe). Fe^{2+} and Fe^{3+} are water soluble with the latter slightly higher in solubility and more stable under neutral to basic conditions [9]. Fe is widely used in wastewater and groundwater remediation due to its low cost and ready available. For aqueous systems containing Fe (in the absence of contaminants), a combination of different species exist, including water, Fe, solid phase iron corrosion products (e.g. FeOOH, Fe_2O_3 and

Fe_3O_4, aqueous Fe^{2+} and Fe^{3+}) and dissolved gases including H_2, CH_4, O_2, H_2S and CO_2 [147].

Iron can be oxidised by many compounds to form ferrous iron, Fe^{2+}. In the presence of water, dissolution of iron occurs, leading to iron corrosion, which is a classical electrochemical process [148, 149]. During anaerobic Fe oxidation in aqueous system, H_2O and H^+ act as electron acceptors with H_2 and OH^- produced (Equations 17 to 18); while under aerobic conditions, H_2O and O_2 act as acceptors generating OH^- (Equation 19). Fe also can be oxidised in presence of organic compound such as chlorinated hydrocarbons (Equation 20) [149].

$$Fe + 2H^+ \longrightarrow Fe^{2+} + H_2 \qquad \text{Equation 17}$$

$$Fe + 2H_2O \longrightarrow Fe^{2+} + H_2 + 2OH^- \qquad \text{Equation 18}$$

$$2Fe + O_2 + 2H_2O \longrightarrow 2Fe^{2+} + 4OH^- \qquad \text{Equation 19}$$

$$Fe + RCl + H^+ \longrightarrow Fe^{2+} + RH + Cl^- \qquad \text{Equation 20}$$

In aqueous systems containing Fe, different mechanisms occur including precipitation, adsorption, co-precipitation and reduction. Crystalline and amorphous iron oxyhydroxides, such as FeOOH, $Fe(OH)_2$, Fe_2O_3, $Fe(OH)_3$ and Fe_3O_4, will precipitate at neutral pH with contaminant molecules adsorbed onto aged and nascent iron oxyhydroxides or being trapped in the nascent iron oxyhydroxide structure during ageing; the first process is known as adsorption while the latter is referred to as co-precipitation. The final step involves migration of contaminant molecules to the surface of Fe, before reduction at the Fe surface [147].

In aqueous systems, Fe undergoes oxidation and generates porous, non-protective and thick oxide films [147, 150]; electrons are released as the Fe is oxidised and the contaminants act as electron acceptors. Ideally oxidation of Fe will occur via electron transfer from the contaminants, however, more often, Fe is oxidised electrochemically, and chemically [151], by water producing a surface oxide layer. Hence, the contaminant molecules have to pass through this oxide film to reach the Fe surface before reduction can take place, while Fe^{2+} has to be transported through the oxide film into the aqueous system, resulting in reduction within the oxide layer [147]; contaminants can be oxidised within the oxide layer via electrons transferred from Fe surface to the contaminant if the majority of oxide layer contains Fe_3O_4 [147, 152].

In summary, contaminant reduction may take place within the oxide layer or at the surface of Fe as the oxide layers are porous; the former is the more favourable process. Here, most of the experiments were conducted under shaking, hence, the generation of an oxide layer at the Fe surface was inhibited and the rate of Fe oxidation increased. Furthermore, precipitation and nucleation of iron oxides in aqueous system were promoted [147].

Table 12 Contaminants that can be reduced by Fe (Source: Adapted from [148])

Contaminant Groups	Chemical Compounds
Chlorinated benzenes	Hexachlorobenzene, pentachlorobenzene, tetrachlorobenzene, trichlorobenzene, dichlorobenzene, chlorobenzene
Chlorinated ethenes	Tetrachloroethene, trichloroethene, cis-dichloroethene, trans-dichloroethene, 1,1-dichloroethene, vinyl chloride
Chlorinated methanes	Carbon tetrachloride, chloroform, dichloromethane, chloromethane
Heavy metal ions	Mercury, silver, nickel, cadmium
Inorganic anions	Dichromate, arsenic, perchlorate, nitrate
Organic dyes	Orange II, chrysoidine, tropaeolin, acid orange, acid red
Other organic contaminants	N-nitrosodimethylamine, TNT
Other polychlorinated hydrocarbons	PCBs, dioxins, pentachlorophenol
Pesticides	DDT, lindane
Trihalomethanes	Bromoform, dibromochloromethane, dichlorobromomethane

Where TNT is trinitrotoluene, PCB is polychlorinated biphenyl and DDT is dichlorodiphenyltrichloroethane

Iron corrosion chemistry has been applied for the removal of toxic and hazardous compounds since the early 1990s [153, 154] and has shown promising results for a wide range of common environmental pollutants, including chlorinated methanes, pesticides, organic dyes, chlorinated benzene and heavy metal ions, as summarised by Zhang W.X [148] (Table 12).

2.4 Adsorption

Adsorption is a process in which the concentration of a component is increased at the interface between two different phases or surfaces; the atoms experience unequal forces of attraction perpendicular to the solid surface plane [155]. The interfacial area plays an important role in concentrating a given component at the surface, and many examples exist where liquids or gases adsorbed on solid surfaces [156].

Adsorption can be divided into physisorption and chemisorption; the former involves weak intermolecular forces such as van der Waals or electrostatic forces, while a chemical bond is formed between the adsorbent surface and adsorbate molecules in the latter. Van der Waals forces are referred to as repulsion-dispersion forces, while electrostatic forces are subject to field dipole, field gradient-quadrupole interactions and polarization as experienced by polar adsorbents; the resulting physisorption occurs quickly and does not involve electron transfer; it is a reversible process with desorption occurring at same temperature and desorption is usually a slow process, due to diffusion effects. Physisorption involves formation of mono and multilayers and is not site specific, with the adsorbed molecules distributed over the entire solid surface. In contrast, chemisorption is a slow and irreversible process, involving electron sharing or electron transfer, causing the formation of chemical bond; limited to the formation of a monolayer, adsorbate molecules adsorb only at specific sites on the surface.

The heat of physisorption is lower compared with chemisorption; the adsorbate may dissociate during chemisorption, while dissociation of molecules is not possible for physisorption. Moreover, chemisorption is favourable at high temperature, hence, it involves higher activation energies compared to physisorption. Both physical and chemical adsorption occur in catalytic processes, while chemical adsorption is limited in separation processes, chemisorption, as it exhibits low capacity and high selectivity, so is only used to remove trace impurities with most of the separation performed by physisorption [155, 157].

In aqueous systems, adsorption using non- polar adsorbents such as silica - rich zeolites and activated carbon (AC) are dominated by van der Waals forces; such materials are known as hydrophobic sorbents and exhibit high affinity for most organic compounds and low affinity towards water. In contrast, electrostatic forces drive adsorption on polar sorbents (e.g. zeolites with high aluminium content), and these materials experience strong interactions with polar species such as water molecules, hence, they are described as hydrophilic sorbents [157].

Many sorbents (activated alumina, zeolites, silica gel and AC) are used in water remediation, and these materials generally possess high surface areas, up to hundreds of $m^2 g^{-1}$ [158]. Among these, AC is one of the most common sorbents used to remove various types of contaminants such as heavy metals [159], Polycyclic Aromatic Hydrocarbons (PAH) [160], chlorinated compounds [161] and dyes [162]. As well as acting as a sorbent, AC has been used as catalyst support and a catalyst for water treatment and chemicals recovery or purification due to its inherent surface chemistry, specific pore structures and high surface area and reactivity. The interactions between the adsorbate molecules and AC surface can be divided into non – electrostatic and electrostatic. Attraction force involved for non – electrostatic interactions are (a) van der Waals, (b) hydrogen bonding and (c) hydrophobicity of

AC that drives solutes from solution to AC surface. Electrostatic interactions can be repulsive or attractive based on (a) chemical properties of the solutes, (b) ion strength of the aqueous system and (c) charge of AC surface [163]. AC surfaces can be divided into three different zones: (a) carbon basal planes (more than 90 % of the AC surface), (b) oxygen containing groups resulting in surface heterogeneity and (c) inorganic ash. For aromatic compounds, most of the molecules are adsorbed on the basal planes, however, the surface functional groups exhibit higher activity, which influences the adsorption uptake [164, 165].

Although AC has successfully removed various types of organics from aqueous systems, such materials are brittle, with carbon fines produced during the treatment process. High regeneration costs are also incurred, hence, polymer resins, with effective and cheaper regeneration processes, are used as an alternative. Polymeric resins also demonstrate a wide range of porosity, surface areas and functional groups, shown to be effective in the removal of certain organic contaminants from water [166-168]. Some polymer materials, such MN200, have controllable pore structures with pores simultaneously in the macro and micro ranges and high surface areas (up to 2000 $m^2 g^{-1}$). Resins can also be regenerated using organic solvents such as acetone, methanol or ethanol [169]. The adsorption of aromatic compounds on non–functionalised polystyrene cross-linked divinylbenzene Macronet MN200 involves van der Waals forces (π-π dispersive interactions) between the benzene rings of the resin and the adsorbate, as well as hydrophobicity of the sorbent, which creates a thermodynamic gradient driving the adsorbate onto the sorbent surface from the bulk solution [170].

Adsorption in aqueous systems is mainly affected by the characteristics of the adsorbate including (a) pK_a, (b) solubility, (c) types of substituents, if the compound is aromatic, and (d) molecular size. If the adsorbate is an electrolyte, then pK_a controls molecular dissociation, which affects the pH of the solution; while the solubility determines the hydrophobic interactions between adsorbate molecules and the sorbent surface. Aromatic substituents can influence the dispersive interactions between sorbent surface aromatic rings and the adsorbate via electron donation or withdrawal. Accessibility of adsorbate molecules to adsorption sites depends on molecular size [171], and the textural properties (i.e. pore size distribution and surface area) and surface chemistry of the sorbent may also influence adsorption [165].

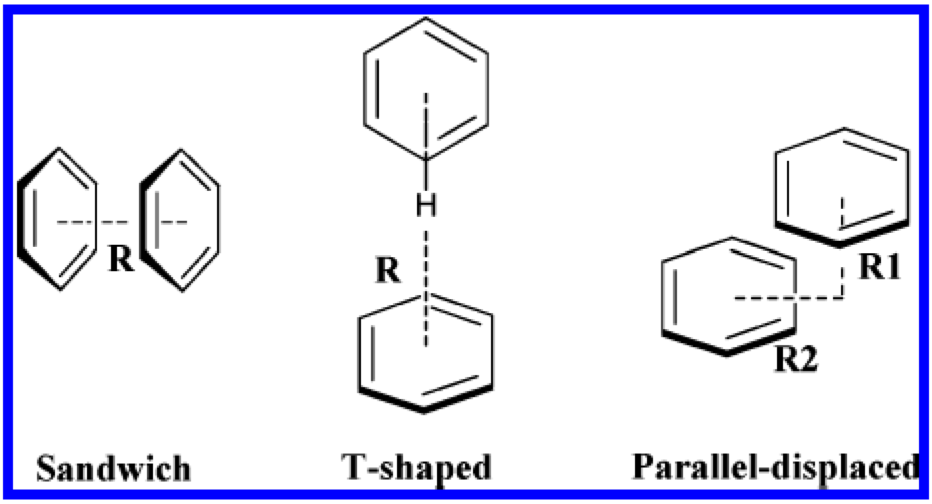

Figure 17 Orientations of aromatic π – π interactions: sandwich, T-shaped, parallel – displaced (Source: Adapted from [172])

Within a benzene ring (C_6H_6), each carbon atom uses sp^2 hybrid orbitals to form sigma bonds with a further carbon atom and a hydrogen atom leaving an un-hybridised 2*p* orbital (an un-paired *p* orbital electron) for each carbon atom, perpendicular to the plane of the ring. The six atomic *p* orbitals, for an aromatic ring, overlap with these *p* orbitals resulting in the generation of six π molecular orbitals, and the six delocalised electrons formed a π electron cloud spread over the planar ring [64, 173]. π - π interactions, also known as pi stacking, are non-covalent attractive interactions between aromatic rings [174], and occur in one of three different orientations: T - shaped, stacked arrangement (sandwich) and point or edge to face (parallel displaced) (Figure 17), where stacked arrangement is most common [172, 175]. Again the presence of aromatic substituents affects the system; an electron withdrawing group, such as $–NO_2$, decreases the electron density of the aromatic ring, which reduces the π – electron repulsion. In contrast, the presence of an electron donating substituent, such as $–NH_2$, increases the electron density of the ring, hence, increases π – electron repulsion [176].

2.5 Removal of Nitrobenzene (NB) from aqueous systems

As a result of NB toxicity, many amelioration techniques have been developed for its removal; however, not all are suitable or efficient. Traditional wastewater treatment processes, such as biological treatments, fail to reduce NB concentrations to the lower limit [34], as a result of inhibition of mineralisation of the NB by microorganisms [34]. It is also known that oxidation of NB is difficult to achieve due to the low electron density of the aromatic ring, which inhibits the donation of electrons [34, 35]. Other remediation technologies, such as adsorption [177], electrochemical reduction [36], advanced oxidation [178] and chemical reduction [179] have also proven to be effective for NB removal.

For degradation of NB via Fenton processes, nitro radicals ($*NO_2$) are generated via ipso substitution of *OH on NB or attack of *OH onto the released of nitro anion (NO_2^-) from the aromatic ring. NB subsequently undergoes nitration with $*NO_2$ and yields 1,3-dinitrobenzene (1,3-DNB) (Figure 18) [34, 146, 178]. 1,3-DNB contains two electron deficient $–NO_2$, hence, 1,3-DNB is more resistant to hydroxyl radical oxidation, so longer treatment periods are required for traditional Fenton processes [178, 180]. The toxicity of 1,3-DNB is reported as ~30 times greater than NB [181], hence, degradation of NB via Fenton is unfavourable. Carlo *et al.* reported that the increased iron dosing results in the increase of 1,3-DNB formation, while the generation of 1,3-DNB decreases at high concentration of H_2O_2 catalyst. In addition, 1,3-DNB is inhibited in the presence of UV radiation; however, these techniques have increased costs and energy consumption since longer UV exposure and more catalyst are required [182].

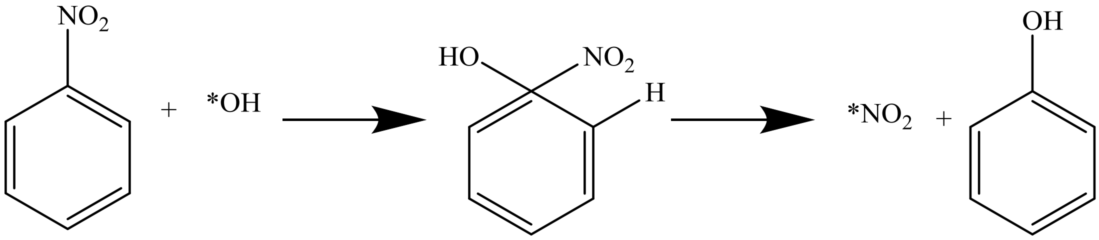

a) Ipso substitution of *OH on NB

$$NO_2^- + {*OH} \longrightarrow {*NO_2} + OH^-$$

b) Attack of *OH on NO_2^-

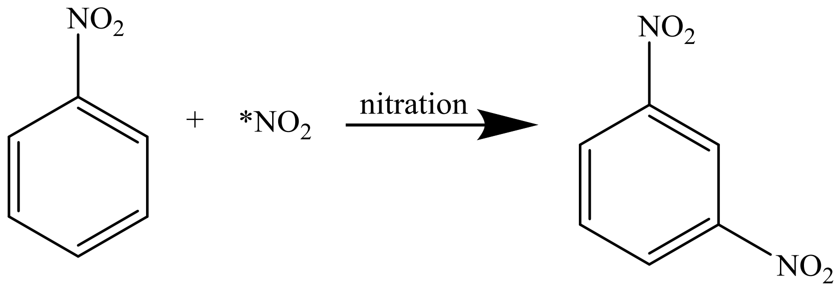

c) Formation of 1,3-DNB via nitration of NB

Figure 18 Nitration of NB via Fenton process (Source: Adapted from [178])

In recent years, iron based Permeable Reactive Barrier (PRB) technologies have been used as alternatives for hazardous waste treatment. PRB has been investigated intensively at the pilot and laboratory scale to study remediation of water polluted by reducible pollutants [183]. In 1996, Agrawal and Tratnyek proposed that NB would be reduced to AN under anaerobic conditions in the presence of iron powder and provided a detailed schematic transformation of nitrobenzene [149]. In Fe – H_2O system, NB undergoes a series of two electron reduction to form AN; firstly, NB is converted into nitrosobenzene (C_6H_5NO), followed by transformation into phenylhydroxylamine (C_6H_5NHOH), finally yielding AN as the product based on the reaction scheme below [149, 184, 185]:

$$C_6H_5NO_2 + Fe^0 + 2H^+ \longrightarrow C_6H_5NO + Fe^{2+} + H_2O \qquad \text{Equation 21}$$

$$C_6H_5NO + Fe^0 + 2H^+ \longrightarrow C_6H_5NHOH + Fe^{2+} \qquad \text{Equation 22}$$

$$C_6H_5NHOH + Fe^0 + 2H^+ \longrightarrow C_6H_5NH_2 + Fe^{2+} + H_2O \qquad \text{Equation 23}$$

The overall reaction is summarised as:

$$C_6H_5NO_2 + 3Fe^0 + 6H^+ \longrightarrow C_6H_5NH_2 + 3Fe^{2+} + 2H_2O \qquad \text{Equation 24}$$

There are several factors such as pH, iron loading and dissolved ions that affect the reduction of NB by iron powder. Several studies have investigated the effect of pH on NB reduction demonstrating that NB reduction is enhanced as pH decreases; while the rate decreases as pH increases [186-189], as iron corrosion is increased in the presence of hydrogen cations (H^+), facilitating the transformation of NB into AN as shown above [187]. Moreover, iron corrosion is favourable at low pH and Fe^{2+} is generated, improving reactivity [187, 190], also oxide layers, such as ferrous hydroxide, on the Fe surface can be removed under acidic conditions, providing more active sites [187, 188]. In contrast, under basic conditions, dissolution of Fe is prevented due to the formation of a passive iron hydroxide layer on the Fe surface resulting in inhibition of mass transport [187].

Previous studies have also reported that iron loading influences the rate of NB reduction with results showing that the rate increases when iron loading increases from 0.5 to 3.0 g L^{-1}, remaining unchanged as the loading increases from 3.0 to 5.0 g L^{-1}, as the reactive sites are in excess at high iron loading and the reduction of NB is limited only by mass transport. The kinetics of NB reduction, in one study, followed pseudo -first order models for all systems except 0.5 g L^{-1} which was described using a pseudo - zero order model [188], while others reported that the pseudo – first order model fitted the data more closely for NB reduction using iron powder [149, 183, 185, 187, 191, 192]. NB reduction was also been seen to be enhanced in the presence of dissolved anions, such as nitrate (NO_3^-), sulphate (SO_4^{2-})

[188] and chloride (Cl^-) ions [193], but inhibited by phosphate ions (PO_4^{3-}) [188], as phosphate ions tend to generate complexes on the Fe surface, via adsorption onto the mineral surface and co-precipitation with iron oxide films causing a decrease in NB reduction [188].

In addition to chemical and biological remediation technologies, physical adsorption has proven to be effective and inexpensive, and is the most frequently adopted method for contaminants removal, especially organic compounds [194], often utilising activated carbons [165, 195-199] due to their structure, chemical stabilities, specific internal structures, surface areas [200] and surface functional groups, which include lactonic and carboxylic groups, that play an important role although they may be present in minimal quantities [195]; the kinetics of NB adsorption have been shown to follow a pseudo-second order model [195, 198]. NB adsorption is affected by AC surface chemistry; oxidation of AC using acid nitric (HNO_3) resulting the increased of oxygen containing acidic functionalities on the surface, while leaving the textural properties, such as pore structure, unchanged. However, treatment using HNO_3 may weaken the $\pi - \pi$ interactions, generating water clusters which reduce NB uptake. A combination of nitric acid and thermal treatment has been shown to lower the amount of acidic functionalities on AC surface and increase the mesopore proportion, promoting NB diffusion, hence, NB uptake [165, 200]. It is noteworthy that AC regeneration via thermal oxidation caused a reduction in NB removal of ~ 50 % after four regeneration cycles [198]. In summary, AC was proven efficient for NB removal, however, several disadvantages, including high regeneration costs, exist.

Wei *et al.* investigated NB adsorption using a low cost synthetic inorganic adsorbent (nanocrystalline hydroxyapatite), noting that NB uptake increased as pH and temperature decreased, as a result of negative charges on the sorbent surface being neutralised, and positive charges being enhanced under acidic conditions; thermodynamic results showed NB adsorption to be a physical process, and increasing temperature resulted in reduced uptake (Section 2.4) [201]. NB has also been successfully removed from water using other siliceous materials such as clay minerals (e.g. montmorillonite [202, 203]), zeolites [204] and MCM-41 [205].

In conclusion, NB degradation via Fenton processes produces 1,3-DNB, which is more toxic than NB, and incurs high operation and capital costs. In the presence of UV radiation, or at higher H_2O_2 concentrations, less 1,3-DNB is formed, however, more energy is consumed, thus, making NB degradation via Fenton unfavourable. Commercial iron powders have been shown to successfully reduce various contaminant types including NB into less toxic compounds; NB is reduced to AN in the presence of Fe, and NB reduction is affected by many factors such as iron loading, pH and the presence of ions. The toxicity of aromatic amines is about 1/500 of nitroaromatics [206], however, AN is hazardous and may require additional remediation steps for removal from aqueous systems. Adsorption is widely used to remove pollutants from water and this method has successfully removed NB at source without contributing to secondary pollution. When selecting a sorbent, surface chemistry, textural properties and regeneration potential must all be considered.

2.6 Removal of AN from aqueous systems

The removal of AN from aqueous systems is essential due to its potential toxicity, as discussed in Section 1.3. Several methods, including adsorption [65, 207, 208], AOPs [209, 210], photo-catalysis [211, 212] and biological treatments [213, 214] have been adopted for AN removal from aqueous systems, however, traditional biological processes are unfavourable, especially for the removal of high AN concentrations as complete degradation of the pollutant is difficult to achieve [48, 62, 215]. AOPs, such as Fenton and ozonation processes, offer an alternative but Fenton processes, fail to remove AN completely and yield NB, phenol and oxalic acid; however, use of an electrical current (electro-Fenton), can enhance AN removal efficiency and rate, the downside being high energy consumption and generation of toxic intermediates [209]; AOPs require acidic conditions i.e. ~ pH 2, and incur high capital and operating costs. Complete AN oxidation pathways have been previously discussed in the literature [209, 216], and are summarised in Figure 19.

Ozonation, catalysed by Fe^{2+} and UV radiation under acidic conditions (pH 3), results in attack of AN by O_3 and *OH to produce NB and benzoquinonimine. NB is further degraded to form maleic acid and NO_3^-; while benzoquinonimine undergoes hydrolytic decomposition and is converted into *p*-benzoquinone and NH_3, which exists as NH_4^+ at < and pH 3, *p*-Benzoquinone is subsequently degraded into maleic acid. A product from both routes, maleic acid is subsequently mineralised and transformed into CO_2 [216]. Combining ultrasound with ozonation has shown promise for AN degradation, however, toxic aromatic by products, such as NB and *p*-benzoquinone cause secondary pollution [217].

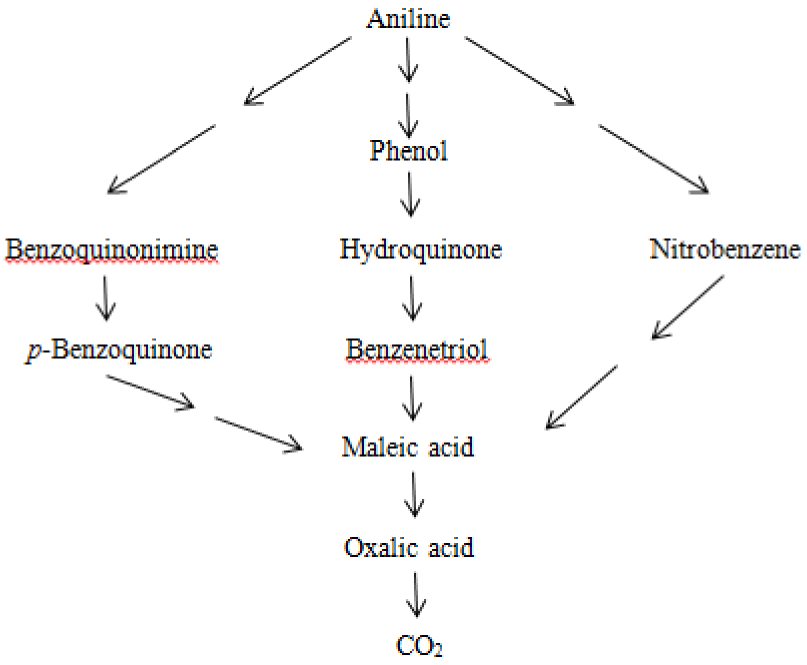

Figure 19 AN oxidation pathways via Fenton or electro-Fenton (Source: Adapted from [209])

Catalytic Wet Air Oxidation (CWAO), used in industrial wastewater treatment, has been used to remove AN from aqueous systems. Carried out in the presence of noble metal catalysts, using air or oxygen as an oxidising agent, under mild conditions such as temperatures of 398 to 493 K and pressures of 5 to 50 bar [218, 219], the process has shown promise for AN removal; however, toxic intermediates, such as phenol [219], HQ [219], NB [220] and nitrophenol [220] are generated, making the process unfavourable due to secondary pollution. Two possible AN oxidation routes, via CWAO, are proposed (Figure 20): (i) $-NH_2$ of AN is oxidised and hydroxylated to form phenol and HQ, followed by ring cleavage of HQ and degradation into CO_2, (ii) oxidation of AN produces di-aromatic substances such as azobenzene and azoxybenzene, with both reactions occurring simultaneously [219].

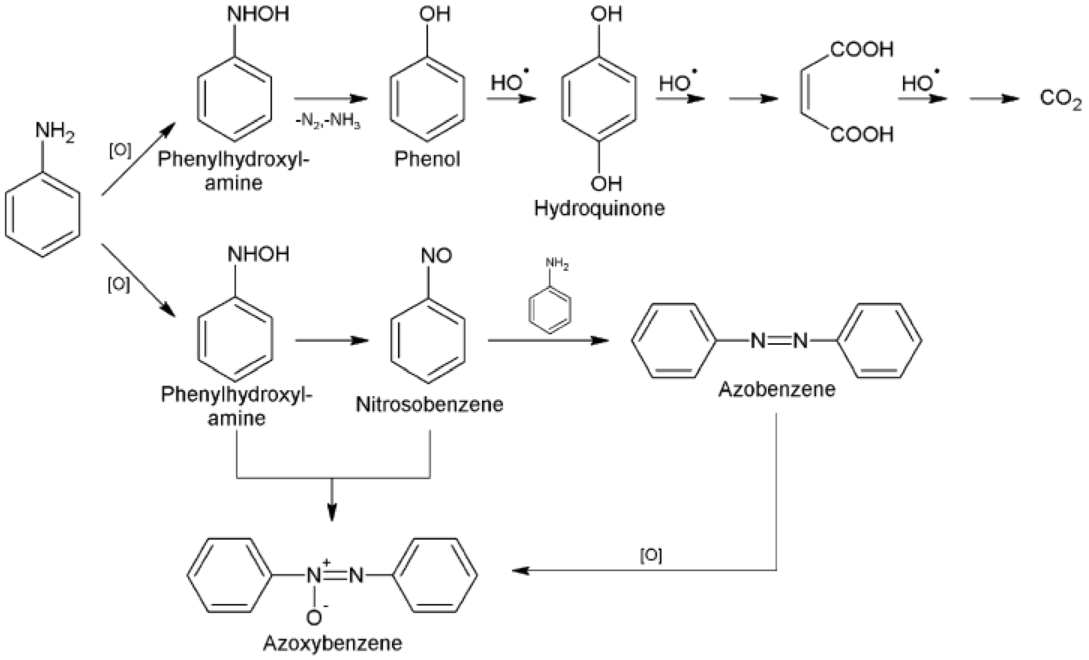

Figure 20 Reaction pathways of CWAO of AN (Source: Adapted from [219])

Adsorption is an efficient environmental remediation technology and has been investigated intensively at laboratory and pilot scale, especially for the treatment of wastewater containing organic pollutants [208]. Different sorbents, such as zeolites [221], montmorillonite [222], polymers [223] and carbon [224] have been used to remove AN from wastewater; among these, carbon materials are the most common sorbents adopted. Previous studies reported that GAC [170, 224-228], carbon nanotubes [229, 230] and AC fibres [62, 231, 232] have successfully removed AN from water; Tang *et al.* reported that AC can be regenerated using hydrochloric acid solution, achieving > 85 % AN uptake for five cycles [226]. Wu *et al.* suggested that AC surface chemistry plays a more important role in AN removal compared to the physical properties of AC; their results demonstrated that the formation of C=C bonds enhanced by oxygen plasma irradiation, resulted in increased π – electrons on the graphene layer, hence, enhanced dispersive interactions between the aromatic rings of AC and AN, consequently increasing AN uptake [228]. Conversely, Li *et al.* (2009, 2010) reported that modification of AC; via nitric acid oxidation caused increased oxygen surface functionalities, which weakened dispersive interactions due to formation of additional water clusters, resulting in lower AN uptake [231, 233].

Siliceous materials have also been used to study AN removal; El-Safty *et al.* used mesoporous aluminosilica monoliths and showed that incorporation of aluminium into silica monoliths increased the acidic sites present, enhancing dispersive interactions and hydrogen bonding; this sorbent was regenerated and reused for 6 cycles [208]. Yang *et al.* found that MCM – 41 with template partially removed has a higher AN adsorption capacity compared to MCM-41 with template completely removed, due to stronger hydrophobicity of the sorbent and greater selectivity towards the adsorbate in the presence of template; this sorbent was regenerated and reused, with ~ 20 % reduction in AN uptake after 3 cycles [234].

Valderrama *et al.* reported that Macronet sorbents, with hyper-cross-linked structures, containing both micro- and macroporosity, can successfully remove AN from aqueous systems [170, 225]. The effect of acidic functionalities of polymeric resins on AN adsorption was investigated by Cai *et al.*, who indicated that macroporous sulphonic functionalised styrene cross-linked with divinylbenzene (LS-2) exhibited a higher AN uptake compared to commercial Amberlite XAD – 4, due to the presence of polar acidic functionalities and higher micropore area [223, 235].

In summary, traditional Fenton oxidation fails to degrade AN completely; electro – Fenton and ozonation successfully degrade AN into harmless products, however, these methods are unfavourable due to high capital and operating costs, and the reaction needs to be carried out in acidic media. Combination of ozonation and ultrasound produces toxic by – products, and, AN removal via CWAO yields di – aromatic compounds, which may contribute to secondary pollution. Various studies report AN removal via adsorption using different sorbents, as discussed above, with AC the most common sorbent used; however, regeneration of AC incurs high costs and polymeric resins are suggested as an alternative due to simpler regeneration methods. Again, surface chemistry of sorbents is crucial and must be considered in line with textural properties and associated costs.

2.7 Removal of PCT from aqueous systems

PCT concentration in aqueous systems is not regulated, however, long term exposure will affect human health [101]; hence, PCT removal from water has been widely studied by researchers, with different technologies, such as AOPs [236-238], biological treatments [239-242] and adsorption processes [243-245] applied for PCT removal. Biological treatments have successfully removed PCT from water streams, however, long treatment were required (2 to 28 days) [240-242]. For AOPs, numerous studies have reported the removal of PCT via Fenton oxidation [92, 143, 238, 246, 247] and the associated degradation routes have been discussed in the literature (Figure 21) [143, 248]. Fenton degradation of PCT is initiated by direct attack of PCT by *OH to produce HQ and acetamide; HQ is converted into benzaldehyde and then transformed into benzoic acid, which is further degraded into carboxylic acids (formic, acetic, malonic and oxalic acids), ketones and alcohols before final mineralisation to CO_2 and water, while acetamide is degraded into carboxylic acid before conversion to nitrates, CO_2 and water [143, 248]. Although PCT may be converted into harmless products, the process must be carried out under acidic conditions and is cost and energy intensive.

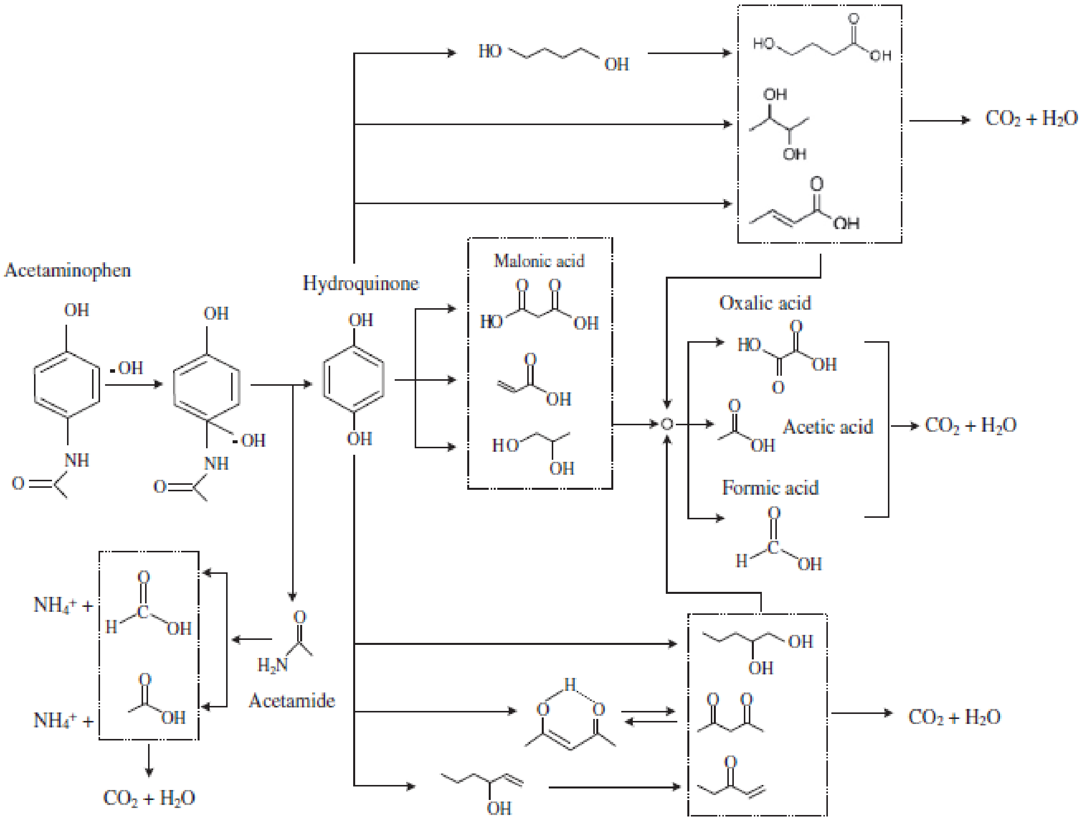

Figure 21 Fenton oxidation and mineralisation pathways of PCT proposed by de Luna *et al.* (2013) (Source: Adapted from [248])

Several studies have investigated photocatalytic degradation of PCT in the presence of solar or UV radiation [237, 249, 250]; titanium dioxide (TiO2) and photo – Fenton are widely adopted for this process with the former acting as photocatalyst [250]. TiO_2 is chemically stable, inexpensive and environmentally friendly [237] and photocatalysis using TiO_2 was successfully degraded PCT at low concentrations (ng L^{-1} to µg L^{-1}) [237, 250], as opposed to Fenton or photo – Fenton oxidation, which have been applied to degrade PCT at higher concentrations (mg L^{-1}) [238, 246]. Since, the concentrations of PCT detected in real water streams are in the range of 0.0095 to 2.4 μg L^{-1}, as discussed in chapter 1, photocatalysis is a viable technology. Jagannathan *et al.* studied the degradation of PCT via sonolysis, photocatalysis and sonophotocatalysis and the results demonstrated that sonophotocatalysis is more efficient and exhibited higher rates compared to the other systems [251].

PCT can also be removed from water via adsorption and numerous studies report PCT adsorption on carbon materials [244, 245, 252]. Terzyk has studied the effects of surface chemistry, pH and temperature on PCT uptake [244, 253-256], and found that PCT removal increased slightly for AC modified with fuming sulphuric acid (creation of acidic sulphate or sulphonic groups) and remained unchanged for AC modified with ammonia (creation of basic amide or imide groups). In contrast, PCT uptake decreased as for AC modified with nitric acid (creation of lactonic, phenolic or carboxylic groups); modification with acids or ammonia contributed to a small change in porosity suggesting that surface chemistry plays an important role in PCT uptake [253]. These phenomena have been ascribed to the interactions between PCT and acid functionalities, e.g. repulsion between the carbonyl groups of AC and PCT, and interaction between basic functional groups and the OH group of PCT [255]. Additionally, based on MOPAC (Molecular Orbital PACkage) calculations, the sorbents can interact with PCT via the phenolic and amide groups of PCT; interaction with the former gave better correlations compared to the latter [244]. As mentioned above, modification with ammonia did not contribute to higher PCT uptake; while modification with sulphuric acid caused a small increase in PCT uptake. For PCT, OH and C=O are electronegative groups; for AC, modified with fuming sulphuric acid, surface functionalities are less electronegative compared to AC modified with nitric acid, as O is more electronegative than S, hence, the resulting C=O is more polar than S=O. Thus, PCT uptake is decreased significantly for AC modified with nitric acid, due to more polar C=O, while less polar S=O is less active, hence, the inhibition of PCT adsorption is prevented.

Ruiz *et al.* also reported that AC modified by wet oxidation lead to an increase in O content and only a small change in porosity, with PCT uptake for unmodified AC double than that of modified AC, ascribed to an increase in adsorbed water molecules for modified AC, which prevents PCT from entering the active sites [243]. Although commercial AC is effective in PCT removal, it nevertheless incurs high regeneration costs; hence, researchers have focussed on low cost sorbents. Cotoruelo *et al.* and Mestre *et al.* investigated PCT removal using AC synthesised from lignin obtained from the cellulose industry and sisal waste; both AC successfully adsorbed PCT from aqueous systems [245, 257]. Meanwhile, Villaescusa *et al.* studied PCT removal using vegetable wastes and found that PCT is dominated adsorption by $\pi - \pi$ dispersive interactions, hydrogen bonding and hydrophobicity, which drives the adsorbate from water to the sorbents [258].

In conclusion, PCT can be removed from water using biological treatment; however, the process is slow. By using AOPs such as Fenton, electro - Fenton or photo – Fenton, PCT may be converted into harmless products (i.e. water and carbon dioxide), but incurs high operational costs. Photocatalysis is proven to successfully to degrade PCT for concentrations in the range ng L^{-1} to mg L^{-1}, and the rate of degradation can be improved by sonophotocatalysis. Physical adsorption is widely applied to remove PCT and commercial AC is the most common sorbent used. The surface chemistry plays important role in PCT uptake, but due to its high associated regeneration costs, alternative sorbents, such as AC synthesised from industries wastes, are of interest for PCT removal.

2.8 Removal of HQ from aqueous systems

The toxicities of phenolic compounds, including HQ, have been discussed in Section 1.5; the presence of HQ in aqueous systems has contributed to adverse environmental and health impacts, hence, remediation techniques, such as catalytic oxidation, electrochemical degradation and extraction, have been used for HQ removal from aqueous systems. These methods are, however, unfavourable due to their associated high operating costs and low efficiencies [116]. AOPs have been studied as an alternative; Ruppert and Bauer reported that mineralisation of HQ via photo – Fenton was 98 % successful over 5 h; however, the mechanisms of degradation were not investigated in their study [259].

Numerous other studies have demonstrated that HQ can be degraded via photocatalysis, another AOPs [260-263], where a pair of conduction band electrons and valence band holes are created on irradiated TiO_2, which reduces O_2 and photolyses H_2O. Active O_2 species such as hydroxyl radicals are generated on the surface of TiO_2, which participate in the degradation mechanism and mineralise of compound [261]. Ksibi *et al.* reported that photocatalytic degradation of HQ may cause the opening of the benzene ring and transformation into carboxylic acids, before final conversion to CO_2 [260]. Although HQ can be degraded and mineralised via photo – Fenton and photocatalysis, detailed mechanisms have not been discussed. In contrast, Yao *et al.* and Tudorache *et al.* have reported the removal of HQ via biocatalytic degradation [264, 265] with proposed mechanisms for HQ degradation using H_2O_2 and enzyme (Serratia marcescens AB 90027), where HQ is initially transformed into *p* – benzoquinone prior to ring cleavage, before further degradation to form maleic acid and oxalic acid and final mineralisation to CO_2 and H_2O, as shown in Figure 22 [264].

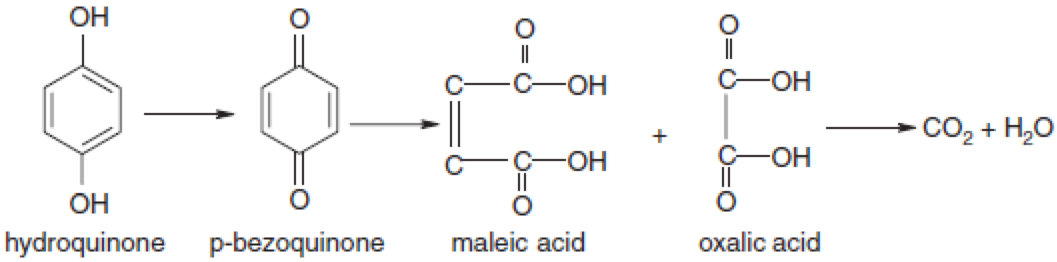

Figure 22 Proposed degradation pathways of HQ (Source: Adapted from [264])

Adsorption, is an alternative to remove HQ from water supplies [116] using a variety of sorbents, e.g. carbon [266], bentonite [267] and silica [268]; among those tested, activated carbon is the most common sorbent used for water treatment due to its specific surface area, textural and chemical properties [104]. Suresh *et al.* and Ayranci and Duman have reported that pH has a significant effect on HQ adsorption on AC [104, 269] with removal enhanced as pH increases between pH 2 to 6 and a reduction thereafter. In addition, HQ uptake increases with AC loading and initial concentration; while AC can be regenerated via thermal treatment with HQ adsorption reduced by ~ 35 % after five cycles [104]. Mohamed *et al.* investigated the effect of surface heterogeneity of AC on HQ adsorption and found that surface area and micropore volumes increased for AC modified with sulphuric acid, however, HQ adsorption decreased due to the increase of acidic functionality capacities blocking the adsorbate molecules from entering the micropores [266]. Magnetic biosorbents, such as β – cyclodextrin – chitosan, with hydrophobic surfaces, low cost and recoverability, has raised interest among researchers; Li and co - workers reported that pH 6 is optimum for HQ adsorption onto β – cyclodextrin – chitosan and regeneration can be achieved using organic solvents, such as ethanol, with < 20 % reduction in HQ uptake after 5 cycles. It is also suggested that HQ removal may involve the formation of hydrogen bonds between the carboxylic groups of the sorbent and HQ, with entrapment of the HQ aromatic ring in the central cavity of the sorbent [116].

Bentonite, a natural clay mineral, is widely used in wastewater treatment due to its low cost and ready available; Yildiz *et al.* modified the surface of bentonite via an ion-exchange reaction to enhance the hydrophobicity, demonstrating that HQ uptake increased with temperature, suggesting an endothermic process. In contrast, HQ adsorption was inhibited at high pH due to the presence of OH^- and increased ionic repulsion between OH groups of HQ and negative charge on the sorbent surface [267]. In addition, Fu and co – workers have investigated HQ removal using mesoporous MCM-41 with varying initial concentration, and they also reported that the surface chemistry of MCM-41 plays an important role in the adsorption process; MCM-41 modified with trimethylchlorosilane and methyltrimethoxysilane, to improve hydrophobicity, increased the interactions driving HQ adsorption by van der Waals and hydrogen bonding forces, with MCM – 41 modified with trimethylchlorosilane exhibiting the lowest HQ uptake. MCM – 41 modified with methyltrimethoxysilane, in contrast showed HQ uptakes is higher than unmodified MCM – 41 at high concentration (>200 mg L^{-1}), while unmodified MCM – 41 performed best at lower initial concentrations (<200 mg L^{-1}) [268]. Polymeric sorbents are also widely used and have shown promise for water remediation due to their surface areas, controllable pore structures and simple regeneration [170], with previous studies reporting that mesoporous resin XAD-4 and microporous hyper-cross-linked sorbent NDA150 were successful in removing HQ from aqueous systems; high overall and micropore surface areas, were important in HQ adsorption, with XAD-4 exhibiting the lowest HQ uptake due to its lower micropore surface area. HQ adsorption is also dependent on pH, exhibiting a maximum for pH < 9 due to the electrostatic repulsion between the OH^- group of HQ and negatively charged sorbents under alkaline conditions. Zhu et al. reported that the adsorption of HQ onto such sorbents is dominated by electrostatic interactions and chemical bonds between sorbent surface and hydroxyl groups of HQ, however, they overlooked van der Waals interactions, which the main forces between aromatics and ACs or polymeric resins; also, adsorption may involve hydrogen bonding between adsorbate and adsorbent [270].

In summary, HQ has been successfully degraded into harmless products via catalytic oxidation and Fenton processes; however, detailed mechanisms involved have not been determined. The mechanism of HQ degradation via biocatalytic processes has been proposed with HQ converted into CO_2 and H_2O. These methods usually involve high cost, hence, are unfavourable. Physical adsorption was shown promise in HQ removal from aqueous systems; with various types of sorbents, such as AC, silica, bentonite, polymeric resins and bio – sorbent, widely adopted.

Adsorption processes, which incur lower capital and operational costs, have raised interest among researchers, and the mechanisms involved discussed in detailed. Again, surface chemistry has great influence on adsorption, while other factors, such as pH and initial concentration, also affect HQ uptake.

CHAPTER 3

3.0 AIMS AND OBJECTIVES

The main goal of this work was to remove different types of organic contaminants from aqueous systems and understand the mechanisms of the processes involved. This was achieved by the realisation of several key objectives.

3.1 Objectives

Within this research, there were five objectives, each consisting of several smaller key aims, as follows:

1) Investigation of the reduction of Nitrobenzene (NB) using commercial iron powder (Fe), by:
    (i) Investigating the effects of iron loading on NB reduction
    (ii) Studying the kinetics of NB reduction using Fe
    (iii) Evaluating the effect of initial pH on NB reduction by Fe

    (iv) Examining the effect of initial concentration on NB reduction using Fe

2) Evaluating the performances of polymeric resins and Granular Activated Carbon (GAC) on Aniline (AN) adsorption, by:
    (i) Investigating the performances of non-functionalised and acidic functionalised sorbents on AN removal
    (ii) Studying the kinetics of AN adsorption onto polymeric resins and GAC
    (iii) Examining the adsorption equilibria of AN using polymeric resins and GAC
    (iv) Evaluating the leaching tendencies of the sorbents used

3) Studying the adsorption of NB onto polymeric sorbents and GAC, by:
    (i) Investigating the performances of non-functionalised and acidic functionalised sorbents on NB adsorption
    (ii) Studying the kinetics of NB adsorption onto polymeric resins and GAC
    (iii) Examining the adsorption equilibria of NB using polymeric resins and GAC
    (iv) Evaluating the leaching tendencies of the sorbents used

4) Examining the performances of polymeric resins and GAC on Paracetamol (PCT) adsorption, by:

    (i) Investigating the performances of non-functionalised and acidic functionalised sorbents on PCT adsorption
    (ii) Studying the kinetics of PCT adsorption onto polymeric resins and GAC
    (iii) Examining the adsorption equilibria of PCT using polymeric resins and GAC
    (iv) Evaluating the leaching tendencies of the sorbents used

5) Investigating Hydroquinone (HQ) adsorption onto polymeric sorbents and GAC, by:
    (i) Investigating the performances of non-functionalised and acidic functionalised sorbents on HQ adsorption
    (ii) Studying the kinetics of HQ adsorption onto polymeric resins and GAC
    (iii) Examining the adsorption equilibria of HQ using polymeric resins and GAC
    (iv) Evaluating the leaching tendencies of the sorbents used

CHAPTER 4

4.0 EXPERIMENTAL

This chapter discusses the methodology used in this study to remove selected organic contaminants (nitrobenzene, aniline, paracetamol and hydroquinone) from aqueous systems, and the principles of analytical techniques employed. The kinetic and adsorption isotherm models used to investigate rates of adsorption, rate limiting steps and adsorption equilibria are also discussed.

4.1 Chemicals

Extra pure nitrobenzene (NB) (99%) and aniline (AN) (99%) were supplied by Acros Organic, UK and Fisher Scientific, UK, respectively. Acetaminophen, also known as paracetamol, (PCT) (BioXtra, $\geq$ 99.0%) and hydroquinone (HQ) ($\geq$99.5%, Reagent Plus) were both supplied by Sigma Aldrich, UK. Stock solutions with initial concentrations, 40 mg L^{-1} for NB and AN, and 80 mg L^{-1} for PCT and HQ, were used to prepare diluted solutions, of required concentrations, using deionized water. pH values of all solutions, determined using a Hanna pH meter, were adjusted using hydrochloric or sodium hydroxide solutions, supplied by Fisher Scientific, UK, as required.

Gas chromatographic quantification, was performed using a dimethyl phthalate (99.6%, analytical grade, Sigma Aldrich, UK) internal standard. A stock solution of dimethyl phthalate (25 mg L^{-1}) was prepared, using methanol (99.9+%) supplied by Fisher Scientific, UK.

Surface functional groups of sorbents used in this study were quantified by Boehm titration methods [271], using sodium hydrogen carbonate ($NaHCO_3$), supplied by VWR International, sodium hydroxide (NaOH) and sodium carbonate (Na_2CO_3), supplied by Sigma Aldrich, UK as reaction bases; excess of base was back titrated using HCl, supplied by Fisher Scientific, UK.

4.2 Materials

NB reduction was performed using two iron powders: electrolytic (Iron 1) and 20 mesh (Iron 2), both supplied by Alfa Aesar, UK. NB, AN, PCT and HQ adsorption studies were performed for a non-functionalised hyper-cross-linked Macronet MN200, two ion exchange resins composed of acidic functionalised polystyrene cross-linked with divinylbenzene (MN500 and S957), all supplied by Purolite, UK; and DARCO GAC, supplied by Sigma Aldrich, UK. All sorbents studied were oven dried at 318 K for 6 h and ground and sieved to obtain particles sized between 150 to 212 µm before use. Textural properties of all samples were determined using nitrogen adsorption analysis (Section 4.4.2), while surface functional groups of polymeric resins were identified using Fourier Transform Infra-Red (FTIR) analysis (Section 4.4.3).

4.3 Experimental methodology

This section outlines the general experimental methodologies used in this study, including NB reduction using commercial iron powders, and AN, NB, PCT and HQ adsorption using selected sorbents. Detailed methodologies adopted for specific targeted contaminant are provided in the relevant discussion chapters.

4.3.1 Iron reduction batch experiments

This methodology was uniquely employed for NB reduction using commercial iron powders (Chapter 6), which was fully probed by studying the effects of pH and NB initial concentration of, allowing both equilibria and kinetic data to be obtained. All experiments were performed in triplicate at room temperature. pH values of NB solutions were adjusted using 0.1 M HCl and 0.1 M NaOH solutions. A known quantity of Iron 1 or Iron 2 and 10 mL of aqueous solution, containing a known amount of NB, were placed in 30 mL glass vials. These batch reactors were shaken using an orbital shaker and the detailed procedures adopted are as follows:

a) To study the effect of shaking speed, 0.2 g of Iron 1 was added to 10 mL of 40 mg L^{-1} NB solution. The reactors were shaken at 0, 75, 125, 175 or 225 rpm for 24 h.

b) To investigate the effect of iron loading, 0, 0.04, 0.2, 0.5, 1 g of Iron 1 was added to 10 mL of 40 mg L^{-1} nitrobenzene solution. The reactors were shaken at 225 rpm for 24 h.

c) To determine the kinetics of NB reduction, 1 g of Iron 2 was added to 10 mL of 40 mg L^{-1} NB solution and the reactors were shaken at 225 rpm.

d) To evaluate the effect of initial concentration, 1 g of Iron 2 was added to 10 mL of 10, 15, 20, 30 and 40 mg L^{-1} NB solution. The reactors were shaken at 225 rpm.

e) To study the effect of pH, the initial NB concentration was set to 40 mg L^{-1} and the pH adjusted to pH 3, 6, or 9. 1 g of Iron 2 was added to 10 mL of NB solution. The reactors were shaken at 225 rpm.

At selected time intervals, a batch reactor was removed and the solution filtered through a 0.22 µm membrane prior to analysis by Gas Chromatography (GC, discussed in detail in Section 4.4.4 to measure the NB concentration.

Solid iron is known to corrode electrochemically to ferrous iron (Fe^{2+}) [149]. NB reduction in an aqueous solution of corroded iron was studied to investigate the role of surface interactions: 1 g of Iron 2 was added to 10 mL of deionised water and this batch reactor was shaken at 225 rpm for 24 h. The solution was filtered and the resulting filtrate mixed with 10 mL of 40 ppm nitrobenzene solution and the resulting mixture shaken at 225 rpm for up to 24 h. At selected time intervals, a batch reactor was withdrawn and the solution filtered through a 0.22 µm membrane prior to GC analysis.

4.3.2 Adsorption of contaminants batch experiments

The kinetics of NB, AN, PCT and HQ adsorption onto MN200, GAC, MN500 and S957 were determined at room temperature. Initially, a batch of reactor was prepared with 40 mg of adsorbent added to 150 mL aqueous solution containing 40 mg L^{-1} of NB, AN, PCT or HQ. The mixture was shaken using an orbital shaker at 225 rpm for up 7 h. At selected time intervals, a 0.3 mL aliquot of solution was withdrawn for GC analysis, until such time that equilibrium was reached.

For equilibrium adsorption studies, 8 mg of adsorbent was added to 30 mL aqueous solution containing a known quantity of targeted contaminant. Detailed procedures for each contaminant are as follows:

a) For NB and AN, equilibrium studies were conducted using solutions with concentrations ranging from 5 to 40 mg L^{-1}.
b) For PCT and HQ, equilibrium studies were performed using solutions with concentrations ranging from 40 to 75 mg L^{-1}.

All solutions were agitated using an orbital shaker at 225 rpm for 24 h, after which a 0.3 mL aliquot was withdrawn and filtered using a 0.22 µm membrane prior to GC analysis.

Leaching tendencies were determined by adding 40 mg of adsorbent to 150 mL of 40 mg L^{-1} NB solution in a sealed vessel, which was subsequently shaken using an orbital shaker at 225 rpm. After 24 h, the solution was filtered and the residue added to 150 mL pure deionised water. 0.3 mL aliquots were withdrawn at pre-determined intervals for GC analysis.

4.4 Analytical methodology

This section details the methodology for qualitative and quantitative analyses used to determine the functional groups and sorbent surface acidic capacities for the sorbent studied using Fourier Transform Infra-Red (FTIR, discussed in detail in Section 4.7) and Boehm titration methods. In addition, the procedures used to quantify NB, AN, PCT and HQ concentrations in solution using Gas Chromatography–Flame Ionisation Detection (GC-FID) are also discussed.

4.4.1 Boehm Titration

The Boehm titration methods used in this work have been reported in a previous study [271] but are summarised here for completeness. Firstly, 0.05 M of reaction bases, $NaHCO_3$, Na_2CO_3 and NaOH, were prepared using deionised water. 1.5 g of GAC, or 0.1 g of either MN500 or S957 was added to 50 mL of each reaction base solution and the resulting mixtures shaken at 225 rpm using an orbital shaker. After 24 h, the solutions were separated using a 0.22 µm membrane filter; 10 mL aliquot samples of each solution were mixed with a known amount of 0.05 M HCl as follows: (a) aliquot of Na_2CO_3 added to 30 mL, (b) aliquot of NaOH or $NaHCO_3$ added to 20 mL. Following this, a drop of phenolphthalein was added to each solution, before back titration using 0.05 M NaOH until the endpoint was reached (colour change from colourless to fuchsia). All Boehm analyses were conducted in triplicate.

4.4.2 Nitrogen adsorption analysis

Nitrogen adsorption analysis was performed to determine the surface areas of Iron 1 and Iron 2 powders. Sorption isotherms were obtained from nitrogen adsorption and analysed using BET theory (as described in Section 4.5), allowing textural properties, including surface area, pore volume and pore size distribution, for the polymeric sorbents and GAC used to be determined. Nitrogen adsorption analysis was performed at 77 K , using a Micrometrics ASAP 2420, prior to which samples were degassed at 373 K (10 K min^{-1}) for 2 h, at a pressure of 10 µmHg.

4.4.3 FTIR analysis

The functional groups of MN200, MN500 and S957 were identified using an Attenuated Total Reflectance–Fourier Transform Infra-Red (ATR-FTIR) spectrophotometer (ABB MB300), using 32 scans and resolution 4 cm^{-1}, with spectra recorded in the range 600 to 4000 cm^{-1}. Before analysis of each sample, a reference spectrum (blank) was performed using single beam mode. Each material was finely ground before analysis via absorbance mode.

4.4.4 Quantification of contaminant concentrations

The concentrations of NB, AN, PCT and HQ were analysed using GC-FID (Shimadzu GC-2014). Helium was used as the carrier gas at a flow rate of 5 mL min^{-1}. Compressed air and high purity hydrogen were used as the combustion gases at flow rates of 300 mL min^{-1} and 30 mL min^{-1}, respectively. Each sampled aliquot was mixed with 0.3 mL of 25 mg L^{-1} dimethyl phthalate, an internal standard, in order to quantify the concentration.

For quantification of NB and AN concentrations, the GC was equipped with a SPB™–5 column (30 m × 0.53 mm × 0.5 µm) for compounds separation. The injector and detector temperatures were adjusted to 383 K and 513 K, respectively. The temperature of the oven was initially programmed to 343 K, increased to 373 K at a rate of 280.5 K min^{-1}, and then increased to 513 K at a rate of 288 K min^{-1} and held for 10 min.

To quanitfy PCT and HQ concentrations, a HP-5 column (30 m × 0.25 mm × 0.25 µm) was used. The GC method used in this study to quantify PCT concentration was previously reported in literature [272] and is also applicable to HQ. The injector and detector temperatures were adjusted to 523 K and 553 K, respectively. The temperature of the GC oven was initially programmed to 343 K (held for 1 min), increased to 393 K at 293 K min^{-1}, increased again to 523 K at 283 K min^{-1}, before finally being raised to 553 K at 278 K min^{-1} (held for 3 min).

4.5 BET theory

Surface areas and porosities of catalysts and sorbents are crucial in determining the overall rate for catalytic reactions or adsorption processes. The performance of a catalyst or sorbent is enhanced with increased surface area, due to more reactive sites being available. In such processes, mesopores are known to be responsible for allowing adsorbate to enter the inner porosity of a sorbent while micopores are usually the active sites for adsorption[243]. It is, therefore, essential to be able to probe the textural parameters of sorbent materials and physical gas adsorption is routinely used to determine the surface area and porosity of a material, often utilising inert gases such as argon and nitrogen as the adsorbate.

BET theory was developed by Brunauer, Emmett and Teller in 1938 and provides an analytical technique to investigate the surface areas and pore size distributions of different types of solid materials. The concept of BET gas adsorption is based on Langmuir theory, which originally stated that adsorption can only occur in the monolayer. However, BET theory takes multilayer adsorption into account, where the first adsorbed layer acts as a substrate for further adsorption, and so on as the layers increase in number. Within monolayer adsorption, there is contact between the adsorbent surface layer and the adsorbed molecules. In contrast, no direct contact exists between the adsorbent surface layer and molecules adsorbed within the multilayers, although the first initial layer will still experience the same forces as any other monolayer. The BET takes account of this difference in interaction type and can be expressed as[273-275]:

$$V = \frac{C\ P\ Po\ V_{mon}}{(Po - P)[Po + P(C - 1)]} \qquad \text{Equation 25}$$

where:

V = volume of gas adsorbed

V_m = volume corresponding to monolayer coverage

C= constant ($C = \exp\left(\frac{\Delta H}{RT}\right)$

P = equilibrium pressure

Po = saturated pressure

The pore widths determined from physisorption measurements can be divided into three categories [274]:

1) Macropores – pore size greater than 50nm

2) Mesopores – pore size between 2nm and 50nm
3) Micropores – pore size less than 2nm

4.5.1 Adsorption isotherms

Adsorption isotherms can be classified as belonging to one or more of six types as proposed by Brunauer, Deming, Deming and Teller [276], most often referred to as the BDDT classification, which has been adopted by IUPAC [274] (Figure 23). Type I isotherms generally signify a solid material with pores less than 2 nm wide and a low surface area; examples include molecular sieve zeolites and microporous activated carbons. Types II and III are characteristic of adsorption on solid materials with pores greater than 50nm in diameter. Type II isotherms can also indicate multilayer adsorption, and point B (marked in Figure 23) represents the completion of monolayer adsorption and the beginning of multilayer formation. Type IV isotherms again indicate multilayer formation but demonstrate hysteresis as the result of mesoporosity within the material (pore widths 2-50 nm); four types of hysteresis loops are commonly observed, which are discussed in detail below. Both Type III and V isotherms are uncommon and form as a result of weak interactions between the adsorbent and adsorbate. Types VI also represent multilayer adsorption, this time on a non - porous surface, where each layer must be complete before subsequent layers can form, related to the energies of interaction. As physisorption is inversely affected by temperature, thermal properties of the system can affect the uptake, hence, sharpness of the steps; the step-height demonstrates the capacity of the monolayer for each adsorbed layer.

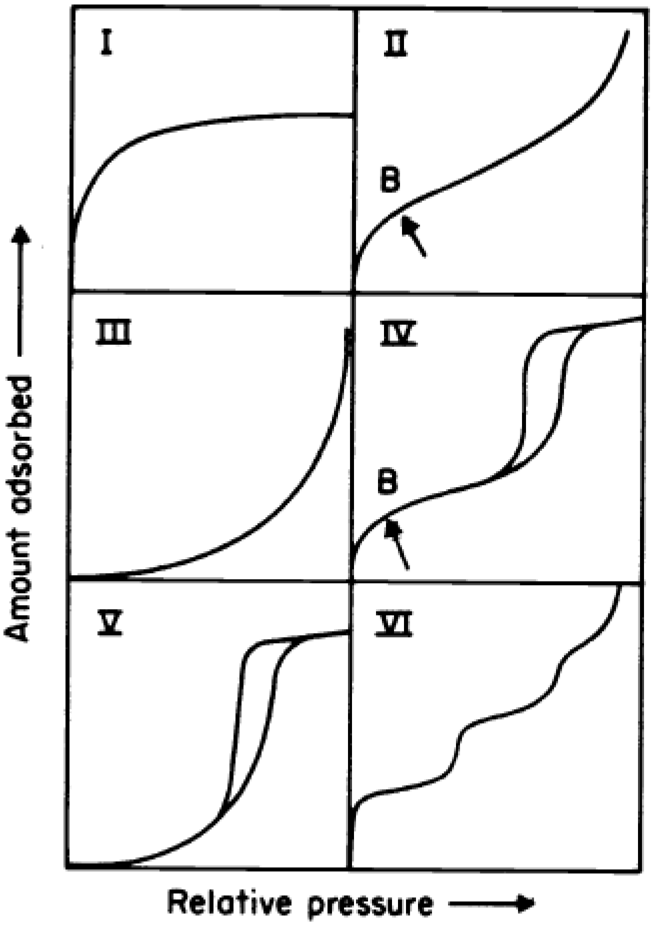

Figure 23 Types of adsorption isotherms exhibited in pysisorbed systems (Source: Adapted from [274])

As stated above, there are four types of hysteresis loops (Figure 24) relate to capillary condensation within the mesoporous structure of the material, and the shape of the loop indicates the shape of the pores found in the material. Type H1 describes porous solid materials that contain uniform spheres agglomerated in a regular array. The pore size distribution and compound morphology are not as well-defined for Type H2 loops and these are, therefore, difficult to interpret. Type H3 is attributed to stacking of plate-like structured particles to produce slit-shaped pores. Materials with narrow slit-shaped pores exhibit Type 4 hysteresis loops.

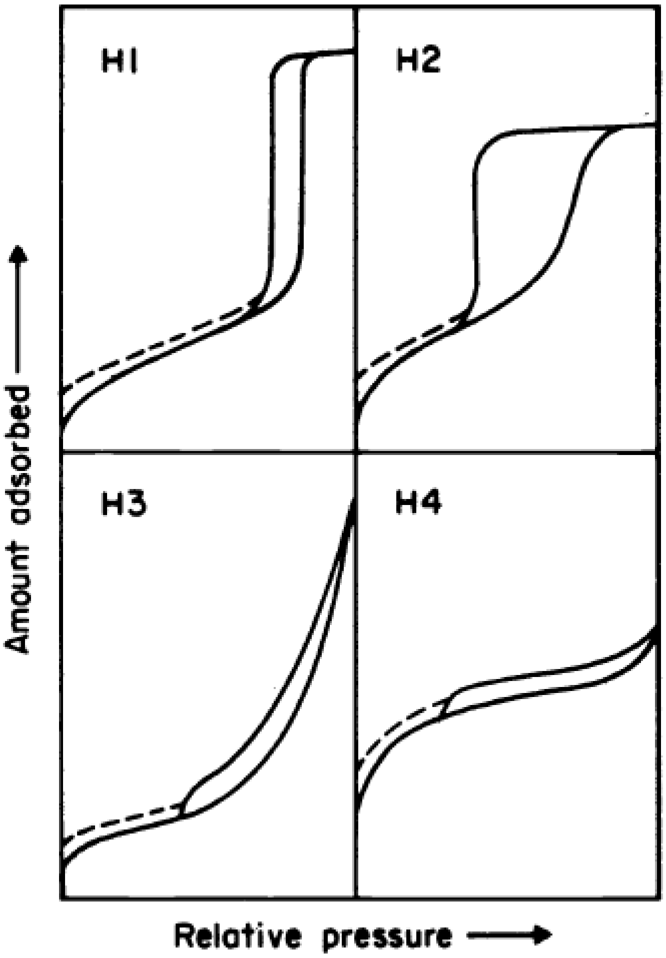

Figure 24 Types of hysteresis loops observed in physisorption (Source: Adapted from [274])

4.6 Gas Chromatography (GC)

GC has been widely used to analyse organic compounds since it was developed in 1952. There are two types of GC: gas-solid and gas-liquid chromatography, the latter is used in this study. During gas-liquid GC analysis, the liquid sample is injected directly, by hypodermic syringe through a rubber septum, into the chromatographic column. The injection port, column and detector are heated to certain preselected temperatures (usually in excess of the boiling point) and the liquid sample is converted into the gaseous state. The injector port and detector are kept at higher temperature to avoid condensation of gaseous compound in the detector and to increase the rate of vaporisation of the injected liquid sample [277].

Inert gases such as helium, nitrogen and argon are used as carrier species and the selected gas passes through the injection port, column and detector continuously from a supplying gas cylinder. The gaseous sample, produced when the liquid is introduced into the heated injection port is carried into the column and is partitioned between the stationary and mobiles phases, allowing separation into the individual components [278].

Finally, the sample is carried to the detector from the column by the carrier gas, where an electrical signal is generated as a function of the quantity of species present. This signal travels to an integrator and is subsequently translated into a chromatogram [278]. A schematic of a GC system is shown in Figure 25.

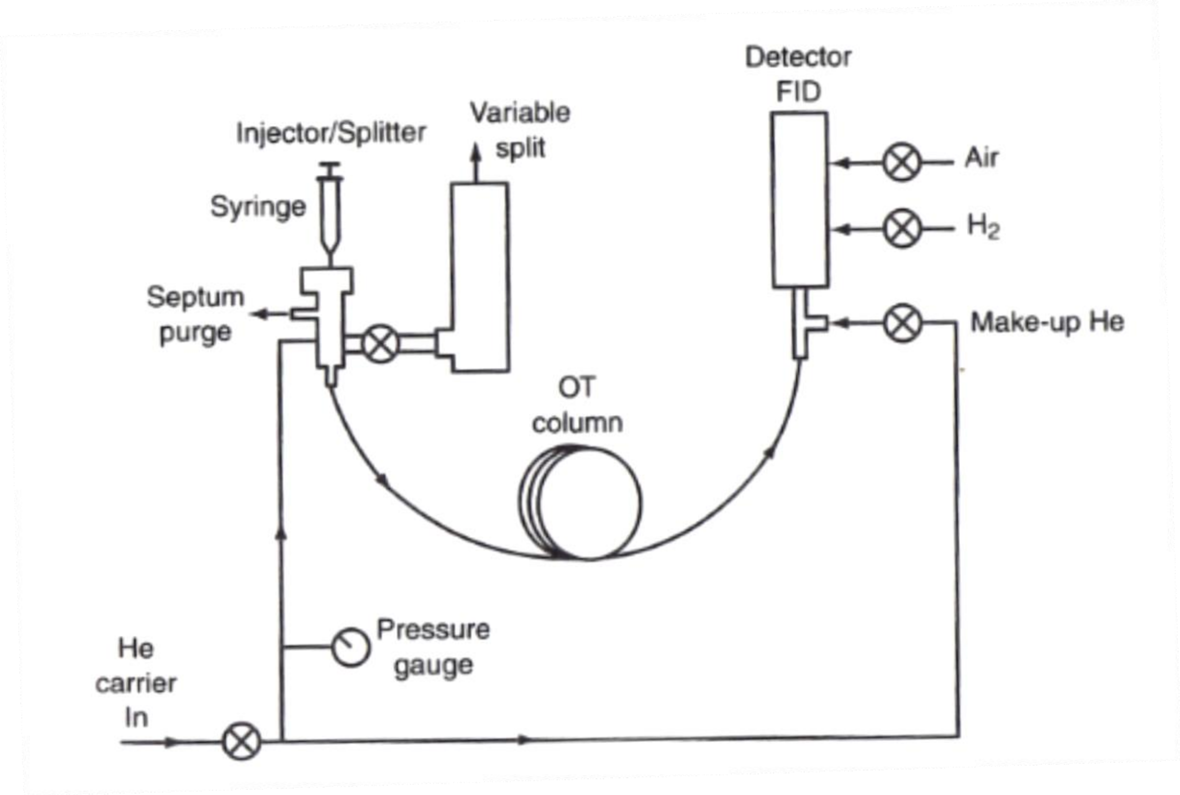

Figure 25 Schematic of a gas-liquid GC system(Source: Adapted from [278])

Different detector types can be employed, such as Flame Ionization Detector (FID), Thermal Conductivity Detector (TCD) and Electron Capture Detector (ECD); the detector used in this study is FID, which is the most popular and widely used detector type. In FID, the effluent from the column is combined with hydrogen and travels to a burner tip, which also contains air at high flow rate. Ions are generated by the oxy-hydrogen flame, which are collected to produce a small current allow the final signal to be obtained [278].

There are advantages to using GC compared with other types of analytical instruments, namely [278]:

1) Low cost
2) High sensitivity

3) High efficiency giving high resolution
4) High accuracy in quantitative analysis
5) Small quantities of samples are required for analysis
6) Simple and reliable

4.7 Fourier Transform Infra-Red (FTIR) Spectrometry

Infrared spectroscopy is widely adopted to identify the functional groups present on a surface and the infrared spectrometers used for analysis can be divided into two types: dispersive and interferrometric. For dispersive spectrometers, the infrared radiation is dispersed, by a grating monochromator, into separate frequencies; while individual frequencies, as well as their intensities, are obtained by Fourier transform analysis of the interference patterns developed via the interaction of infrared frequencies within interferrometric spectrometers. Both types of instruments require an appropriate infrared source and suitable detectors to determine the intensities; the most common infrared sources used are rods composed of ceramic materials or silicon carbide, which are heated to ~1800˚C. The infrared light is diffracted using a prism monochromator for basic infrared spectrometers; while diffraction gratings are adopted for dispersive spectrometers as shown in Figure 26. Monochromatic gratings are used in interferrometric systems, creating interference at specific angles as the incoming radiation is reflected and diffracted; hence, constructive interference of certain wavelengths is developed. Thermopile detectors, used for the dispersive systems, usually contain a few thermocouples connected in series to enhance the sensitivity. The detector is constructed inside a vacuum Dewar flask which contains liquid N_2; the inner wall consisting of mercury cadmium telluride (MCT), a homogeneous semiconductor, while the outer wall is usually an infrared transparent window (Figure 26).

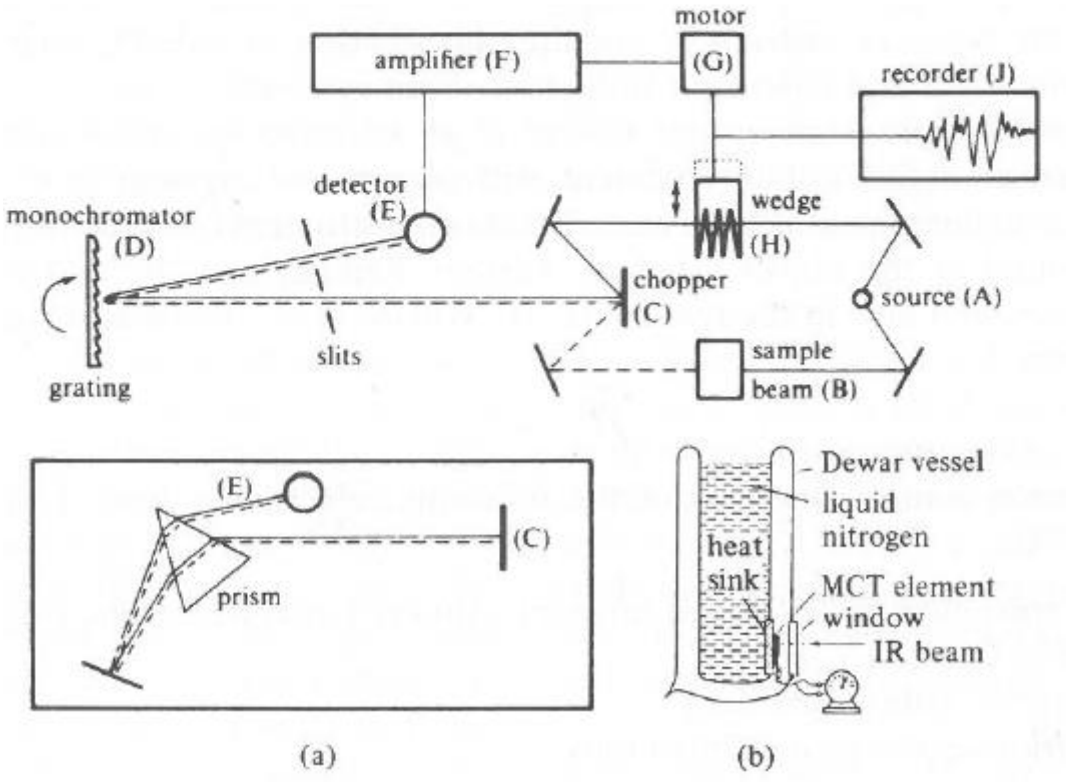

Figure 26 Schematic diagram of dispersive spectrometer: (a) prism monochromator and (b) MCT detector (Source: Adapted from [279])

For dispersive spectrometers, the light emitted from the source (Figure 26, point marked A) is split into a reference beam and a sample beam, the beam that passes through the sample being analysed), both of which are reflected onto a chopper (C) that contains a rotating segmented mirror. These beams are subsequently reflected onto the rotating monochromator grating (D), by the chopper, and the separate frequencies are generated and collected by the thermopile detector (E) before finally being transformed into electrical energy. The individual frequencies generated are absorbed, as appropriate, by the sample being analysed, and as the sample and reference beams are sent alternately from the chopper to the detector, this allows comparison of the generated and absorbed beams. The current generated at the detector is amplified (F). The movement of an optical wedge (H) creates the absorption bands in a printed spectrum but this has been superseded in recent years by digital recording for on screen display. It is worth noting that dispersive spectrometers suffer the disadvantages of poor sensitivity and inaccurate wavelength.

Interferometric spectrometers, also known as Michelson interferometers, were developed by Albert Michelson in 1887 (Figure 27). The radiation source produces a monochromatic light beam (A) which travels to a beam splitter (B), from which two equal beams (Beam (C) and (E)) are transmitted onto flat mirrors, (D) and (F), respectively, before reflection back to B. Recombined as beam G, these are then transported to a detector. The principle of FTIR is based on such interferometric spectrometers where the sample absorbs specific frequencies as the light beam is introduced; the speed movement of the mirror (F) at which the infrared spectrum is recorded is denoted the scan time [279].

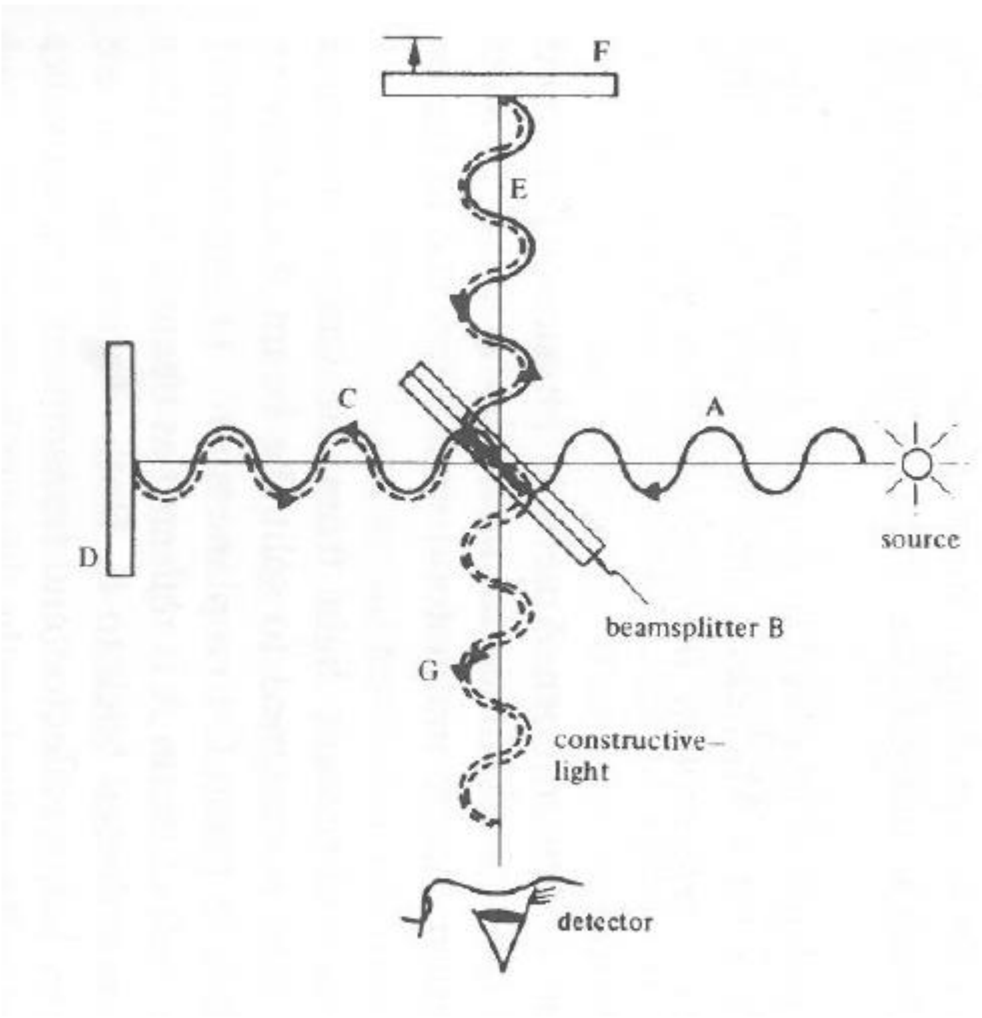

Figure 27 Schematic diagram of interferometric spectrometer: The detector will receive dark and light images alternately as mirror F is moved. FTIR is operated in single beam mode and the sample is located between the infrared source and beamsplitter (Source: Adapted from [279])

In this study, Attenuated Total Reflectance (ATR) – FTIR was adopted to determine the functional groups of the sorbents used; when the sample is subjected to light, changes are detected in the totally internally reflected infrared beam, as determined by ATR. The infrared light beam is introduced at a specific angle and transported to a high refractive index crystal; a wave is generated by the internal reflectance and directed to the sample, which is held in direct contact with an optically dense crystal, which is attenuated as the sample absorbs energy. The attenuated wave travels back to the infrared beam and is discharged from the opposite end of the crystal, finally being directed to the detector, thus, an infrared spectrum is produced [280]. The multiple reflections of ATR-FTIR are shown in Figure 28.

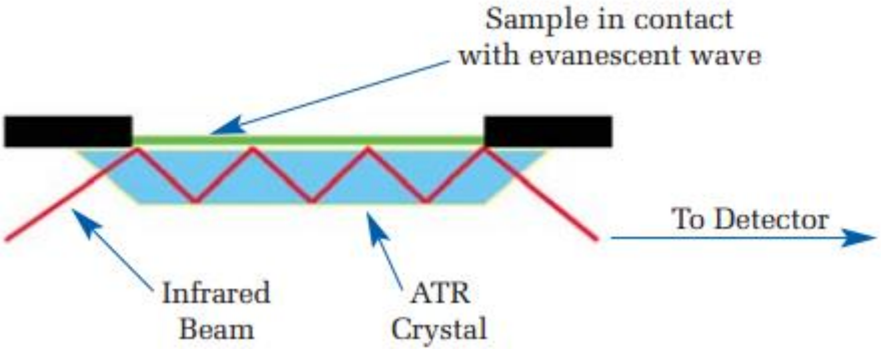

Figure 28 Schematic diagram of multiple reflection of ATR-FTIR system (Source: Adapted from [280])

4.8 Kinetic reaction models

In this study, the adsorption kinetics for nitrobenzene (NB), nniline (AN), paracetamol (PCT) and hydroquinone (HQ) onto Granular Activated Carbon (GAC) and hyper-cross-linked polymeric resins MN200, MN500 and S957 were investigated using pseudo-first, pseudo-second and Elovich models. Several studies have demonstrated that the adsorption of organic compounds can be described by a pseudo-first order kinetic model [177, 225]; the pseudo-first order model proposed by Lagergren [281], is based on a proportional relationship between overall adsorption rate ($\frac{dq_t}{dt}$) and driving force ($q_e - q_t$) [282]:

$$\frac{dq_t}{dt} = k_1 (q_e - q_t)$$ Equation 26

By integrating Equation 26 with $q_t = 0$ at $t = 0$ and q_t at $t = t$, then Equation 26 becomes:

$$q_t = q_e(1 - e^{-k_1 t})$$ Equation 27

Other previous works have reported that the adsorption kinetics of organic species can be described by pseudo-second order models [225, 283]. The pseudo-second order model states that there is a proportional relationship between overall adsorption rate and the square of the driving force [282], as proposed by Ho [284]:

$$\frac{dq_t}{dt} = k_2 (q_e - q_t)^2$$ Equation 28

By integrating Equation 28 with $q_t = 0$ at $t = 0$ and q_t at $t = t$, then Equation 28 becomes:

$$q_t = (k_2 t q_e^2)/(1 + k_2 t q_e)$$ Equation 29

where q_t (mg g^{-1}) and q_e (mg g^{-1}) are uptake capacity of NB at t time and equilibrium, respectively; k_1 (min^{-1}) and k_2 (g mg min^{-1}) are the pseudo-first and pseudo-second order rate constants, respectively.

In addition, the Elovich model has previously been adopted to study the kinetics of adsorption processes [285, 286]. This model assumes that the adsorption process involves several mechanisms, e.g. diffusion in the mass of dissolution, surface diffusion and activated catalytic surfaces [170]. However, the Elovich model is restricted to early stage sorption when the system is far from equilibrium [287]. The equation can be expressed as:

$$\frac{dq_t}{dt} = a \exp(-bq_t) \qquad \text{Equation 30}$$

By integrating Equation 30 with $q_t = 0$ at $t = 0$ and q_t at $t = t$, then Equation 30 becomes:

$$q_t = \left(\frac{1}{b}\right)\ln(ab) + \left(\frac{1}{b}\right)\ln(t) \qquad \text{Equation 31}$$

where a and b are desorption constants and initial adsorption rate, respectively; a, b and $t \geq 1$

4.9 Kinetic diffusion models

An adsorption process can be described in three stages: 1) migration of solute to sorbent's surface from bulk solution, known as film diffusion; 2) diffusion into pores and intraparticle diffusion, called particle diffusion; and 3) adsorption of solute into pore's inner surface and between the capillary spaces of the sorbent. The last step occurs relatively quickly, hence, it will not influence the adsorption rate. Therefore, the overall rate is controlled by either film or particle diffusion, and the slowest step is the rate limiting step [155].

The Homogeneous Particle Diffusion Model (HPDM) can be applied to determine the rate limiting step of an adsorption process. HPDM takes into account several sorption mechanisms, which involve transport of solute molecules from bulk solution to the sorbent's external surface, then diffusion through the liquid/solid interface and into the bulk particles of the sorbent, and interaction with the moieties of the sorbent's surface. This adsorption process can be described using Fick's law which applies to quasi-homogeneous media [170] as shown below:

$$X(t) = 1 - \frac{6}{\pi^2}\sum_{z=1}^{\infty}\frac{1}{z^2}\exp[\frac{-z^2\pi^2 D_e t}{r^2}] \qquad \text{Equation 32}$$

Equation 32 can be fitted using Vermeulen's approximation in the range of $0 < X(t) < 1$ by assuming the adsorbent particles are spherical, giving the film diffusion control expression:

$$-\ln[1 - X(t)] = \frac{3DC}{rC_r}t \qquad \text{Equation 33}$$

In contrast, if particle diffusion controls the sorption rate, the expression becomes:

$$-\ln[1 - X^2(t)] = \frac{2\pi^2 D_e}{r^2}t \qquad \text{Equation 34}$$

Where $X(t) = \frac{q_t}{q_e}$, is the fractional attainment of equilibrium at time t; D and D_e are the effective diffusion coefficient of sorbates in solution and sorbent phase, respectively (m^2 s^{-1}); C and C_r are total concentration of adsorbed compounds and adsorbed species in sorbent phase (mg L^{-1}), respectively; and r is the radius of the sorbent particle (m).

If the particle diffusion control equation fits the kinetic data more closely, by providing a better correlation (higher R^2 values), the intraparticle diffusion model, can subsequently be applied to further confirm that the rate is dominated by particle diffusion:

$$q_t = K_i t^{0.5} + I \qquad \text{Equation 35}$$

Where q_t (mg g^{-1}) is uptake capacity of compound at t time, K_i (mg g^{-1} min^{-1}) is the intra-particle diffusion rate constant, and I (mg g^{-1}) indicates the thickness of the boundary layer. In the case of a single linear slope, with $I = 0$, the rate is only limited by particle diffusion.

4.10 Adsorption equilibria

In adsorption processes, the solute migrates from the bulk solution and is adsorbed onto the sorbent; however, the sorbed molecule tends to desorb from the sorbent back into the solution. Adsorption equilibrium is a state at which the rates of adsorption and desorption are equal, and the concentration of solution remains unchanged either in the bulk solution or at the sorbent's surface [155]. In order to understand the mechanism of contaminants adsorption, adsorption isotherms were investigated in this study, which present the amount of solute adsorbed, per weight of adsorbent, as a function of concentration. The adsorption of solute can be described using the Langmuir adsorption isotherm; however, for heterogeneous surfaces, the Freundlich adsorption isotherm has been found to provide a more appropriate fit.

The Langmuir adsorption isotherm is widely used to describe monolayer adsorption, where it is assumed that each molecule is adsorbed on a specific site within the sorbent's surface and the adsorption energy is constant at all active sites due to homogeneous surface. Furthermore, since the adsorption of solutes onto a sorbent surface is localised, the molecules will be adsorbed on definite sites. Therefore, this model is also known as the ideal localised monolayer model [288, 289]. The Langmuir adsorption equation can be expressed in the following form:

$$q_e = \frac{q_m K_L C_e}{(1 + K_L C_e)} \qquad \text{Equation 36}$$

Where q_e (mg g^{-1}) and C_e (mg L^{-1}) are the equilibrium uptake capacity and equilibrium concentration, respectively. K_L (L mg^{-1}) is the Langmuir adsorption constant and q_m (mg g^{-1}) is the monolayer adsorption capacity of the sorbent [290].

The Freundlich adsorption isotherm, on the other hand, assumes that adsorption interactions with heterogeneous surface sites with different adsorption energies are not equally likely [290, 291], and the Freundlich adsorption equation can be written as following:

$$q_e = K_f C_e^{\frac{1}{n}} \qquad \text{Equation 37}$$

Where C_e (mg L^{-1}) and q_e (mg g^{-1}) are equilibrium concentration and uptake capacity, respectively. K_f (mg g^{-1} (L mg^{-1})$^{1/n}$) is the Freundlich adsorption constant and n represents a constant related to the adsorption affinity. K_f and n describe the magnitude of the driving force in a sorption process and the distribution of energy sites on the sorbent's surface [282]. The value of n reflects adsorption favourability. For $n < 1$, sorption is unfavourable, n of 1 to 2 indicates sorption is moderate to difficult, n between 2 and 10 indicates good sorption characteristics [290]. In addition, adsorption is a chemical process if $n < 1$, and a physical process if $n > 1$ [194, 201].

CHAPTER 5

5.0 MATERIALS CHARACTERISATION

This chapter provides the results of materials characterisation using Boehm titration, Fourier – Transform Infrared (FTIR) spectrometry and nitrogen adsorption analysed using BET theory. The surface areas of the granular activated carbon, iron powders and polymeric resins used in this study are discussed in conjunction with the resulting pore size distributions. The acidic capacities of functionalised sorbents are determined and the FTIR spectra of the polymeric sorbents used are also discussed in detail.

5.1 Boehm titration

As detailed in Chapter 2, the surface chemistry of a sorbent can significantly affect its performance in contaminants removal from aqueous systems. In this study, the total acidic capacities of S957, MN500 and Granular Activated Carbon (GAC) are examined via Boehm acid-base titration, which involves neutralisation of an acid and a base in equal quantities [292]. The method is based on the principle that bases with varying degrees of basicity can neutralise different acidic surface functionalities. Sodium bicarbonate ($NaHCO_3$), the weakest base, only neutralises carboxylic groups; sodium carbonate (Na_2CO_3) neutralises both lactonic and carboxylic groups, while sodium hydroxide (NaOH), the strongest base, neutralises all categories of acid surface groups i.e. phenolic, lactonic and carboxylic groups. The amount of base used is determined by back titration with an acid; quantification of the individual acidic groups for each sorbent can, therefore, be obtained from the difference in the quantities of each reactive base required for neutralisation [271, 293].

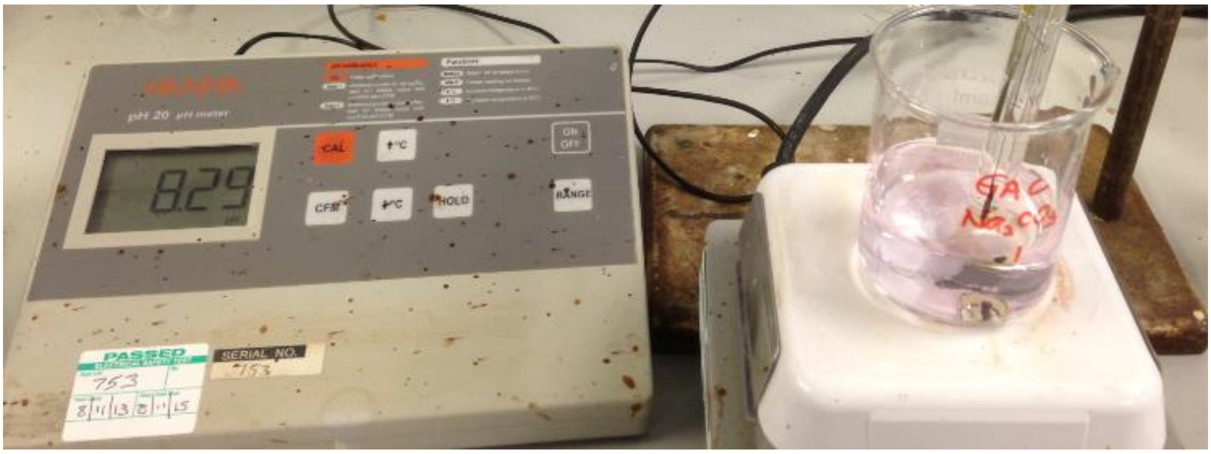

Figure 29 Boehm titration: Quantification of sorbent acidic surface functionalities. Phenolphthalein indicator is used (solution is colourless at acidic pH, and fuchsia at pH > 8).

As the end point indicates complete neutralisation of the remaining base, an indicator is added to the solution, which usually undergoes a visible colour change when the end point is achieved. The indicator chosen is usually a weak base or acid containing conjugated organic constituents, hence, the colour varies with pH. In this study, phenolphthalein, a weak acid, was used as the indicator for Boehm titrations, undergoing a colour change from colourless to red violet/fuchsia at pH 8 [271, 292], as shown in Figure 29. The volumes of each reaction base required to neutralise the corresponding acidic functionalities completely were recorded and are shown in Table 13.

Table 13 Boehm titration: Volumes of reaction bases required to obtain acidic group neutralisation

	V_1 (mL)	V_2 (mL)	V_3 (mL)	V_{av} (mL)
GAC				
NaOH	14.5	14.35	14.65	14.5
Na_2CO_3	23.7	23.9	23.8	23.8
$NaHCO_3$	12.3	12.5	12.4	12.4
MN500				
NaOH	11.05	10.95	11	11
Na_2CO_3	0	0	0	0
$NaHCO_3$	0	0	0	0
S957				
NaOH	13.6	13.6	13.6	13.6
Na_2CO_3	0	0	0	0
$NaHCO_3$	0	0	0	0

The concentrations of acidic functionalities of sorbents can be determined using basic stoichiometry where one mole of acid is required to neutralise one mole of base. Detailed calculations are as shown below:

<u>To calculate total acidic capacities of acidic functionalities:</u>

$$1 \text{ mol of } H^+ \longrightarrow 1 \text{ mol of } OH^-$$

Given that X_1 = molarity of remaining reaction base after 24 h, mol L^{-1}

X_2 = molarity of titrant (NaOH), mol L^{-1} (0.05 mol L^{-1})

X_3 = molarity of HCl added, mol L^{-1} (0.05 mol L^{-1})

V_a = volume of aliquot of filtered reaction base solution, L (0.01 L)

V_b = volume of titrant (NaOH) required to obtain end point, L

V_c =volume of HCl added, L

m_1 = moles of base reacted in back-titration, mol

m_2 = moles of acid reacted in back-titration, mol where $m = V \cdot X$

<u>To calculate the reaction base concentration after 24 h, (X_1):</u>

Based on stoichiometry (for neutralisation), the number of moles of acid is equal to the number of moles of base, hence,

$m_1 = m_2$

$(V_a \cdot X_1) + (V_b \cdot X_2) = (V_c \cdot X_3)$

$(0.01\ \mathrm{L} \cdot X_1) + (0.0145\ \mathrm{L} \cdot 0.05\ \mathrm{mol\ L^{-1}}) = (0.02\ \mathrm{L} \cdot 0.05\ \mathrm{mol\ L^{-1}})$

$(0.01\ \mathrm{L} \cdot X_1) + (7.25 \cdot 10^{-4}\ \mathrm{mol}) = 1 \times 10^{-3}\ \mathrm{mol}$

$(0.01\ \mathrm{L} \cdot X_1) = 2.75 \times 10^{-4}\ \mathrm{mol}$

$X_1 = \underline{0.0275\ \mathrm{mol\ L^{-1}}}$

The number of moles of total acidic functionalities can be determined from the number of moles of base that has been reacted after 24 h (the difference between the initial number of moles of base and the number of moles of base after 24 h):

Moles of total acidic functionalities $= (0.05\ \mathrm{L} \cdot 0.05\ \mathrm{mol\ L^{-1}})$ -

$(0.05\ \mathrm{L} \cdot 0.0275\ \mathrm{mol\ L^{-1}})$

$= (2.5 \times 10^{-3}\ \mathrm{mol}) - (1.375 \times 10^{-3}\ \mathrm{mol})$

= $\underline{1.125 \times 10^{-3} \text{ mol}}$

Capacity of acidic functionalities, mol g^{-1} = 1.125×10^{-3} mol / 1.5 g

= $\underline{0.75 \text{ mmol g}^{-1}}$

These calculations, were applied to the data obtained for GAC (Na_2CO_3: Appendix A; $NaHCO_3$: Appendix B) to determine the capacities for lactonic, phenolic and carboxylic groups (Appendix C). It was also possible to determine the total acidic capacities for MN500 (Appendix D) and S957 (Appendix E) with all results summarised in Table 14.

Table 14 Acidic capacities obtained via Boehm titration for GAC, MN500 and S957

Functional groups (mmol g^{-1})	GAC (phenolic, lactonic, carboxylic)	MN500 (sulfonic)	S957 (sulfonic-phosphonic)
Total acidic	0.750	2.500	9.000
Carboxylic	0.400	-	-
Phenolic	0.316	-	-
Lactonic	0.034	-	-
Sulfonic	-	2.500	-
Sulfonic-phosphonic	-	-	9.000

5.2 Nitrogen adsorption analysis

Textural properties of non-functionalised hyper-cross-linked polymeric sorbent Macronet MN200, GAC, sulfonic functionalised polystyrene cross-linked divinylbenzene MN500 and phosphonic/sulfonic functionalised polymeric resin S957 were analysed using nitrogen adsorption; pore size distributions and sorption isotherms for all sorbents are shown in Figure 30 and Figure 31, respectively. It can be observed that MN200 and MN500 contain pores ranging from micro (< 2 nm) to macro-pore size (> 50 nm) while S957 has only meso (2-50 nm), and macro-pores, by contrast GAC exclusively contains meso-pores (Figure 30). The isotherms (Figure 31) obtained for MN200 and MN500 can be classified as Type I, indicating that MN200 and MN500 are microporous sorbents; while it is Type II for GAC and S957[274], representing monolayer-multilayer adsorption. The hysteresis loops observed for all samples are Type H3, where adsorption is not restricted, even at high relative pressure. This indicates that within the materials are composed of plate like particles stacked together to form aggregates with slit-shape pores. Additionally, the surface areas and total pore volumes of all sorbents were again obtained using nitrogen adsorption; it was found that MN200 exhibited the highest surface area, followed by GAC, MN500 and S957. The total pore volume is highest for GAC, while S957 exhibited the lowest total pore volume and all results obtained are shown in Table 15. For the iron powders used in this work, both samples showed surface areas of less than 1 m^2 g^{-1}.

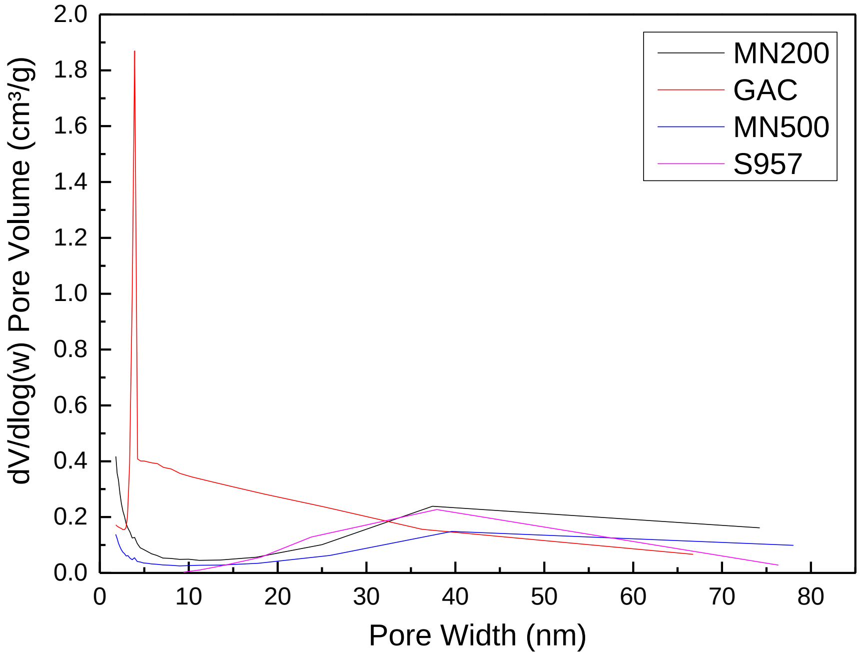

Figure 30 Pore size distributions for MN200, GAC, MN500 and S957, analysed using BJH, Harkins and Jura Models with Faas Correction

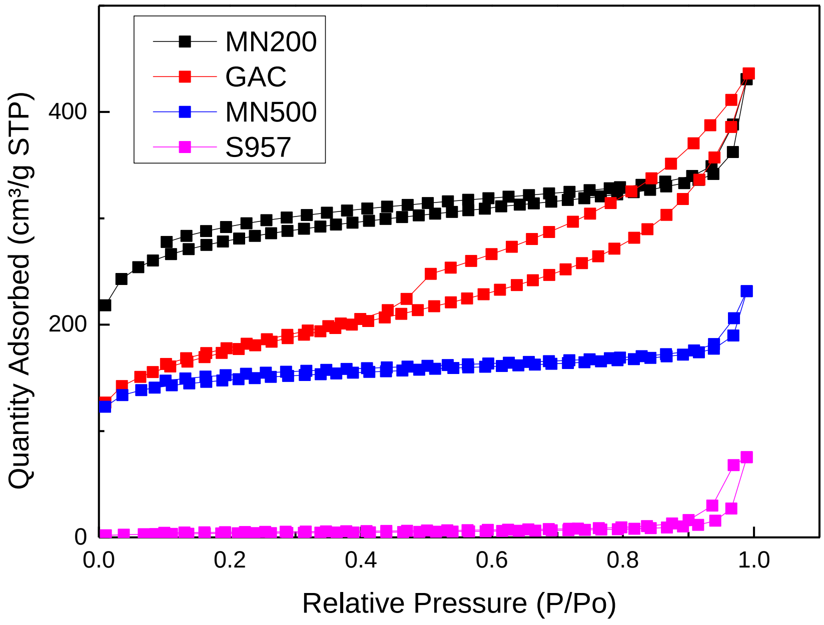

Figure 31 Nitrogen sorption isotherms for MN200, GAC, MN500 and S957

Table 15 BET surface areas and total pore volumes for sorbents used in this study

Sorbent	MN200	GAC	MN500	S957
BET surface area (m^2 g^{-1})	882.1	579.3	460.8	13.1
Predominant pore structure	Microporous	Mesoporous	Microporous	Nonporous
Total pore volume (cm^3 g^{-1})	0.666	0.674	0.358	0.116

5.3 FTIR analysis

The qualitative analysis of polymeric resins MN200, MN500 and S957 was conducted using FTIR to identify the functional groups available for contaminants adsorption; the results are shown in Figure 32. The FTIR spectra for MN200 has been discussed in a previous study, which demonstrated the presence of vibrations (stretching mode) of the aromatic ring, -CH_2 and –CH; the results obtained are compared to the literature [294, 295] and summarised in Table 16. It can be observed that the absorption bands of MN200 are consistent with those observed in the previous study, in addition, the absorption bands above 2800 cm^{-1}, which were not been previously discussed, are also assigned in this study. The IR spectra for MN500 and S957 are similar to MN200; however, additional strong absorption bands, representing the presence of surface functional groups, were found for MN500 and S957. For MN500, two bands were found at 1030 and 1165 cm^{-1}, indicating the presence of R- SO_3^-, with absorption bands also observed at these values for S957. Furthermore, S957 exhibited two additional absorption bands at 960 and 1000 cm^{-1}, which represent the presence of RPO_3^{2-} [295].

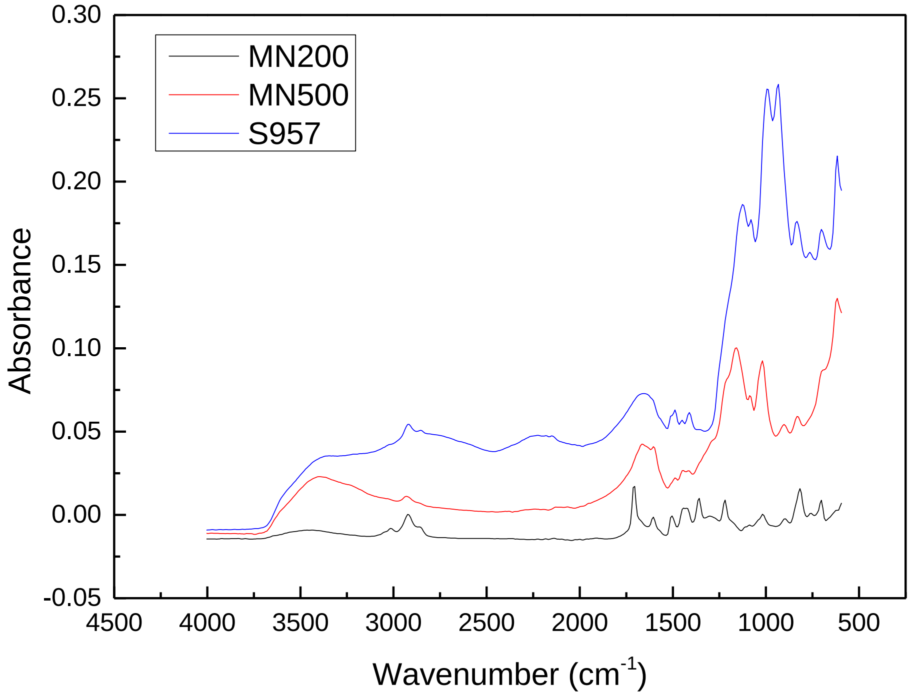

Figure 32 IR spectra of MN200, MN500 and S957

Table 16 Absorption bands obtained from IR spectra for MN200 and comparison with [294]

Absorption band (cm^{-1})	Compound	Absorption band (cm^{-1}) from [294]
715	mono – substituted aromatic ring (polystyrene)	700
700 - 900	aromatic out – of – plane and benzene out – of – plane –CH vibrations	700-900
1220	aryl ketones	1200
1015 and 1355	possibility C-(C=O)-C and C-C-C bending	1018 and 1295

1355 - 1505	phenyl carbon stretch	1295 - 1384
1615 - 1702	benzene C-C	-
2800 – 3030	aromatic C-H stretch	-

CHAPTER 6

6.0 METHODS FOR AMELIORATION OF NITROBENZENE AND RELATED PRODUCTS

This chapter discusses the results of nitrobenzene removal via reduction and adsorption; the effects of agitation speed, iron loading, initial contaminant concentration and pH on nitrobenzene reduction were studied; while for nitrobenzene adsorption kinetics, equilibria and leaching tendencies were investigated for a series of polymeric resins and granular activated carbon.

6.1 Introduction

As outlined in Chapters 1 and 2, there is a need to remove nitrobenzene (NB) and related products from aqueous systems due to their toxicity. In this study, commercial iron powder was used to reduce NB, generating aniline (AN) as a by–product; hence, polymeric resins and granular activated carbon were adopted to remove AN in order to prevent secondary contamination. Since the degradation of NB using iron required this additional remediation step to completely remove all contaminant species; this study subsequently investigated the adsorption of NB at source. A simplified schematic diagram for NB and AN removal from aqueous systems is shown in Figure 33.

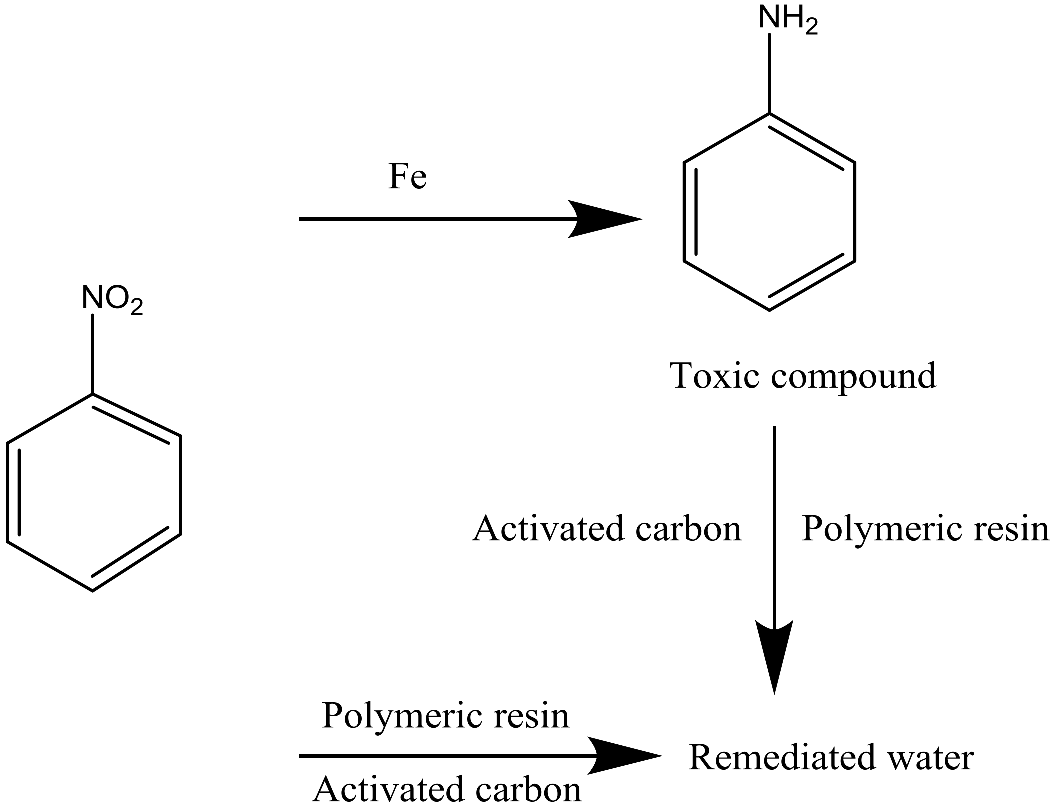

Figure 33 A simplified schematic diagram for NB and AN removal from aqueous systems via iron reduction or adsorption

6.2 Reduction of NB using iron powder

6.2.1 Quantification of NB using Gas Chromatography – Flame Ionisation Detection (GC-FID)

NB can be analysed qualitatively, and quantitatively, using GC-FID; for qualitative analysis, the peak of NB is identified from the retention time, while the concentration of NB can be determined from proportionality to the peak area for quantitative analysis - the greater the concentration, the larger the area under the peak. A calibration curve is used to quantify concentration, with an internal standard (IS) of known concentration added to the aliquots of samples to be analysed prior to injection in the GC, an additional peak is observed for the added IS. The aliquots of sample and IS are mixed in equal volumes and the calibration curve constructed using the ratio of peak area of analysed compound to that of IS [292]. In this study, dimethyl phthalate was used as the IS.

The retention times of peaks obtained for NB and dimethyl phthalate are approximately 5.8 and 9.8 min, respectively (Figure 34). The peak areas of NB and IS with the resultant ratios are shown in Tables 17 to 19. The calibration curve measurements were performed following each conditioning of the column or whenever a new stock solution was prepared. A calibration curve was determined for stock solutions of 10, 20 and 40 mg L^{-1} NB. It can be observed that the ratio obtained increases with NB concentration, as expected.

Figure 34 Chromatogram of NB (retention time: 5.8 min) and dimethyl phthalate (retention time: 9.8 min) with 40 mg L^{-1} of NB and 25 mg L^{-1} of dimethyl phthalate (IS)

Table 17 Peak areas of 10 mg L^{-1} NB and 25 mg L^{-1} dimethyl phthalate, and resultant ratios

Run number	NB peak area	Dimethyl phthalate (IS) peak area	Ratio (NB : IS)
1	37675	48942	0.7698
2	38775	49351	0.7857
3	38685	49031	0.7890
Average	38378	49108	0.7815

Table 18 Peak areas of 20 mg L^{-1} NB and 25 mg L^{-1} dimethyl phthalate, and resultant ratios

Run number	NB peak area	Dimethyl phthalate (IS) peak area	Ratio (NB : IS)
1	75271	47965	1.5693
2	77661	48776	1.5922
3	76263	47922	1.5914
Average	76395	48221	1.5843

Table 19 Peak areas of 40 mg L^{-1} NB and 25 mg L^{-1} dimethyl phthalate, and resultant ratios

Run number	NB peak area	Dimethyl phthalate (IS) peak area	Ratio (NB : IS)
1	149469	44357	3.3697
2	154090	46745	3.2964
3	148072	45089	3.284
Average	150570	45397	3.3167

Aliquots of solutions containing 10, 20 and 40 mg L^{-1} NB were mixed with IS and analysed via GC-FID with all analyses conducted in triplicate; the ratios were obtained by dividing peak areas for NB by peak areas for IS. A NB calibration curve was created by plotting the average ratio obtained for each NB concentration used versus NB concentration. From Figure 35, it can be seen that the data fit a linear line with $R^2 > 0.99$ of equation, peak area ratio = 0.08251 [NB] -0.0501. Hence, NB concentrations were quantified by using the peak area ratio obtained for an unknown concentration of NB in the formula determined from the calibration plot.

For example, if the ratio of peak areas of NB to IS is 2.6458:

Peak area ratio = 2.6458 = 0.08251 [NB] -0.0501

rearranging and evaluating gives [NB] = 32.6736. Hence, the concentration of NB is 32.6736 mg L^{-1}, and this method was employed to calculate all NB concentrations determined in this study.

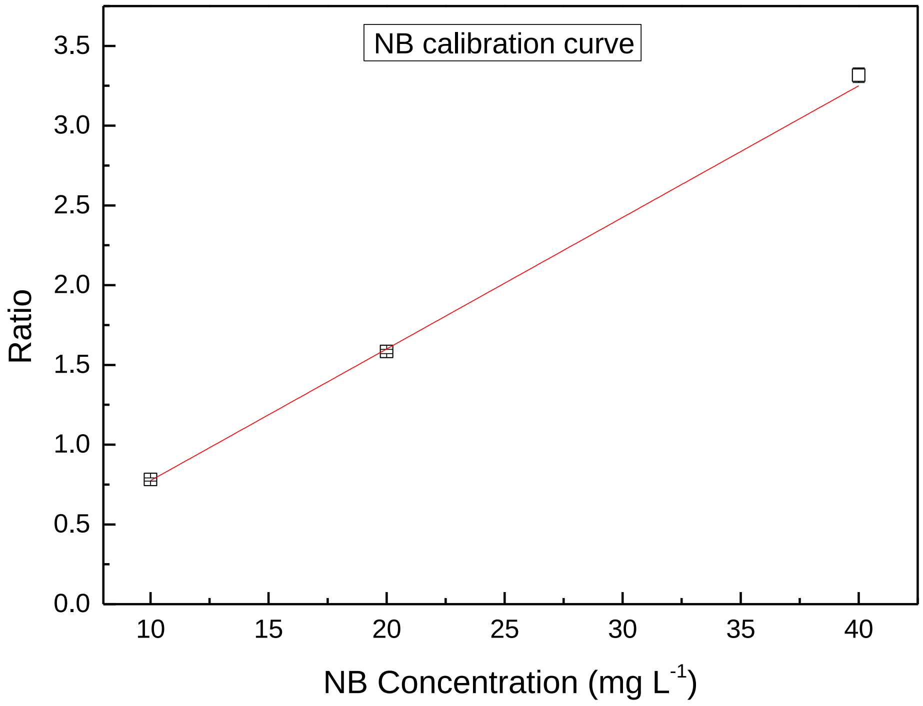

Figure 35 NB calibration curve. Errors shown are for repeat runs (n = 3).

6.2.2 Effect of agitation speed on NB reduction

In presence of iron, NB undergoes reduction to yield AN (this can be proven by Gas Chromatography (GC) where the intensity of NB would be reduced and an AN peak observed, as shown in Appendix F). To study the effect of agitation speed on NB reduction, batch reactors containing 40 mg L^{-1} of NB solution were agitated using an orbital shaker at 0, 75, 125, 175 or 225 rpm for 24 h. The results obtained (Figure 36) demonstrate that the efficiency of NB degradation is enhanced with agitation speed, i.e. a greater amount of NB is degraded at higher agitation speed. Agrawal and Tratnyek have previously investigated the effect of mixing rate on NB reduction, and their results demonstrated that the pseudo-first-order rate constant of NB reduction increased with mixing rate (rpm) [149], indicating that mixing rate has a significant influence on NB reduction. This is likely the result of limitation of the rate of NB reduction by mass transport effects. It was visually observed, in this study, that iron powder tends to settle without agitation, and the distribution of iron powder in NB solution is more even as agitation speed is increased. An increased shaking speed, therefore, maximises mixing of the iron and NB resulting in greater reaction, hence, the efficiency of NB reduction is enhanced.

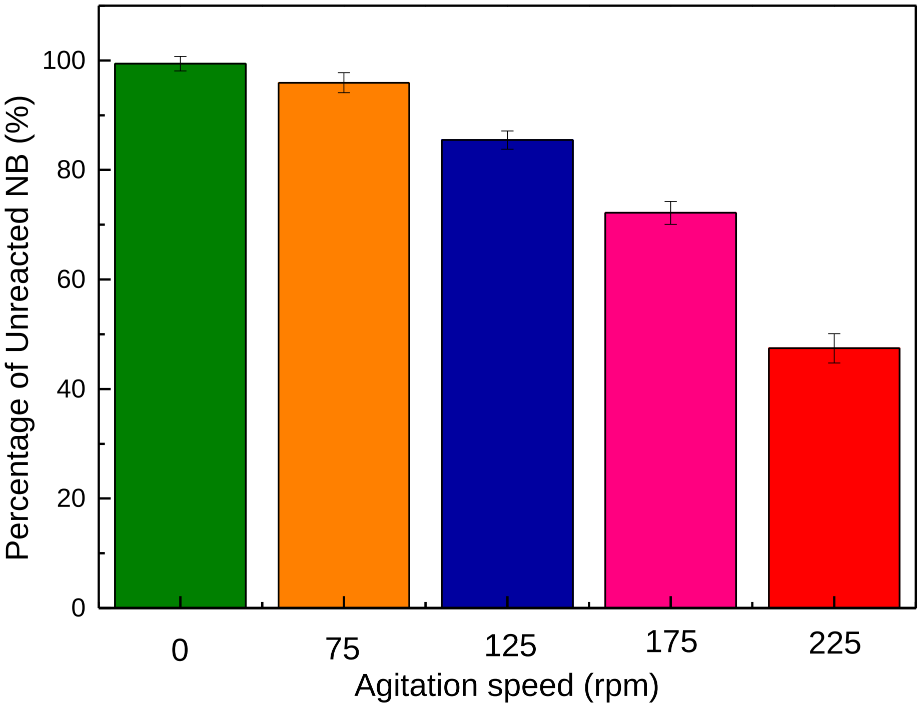

Figure 36 Percentage of unreacted NB at different agitation speed over 24 h. Errors shown are for repeat runs (n = 3).

6.2.3 Effect of iron loading on NB reduction

The effect of iron loading on NB reduction was studied by varying the iron dosage (4 to 20, 50 or 100 g L^{-1}) added to a reaction system containing an initial concentration of 40 mg L^{-1} NB; the results demonstrate that NB reduction is enhanced as iron loading is increased in the system (Figure 37). These findings are consistent with previous studies, which also report that the efficiency of NB reduction is enhanced with iron dosage [188, 189, 296] due an increase in the number of reactive sites for NB reduction to AN [188].

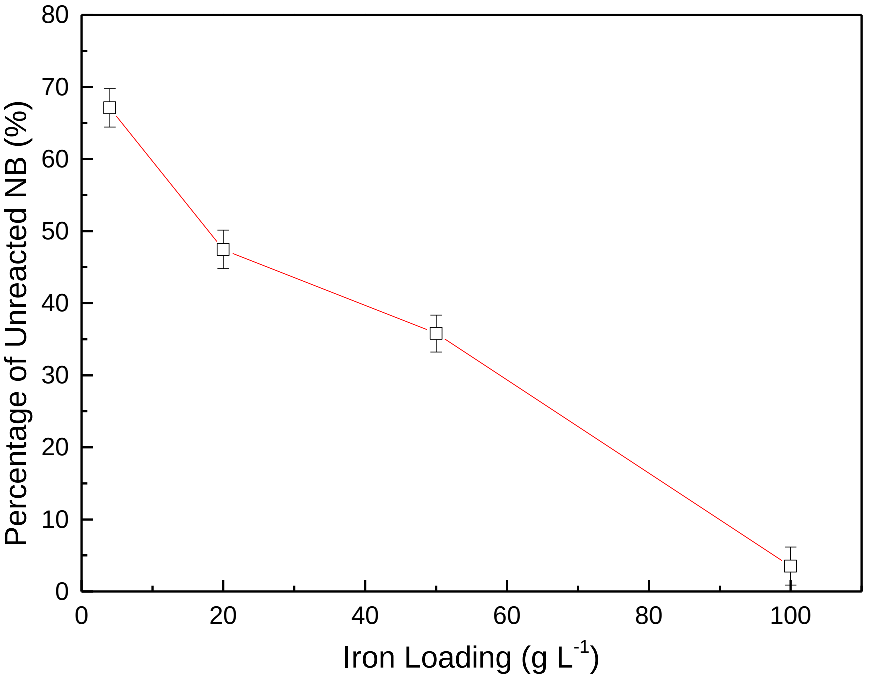

Figure 37 Percentage of unreacted NB at different iron loading over 24 h. Errors shown are for repeat runs (n = 3).

6.2.4 Kinetics of NB reduction

Several previous studies have reported that the kinetics of NB reduction follow a pseudo- first order model [149, 187, 296], however, one study shows the kinetics to be described by a pseudo-zero order model [188], however, this applied to low iron loadings, in contrast to the excess quantities used here. This study investigated the kinetics of NB reduction using iron powders (herein referred to as Iron 1 (electrolytic) and Iron 2 (20 mesh)) and a control experiment conducted in the absence of iron. The results obtained indicate that NB reduction was complete within 24 h for Iron 1 and 6 h for Iron 2, with the concentration of NB remaining unchanged over the reaction period for the control experiment. The consumption of NB in the presence of either iron powder (Figure 38) can be expressed by nonlinear regression to an integrated pseudo-first order kinetic model:

$$[NB]_t = [NB]_0\, e^{-k_3 t} \qquad \text{Equation 38}$$

where k_3 (h^{-1}/ min^{-1}) is rate constant of NB reduction.

The values of k_3 observed were 0.138 h^{-1} and 0.665 h^{-1} for Iron 1 and Iron 2, respectively, with $R^2 > 0.99$ for both systems. Hence, it can be concluded that the degradation of NB using commercial iron powders follows a pseudo-first order model, in line with the previous results mentioned above.

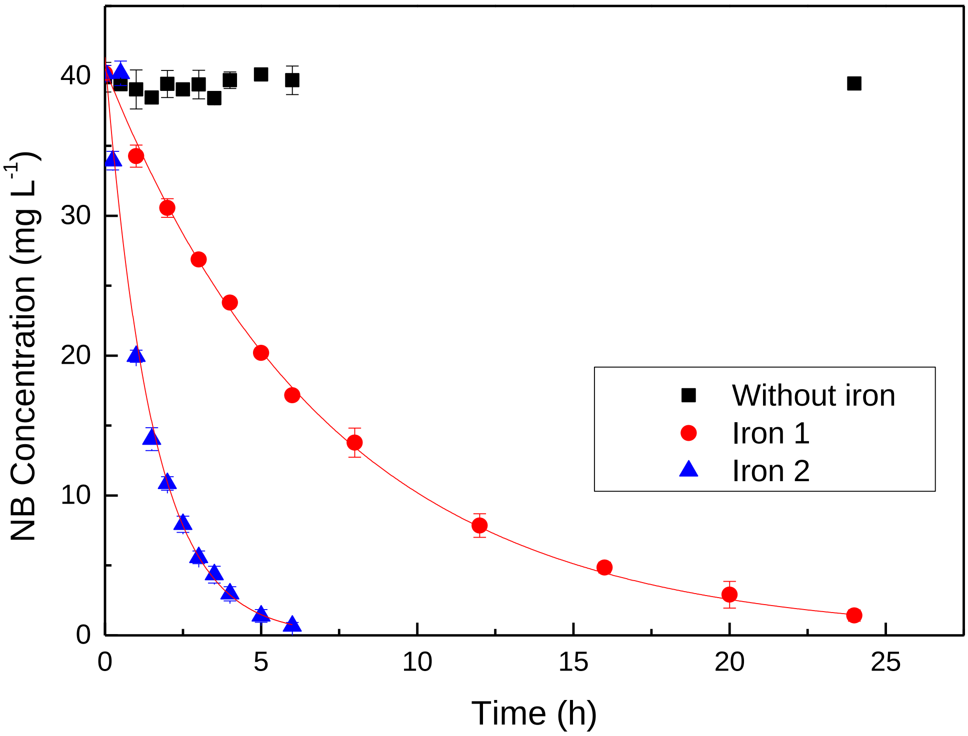

Figure 38 Kinetic study of NB reduction by commercial iron powders, fitted using a pseudo-first order model. Errors shown are for repeat runs (n = 3).

6.2.5 Effect of initial concentration on NB reduction

Although the results of the kinetic study agree with several previous studies showing NB reduction to follow a pseudo-first order kinetic model, there is lack of information regarding the effect of parameter variation on the kinetics of the process and this study serves to quantify these relationships. Firstly, the effect of initial NB concentration on the kinetics of NB reduction using Iron 2 was investigated. The results for 10 - 40 mg L^{-1} NB (Figure 39) demonstrate that increasing initial NB concentration significantly increases the time required for complete NB degradation.

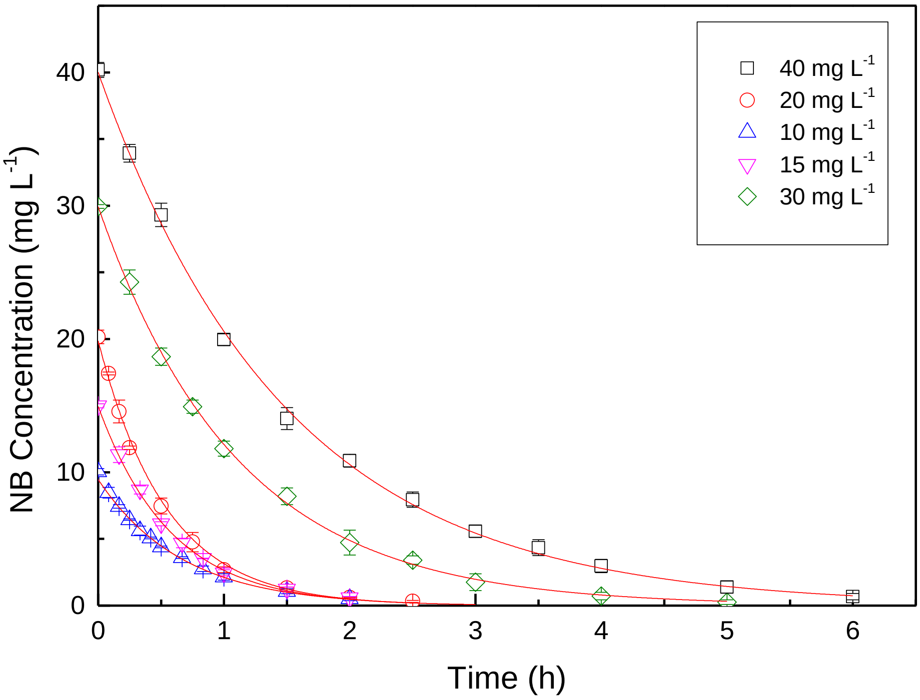

Figure 39 Kinetic study of NB reduction by Iron 2 at 10, 15, 20, 30 and 40 mg L^{-1}, fitted using a pseudo-first order model. Errors shown are for repeat runs (n = 3).

Fitting the data obtained for the five different initial NB concentrations, using a pseudo-first order kinetic model shows the rate constant to increase initially up to 20 mg L^{-1}, before decreasing again for concentrations > 20 mg L^{-1} (Table 20). These results are consistent with those obtained by Xu *et al.* who studied initial concentrations in the range 200 – 1900 mg L^{-1}, observed a peak in rate constant at 900 mg L^{-1}, which the authors ascribed to competition between the reduction of NB at the iron surface and adsorption of NB on to reactive sites, meaning NB reduction is limited by mass transport at higher concentrations [297]; it should be noted that shaker model and speed significantly affect the levels at which mass transport effects become evident, hence, the mass transport limitations for the lower values of NB used in this study may be affected by the operational conditions adopted.

Table 20 Time taken for complete NB removal, and resulting kinetic parameters, using Iron 2. Data fitted using a pseudo-first order model.

	NB initial concentration (mg L^{-1})				
	10	15	20	30	40
Time taken for 100% NB removal (h)	2	2.5	3	5	6
k_3 (h^{-1})	1.49	1.73	1.84	0.91	0.637
R^2	0.996	0.999	0.997	0.999	0.999

6.2.6 Effect of pH on NB reduction

As previous studies have demonstrated, hydrogen ions (H^+) affect NB reduction rate and iron corrosion [187, 189, 298], this study investigated the effect of pH on NB reduction. This was achieved by studying the kinetics of NB reduction using Iron 2 with varied pH (3 to 9); the results obtained (Figure 40) demonstrate that the time taken to completely remove NB increases as the pH becomes more basic. The kinetic data for all pH values used can be described by a pseudo-first order model (R^2>0.99), and the rate increases as initial pH decreases, indicating that reduction is inhibited at basic pH; similar phenomena have been observed by other researchers [187-189, 299]. Increased NB reduction at low pH occurs as iron corrosion is promoted under acidic conditions [187, 298], the stepwise transformation of NB to AN is favoured by the presence of H^+ [187, 189], and the surface hydroxide layer, present under basic conditions, which results in mass transfer limitations [187, 298], is eliminated at low pH [188, 189]. To rule out the possibility that acidic pH alone controls NB reduction, a control experiment was performed in the absence of iron powder and at pH 3; the results demonstrate that the concentration of NB remains unchanged over an extended period, hence iron itself is required to facilitate degradation.

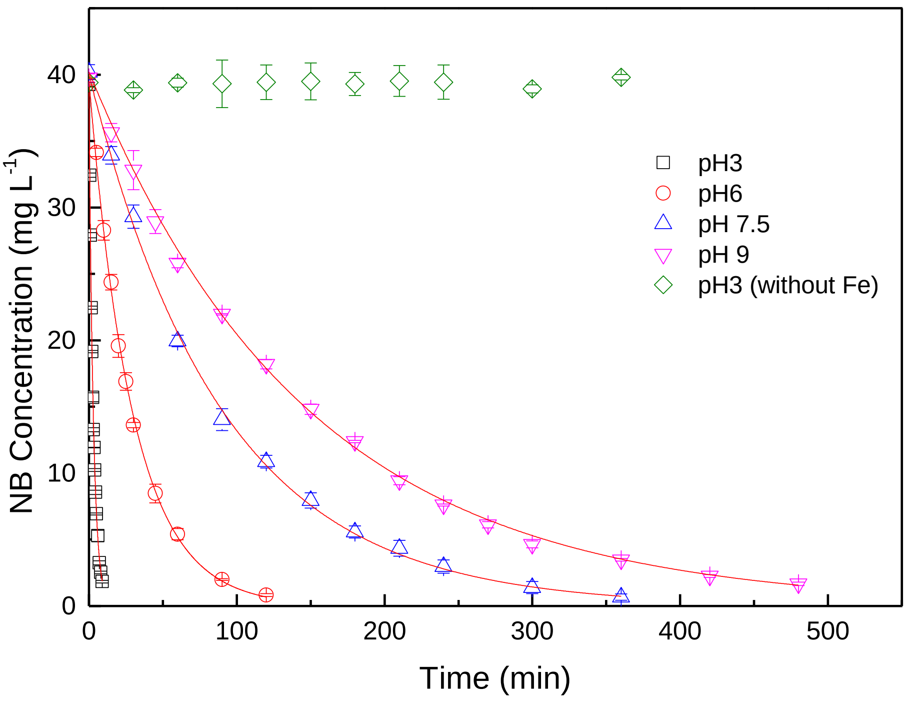

Figure 40 Kinetics of NB reduction by Iron 2 at pH 3, 6, 7.5 and 9, fitted using a pseudo-first order model. Errors shown are for repeat runs (n = 3).

6.2.7 NB reduction in an aqueous solution of corroded iron

Iron powder can undergo corrosion in aqueous solution, causing dissolution of the iron solid to ferrous iron cations, which are reportedly involved in direct electron transfer from the iron surface [149]. However, NB reduction in a purely aqueous solution of corroded iron has not been previously investigated to define the separate roles of the iron surface and the corroded iron. NB reduction in pre-filtered solutions of aqueous corroded iron showed that no degradation of NB occurred, with the initial concentration remaining unchanged after 24 h (Figure 41). Hence, it can be concluded that NB reduction only occurs on the surface of iron particles, which involves the transfer of two electrons from the iron surface to produce AN. Thus, these results validate the reduction of NB at the metal surface only, as proposed by Agrawal and Tratnyek [149].

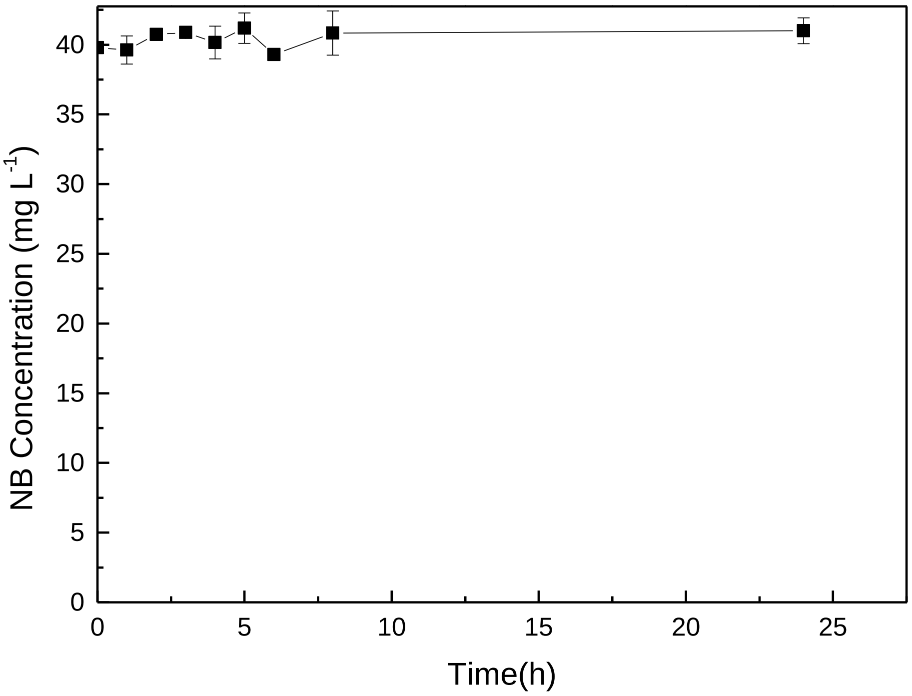

Figure 41 Concentration of NB with time to investigate whether NB reduction occurs in aqueous media filtered from a corroded iron solution. Errors shown are for repeat runs (n = 3).

6.3 Adsorption of Aniline (AN) using polymeric resins and granular activated carbon

6.3.1 Quantification of AN using GC – FID

AN in aqueous sample is analysed qualitatively and quantitatively using GC-FID; the concentration of AN can be obtained from the peak observed at the retention time known to correspond to AN, by comparison of the peak area of that of an internal standard (IS: dimethyl phthalate). A calibration curve can then be developed by plotting a graph of the peak area ratios obtained vs. AN concentration. In this study, a calibration curve for AN was plotted at 0, 10, 20 and 40 mg L^{-1}, as shown in Figure 43.

From Figure 42, the peaks of AN and dimethyl phthalate were found to occur at 4.3 and 9.8 min, respectively, with the peak areas obtained and the ratios calculated tabulated in Table 21 to 23. It can be seen that the peak area of AN increases with concentration, resulting in a greater ratio at higher concentration; these findings are consistent with those observed for NB (Section 6.2.1). By using a linear regression method to fit the data, a linear relationship of with peak area ratio = 0.07729 [AN] – 0.00616 ($R^2 > 0.99$) was obtained, as shown in Figure 43.

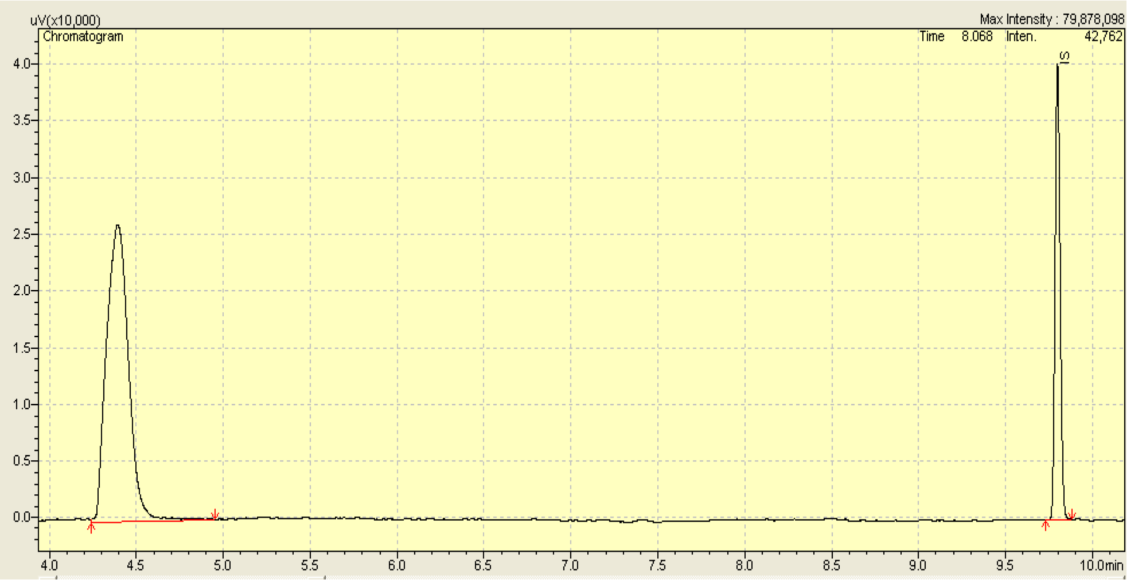

Figure 42 Chromatogram of AN (retention time: 4.3 min) and dimethyl phthalate (retention time: 9.8 min) with 40 mg L^{-1} of AN and 25 mg L^{-1} of dimethyl phthalate (IS)

Table 21 Peak areas of 10 mg L^{-1} AN and 25 mg L^{-1} dimethyl phthalate, and resulting ratios

Number of run	Peak area of AN	Peak area of dimethyl phthalate (IS)	Ratio (AN : IS)
1	48397	67831	0.7135
2	57655	69015	0.8354
3	54045	68918	0.7842
Average	53342	68588	0.7777

Table 22 Peak areas of 20 mg L^{-1} AN and 25 mg L^{-1} dimethyl phthalate, and resulting ratios

Number of run	Peak area of AN	Peak area of dimethyl phthalate (IS)	Ratio (AN : IS)
1	90599	61328	1.4773
2	110386	69421	1.5901
3	99160	65826	1.5064
Average	99902	65525	1.5246

Table 23 Peak areas of 40 mg L^{-1} AN and 25 mg L^{-1} dimethyl phthalate, and resulting ratios

Number of run	Peak area of AN	Peak area of dimethyl phthalate (IS)	Ratio (AN : IS)
1	190142	70864	2.6832
2	199142	71934	2.7684
3	194583	71441	2.7237
Average	194604	71413	2.7251

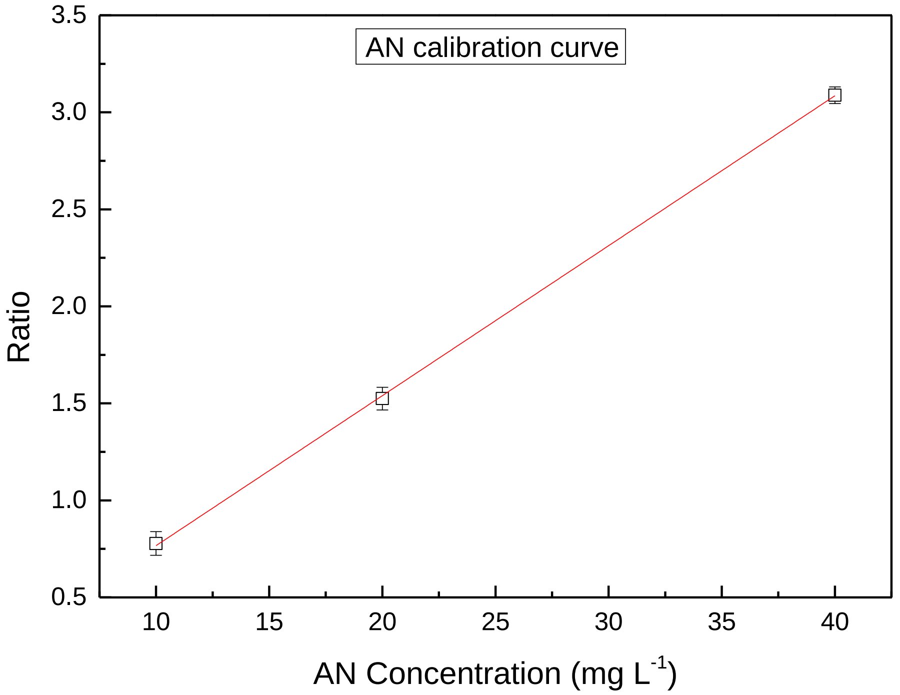

Figure 43 AN calibration curve. Errors shown are for repeat runs (n = 3).

Hence, AN concentrations were quantified by using the peak area ratio obtained for an unknown concentration of AN in the formula determined from the calibration plot.

For example, if the ratio of peak areas of AN to IS is 1.9547:

Peak area ratio = 1.9547 = 0.07729 [AN] -0.00616

rearranging and evaluating gives [AN] = 25.3701. Hence, the concentration of AN is 25.3701 mg L^{-1}, and this method was employed to calculate all AN concentrations determined in this study.

6.3.2 Equilibrium uptake capacities of AN onto polymeric resins and GAC

The removal of AN is neccessitated by its toxic nature, and its formation during the degradation of NB, causing secondary pollution. In this study, AN was removed from aqueous systems via adsorption using sulfonic-phosphonic functionalised polymeric resin S957, sulfonic functionalised polymeric sorbent MN500, non – functionalised Macronet MN200 and Granular Activated Carbon (GAC). The equilibrium uptake profiles for S957 (131.63 mg g^{-1}; 120 min), MN500 (110.48 mg g^{-1}; 90 min), GAC (40.43 mg g^{-1}; 120 min) and MN200 (31.67 mg g^{-1}; 120 min), are shown in Figure 44.

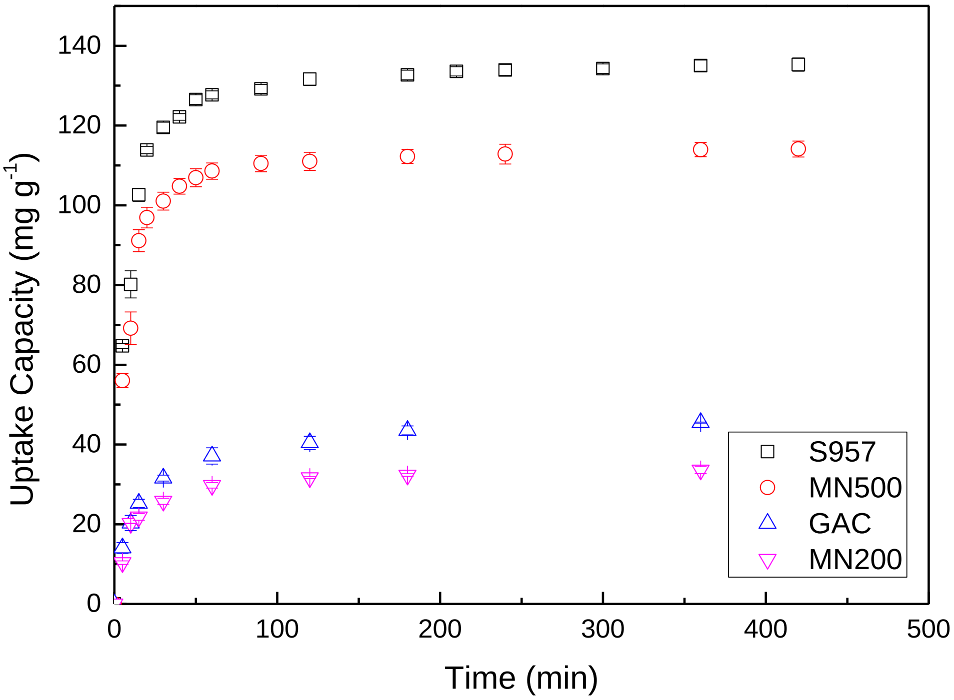

Figure 44 Uptake capacity profiles of AN for S957, MN500, MN200 and GAC (initial concentration 40 mg L^{-1}). Errors shown are for repeat runs (n = 2).

6.3.3 Kinetics of AN adsorption

AN adsorption kinetics were investigated using a pseudo-first order, a pseudo-second order and the Elovich kinetic models. The parameters obtained are summarised in Table 24 and kinetic fits are shown in Figures 45 and 46. The results demonstrate that AN adsorption kinetics, for all sorbents, can be most appropriately described using pseudo-second order models. These findings are consistent with previous studies, which report that AN adsorption onto sorbents such as lignin [65], bentonite [61], activated carbon [170, 228] and polymers [170, 223] followed pseudo-second order models. Adsorption of aromatic compounds onto GAC involves two forces: 1) π-π dispersive interactions between the AN aromatic ring and the basal planes of GAC and 2) electrostatic repulsion and attraction of any ions present [170]. However, adsorption of AN onto non-functionalised sorbents, such as MN200 ,experiences van der Waals forces and the hydrophobicity of the sorbents creates a thermodynamic gradient driving solute from the aqueous solution [170]. AN uptake capacities onto all sorbents increased with total acidic content (refer to Table 24, Figure 45 and 46): S957 > MN500 > GAC > MN200. The higher uptake capacities observed for the acidic functionalised sorbents (S957, MN500 and GAC) than the non-functionalised sorbent (MN200) may be due to the presence of polar groups, such as carboxyl and sulfonic groups enhancing surface contact with the aqueous solution. In addition, the interactions between these acidic groups and basic amino groups of AN results in increased adsorption uptakes [223, 235]; hence, higher acidic sorbent capacities contribute to stronger interactions between acidic groups of the specific sorbent and $–NH_2$ group of AN, thus, S957 exhibits the highest overall acid content so the highest adsorption capacity. The rate of adsorption (k_2

values in Table 24), increases as acidic capacity decreases; k_2 is highest for MN200, ~ 2 times that of GAC, MN200 and S957, which suggests that the rate of AN adsorption onto MN200 is fastest for the non-functionalised sorbent. Formation of hydrogen bonding between the acidic groups and water, causing the development of water cluster networks, may prevent AN molecules from entering the pores [165], while increased acidic capacity causes a reduced surface area that may also inhibit AN adsorption. Hence, there is a clear interplay between the role of acidic groups interacting with the basic amino groups of AN, enhancing AN adsorption, while inhibiting the rate of adsorption.

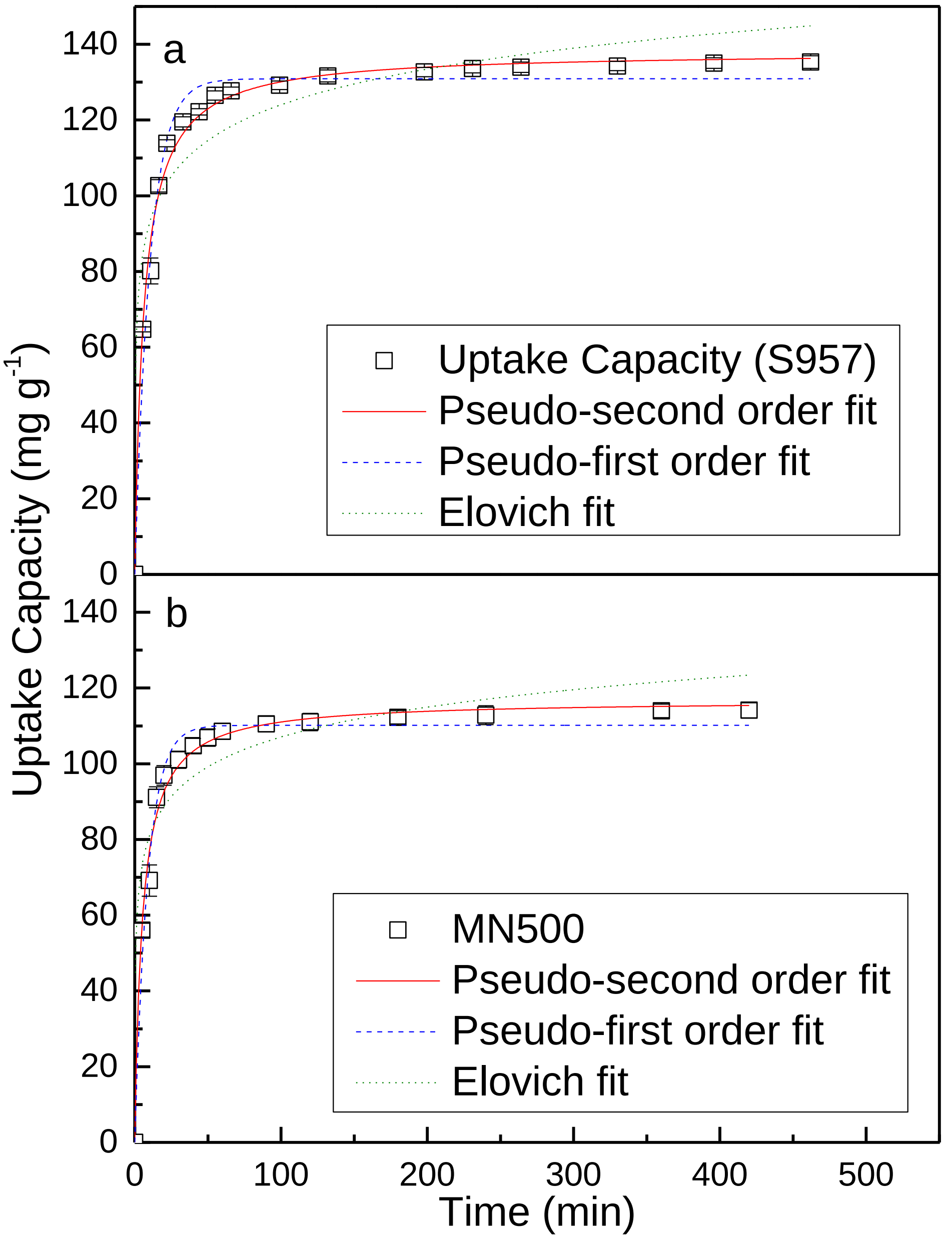

Figure 45 Kinetic data for AN adsorption, fitted using pseudo-first order (dash line), pseudo-second order (solid line) and Elovich (dot line) models for (a) S957 and (b) MN500. Errors shown are for repeat runs (n = 2).

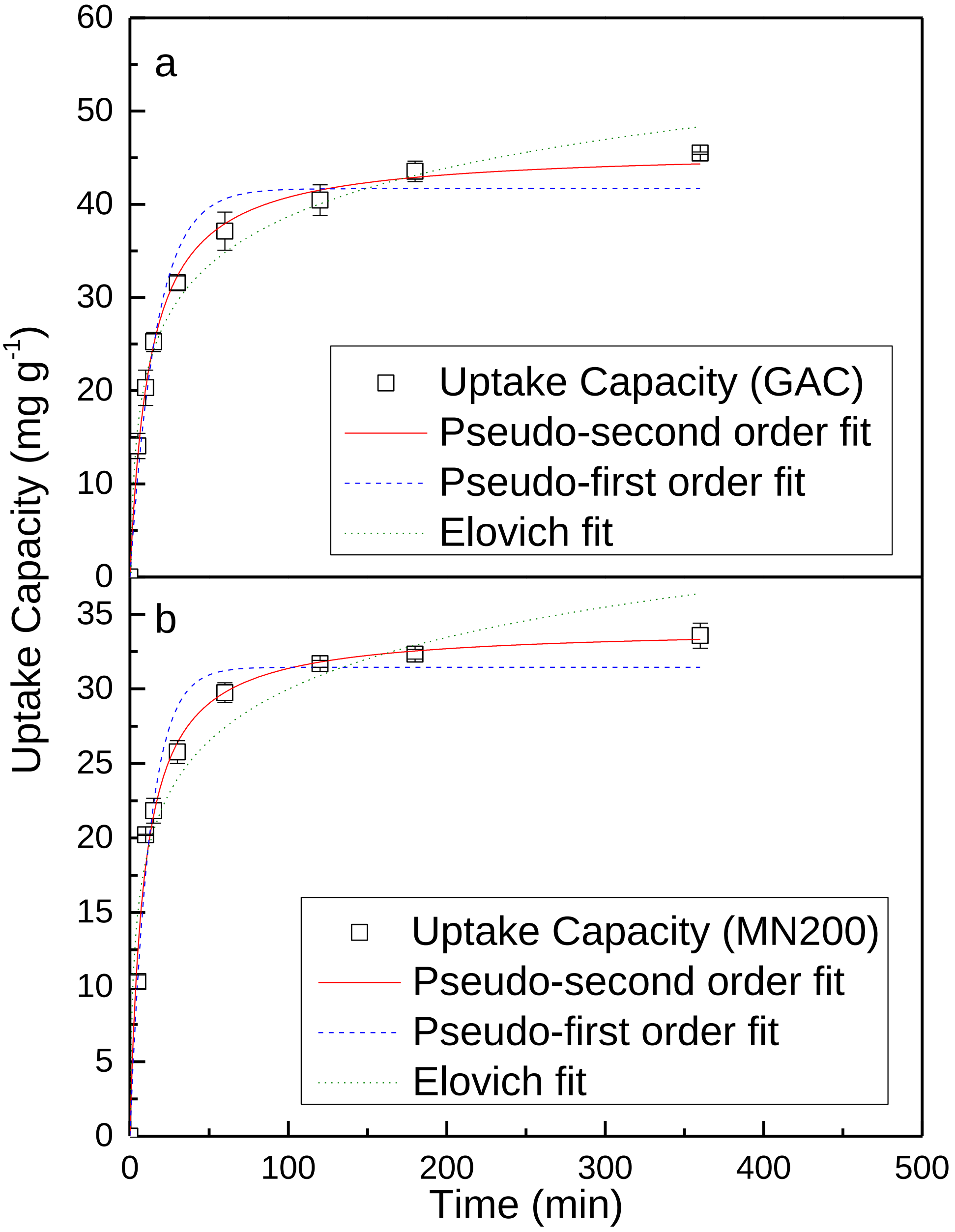

Figure 46 Kinetic data for AN adsorption, fitted using pseudo-first order (dash line), pseudo-second order (solid line) and Elovich (dot line) models for (a) GAC and (b) MN200. Errors shown are for repeat runs (n = 2).

Table 24 Kinetic parameters of S957, MN500, GAC and MN200 fitted using a pseudo-first order, a pseudo-second order and the Elovich models.

Model	S957	MN500	GAC	MN200
Pseudo-first order				
q_e (mg g^{-1})	130.9	110.2	41.7	31.4
k_1 (min^{-1})	0.104	0.112	0.060	0.082
R^2	0.982	0.983	0.966	0.973
Pseudo-second order				
q_e (mg g^{-1})	138.1	116.8	45.9	34.1
k_2 (g mg^{-1} min^{-1})(x10^{-4})	13.0	16.4	17.0	33.3
R^2	0.992	0.991	0.996	0.990
Elovich				
a (mg g^{-1} min^{-1})	1345.5	1383.0	12.8	19.9
b (g mg $^{-1}$)	0.073	0.087	0.132	0.199
R^2	0.928	0.924	0.985	0.951

6.3.4 Determination of rate limiting step

In order to determine the rate limiting step of AN adsorption onto MN200, GAC, MN500 and S957, the Homogeneous Particle Diffusion Model (HPDM) [170] was applied to the kinetic data obtained (Figures 47 and 48); the results indicate that, for all samples, AN adsorption is controlled by particle diffusion (higher R^2 values), consistent with previous studies reporting AN adsorption onto GAC and polymeric resin are limited by particle diffusion [170].

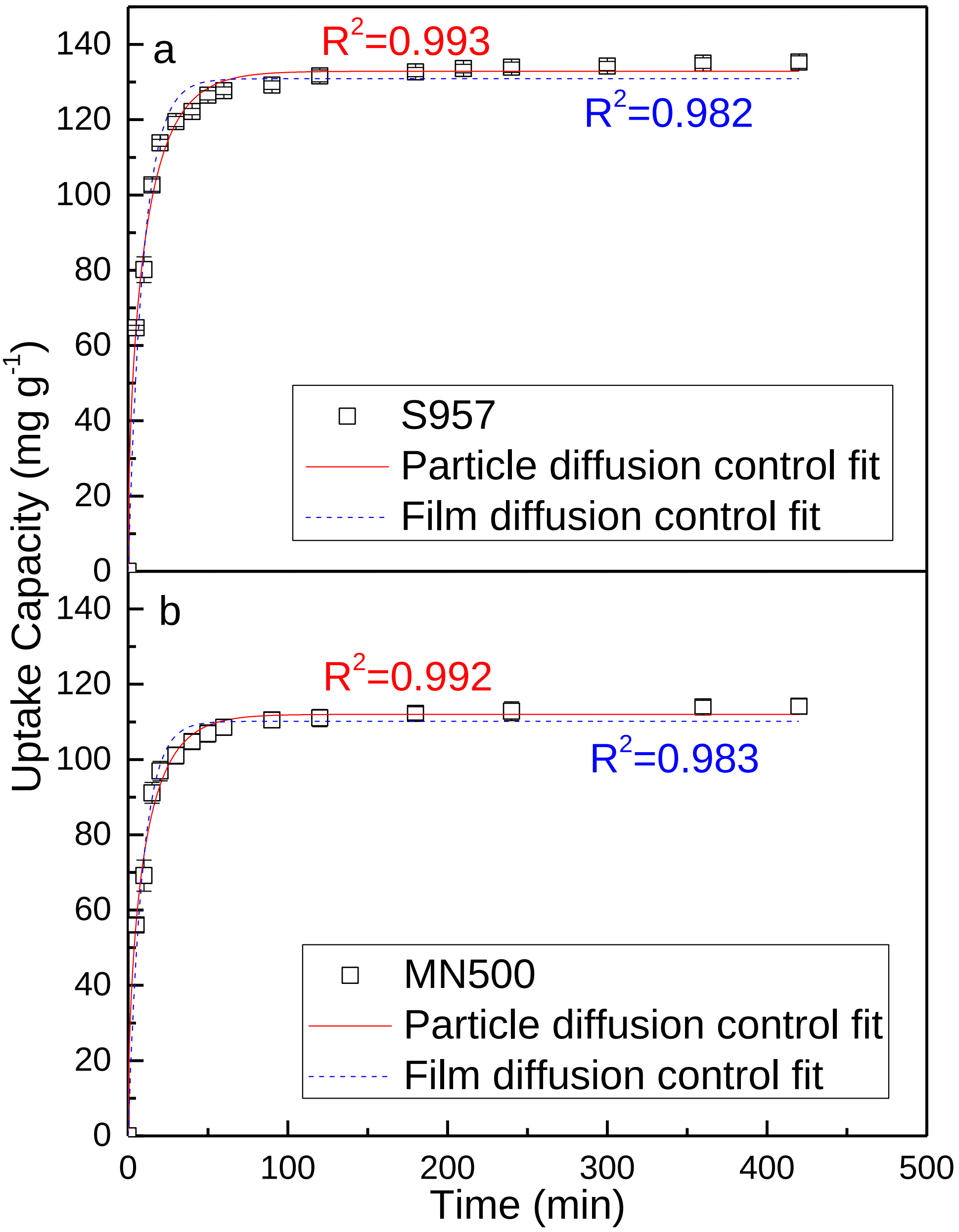

Figure 47 AN uptake capacities fitted using HPDM, showing particle diffusion (solid line) and film diffusion (dash line) control for (a) S957 and (b) MN500. Errors shown are for repeat runs (n = 2).

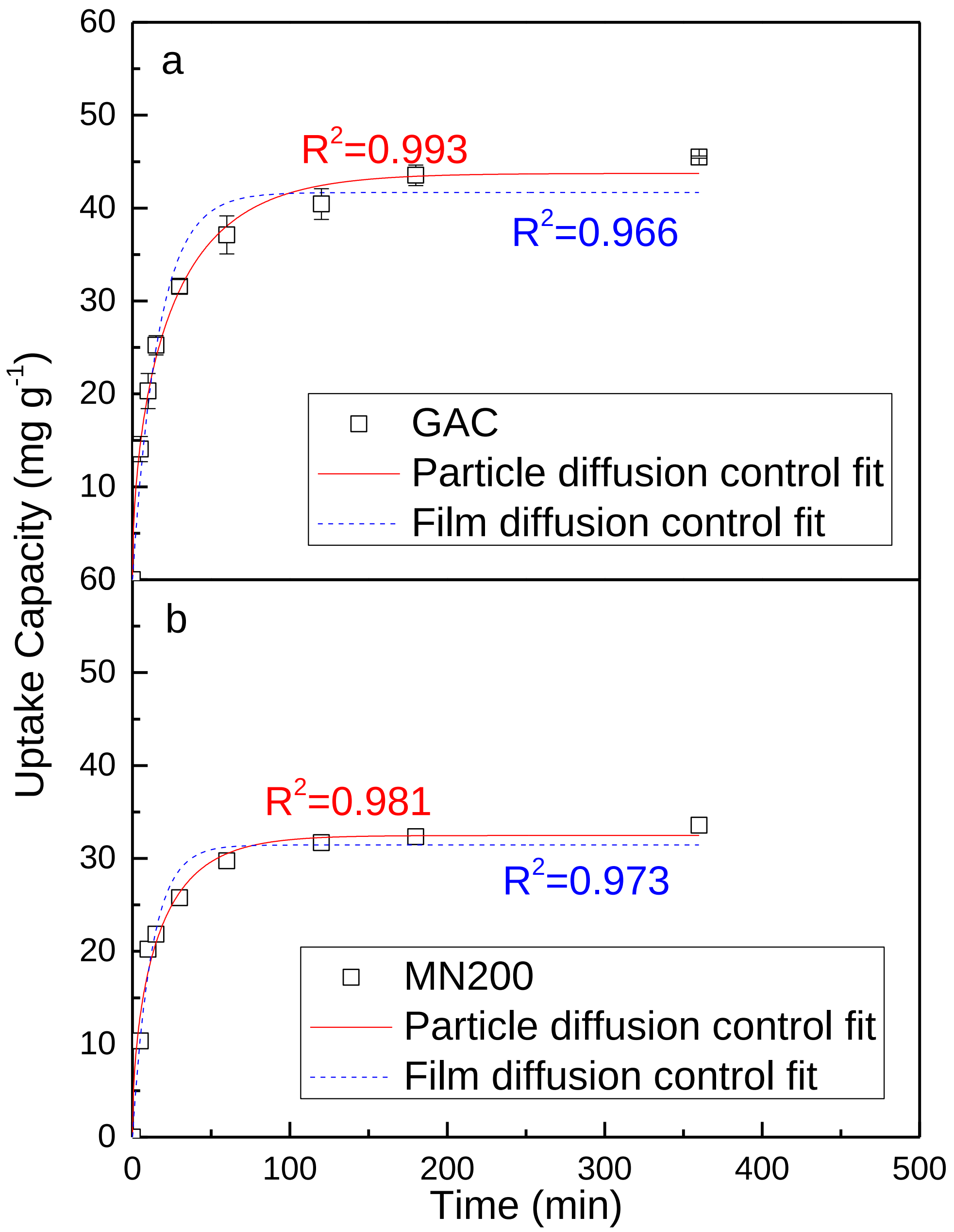

Figure 48 AN uptake capacities fitted using HPDM, showing particle diffusion (solid line) and film diffusion (dash line) control for (a) GAC and (b) MN200. Errors shown are for repeat runs (n = 2).

In order to confirm that the adsorption of AN onto all sorbents is dominated by particle diffusion, the intraparticle diffusion model is applied [170]. From Figure 49, it can be observed that more than one gradient is obtained for each plot, indicating that the rate of AN adsorption is controlled by several steps for all sorbents, with parameters obtained shown in Table 25. The first portion represents diffusion of AN on to the external sorbent surface from the bulk solution, which occurs at the initial stage of adsorption and is the fastest, providing the highest values of k_{i1} for all sorbents. The second slope, in all plots, with lower values of k_{i2}, indicating slower rate of diffusion compared to film diffusion, can be ascribed to intraparticle diffusion and adsorption of solutes in macro and mesopores. The third section corresponds to micropore diffusion, establishing AN adsorption equilibrium. As the third portions have the shallowest gradients, hence, the values of k_{i3} are the smallest, the rate of intraparticle diffusion within the micropores is slowest, due to an enhanced diffusional resistance. Film diffusion only occurs at the initial stage of adsorption; hence, the overall rates, for AN adsorption onto all sorbents are controlled by particle diffusion, in line with previous studies [170, 228].

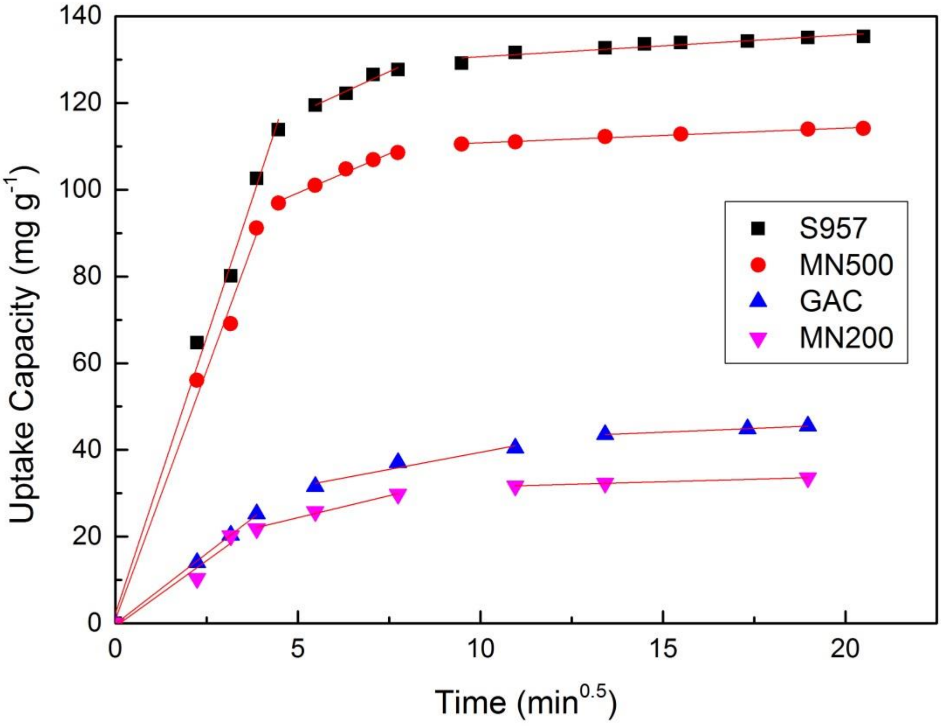

Figure 49 Kinetic fits of AN adsorption using the intraparticle diffusion model for S957, MN500, GAC and MN200.

Table 25 Intraparticle diffusion rate constants for AN adsorption by S957, MN500, GAC and MN200

Adsorbent	k_{i1}	R^2	k_{i2}	R^2	k_{i3}	R^2
S957	25.49	0.991	3.83	0.952	0.50	0.877
MN500	16.80	0.983	8.74	0.955	0.43	0.896
GAC	6.49	0.999	1.58	0.884	0.34	0.998
MN200	6.06	0.904	2.02	0.982	0.23	0.996

6.4.5 Adsorption equilibria study

The kinetic results obtained in this work (Figures 45 and 46) show S957 and MN500 to have higher AN uptakes compared to GAC and MN200; hence, S957 and MN500 were selected for further investigation, including detailed isothermal studies to provide additional understanding of the mechanism of AN adsorption. The resulting adsorption isotherms were analysed using both the Freundlich and Langmuir isotherm models (Figure 50); and the parameters obtained are tabulated in Table 26. The results demonstrate that the Freundlich equation fits the data more appropriately for both S957 and MN500. The value of K_f reflects the AN adsorption capacity; thus, higher adsorption capacities result in higher values of K_f.

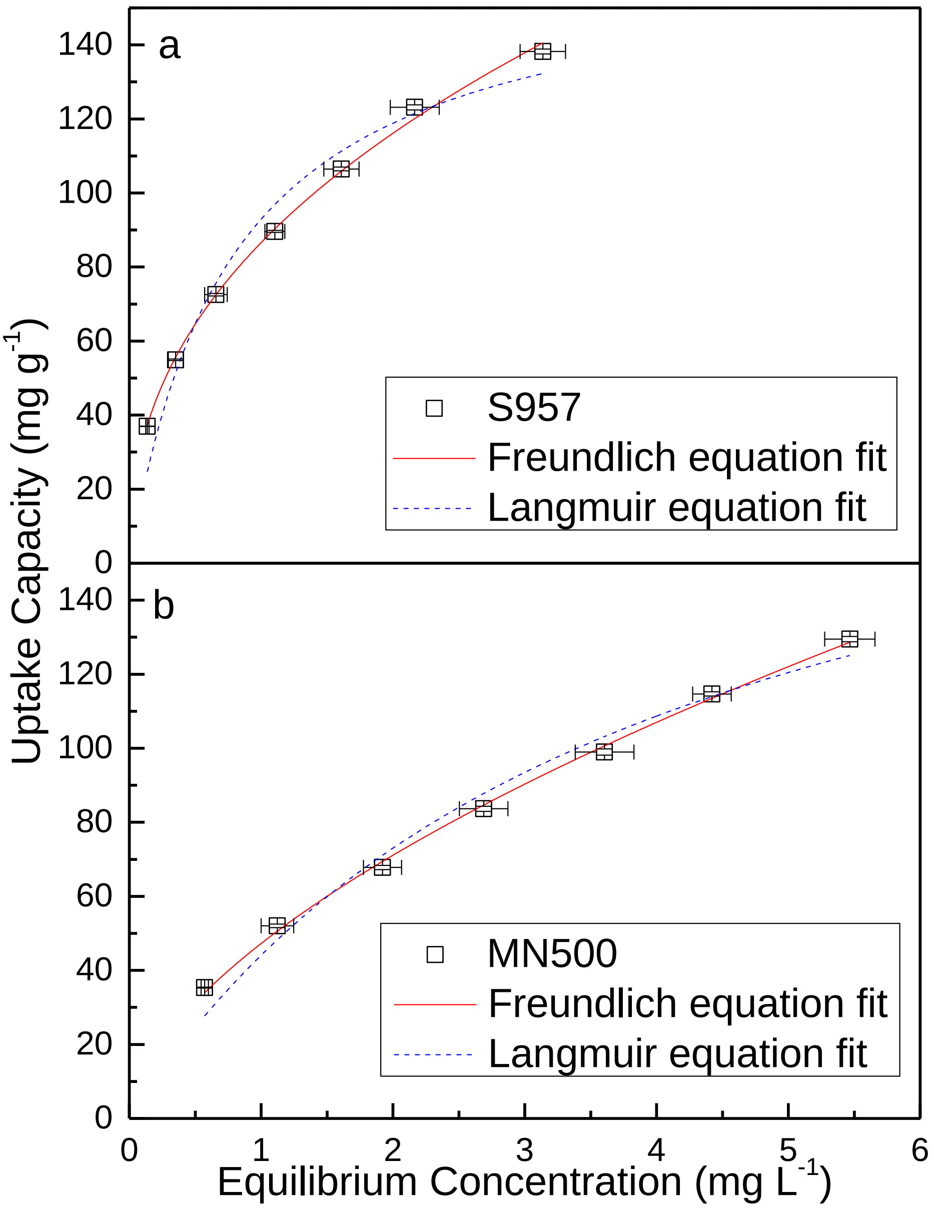

Figure 50 AN uptake capacities fitted using Freundlich (solid line) and Langmuir (dash line) equations for (a) S957 and (b) MN500. Errors shown are for repeat runs (n = 2).

The data presented in Table 26 show that the value of K_f for S957 is higher than MN500, indicating AN uptake is higher for S957 compared to MN500, which is consistent with previous results showing a higher value of K_f for an acidic functionalised polymeric sorbent compared to a non-functionalised resin [223, 235]. The acidic functionalities of S957 are more abundant on the surface and form stronger interactions with the basic amine groups of AN, despite the smaller surface area of the material itself; hence, the surface chemistry plays a more significant role than the textural properties with regards to AN uptake capacity. In addition, the data shown in Table 26 indicate that AN adsorption onto S957 is favourable, while it is moderately favourable for MN500; the n values obtained also show AN adsorption onto S957 and MN500 to be a physical process. Hence, S957 appears the better candidate for AN adsorption, providing easy regeneration as the process involves physisorption.

Table 26 Isotherm parameters obtained by fitting Freundlich and Langmuir equations to the data of AN adsorption onto S957 and MN500

Adsorbent	S957	MN500
Freundlich model		
K_f (mg g^{-1} (L mg^{-1})$^{1/n}$	86.59	47.25
n	2.361	1.696
R^2	0.997	0.997
Langmuir model		
q_m (mg g^{-1})	165.0	212.5
K_L (L mg^{-1})	1.287	0.2618
R^2	0.957	0.975

6.4.6 Leaching tendencies

In pollutant removal processes, it is not only important to determine the adsorption dynamics of a system, such as kinetics and the mechanism of adsorption, but is also essential to investigate the leaching tendencies of any sorbents used. From the kinetic results, S957 and MN500 were shown to exhibit moderately slower kinetics compared to GAC and MN200; however, AN uptake capacities for S957 and MN500 were higher, hence, only the leaching tendencies of S957 and MN500 were investigated, as they offer more promise as AN sorbents. Leaching experiments were performed by adding known amounts of pure deionised water to fully AN loaded sorbents (Figure 51) and the leaching tendency of each sorbent can be obtained from:

$$Leaching\ tendencies = \frac{Amount\ of\ AN\ leached}{Amount\ of\ AN\ adsorbed}\ x\ 100\% \qquad \text{Equation 39}$$

The results indicate that, over a period of 80 h, 19% of AN was leached from MN500; while only 12% of AN leached from S957, this behaviour is ascribed to the higher acidic capacity of S957, which results in stronger interactions between the basic amine groups of AN and the acidic functionalities on the sorbent. A steep increase in AN desorption rate was also observed initially, with 7% and 11% of AN leached over 6 h from S957 and MN500, respectively, but dramatic decreases in leaching rate were observed for both sorbents thereafter.

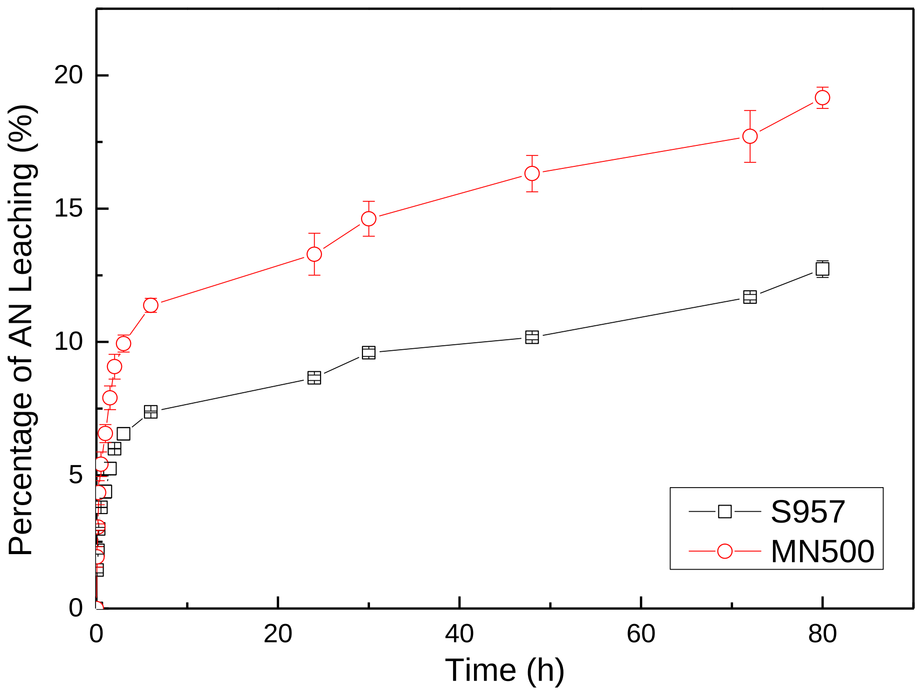

Figure 51 Percentage of adsorbed AN leached from S957 (empty square) and MN500 (empty circle). Errors shown are for repeat runs (n = 2).

6.4 Adsorption of NB using polymeric resins and GAC

6.4.1 Equilibrium uptake capacities for NB onto polymeric resins and GAC

The direct removal of NB from solution was considered to simplify its removal from aqueous systems, hence, adsorption of NB from aqueous systems was investigated using polymeric resin MN200, MN500 and S957, with the observed performances compared to GAC and all results shown in Figure 52. The equilibrium uptake capacities were determined as 125.6 mg g^{-1} (90 min) and 119.1 mg g^{-1} (180 min) for MN200 and GAC, respectively. However, it was found that less than

10% of the NB available within the system is adsorbed by using the acidic functionalised polymeric sorbents MN500 and S957, over 24 h. NB uptake is less than 15 mg g^{-1} for both sorbents, which may be due to repulsive forces between the acidic functionalities of these sorbents with the electronegative nitro group of NB, inhibiting uptake.

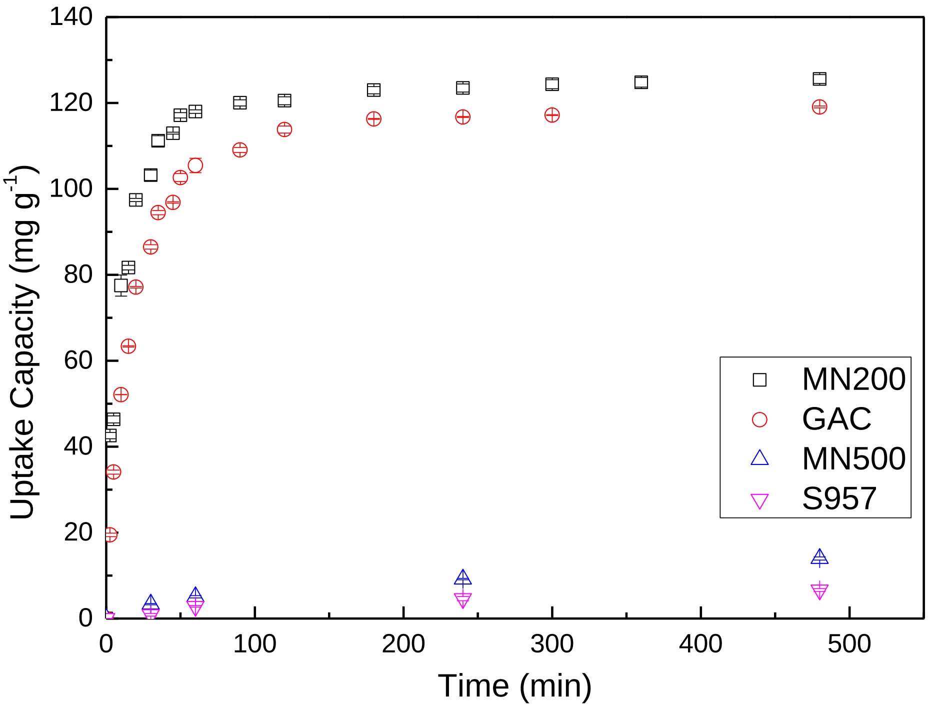

Figure 52 Uptake capacities for NB with time for MN200, GAC, MN500 and S957. Errors shown are for repeat runs (n = 2).

6.4.2 Kinetics of NB adsorption

The NB kinetic study focussed on only MN200 and GAC due to the poor uptake performances of MN500 and S957; the data obtained are presented in Figure 53 and the parameters obtained are summarised in Table 27. As outlined previously for the AN kinetic study, the kinetic data obtained were fitted using a pseudo-first order, a pseudo-second order and the Elovich models. The results demonstrate that a pseudo-second order model fits the data more closely for both sorbents. Adsorption of AN onto MN200 is known to involve two forces:1) van der Waals interactions and 2) the hydrophobic nature of the sorbent attracting the solute from bulk solution [170]. In contrast, NB adsorbed onto GAC experiences only π-π dispersive interactions between the aromatic rings of the basal planes of GAC and NB [165]. The kinetic data, shown in Table 27, indicate that k_2 for MN200 is approximately double that of GAC; suggesting adsorption is faster for MN200 compared to GAC. This difference may be due to the higher surface area of MN200, or possibly the formation of water clusters via hydrogen bonding to the surface functionalities of GAC, blocking solute from entering the pores [165].

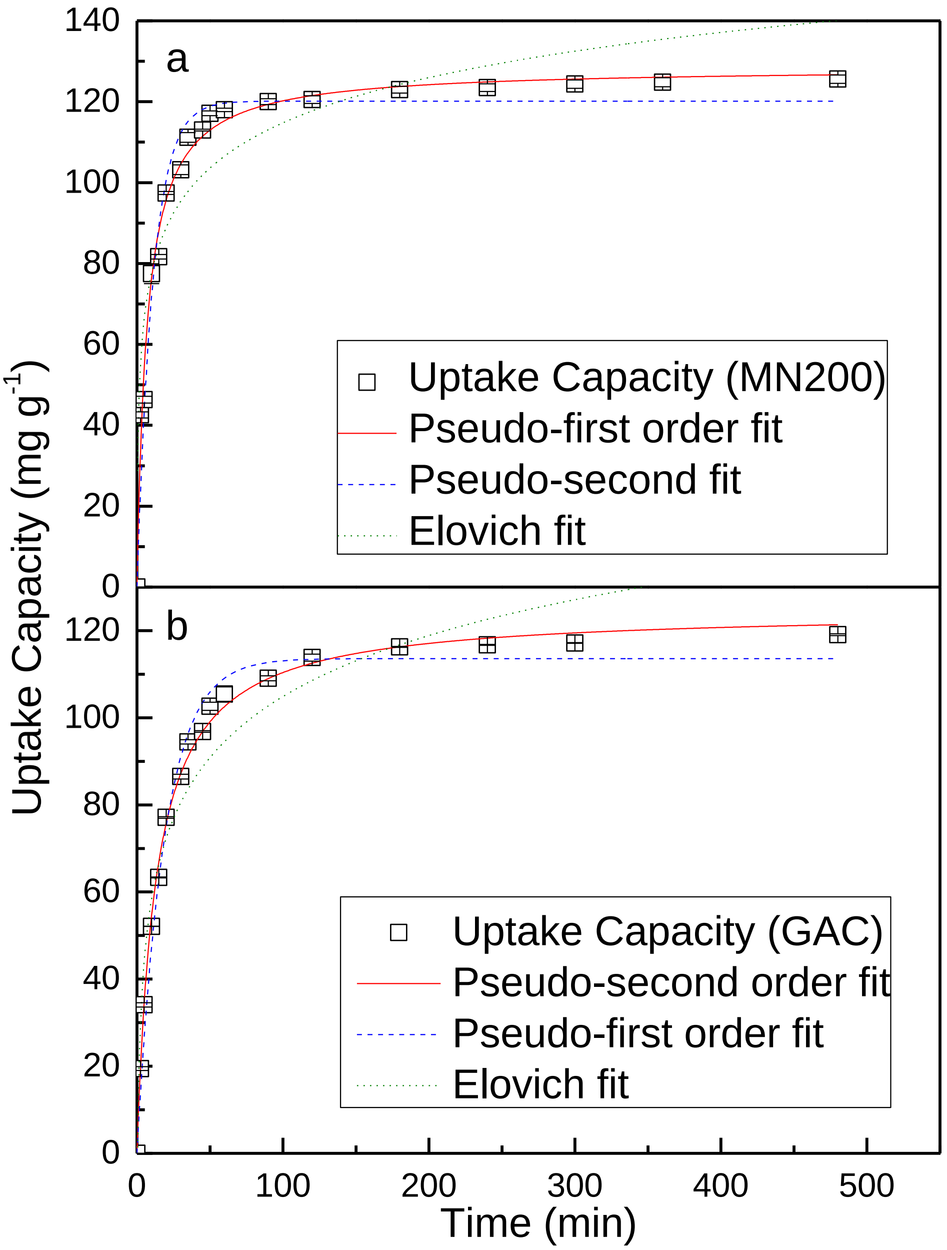

Figure 53 Kinetic data for NB adsorption, fitted using a pseudo-first order (dash line), a pseudo-second order (solid line) and the Elovich (dot line) models for (a) MN200 and (b) GAC. Errors shown are for repeat runs (n = 2).

Table 27 Kinetic parameters of MN200 and GAC fitted using a pseudo-first order, a pseudo-second order and the Elovich models

Model	MN200	GAC
Pseudo-first order		
q_e (mg g^{-1})	120.14	113.59
k_1 (min^{-1})	0.09	0.05
R^2	0.967	0.986
Pseudo-second order		
q_e (mg g^{-1})	128.46	124.61
k_2 (g mg^{-1} min^{-1})(x10^{-4})	11.3	6.22
R^2	0.988	0.996
Elovich		
a (mg g^{-1} min^{-1})	198.94	36.00
b (g mg $^{-1}$)	0.06	0.04
R^2	0.911	0.938

6.4.3 Determination of rate limiting step

In order to determine the rate limiting step of NB adsorption, the Homogeneous Particle Diffusion Model (HPDM) was applied [170] (Figure 54), with the results demonstrating that the particle diffusion regression provides a closer fit for both MN200 and GAC; hence, the adsorption rate is dominated by particle diffusion.

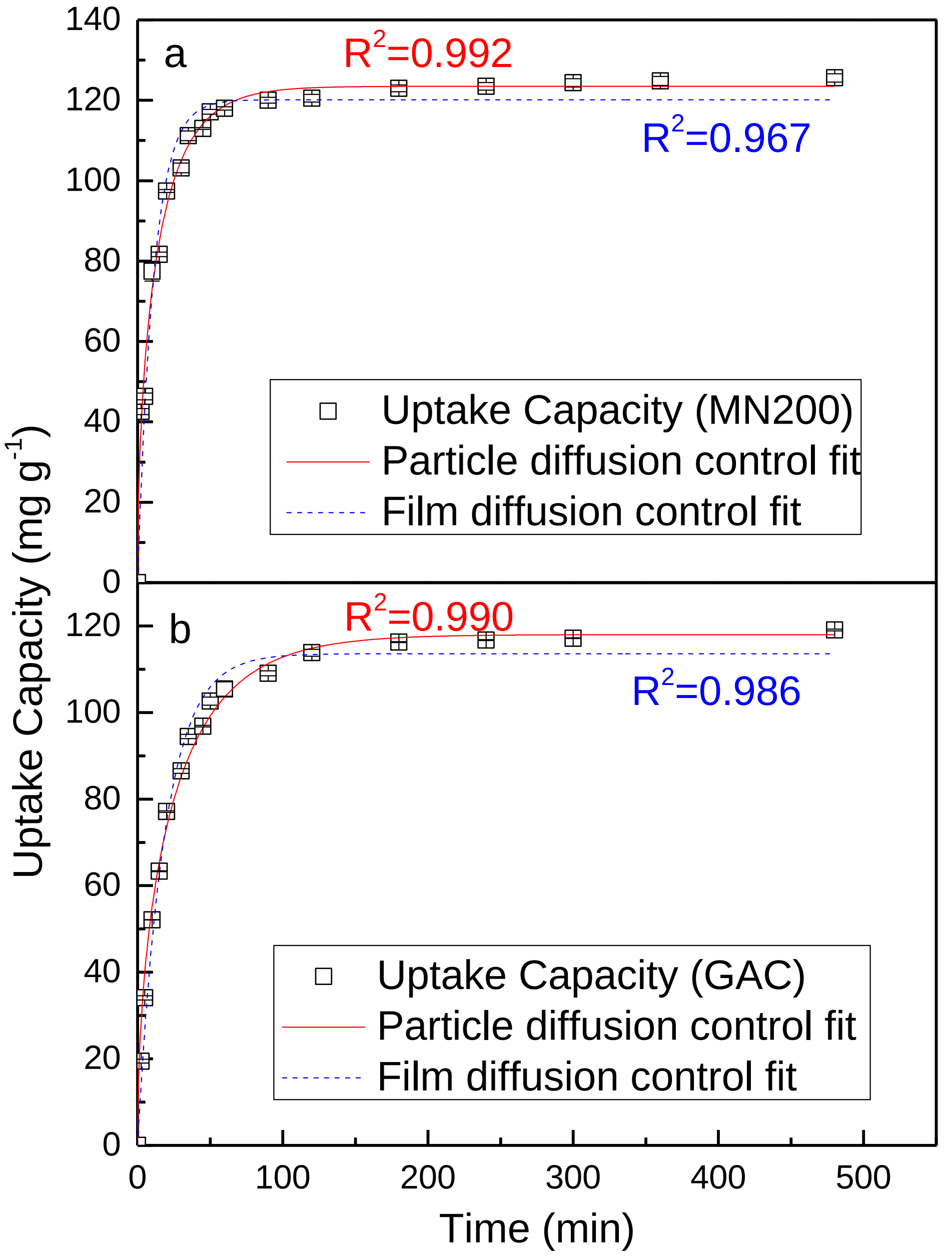

Figure 54 NB uptake capacities fitted using HPDM, showing particle diffusion (solid line) and film diffusion (dash line) control for (a) MN200 and (b) GAC. Errors shown are for repeat runs (n = 2).

In order to prove that the rate of adsorption is dominated by particle diffusion, the intraparticle diffusion model [170] was applied. From Figure 55, it can be observed that multi-linear lines are obtained for each plot and the slopes are reported in Table 28; hence, the rate of adsorption is limited by more than one step. The linear line obtained at short times is related to film diffusion, while the second slope represents intra-particle diffusion and the third slope, fitted to the longer time data, refers to micropore diffusion, which lasts until the equilibrium uptake capacity is reached [198]. From both plots, it is evident that film diffusion only occurs at the initial stages of the entire adsorption process; therefore, the rate is limited by particle diffusion for both MN200 and GAC.

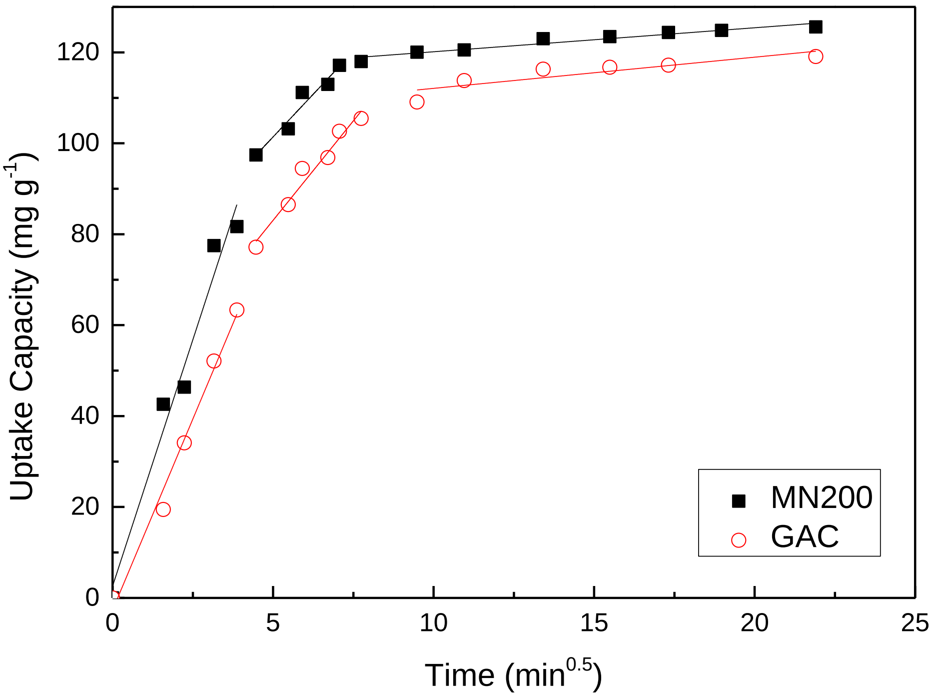

Figure 55 Kinetic fits of NB adsorption using intraparticle diffusion model for MN200 (filled square symbol) and GAC (empty circle symbol).

Table 28 Intraparticle diffusion rate constants for NB adsorption by MN200 and GAC

Adsorbent	k_{i1}	R^2	k_{i2}	R^2	k_{i3}	R^2
MN200	21.67	0.961	7.51	0.929	0.52	0.927
GAC	16.80	0.983	8.74	0.955	0.43	0.896

The intraparticle diffusion constants (k_{i1}, k_{i2}, k_{i3}) obtained from the slope of each linear line show that $k_{i1} > k_{i2} > k_{i3}$ for both MN200 and GAC. This trend indicates that the rate of NB adsorption is highest at the beginning of adsorption process and lowest in the final stages for both sorbents. The transport of solute from the solution to the surface of the sorbents is relatively fast, hence, k_{i1} is fastest rate for MN200 and GAC. k_{i2} refers to adsorption of solutes onto external surfaces, and k_{i3} is attributed to internal surface sorption processes within the sorbent particles and sorption equilibrium approach. Intraparticle diffusion is initiated by adsorption of solute on external adsorbent particle surfaces i.e. the macroporous structure; therefore, the rate is higher compared to the latter step. Once adsorption within the macropores reaches equilibrium, the molecules adsorb onto the internal surface of the particles before finally diffusing into the microporous structure. The final step exhibits an enhanced diffusion resistance, which contributes to a lower adsorption rate. This phenomenon has previously been discussed in detail in the literature [169, 170, 300]. Since rate is controlled by the migration of NB solutes from the bulk to the sorbent surface in the early stages of adsorption, hence, the overall rate of AN adsorption is limited by intraparticle diffusion.

6.4.4 Adsorption equilibria study

In order to understand the mechanism of NB adsorption, isotherms for both MN200 and GAC, again selected as a result of their superior capacities, were investigated in this study. The data obtained were fitted using Freundlich and Langmuir equations, as shown in Figure 56, and the parameters obtained are tabulated in Table 29. It was found that the Freundlich model fitted the data more accurately compared to the Langmuir model with better correlation coefficients, R^2, for both sorbents. The results obtained here demonstrate that the values of n, for both MN200 and GAC, are greater than 2, which suggests that NB adsorption is favourable. Moreover, since both n values for MN200 and GAC > 1, this indicates that adsorption of NB onto both sorbents is a physical process, which has implications for leaching from loaded sorbents. From Table 29, the value of K_f for MN200 is slightly higher than that for GAC, which suggests that the adsorption capacity of MN200 is higher than GAC. This may be due to hydrogen bonding of water onto the acidic functional groups forming clusters, which inhibit the sorption of NB molecules onto available adsorption sites. Further to this, the π-electron density of GAC is reduced as a result of acidic functional groups attracting π-electrons from the basal planes of the carbon structure; hence, interactions between π-electrons of GAC basal planes and the aromatic ring of NB are weakened, reducing the NB uptake capacity [200].

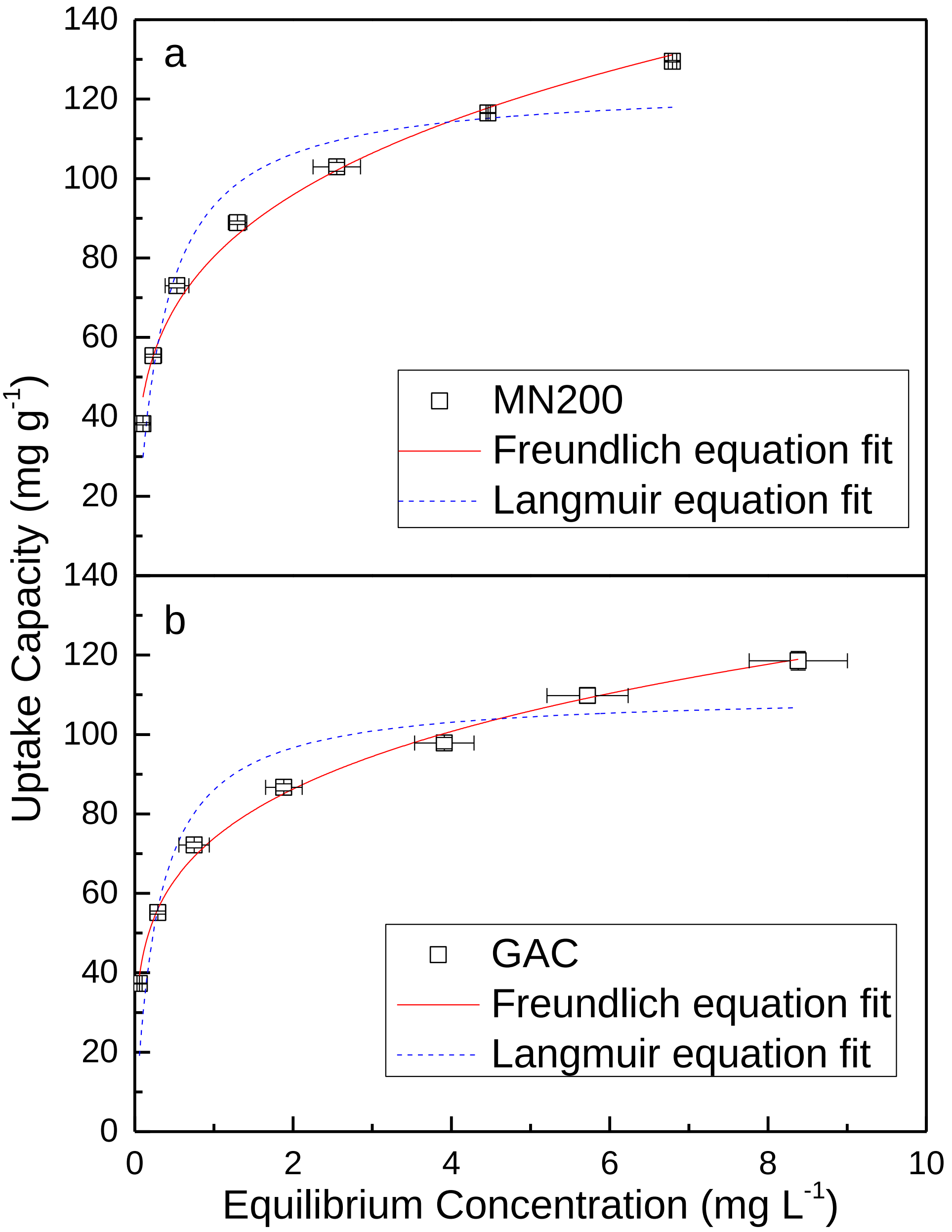

Figure 56 NB uptake capacities fitted using Freundlich (solid line) and Langmuir (dash line) equations for (a) MN200 and (b) GAC. Errors shown are for repeat runs (n = 2).

Table 29 Isotherm parameters obtained by fitting Freundlich and Langmuir equations to the data of NB adsorption onto MN200 and GAC

Adsorption isotherms	MN200	GAC
Freundlich		
K_f (mg g^{-1} (L $mg^{-1})^{1/n}$	80.315	73.852
n	3.906	4.462
R^2	0.985	0.994
Langmuir		
q_m (mg g^{-1})	123.611	110.341
K_L (L mg^{-1})	3.057	3.539
R^2	0.930	0.845

6.4.5 Leaching tendencies

As outlined for AN adsorption, for contaminants removal via sorption processes, it is vital to investigate the leaching tendencies of sorbents, even if the sorbents exhibit high uptake capacities and fast kinetics. In this study, leaching tendencies of MN200 and GAC were investigated by adding known amounts of pure deionised water to sorbents fully loaded with NB. The percentages of adsorbed NB leached from MN200 and GAC, as a function of time, determined using Equation 39, are shown in Figure 57. The results show that 29% of adsorbed NB is leached from MN200 after 80 h; while 25% of adsorbed NB is leached from GAC within the same time period. Furthermore, a higher leaching rate was observed in the initial stages, with 19% and 16% of NB leached in just 7 h from MN200 and GAC, respectively; the desorption rate decreased significantly after this point. The higher leaching rates found for MN200 compared to GAC may be due the wider pore sizes of the latter allowing easy loss of adsorbate.

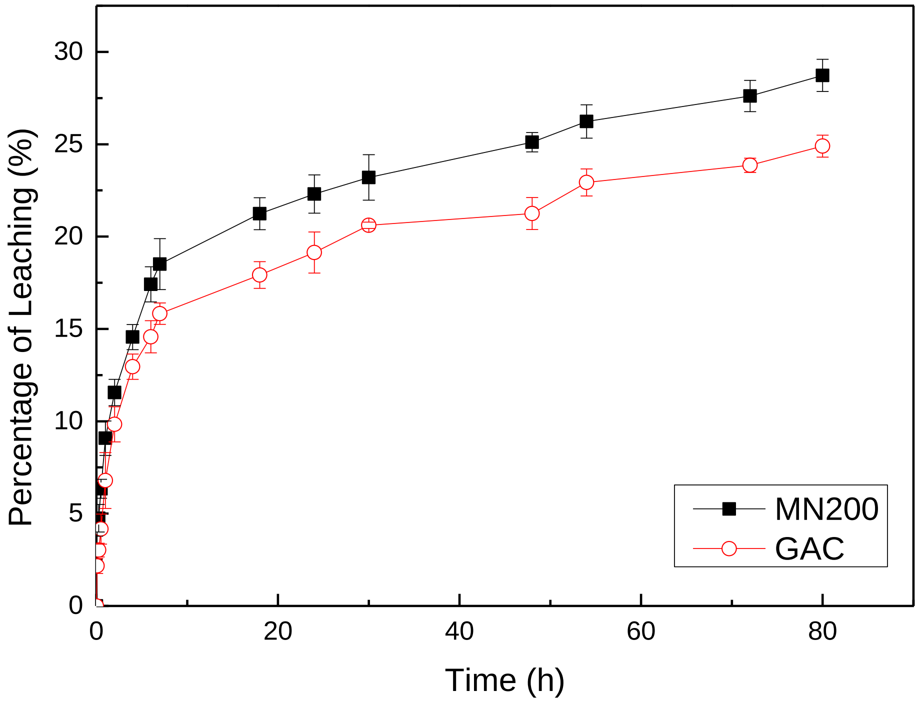

Figure 57 Percentage of adsorbed NB leached from MN200 (filled square) and GAC (empty circle). Errors shown are for repeat runs (n = 2).

CHAPTER 7

7.0 METHODS FOR AMELIORATION OF PARACETAMOL AND RELATED PRODUCTS

This chapter discusses the results of paracetamol and hydroquinone removal via adsorption; the kinetics, equilibria and leaching tendencies were studied. For both contaminants, polymeric resins and granular activated carbon were used and adsorption process variables determined.

7.1 Introduction

Paracetamol (PCT), also known as acetaminophen, is a widely used pharmaceutical and the resulting large consumption means that PCT is detected in water streams; hence, PCT removal from aqueous systems has been investigated intensively by the researchers. Methods adopted for remediation include Advanced Oxidation Processes (AOPs), which have shown promise; however, PCT degradation via Fenton oxidation yields a number of toxic intermediates, such as Hydroquinone (HQ), it is, therefore, unfavourable. Direct adsorption of PCT is, therefore, an alternative, which has been shown to successfully remove PCT at source, without the production of toxic intermediates. This study focusses on the removal of PCT and potential toxic Fenton oxidation intermediate HQ from water via adsorption. A simplified schematic diagram for the direct adsorption of PCT and HQ is shown in Figure 58.

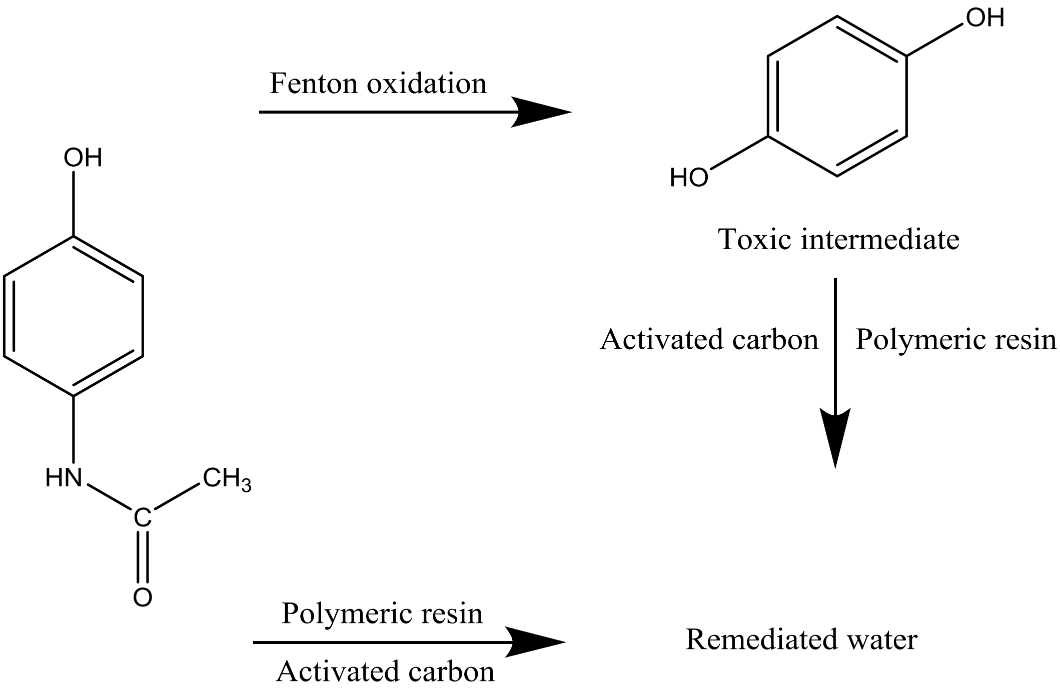

Figure 58 A simplified schematic diagram for PCT and HQ removal from aqueous systems via adsorption

7.2 Adsorption of HQ using polymeric resins and GAC

7.2.1 Quantification of HQ using GC-FID

In this study, the qualitative and quantitative analysis of HQ was conducted using GC-FID. A mixture of HQ and dimethyl phthalate (internal standard, IS) was injected and analysed by GC; the peaks of HQ and IS are observed at different retention times and HQ concentration can be determined from the peak area obtained at the appropriate retention time; the higher the concentration, the larger the area under the peak. A calibration curve was built by plotting the ratio of peak areas of HQ to IS against HQ concentration.

The peaks for HQ and IS were found at 5.1 min and 11.6 min, respectively (Figure 59). The peak areas of PCT and IS, as well as the resulting ratios are shown in Table 30 to 32. The HQ calibration curve is determined at higher concentrations (20, 40 and 80 mg L^{-1}) compared to NB and AN due to the small peak areas for HQ at low concentrations.

Figure 59 Chromatogram of HQ (retention time: 5.1 min) and dimethyl phthalate (retention time: 11.6 min) with 80 mg L^{-1} of HQ and 25 mg L^{-1} of dimethyl phthalate(IS)

Table 30 Peak areas of 20 mg L^{-1} HQ and 25 mg L^{-1} dimethyl phthalate, and resulting ratios

Number of run	Peak area of HQ	Peak area of dimethyl phthalate (IS)	Ratio (HQ : IS)
1	18464	60120	0.3074
2	17005	58379	0.2913
3	17094	57364	0.2980
Average	17521	58621	0.2989

Table 31 Peak areas of 40 mg L^{-1} HQ and 25 mg L^{-1} dimethyl phthalate, and resulting ratios

Number of run	Peak area of HQ	Peak area of dimethyl phthalate (IS)	Ratio (HQ : IS)
1	48501	59628	0.8134
2	38382	54983	0.7022
3	43770	55624	0.7869
Average	43551	56745	0.7675

Table 32 Peak areas of 80 mg L^{-1} HQ and 25 mg L^{-1} dimethyl phthalate, and resulting ratios

Number of run	Peak area of HQ	Peak area of dimethyl phthalate (IS)	Ratio (HQ : IS)
1	102212	51704	1.9534
2	82765	48933	1.6914
3	85611	49867	1.7168
Average	90196	50468	1.7872

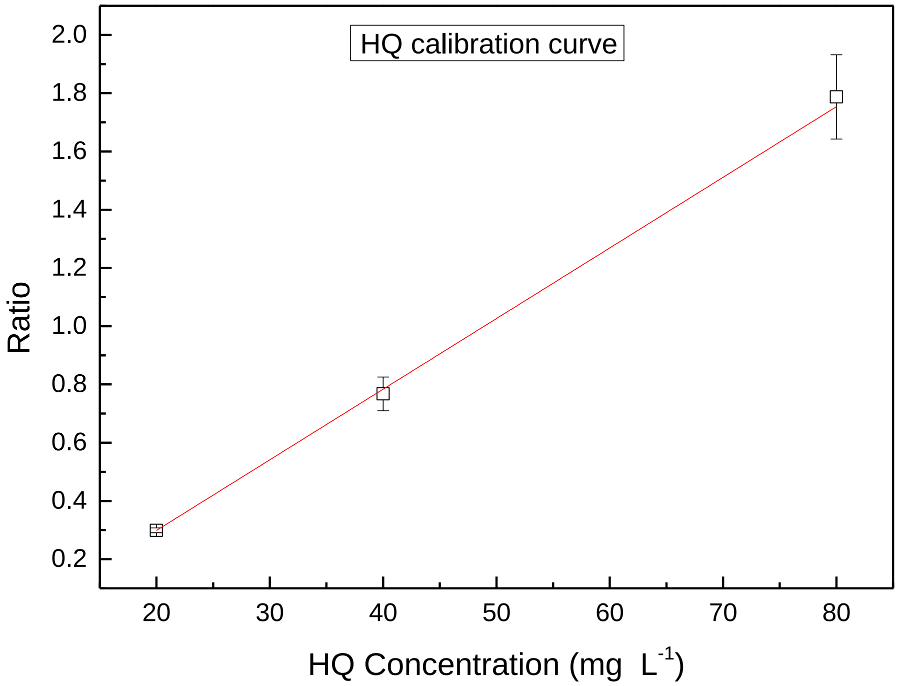

Figure 60 HQ calibration curve. Errors shown are for repeat runs (n = 3).

Ratios were determined by dividing the peak area for HQ by the peak area for dimethyl phthalate. Figure 60, shows the data to fit a linear line with $R^2 > 0.99$ of equation, peak area ratio = 0.02425 [HQ] -0.18633.

Hence, HQ concentrations were quantified by using the peak area ratio obtained for an unknown concentration of HQ in the formula determined from the calibration plot.

For example, if the ratio of peak areas of HQ to IS is 1.4283:

Peak area ratio = 1.4283 = 0.02425 [HQ] -0.18633 rearranging and evaluating gives [HQ] = 66.5827. Hence, the concentration of HQ is 66.5827 mg L^{-1}, and this method was employed to calculate all HQ concentrations determined in this study.

7.2.2 Equilibrium uptake capacities of HQ onto polymeric resins and GAC

HQ removal from water via adsorption, onto non – functionalised hyper-cross-linked Macronet MN200, GAC, acidic functionalised polystyrene cross-linked divinylbenzene MN500 and S957, was investigated with time, and the results obtained are shown in Figure 61. Low HQ uptakes are observed for MN500 and S957; due to the presence of repulsive forces between the acidic functional groups of the sorbents with the acidic hydroxyl groups of the HQ molecules. In contrast, higher uptakes were observed for MN200 and GAC, which had equilibrium uptake capacities of 80.1 mg g^{-1} (120 min) and 52.1 mg g^{-1} (120 min), respectively.

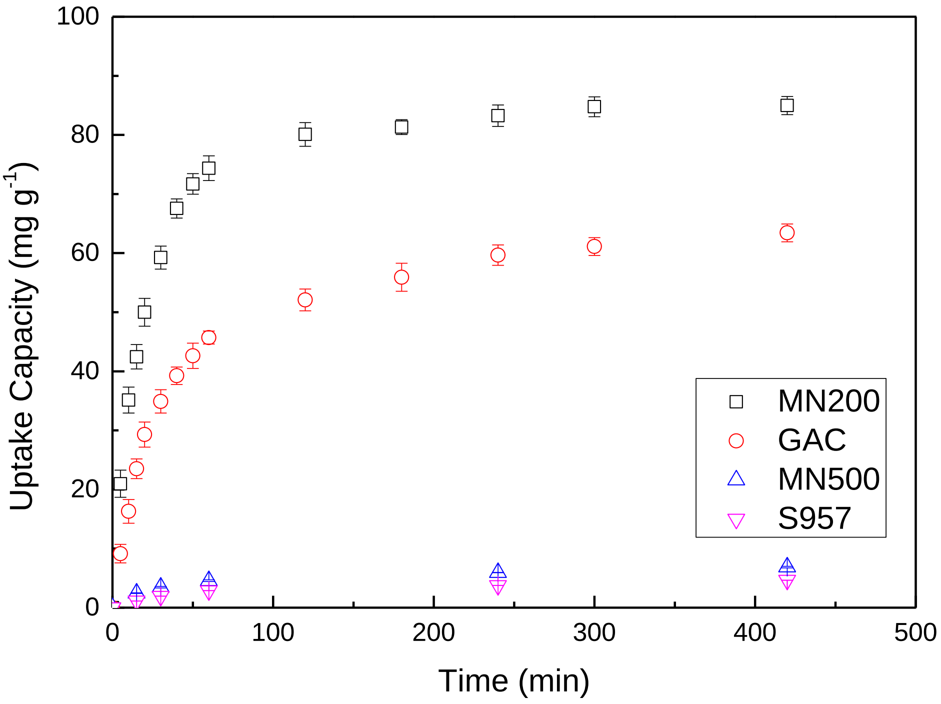

Figure 61 Uptake capacity of HQ with time for MN200, GAC, MN500 and S957 (initial concentration 40 mg L^{-1}). Errors shown are for repeat runs (n = 2).

7.2.3 Kinetics of HQ adsorption

To investigate the kinetics of adsorption, this study focussed on HQ removal using macroporous polymeric resin MN200 and microporous GAC, due to the low uptakes for macroporous MN500 and S957. Pseudo-first order, pseudo-second order and Elovich models (Figure 62) were applied to determine the kinetics of HQ sorption and the results demonstrate that the adsorption of HQ can be most closely described using a pseudo-second order equation for both sorbents (Table 33). The interactions involved in adsorption on the different sorbents are varied. The adsorption of aromatics onto MN200 will involve van der Waals forces and the hydrophobicity of the sorbent will drive solute molecules from the aqueous system to the surface of the sorbent [170]. In contrast, adsorption of aromatic compounds onto GAC is driven by dispersion forces between HQ benzene ring π-electrons and the basal planes of GAC [104, 170, 266], as well as hydrogen bonding [104, 116]; electrostatic repulsive and attractive forces, which may contribute if ions are present [170].

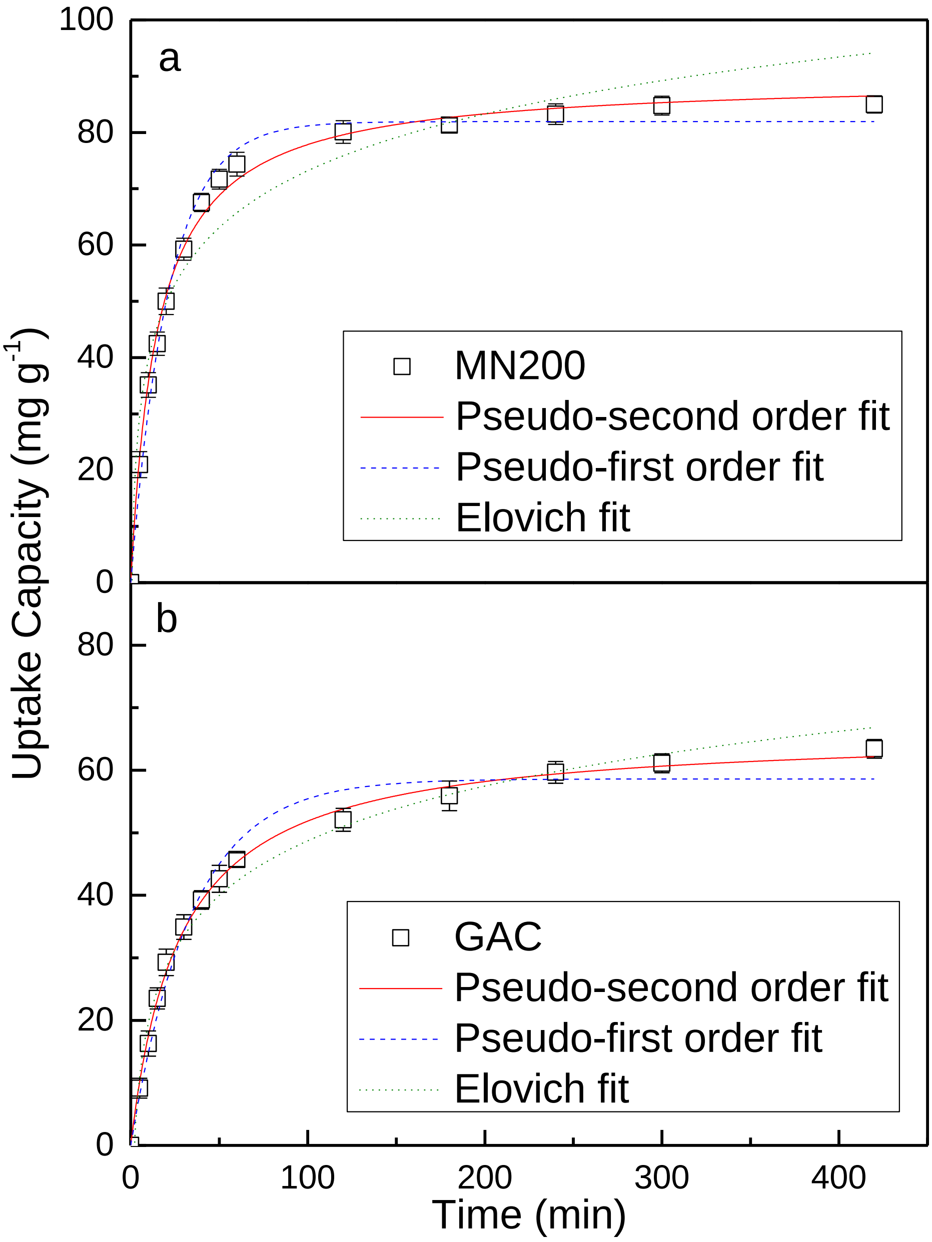

Figure 62 Kinetic data for HQ adsorption, fitted using a pseudo-first order (dash line), a pseudo-second order (solid line) and Elovich (dot line) models for (a) MN200 and (b) GAC. Errors shown are for repeat runs (n = 2).

Table 33 Kinetic parameters of MN200 and GAC fitted using a pseudo-first order, a pseudo-second order and Elovich models

Adsorbent	MN200	GAC
Pseudo-first order		
q_e (mg g^{-1})	82.53	58.66
k_1 (min^{-1})	0.04	0.03
R^2	0.990	0.979
Pseudo-second order		
q_e (mg g^{-1})	90.25	66.34
k_2 (g mg^{-1} min^{-1})(x10^{-4})	7.22	5.37
R^2	0.996	0.996
Elovich		
a (mg g^{-1} min^{-1})	21.69	0.08
b (g mg^{-1})	0.07	0.08
R^2	0.946	0.987

It was found that equilibrium HQ uptake is predicted to be higher for MN200 compared to GAC (Table 33), which may be due to its higher surface area, providing more active sorption sites for HQ molecules. Furthermore, MN200 exhibits faster adsorption rates compared to GAC, indicating that HQ adsorption is hindered by increased acidic group functionalisation of the sorbent. Formation of water cluster networks via hydrogen bonding between sorbent acidic functionalities and water molecules is thought to prevent HQ molecules from entering the sorbent microporosity [301], additionally reducing HQ uptake for the acid functionalised sorbent despite the relatively large surface area. The presence of oxygen containing functional groups on GAC is considered to reduce the electron density of the basal planes, hence, weakening the π-π dispersive interactions between the adsorbate and sorbent [266].

7.2.4 Determination of rate limiting step

To further investigate the mechanism involved in HQ uptake, the Homogeneous Particle Diffusion Model (HPDM) was applied to determine the rate limiting step [170], with the overall rates of HQ adsorption onto both MN200 and GAC found to be limited by particle diffusion (Figure 63).

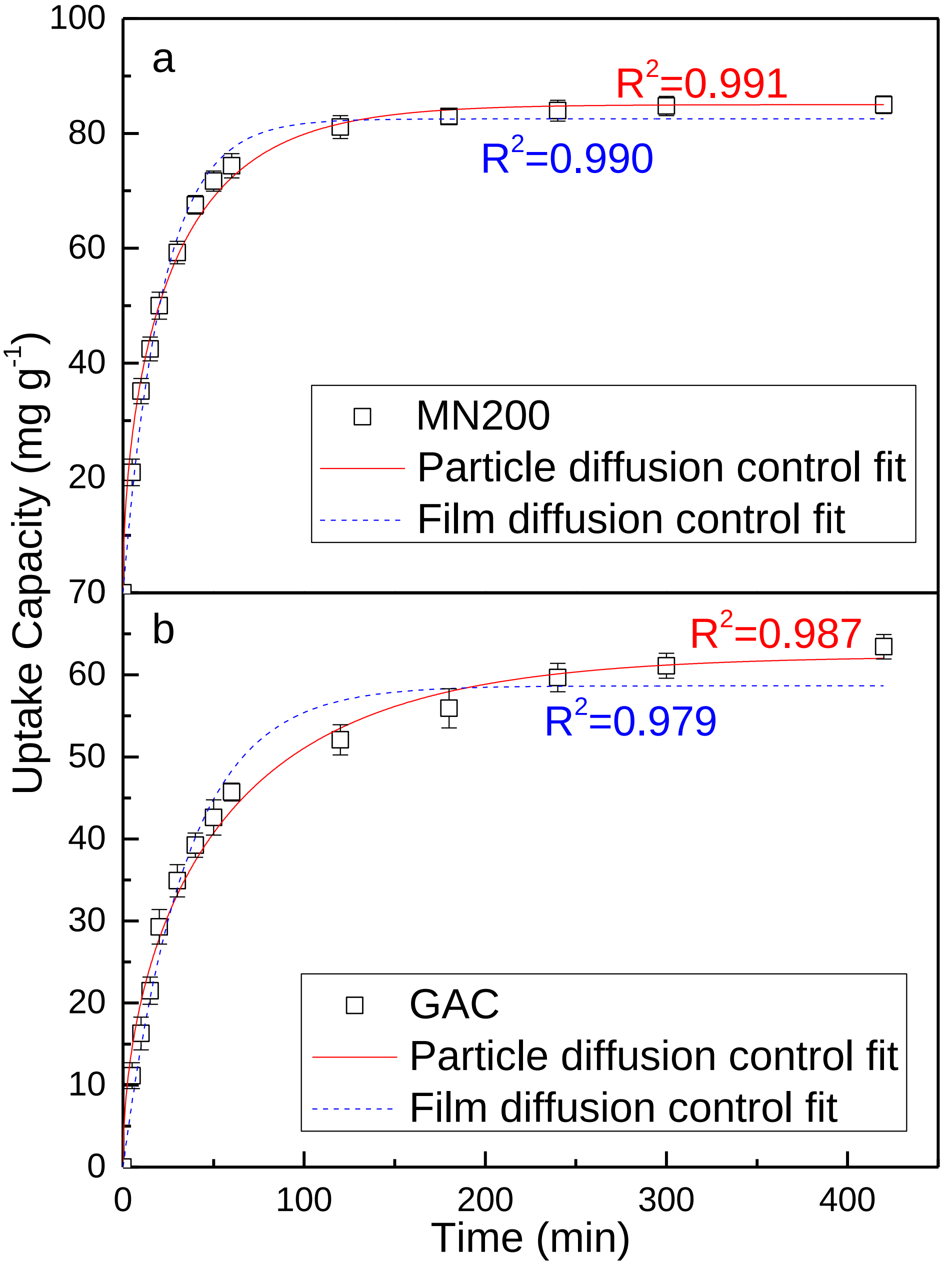

Figure 63 HQ uptake capacities fitted using HPDM, showing particle diffusion (solid line) and film diffusion (dash line) control for (a) MN200 and (b) GAC, Errors shown are for repeat runs (n = 2).

An intraparticle diffusion model [170] (Figure 64) was adopted to further confirm HQ adsorption is dominated by particle diffusion. It was found that there was more than one slope for both sorbents, indicating that rates of HQ adsorption were governed by multi-steps (Table 34). The first linear slopes represent film diffusion, while the second linear slopes indicate particle diffusion and the third slopes represent diffusion of solutes into the micropores of the sorbent [282]. Film diffusion occurs relatively quickly (initial stages of adsorption); hence, the rate of HQ adsorption onto both sorbents was controlled by particle diffusion. Moreover, the rate of HQ uptake can be indicated by the value of the slope, which increases with rate. Since the migration of HQ molecules to the external surface of the sorbent from bulk solution happens very quickly, this provides the highest rate for both MN200 and GAC. The values of k_{i2} are found to be lower than k_{i1} representing slower rates for diffusion of HQ molecules into macro- and mesoporosity for both sorbents. Furthermore, the diffusional resistance increased when the molecules diffused into the microporosity providing the lowest diffusion rate (k_{i3} values).

Table 34 Intraparticle diffusional rate constants for HQ adsorption by MN200 and GAC

Adsorbent	k_{i1}	R^2	k_{i2}	R^2	k_{i3}	R^2
MN200	11.11	0.993	4.80	0.981	0.41	0.845
GAC	5.44	0.991	5.00	0.997	1.20	0.940

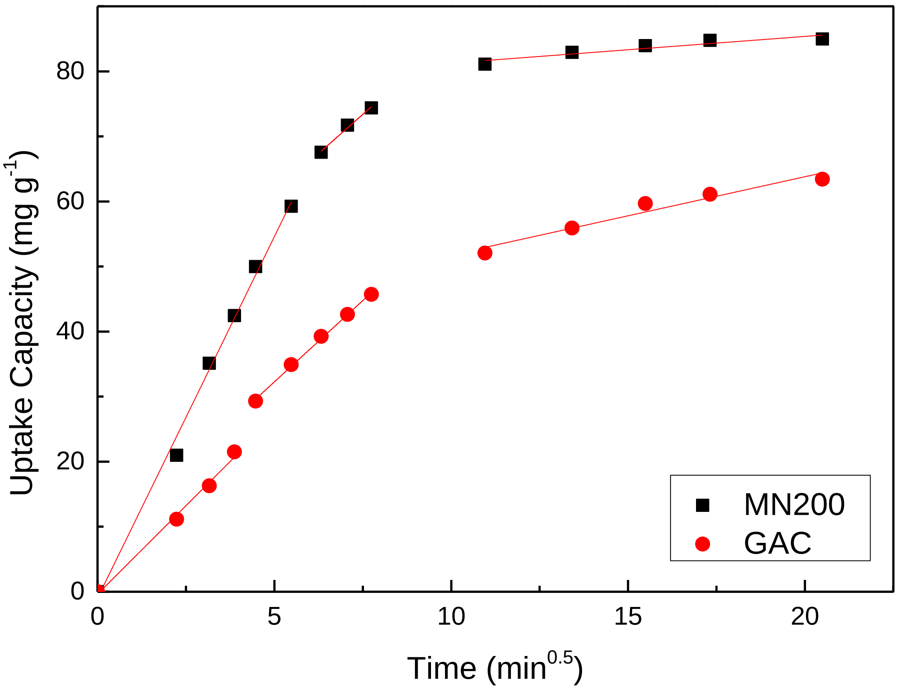

Figure 64 Intraparticle diffusional kinetic fits for HQ adsorption by MN200 (squares) and GAC (circles). Errors shown are for repeat runs (n = 2).

7.2.5 Adsorption equilibria study

To further understand the mechanism of HQ uptake by MN200 and GAC, the Freundlich and Langmuir models were applied to the equilibria data obtained, with the parameters obtained shown in Table 35. The results (Figure 65) demonstrate that the Freundlich equation fitted the data more closely (higher R^2 values) for both sorbents, compared to Langmuir regression. The Freundlich adsorption constant, K_F, gives an indication of adsorption capacity, i.e. the higher K_F , the higher the capacity [282]. It can be seen that K_F is higher for MN200 than GAC, hence, the HQ uptake is expected to be higher for MN200, which is consistent with the kinetic studies, and may due to the formation of cluster networks between water molecules and acidic functionalised GAC preventing the HQ molecules from entering the inner pores. Additionally, the acidic functional groups of GAC may attract π-electrons from the GAC basal planes, which reduces the π-electron density of GAC. As a result, the interactions between π-electrons of HQ benzene rings and GAC basal planes are weakened [200]. The value of n indicates adsorption favourability; and the results obtained here show that the values of n, for both sorbents, are greater than 1, indicating that HQ adsorption onto MN200 and GAC is a physical process. In addition, since both n values are between 1 and 2, this suggests that HQ adsorption is moderately favourable for both sorbents.

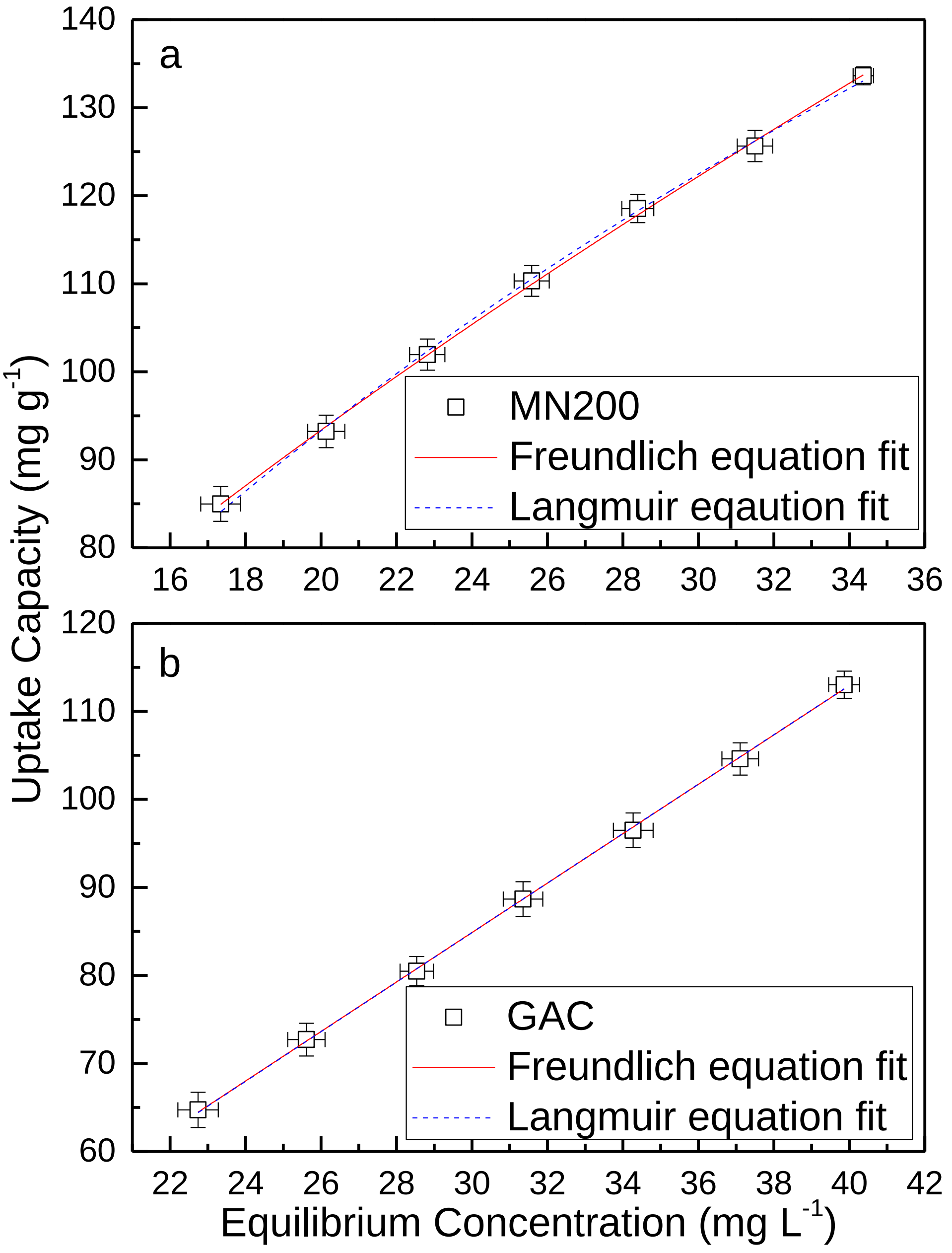

Figure 65 HQ uptake capacities fitted using Freundlich (solid line) and Langmuir (dash line) equations for (a) MN200 and (b) GAC. Errors shown are for repeat runs (n = 2).

Table 35 Isothermal parameters obtained by fitting Freundlich and Langmuir equations to the data of HQ adsorption onto MN200 and GAC

Adsorbent	MN200	GAC
Freundlich		
K_f (mg g^{-1} (L $mg^{-1})^{1/n}$	12.79	2.90
n	1.51	1.01
R^2	0.9991	0.9996
Langmuir		
q_m (mg g^{-1})	326.66	14692.83
K_L (L mg^{-1}) ($x10^{-4}$)	199.9	1.93
R^2	0.9987	0.9995

7.2.6 Leaching tendencies

Experiments to probe the leaching tendencies of the best performing sorbents were conducted by adding deionised water to fully HQ loaded sorbent particles and the results (Figure 66) demonstrate that 29% and 26% of HQ was leached from M200 and GAC, respectively, over 80 h. More HQ was observed to leach from MN200 as it is easier for the molecules to leach from the wider macroporosity of this sorbent than the predominantly mesoporous GAC. Furthermore, it was found that the leaching rates for both sorbents were higher in the initial stages (first 7 h) during which time 19% and 16% of HQ was leached from MN200 and GAC, respectively; after which the leaching rates for both sorbents reduced dramatically.

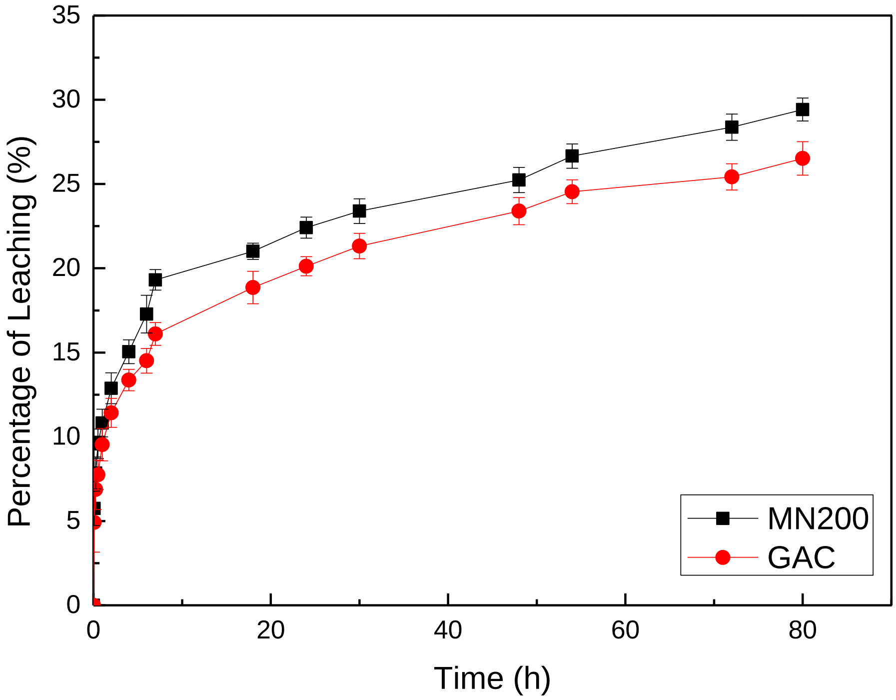

Figure 66 Percentage of adsorbed HQ leached from MN200 and GAC. Errors shown are for repeat runs (n = 2).

7.3 Adsorption of PCT using polymeric resins and GAC

7.3.1 Quantification of PCT using Gas Chromatography – Flame Ionisation Detection (GC-FID)

PCT can be analysed qualitatively, providing the retention time, and quantitatively, giving information relating to concentration, both using GC-FID. The area under the peak obtained at the retention time corresponding to PCT indicates the relative concentration, and peak area increases with PCT concentration. For GC analysis, an aliquot, containing a mixture of PCT solution and dimethyl phthalate (internal standard, IS) in equal volumes, is injected to GC- FID, allowing a PCT calibration curve to be developed by analysing solutions containing different PCT concentrations. In Chapter 4, a calibration curve for nitrobenzene (NB) and aniline (AN) were determined at 10, 20 and 40 mg L^{-1}; however, due to the very small peak area for 10 mg L^{-1} PCT, which is difficult to detect, the calibration curve for PCT was determined at 20, 40 and 80 mg L^{-1}.

The peaks for PCT and IS were found around 14.4 and 11.6 min, respectively (Figure 67); peak areas obtained for PCT and IS, as well as the resulting ratios are tabulated in Tables 36 to 38. It can be seen that the peak areas for PCT increase with concentration, as expected; which can be ascribed to the constant concentration of IS while the concentration of PCT, hence, the area obtained increased.

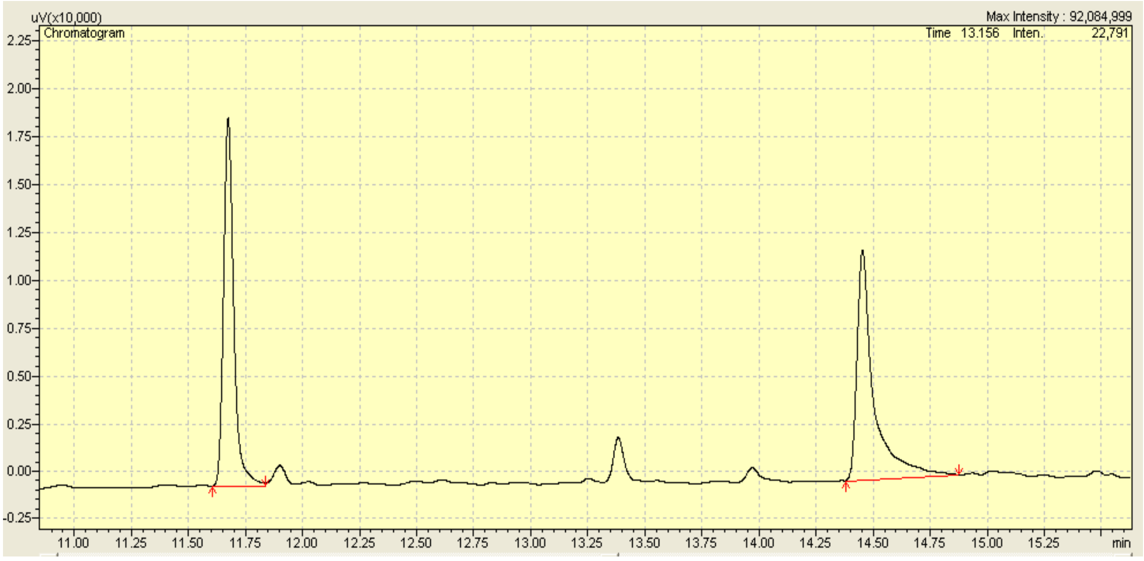

Figure 67 Chromatogram of PCT (retention time: 14.4 min) and IS (retention time: 11.6 min) with 80 mg L^{-1} of PCT and 25 mg L^{-1} of dimethyl phthalate (IS)

Table 36 Peak areas of 20 mg L^{-1} PCT and 25 mg L^{-1} dimethyl phthalate, and resultant ratios

Number of run	Peak area of PCT	Peak area of dimethyl phthalate (IS)	Ratio (PCT : IS)
1	15607	63574	0.2455
2	16175	64289	0.2516
3	13446	60675	0.2226
Average	15076	62846	0.2399

Table 37 Peak areas of 40 mg L^{-1} PCT and 25 mg L^{-1} dimethyl phthalate, and resultant ratios

Number of run	Peak area of PCT	Peak area of dimethyl phthalate (IS)	Ratio (PCT : IS)
1	32487	66681	0.4872
2	30348	61986	0.4896
3	31524	62577	0.5034
Average	31453	63748	0.4934

Table 38 Peak areas of 80 mg L^{-1} PCT and 25 mg L^{-1} dimethyl phthalate, and resultant ratios

Number of run	Peak area of PCT	Peak area of dimethyl phthalate (IS)	Ratio (PCT : IS)
1	70507	67939	1.0378
2	71777	65341	1.0985
3	63969	64279	0.9957
Average	68751	65853	1.044

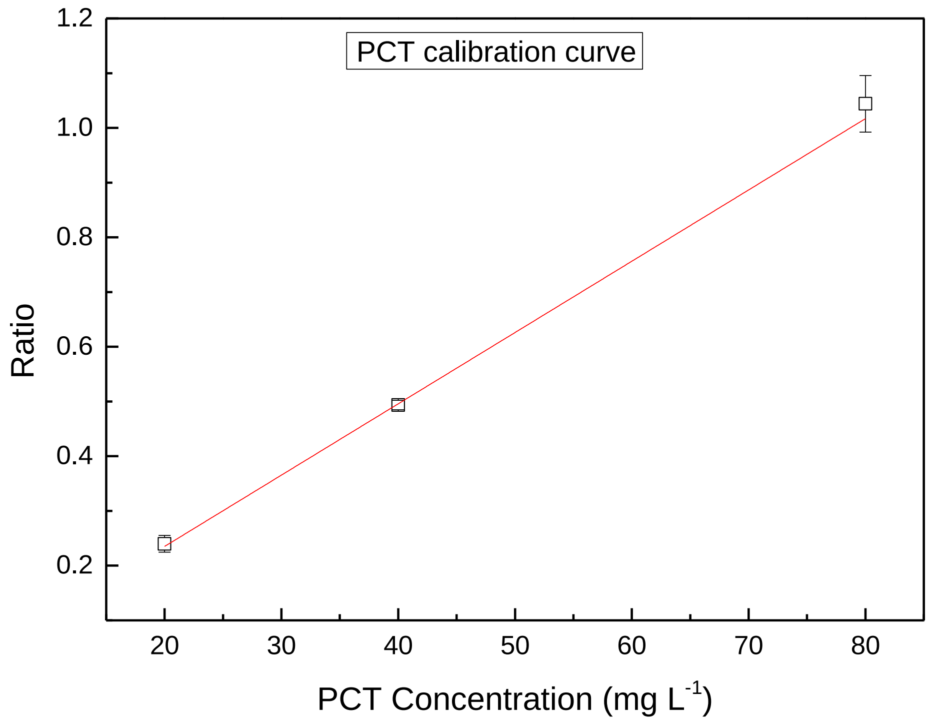

Figure 68 PCT calibration curve. Errors shown are for repeat runs (n = 3).

From the data presented in the tables above, peak area ratios can be calculated by dividing the peak area for PCT by the peak area for IS, hence, the calibration curve is developed by plotting the average peak area ratio of vs. PCT concentration. From Figure 68, it can be seen that the data fit a linear line with $R^2 > 0.99$ of equation peak area ratio = 0.01303 [PCT] -0.02542. Hence, PCT concentrations were quantified by using the peak area ratio obtained for an unknown concentration of PCT in the formula determined from the calibration plot.

For example, if the ratio of peak areas of PCT to IS is 0.7465:

Peak area ratio = 0.7465 = 0.01303 [PCT] -0.02542 rearranging and evaluating gives [PCT] = 59.2417. Hence, the concentration of PCT is 59.2417 mg L^{-1}, and this method was employed to calculate all PCT concentrations determined in this study.

7.3.2 Equilibrium uptake capacities of PCT onto polymeric resins and GAC

In this study, PCT is removed from aqueous systems via adsorption process using non – functionalised hyper-cross-linked Macronet MN200, GAC, acidic functionalised MN500 and S957. The PCT uptake profiles for MN200 (105.67 mg g^{-1}, 90 min), GAC (91.97 mg g^{-}1, 90 min),, MN500 (65.09 mg g^{-1}, 120 min) and S957 (56.47 mg g^{-1}, 120 min), are, shown in Figure 69.

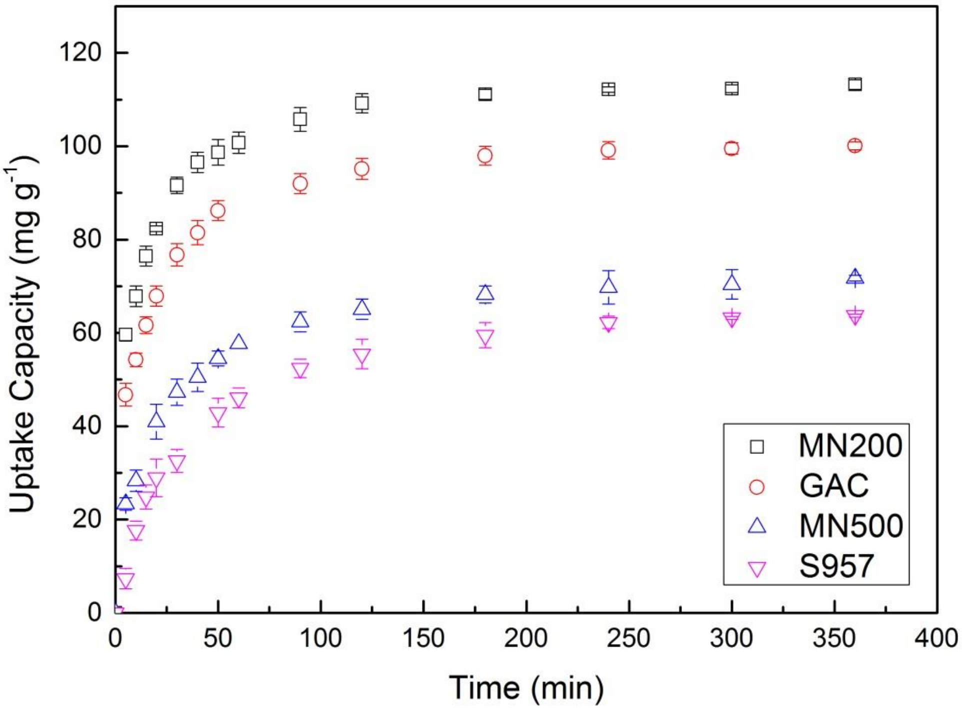

Figure 69 Uptake capacity of PCT with time for MN200, GAC, MN500 and S957 (initial concentration 40 mg L^{-1}). Errors shown are for repeat runs (n = 2).

7.3.3 Kinetics of PCT adsorption

A pseudo-first order, a pseudo-second order and the Elovich models were applied to study the kinetics of PCT adsorption onto MN200, GAC, MN500 and S957; the resulting kinetic fits, and the parameters obtained, are shown in Figures 70 and 71 and Table 39, respectively. Numerous studies have reported the removal of PCT from water via adsorption processes using different types of carbonaceous materials including commercial GAC [243, 252, 302], AC synthesised from sisal wastes [257] and biomass residues [245], with the kinetics described using either a pseudo-second order model [243, 257]. or, as in one case, a pseudo-first order model [258].

In this study, the PCT was successfully removed from aqueous systems using MN200, GAC, MN500 and S957 and a pseudo-second order equation more closely fitted the data obtained. The surface of GAC can be divided into several different categories, which are inorganic ash, acidic functionalised groups, such as carbonyl and carboxylic groups, and basal planes, which typically comprise ~90% of a carbons surface. Most aromatic molecules adsorb on the basal planes of a carbon based sorbent; however, heterogeneous acidic surface groups demonstrate higher chemical activity, which may also affect contaminant uptakes [164, 165]. Therefore, PCT adsorbing on to GAC will experience several different interactions, including dispersion forces between the π electrons of the graphene layers of GAC and the aromatic ring of PCT; as well as electrostatic repulsive or attractive forces if ions are present [170]. Furthermore, water adsorption via hydrogen bonding with the heterogeneous surface oxygen groups has also been observed during the adsorption of aromatic compounds onto carbons [164]. In contrast, the adsorption of aromatics onto MN200 will be thermodynamically gradient driven, due to the hydrophobicity of the sorbent that driving the solute from the bulk in conjunction with van der Waals forces [170].

The results obtained here demonstrate that MN200 had the highest PCT uptake capacity, due to its higher surface area; while S957 had the lowest. This indicates that PCT adsorption increases as the acidic capacity of the sorbent decreases, following the sequence: MN200 > GAC > MN500 > S957. A similar trend was found for the pseudo-second order rate constants, k_2 with the highest rate obtained for MN200 and the lowest for S957. Lower sorbent acidic capacities contribute to higher PCT uptakes and faster kinetics by inhibiting PCT solute from entering the micropores of the sorbent via formation of hydrogen-bonded water clusters on the acidic functionalities. Such phenomena have been found previously for adsorption of other aromatic compounds onto acidic functionalised sorbents [164, 165]. Additionally, the presence of oxygen containing functional groups, such as carbonyl, on AC surface will create repulsive forces between the AC surface and the carbonyl groups of PCT, reducing the uptake capacity [255]. In summary, the presence of acidic functional groups in sorbents will significantly affect contaminants removal, as observed for PCT removal here.

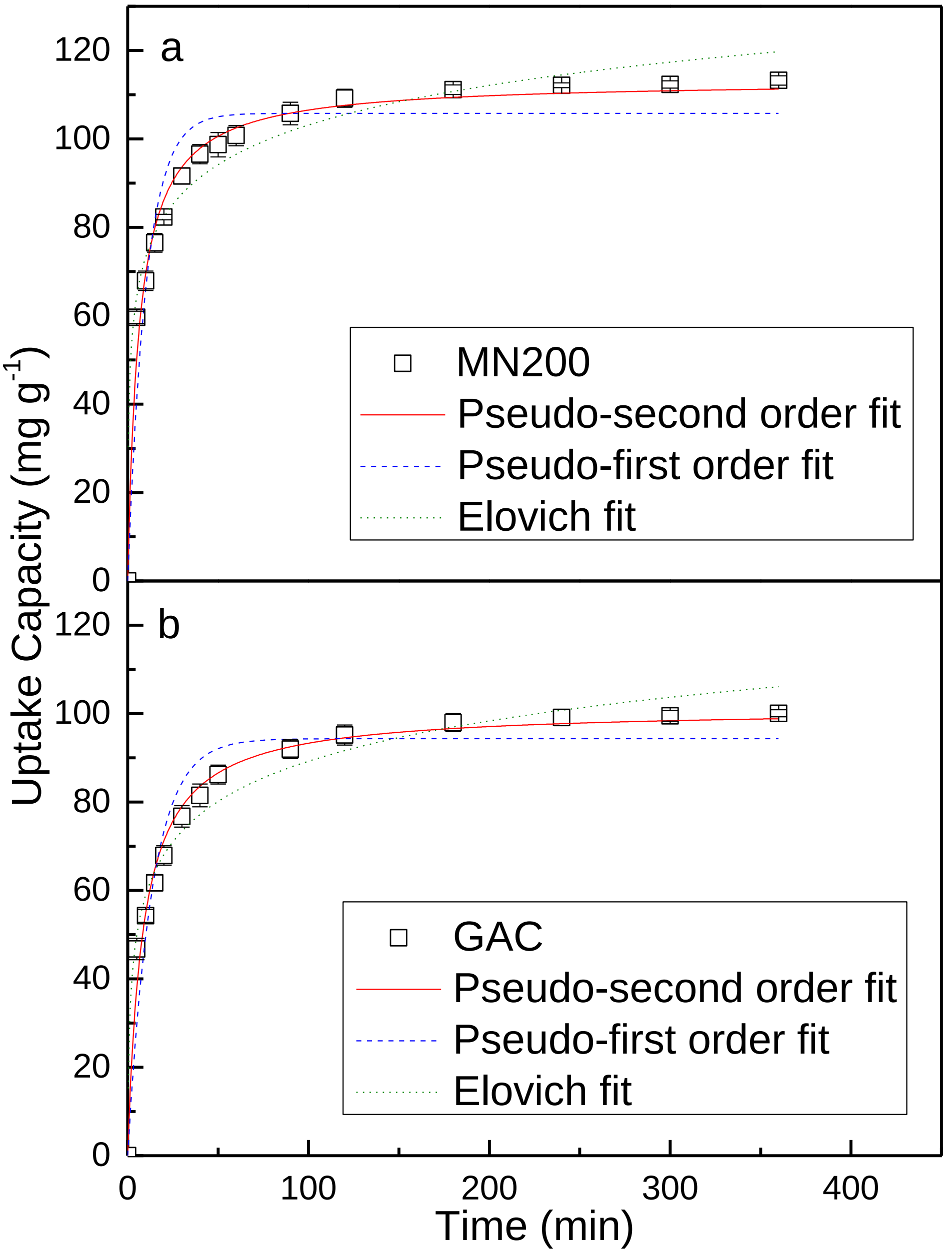

Figure 70 Kinetic data for PCT adsorption, fitted using a pseudo-first order (dash line), a pseudo-second order (solid line) and Elovich (dot line) models for (a) MN200 and (b) GAC. Errors shown are for repeat runs (n = 2).

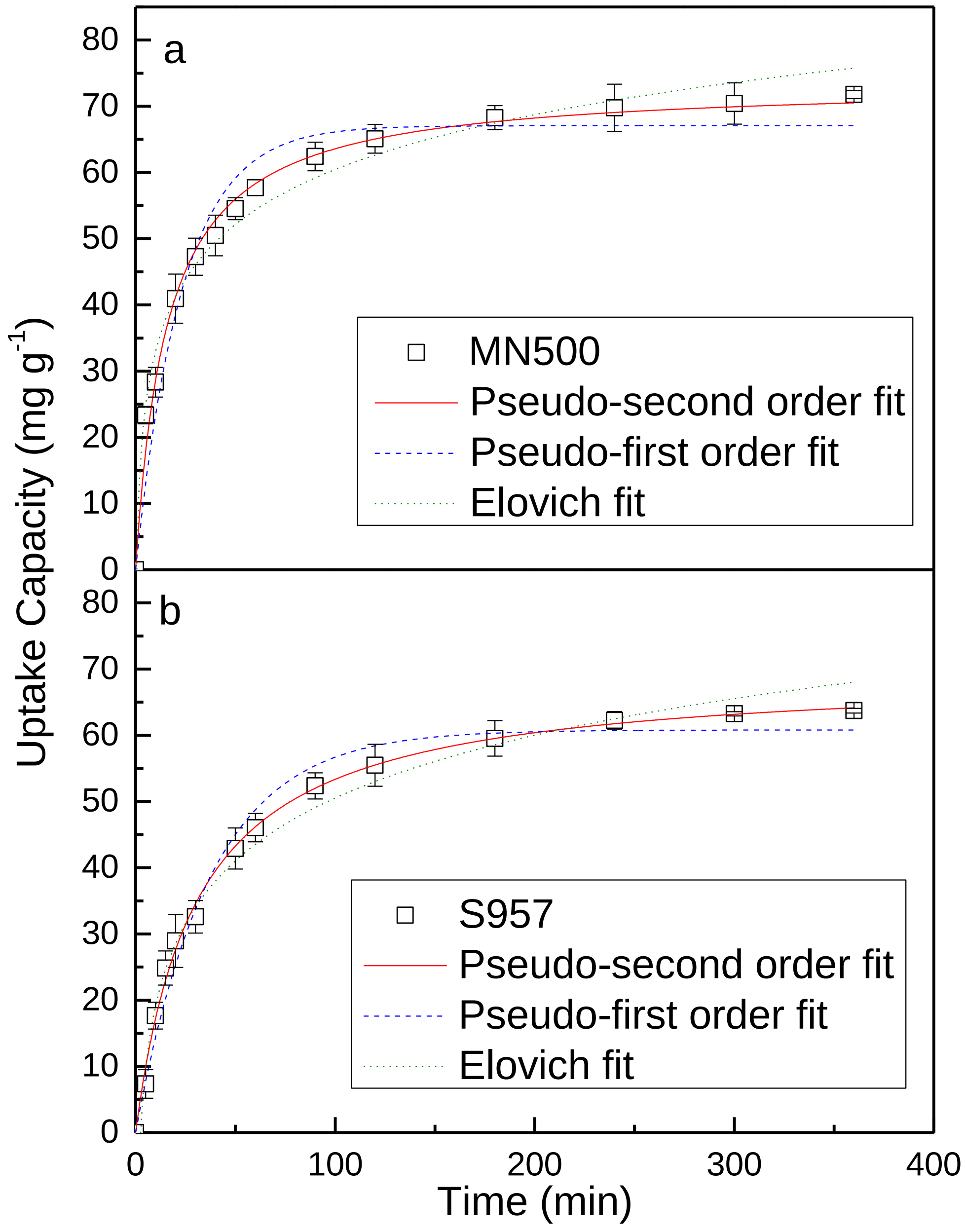

Figure 71 Kinetic data for PCT adsorption, fitted using a pseudo-first order (dash line), a pseudo-second order (solid line) and Elovich (dot line) models for (a) MN500 and (b) S957. Errors shown are for repeat runs (n = 2).

Table 39 Kinetic parameters of MN200, GAC, MN500 and S957 fitted using a pseudo-first order, a pseudo-second order and the Elovich models

Model	MN200	GAC	MN500	S957
Pseudo-first order				
q_e (mg g^{-1})	105.783	94.328	67.072	60.806
k_1 (min^{-1})	0.098	0.074	0.042	0.026
R^2	0.930	0.935	0.952	0.982
Pseudo-second order				
q_e (mg g^{-1})	113.215	101.155	73.595	69.572
k_2 (g mg^{-1} min^{-1})(x10^{-4})	14.1	11.7	8.629	4.728
R^2	0.987	0.987	0.991	0.997
Elovich				
a (mg g^{-1} min^{-1})	372.504	115.985	18.763	5.494
b (g mg $^{-1}$)	0.077	0.075	0.083	0.073
R^2	0.979	0.979	0.983	0.989

7.3.4 Determination of rate limiting step

In this study, the Homogeneous Particle Diffusion Model [170] was adopted to investigate the rate limiting step in PCT adsorption (Figures 72 and 73); previous studies have reported that PCT adsorption onto GAC is controlled by particle diffusion [243]. This is agreement with the observations in this study, as the particle diffusion control regression fitted the obtained data more closely, indicating that the overall rate of PCT adsorption was limited by particle diffusion for all sorbents.

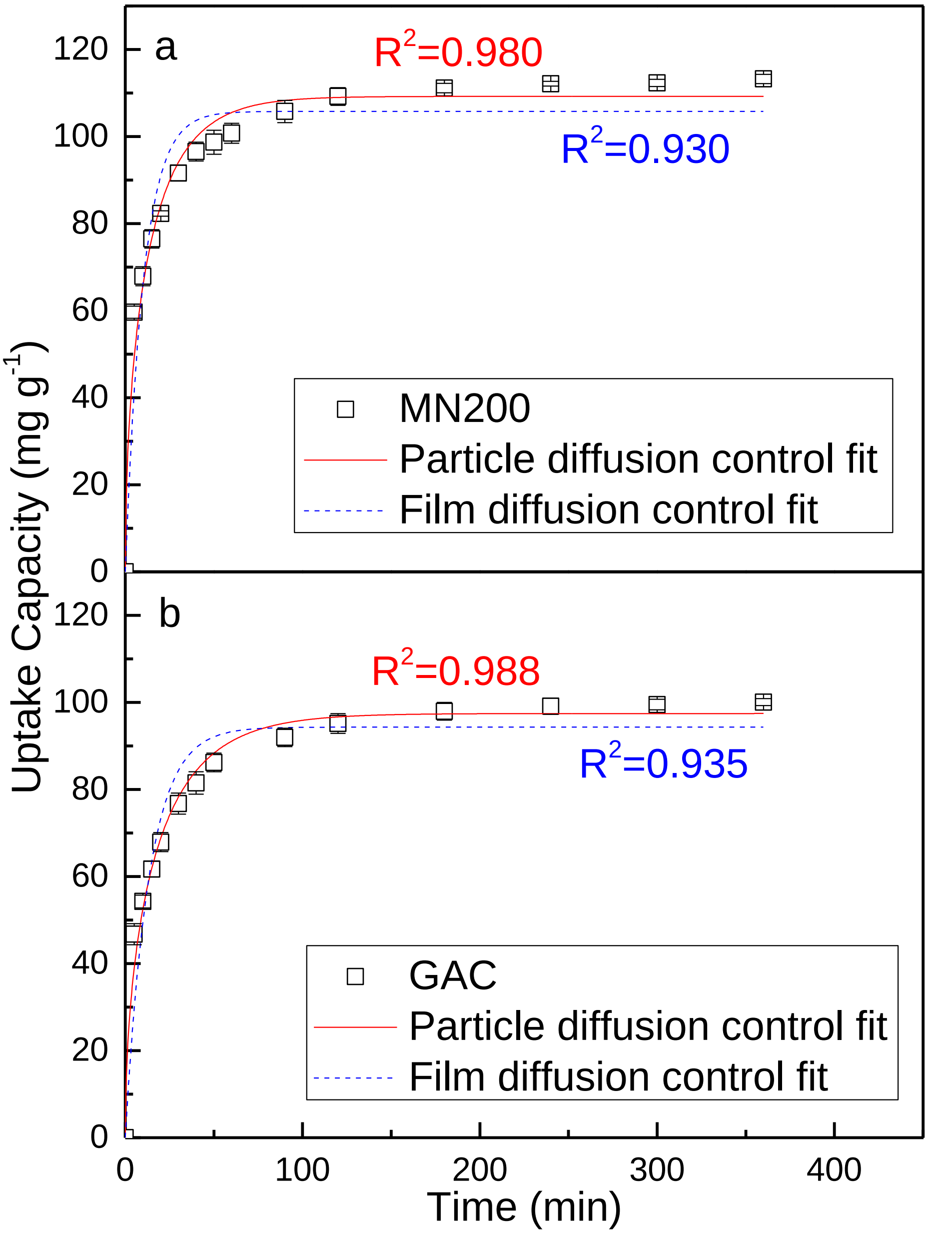

Figure 72 PCT uptake capacities fitted using HPDM, showing particle diffusion (solid line) and film diffusion (dash line) control for (a) MN200 and (b) GAC. Errors shown are for repeat runs (n = 2).

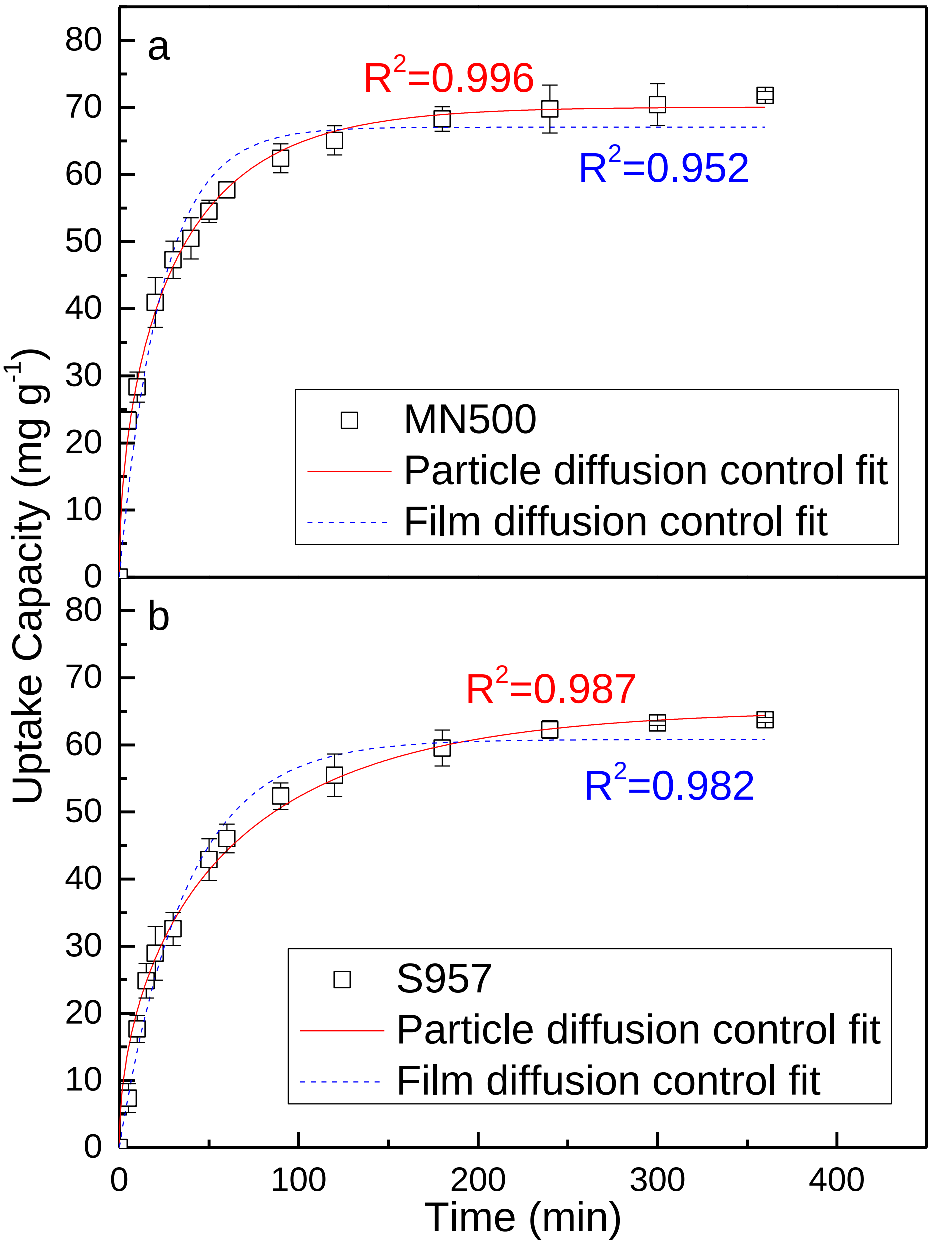

Figure 73 PCT uptake capacities fitted using HPDM, showing particle diffusion (solid line) and film diffusion (dash line) control for (a) MN500 and (b) S957. Errors shown are for repeat runs (n = 2).

In order to further confirm that PCT adsorption onto all sorbents is dominated by particle diffusion, the intraparticle diffusion model [170] was applied. From Figure 74, it can be seen that there are multi-linear sections for each plot, indicating that the rate of PCT uptake by each sorbent is limited by more than one step, and the parameters obtained are shown in Table 40. The value of the slope for each line represents the rate of PCT uptake, i.e. the rate is higher if the value of the slope is larger. The first slope, k_{i1}, for all sorbents, represents the initial step in sorption process, which is the diffusion of PCT molecules from the bulk into the external surface of the sorbent. This step happens relatively quickly providing the highest value of k_i for all systems. The second slope corresponds to intraparticle diffusion, and the adsorption of molecules in the macro and meso-sized pores; however, this step is slower than the first resulting in lower values of k_{i2} for all sorbents. The last slope, with the lowest values of k_{i3}, represents diffusion within the micropores of the sorbent until equilibrium is achieved; the associated increase in diffusional resistance contributes to a lower diffusion rate compared to the two previous steps. Although PCT adsorption rates are governed by multiple steps, film diffusion occurs very quickly (within 6 min), hence it can be concluded that the overall PCT uptake, by all sorbents, is controlled by particle diffusion. These trends have also been previously reported for PCT removal using AC [243].

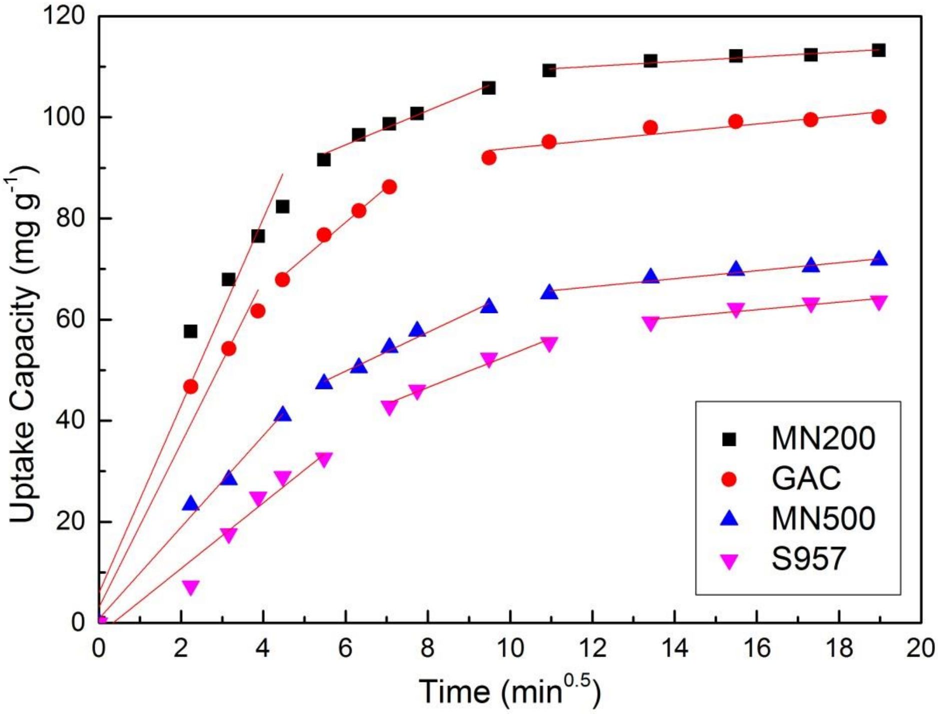

Figure 74 Kinetic fits of PCT adsorption using intraparticle diffusion model for MN200, GAC, MN500 and S957

Table 40 Intraparticle diffusion rate constants for PCT adsorption by MN200, GAC, MN500 and S957

Adsorbent	k_{i1}	R^2	k_{i2}	R^2	k_{i3}	R^2
MN200	18.52	0.940	3.38	0.964	0.47	0.923
GAC	16.20	0.947	6.94	0.983	0.80	0.846
MN500	9.05	0.987	3.85	0.971	0.78	0.940
S957	6.49	0.940	3.24	0.971	0.74	0.856

7.3.5 Adsorption equilibria study

Although the kinetics of PCT adsorption onto GAC and polymeric resins are known to be pseudo-second order, a detailed mechanism is not provided by the kinetic study. In order to further understand the mechanism of PCT removal by MN200, GAC, MN500 and S957, adsorption isotherms, for all sorbents, were analysed using the Freundlich and Langmuir models, which present the uptake capacity as a function of equilibrium concentration. Here, adsorption equilibrium studies were conducted at higher concentrations compared to NB and AN, in the range 40 to 75 mg L^{-1}, due to the small PCT peak at low concentration.

From Figures 75 and 76, both the Freundlich and Langmuir equations successfully describe the equilibria data obtained; however, Freundlich regression fitted the data more closely, providing higher R^2 values for all sorbents, with the parameters obtained shown in Table 41. Hence, the following discussions focus on the Freundlich model. The results demonstrate that the value of K_f is highest for MN200, followed by GAC, then MN500, and finally S957, indicating that uptake decreases as acidic functionality capacity increases, consistent with the kinetic study. This observation may be ascribed to the greater surface area of MN200 providing more active sites for sorption of PCT molecules; and the formation of hydrogen bonds between acidic functional groups and water molecules generating water clusters, which inhibit PCT solute from entering the microporosity of the sorbents [164]. It is also worth noting that previous studies have reported that increasing oxygen O content of AC by surface modification significantly reduces PCT uptake [243, 253], due to increased density of acidic carbonyl groups on AC surface increasing the repulsive forces with PCT molecules, decreasing PCT uptake [255]. Additionally, increased acidic functionalisation (MN200 < GAC < MN500 < S957) may also increase the repulsive forces between the sorbent surface and the weak acidic phenol of PCT, as a consequence of the electron withdrawing properties of the polar surface groups. Therefore, the presence of acidic functionalities significantly affects the removal of PCT from aqueous system, as observed in this study.

In addition, the results show that the values of *n* were greater than 1 for MN200, GAC, MN500 and S957, suggesting that PCT adsorption onto all sorbents is a physical process. Furthermore, the value of *n* indicates the favourability of adsorption; from Table 41, it can be seen that the values of *n* for MN500 and S957 were between 1 and 2, hence, sorption is moderately favourable for both sorbents. In contrast, the *n* values for MN200 and GAC were greater than 2 suggesting that PCT adsorption onto both sorbents is favourable.

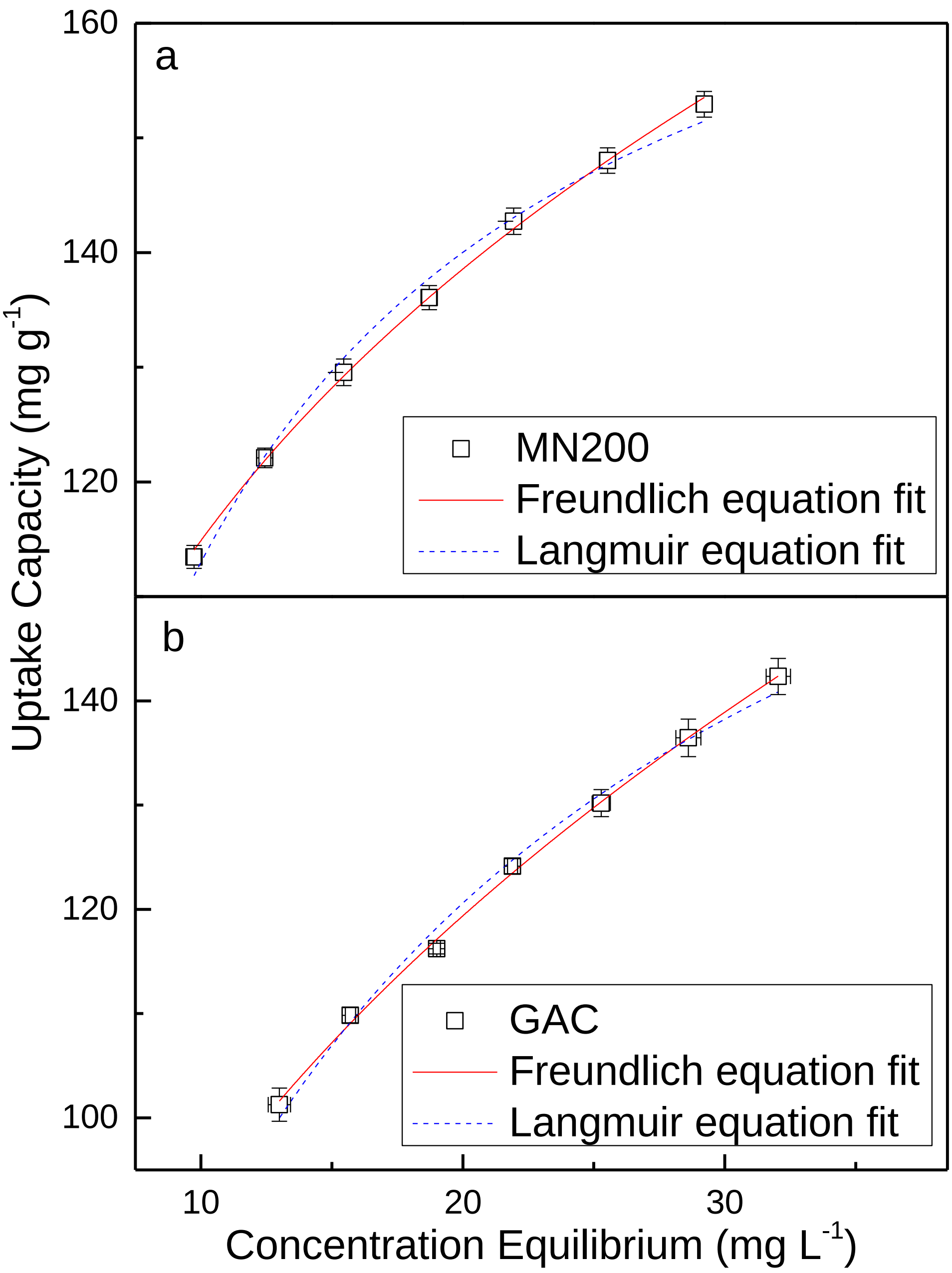

Figure 75 PCT uptake capacities fitted using Freundlich (solid line) and Langmuir (dash line) equations for (a) MN200 and (b) GAC. Errors shown are for repeat runs (n = 2).

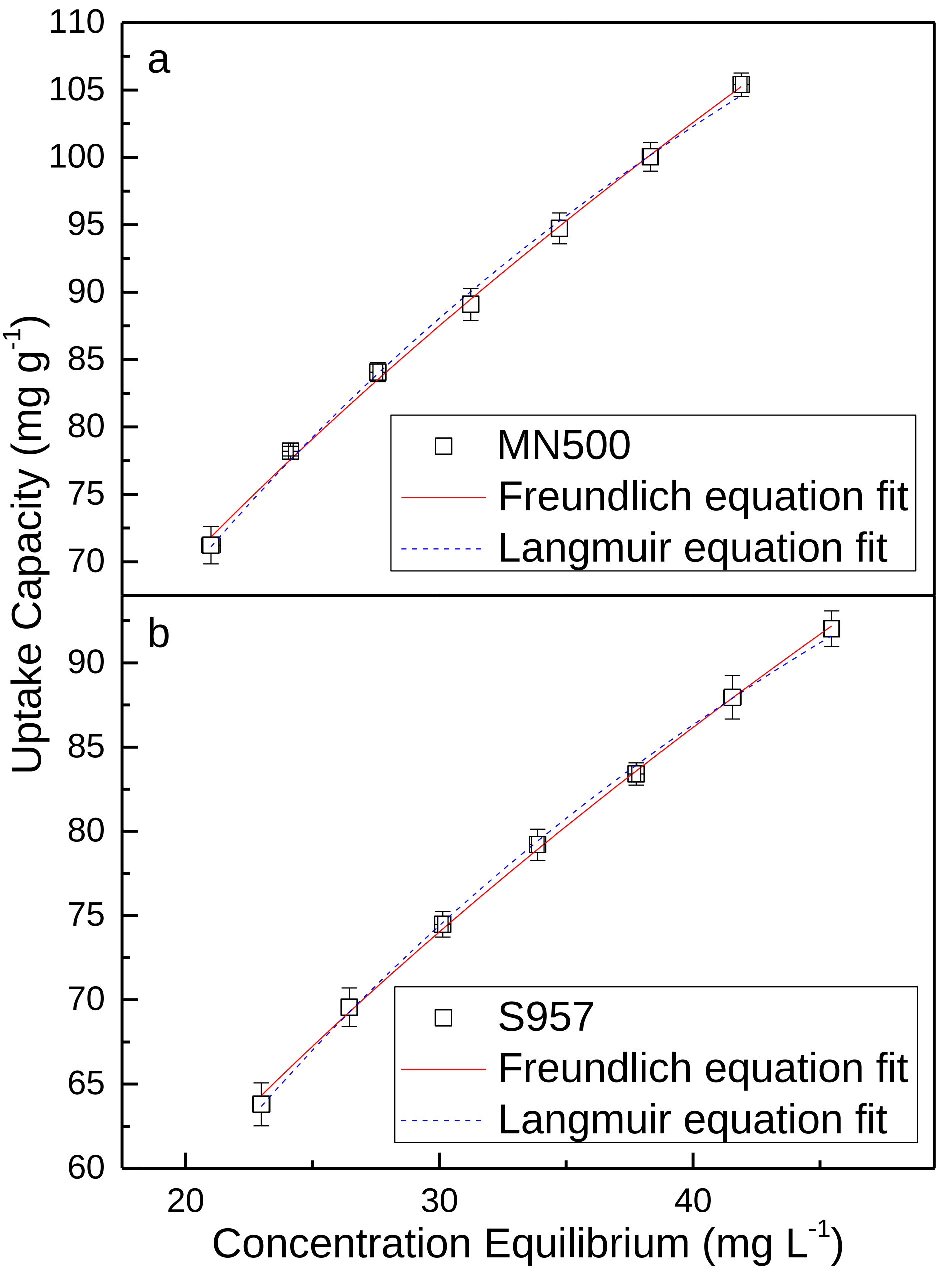

Figure 76 PCT uptake capacities fitted using Freundlich (solid line) and Langmuir (dash line) equations for (a) MN500 and (b) S957. Errors shown are for repeat runs (n = 2).

Table 41 Isothermal parameters obtained by fitting Freundlich and Langmuir equations to PCT adsorption data for MN200, GAC, MN500 and GAC

Adsorption isotherms	MN200	GAC	MN500	S957
Freundlich				
K_f (mg g^{-1} (L $mg^{-1})^{1/n}$)	61.615	38.949	13.333	12.289
n	3.696	2.674	1.807	1.894
R^2	0.998	0.998	0.998	0.998
Langmuir				
q_m (mg g^{-1})	184.104	195.453	198.716	166.252
K_L (L mg^{-1})	0.158	0.080	0.026	0.027
R^2	0.990	0.991	0.996	0.998

7.3.6 Leaching tendencies

Despite the kinetics and mechanism of PCT uptake by MN200, GAC, MN500 and S957 being known, it is still vital to investigate the leaching tendencies of each sorbent in order to fully understand the PCT adsorption systems. As discussed in Section 7.2.3, although MN200 exhibits faster kinetics and a higher PCT uptake capacity compared to the other sorbents tested, no one material presented itself as an outstanding candidate for PCT removal; hence, all sorbents were tested for leaching tendency by adding pure deionised water to fully PCT loaded sorbents. The results obtained (Figure 77) indicate that approximately 29%, 28%, 26% and 22% of PCT was leached from MN200, MN500, S957 and GAC, respectively, after 80 h. MN200, MN500 and S957 exhibit marginally higher leaching tendencies compared to GAC, which may be due the inherent macroposity of these samples. In contrast, GAC contains only mesopores, contributing to a lower PCT leaching rate. It can also be noted that the desorption rates were higher during the initial stages with

21%, 19%, 17% and 14% of PCT leached from MN200, MN500, S957 and GAC, respectively, over 6 h, where after PCT desorption rates decreased significantly.

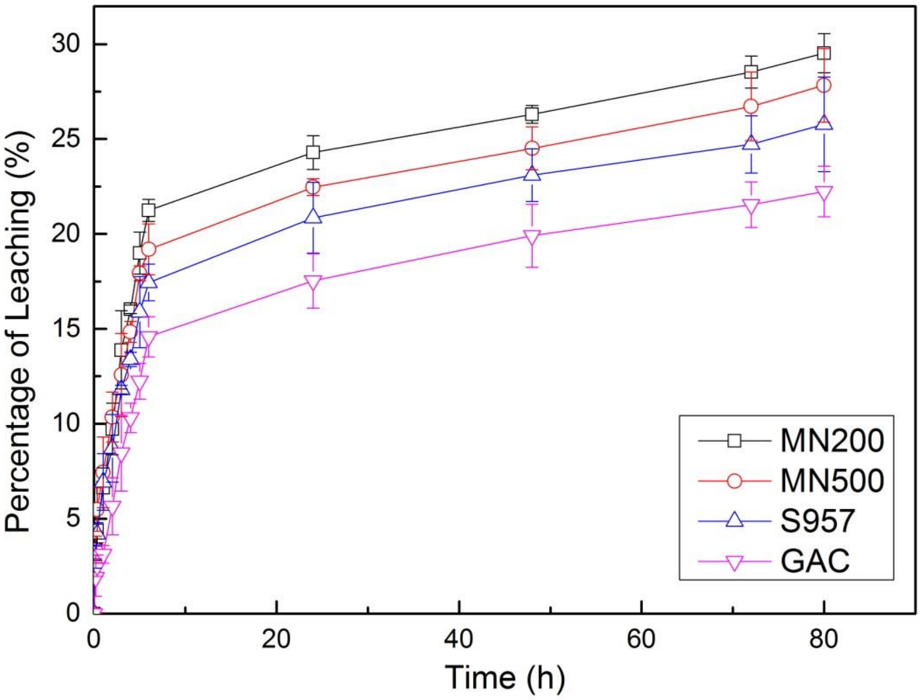

Figure 77 Percentage of adsorbed PCT leached from MN200, MN500, S957 and GAC. Errors shown are for repeat runs (n = 2).

CHAPTER 8

8.0 CONCLUSION

The combination of an increasing human population and limitations of available fresh water stores have contributed to a shortage of potable water supplies. In addition to this, improper waste management, including disposal of effluents from industrial activities has further contaminated water streams. Hence, recent research has focussed on the removal of a range of pollutants from aqueous systems. Different types of contaminants, such as organics, inorganics, and heavy metals, have been detected in water courses, and aromatics are a growing class of organic pollutants that are now classified as major contaminants, being listed as priority substances by the U.S. Environmental Protection Agency (USEPA). This study, therefore, focussed on water supply remediation, specifically studying the removal of organic aromatic substances from aqueous systems.

Four organic compounds (nitrobenzene (NB), aniline (AN), hydroquinone (HQ) and paracetamol (PCT)) were chosen as target contaminants in this study. NB is a nitroaromatic, widely used in industry to produce pesticides and dyes; however, poor wastewater treatments mean NB is released into ground and surface waters causing serious health problems, such as methemoglobinemia. Furthermore, NB is a suspected carcinogen and is listed as a priority pollutant. AN is an aromatic amine used to manufacture dyes, rubber and polymers; it is a suspected anthropogenic carcinogen, hence, the release of AN into the environment may have biological consequences. PCT is an emerging organic pollutant, widely consumed as an antipyretic analgesic, consequently, it is found in effluent streams and surface waters; it is toxic to blood and may affect the thyroid and salivary glands. HQ, is a phenolic compound used extensively to generate rubber and cosmetic products; a suspected carcinogen, it is toxic to the kidneys and stomach.

Different remediation technologies have been applied for contaminant removal from water streams; among these, reactive treatment walls are the most commonly used due, to the low cost and high efficiency of such processes, which Can include advanced oxidation processes, to oxidise the contaminants. Related to this, commercial iron powder (Fe) has shown promise contaminant degradation, while adsorption is an alternative proven to be effective for pollutant removal at low cost, using sorbents such as activated carbon, zeolites and polymer resins.

Utilising Fenton oxidation to degrade NB is ineffective and yields 1,3-dinitrobenzene (DNB) which is 30 times more toxic than NB. Hence, this study focussed on alternative treatment methods, transformation to the more biodegradable AN using iron mediated processes, and adsorption.

8.1 Reduction of NB to AN

Commercial iron powders were used to degrade NB to AN, with the effects of initial concentration and pH investigated in detail. The rate of NB degradation increased with decreasing pH, as corrosion of iron is favoured under acidic conditions. However, the rate constant of degradation showed a more complex relationship with initial concentration, due to the mass transfer effects within the reaction system. Although these experimental parameters affected the reaction rate, the kinetics of NB reduction can all be described by pseudo-first-order models. In addition, control experiments showed that the concentration of NB remained unchanged in the absence of iron catalyst even at pH 3, supporting the theory that NB degradation takes place at the iron metal surface.

8.2 Adsorption of the NB reduction product AN

Since AN is produced in the reduction of NB using Fe, it will be necessary remove it to prevent secondary pollution; adsorption processes have potential for such remediation and non-functionalised hyper-cross-linked Macronet MN200, Granular Activated Carbon (GAC), sulfonic functionalised polystyrene cross-linked with divinylbenzene MN500 and sulfonic-phosphonic functionalised polymeric resin S957 were used as sorbents in this study.

The results demonstrated that higher uptake capacities were obtained for materials with greater levels of acid functionalisation, with rates obeying pseudo-second order kinetic models that showed the rate of adsorption to decrease as acid functionalisation increased, attributable to an associated decrease in surface area. Overall, rates followed the trend S957 < MN500 < GAC < MN200, as acidic functionalities promoted water cluster formation via hydrogen bonding, inhibiting AN from entering the pores.

Adsorption on S957 and MN500 is a physical process, controlled by particle diffusion; adsorption of AN on MN500 is moderately favourable, while it is favourable for S957, as a result of the high degree of acid functionalisation, however, both sorbents exhibit low leaching tendencies (< 20% over 80 h). These results, therefore, suggest that acid functionalised sorbents are promising candidates for AN removal from aqueous systems.

8.3 Direct adsorption of NB

NB degradation followed by AN adsorption can be simplified by considering the direct adsorption of NB at source; this was tested using the non-functionalised hyper-cross-linked polymeric resin MN200 and a commercial granular activated carbon (GAC) with acidic functionalities. Resins MN500 and S957 were discounted from in-depth studies as they demonstrated relatively low uptakes, due to electrostatic repulsion between the nitro groups of NB and the surface acidic functionalities. The resulting kinetics of NB removal by MN200 and GAC could be described by pseudo-second order kinetic models with similar equilibrium uptakes, however, MN200 exhibited faster kinetics, due to its larger surface area and lack of surface functionalisation. NB adsorption was a favourable, physical process, limited by particle diffusion, for both sorbents and <30% leaching occurred within 80 h. The results obtained suggest that non-functionalised sorbents would be most promising for NB removal.

8.4 Adsorption of the PCT reduction by-product HQ

HQ is produced in the reduction of PCT, hence, its remediation is required; here, HQ adsorption, using non-functionalised hyper-cross-linked Macronet MN200, Granular Activated Carbon (GAC), sulfonic functionalised polystyrene cross-linked with divinylbenzene MN500 and sulfonic-phosphonic functionalised polymeric resin S957 was studied. In-depth analysis focussed on MN200 and GAC, due to poor equilibrium performance of MN500 and S957, And the results obtained demonstrate that HQ adsorption is a moderately favourable, physical process, limited by particle diffusion for both sorbents. MN200 exhibits a higher uptake and faster rate of adsorption compared to GAC due to its larger surface area, and the fact that water clusters form, via hydrogen bonding with acidic functionalities on the surface of GAC, inhibiting HQ from entering the pores; however, both sorbents exhibit similar leaching tendencies with <30% leached over 80 h. The results obtained suggest that non - functionalised sorbents are promising candidates for HQ removal.

8.5 Adsorption of PCT

PCT degradation followed by HQ adsorption can be simplified by considering the direct adsorption of PCT at source; this was tested using non-functionalised hyper-cross-linked Macronet MN200, Granular Activated Carbon (GAC), sulfonic functionalised polystyrene cross-linked with divinylbenzene MN500 and sulfonic-phosphonic functionalised polymeric resin S957. The results of in-depth adsorption studies showed that all systems obeyed pseudo-second order kinetic models with rates controlled by particle diffusion. PCT uptakes and adsorption rates increased with decreasing acid functionalisation due to the formation of water clusters at acidic sites, which inhibits PCT from entering the microporosity of the sorbents. Furthermore, there are competing effects from (i) the interaction of acidic functionalities with the PCT basic amide groups and (ii) repulsive forces, which exist between the phenol and carbonyl acid groups of PCT with acidic surface functionalities. Adsorption of PCT onto all sorbents is a physical process, favourable for MN200 and GAC, but only moderately favourable for MN500 and S957; all systems were also observed to leach < 30 % PCT over 80 h. The results obtained suggest that a non-functionalised sorbent, here most favourably MN200, is viable for adsorption of PCT.

8.6 Overall conclusions

Direct adsorption of NB is an effective alternative to reduction and subsequent adsorption of AN. Polymeric resins have been shown to be promising sorbents for the removal of all targeted organic contaminants used in this study; non-functionalised Macronet MN200 exhibited higher uptake and faster kinetics for the removal of NB, PCT and HQ with the performance enhanced as a result of the low acid functionality content, ascribed to repulsive forces between acidic groups and the target contaminant molecules. In contrast, S957, with the highest capacity of acidic functionalities, demonstrated better performance in the removal of AN, as a result of stronger interactions with the basic $–NH_2$ group of AN. Adsorption was a physical process, limited by particle diffusion, for all combinations of contaminants and sorbents, which has implications for bed design for industrial application, and all systems obeyed pseudo-second order kinetic models; with a decrease in adsorption rate with increasing acid functionalisation as a consequence of the formation of water clusters, which block the contaminant molecules from entering the inner pores.

The results have significance for the design of adsorption beds for water remediation, demonstrating the need to balance surface functionalisation for specific contaminant removal, while simultaneously addressing significant kinetic effects.

CHAPTER 9

9.0 FUTURE WORK

The future work suggested by the results of this study includes an investigation of the effects of pH and temperature on the adsorption of nitrobenzene (NB), aniline (AN), paracetamol (PCT) and hydroquinone (HQ) onto non – functionalised and acidic functionalised macronet materials, as well as activated carbon, with particular reference to the sorbents studied here. As stated previously, adsorption of aromatic compounds involves a combination of dispersive and electrostatic interactions; the surface of a sorbent will be positively charged under acidic conditions, while it will be negatively charged under basic conditions, resulting in the favourable adsorption of cations at high pH and favourable adsorption of anions at low pH [165], this will, therefore, affect adsorption of the target contaminants used here as they contain polar bonds and aromatic structures. It would, therefore, be useful to determine the points of zero charge for all sorbents, to provide working pH ranges for additional studies. It is vital to evaluate the effect of temperature to further understand the adsorption mechanisms involved, hence, thermodynamic studies at different temperatures would allow parameters, including the enthalpy, entropy and Gibbs free energy to be obtained [230].

The leaching behaviour of the sorbents studied here, involved desorption of the contaminants in pure deionised water, however, previous studies also investigated desorption of contaminants in different types of solvents, as may be used in industrial regeneration processes [169], such as nitric acid, hydrochloric acid, ethanol, acetone and sodium hydroxide [198, 227]. Therefore, it is also suggested that the future work may investigate the effect of regeneration solvent on contaminant desorption to determine both leaching behaviour and potential regenerative media.

Since non-functionalised sorbent showed promise for three of the target species studied, it is suggested that another potential area for future study would be the competitive adsorption of these target species using the same four sorbents to investigate whether the presence of competing species affects the adsorption behaviour for individual contaminants.

REFERENCES

1. Drinan, F.R.S.J., *The Drinking Water Handbook*2000, Pennsylvania: Technomic Publishing Company, Inc. 260.
2. Kolpin, D.W., et al., *Pharmaceuticals, hormones, and other organic wastewater contaminants in US streams, 1999-2000: A national reconnaissance.* Environmental Science & Technology, 2002. **36**(6): p. 1202-1211.
3. Daughton, C.G. and T.A. Ternes, *Pharmaceuticals and personal care products in the environment: Agents of subtle change?* Environmental Health Perspectives, 1999. **107**: p. 907-938.
4. Ohe, T., T. Watanabe, and K. Wakabayashi, *Mutagens in surface waters: a review.* Mutation Research-Reviews in Mutation Research, 2004. **567**(2-3): p. 109-149.
5. Merriam-Webster. *Water pollution.* cited 2014 [12 February 2014]; Available from: http://visual.merriamwebster.com/earth/environment/water-pollution.php.
6. Ikonet. 2014 [18 December 2014]; Available from: http://www.ikonet.com/en/.
7. Hendricks, D., *Fundamentals of water treatment unit processes: Physical, chemical, and biological*2011, United States of America: Taylor and Francis Group, LLC. 883.
8. Masschelein, W.J., *Unit processes in drinking water treatment*1992, New York: Marcel Dekker, Inc. 635.
9. Cundy, A.B., L. Hopkinson, and R.L.D. Whitby, *Use of iron-based technologies in contaminated land and groundwater remediation: A review.* Science of the Total Environment, 2008. **400**(1-3): p. 42-51.
10. USEPA. *Priority Pollutants.* [15 July 2014]; Available from: http://water.epa.gov/scitech/methods/cwa/pollutants.cfm.

11. Snellinx, Z., et al., *Biological remediation of explosives and related nitroaromatic compounds.* Environmental Science and Pollution Research, 2002. **9**(1): p. 48-61.

12. Marvinsikkema, F.D. and J.A.M. Debont, *Degradation of nitroaromatic compounds by microorganisms.* Applied Microbiology and Biotechnology, 1994. **42**(4): p. 499-507.

13. Chondo, Y., et al., *Determination of Selected Nitropolycyclic Aromatic Hydrocarbons in Water Samples.* Chemical & Pharmaceutical Bulletin, 2013. **61**(12): p. 1269-1274.

14. Priego-Capote, F., U. Luque-Garcia, and M.D.L. de Castro, *Automated fast extraction of nitrated polycyclic aromatic hydrocarbons from soil by focused microwave-assisted Soxhlet extraction prior to gas chromatography-electron-capture detection.* Journal of Chromatography A, 2003. **994**(1-2): p. 159-167.

15. Luque-Garcia, J.L. and M.D.L. de Castro, *Static pressurised liquid extraction of nitrated polycyclic aromatic hydrocarbons from soils with on-line filtration-preconcentration prior to gas chromatography-mass spectrometry detection.* Analyst, 2003. **128**(7): p. 980-985.

16. Araki, Y., et al., *Analysis of Atmospheric Polycyclic Aromatic Hydrocarbons and Nitropolycyclic Aromatic Hydrocarbons in Gas/Particle Phases Separately Collected by a High-volume Air Sampler Equipped with a Column Packed with XAD-4 Resin.* Journal of Health Science, 2009. **55**(1): p. 77-85.

17. Zielinska, B. and S. Samy, *Analysis of nitrated polycyclic aromatic hydrocarbons.* Analytical and Bioanalytical Chemistry, 2006. **386**(4): p. 883-890.

18. IARC. *Agents Classified by the IARC Monographs*. 2012; Available from: http://monographs.iarc.fr/ENG/Classification/ClassificationsAlphaOrder.pdf.

19. Sigma-Aldrich. *Safety Data Sheet: 2-Nitrofluorene*. 2014 [4 September 2014]; Available from: http://www.sigmaaldrich.com/MSDS/MSDS/DisplayMSDSPage.do?country=GB&language=en&productNumber=N16754&brand=ALDRICH&PageToGoToURL=http%3A%2F%2Fwww.sigmaaldrich.com%2Fcatalog%2Fproduct%2Faldrich%2Fn16754%3Flang%3Den.

20. Medina, V.F., et al., *Phyto-removal of trinitrotoluene from water with batch kinetic studies.* Water Research, 2000. **34**(10): p. 2713-2722.

21. Ayoub, K., et al., *Electro-Fenton removal of TNT: Evidences of the electro-chemical reduction contribution.* Applied Catalysis B-Environmental, 2011. **104**(1-2): p. 169-176.

22. Hatzinger, P.B., et al., *Enhancing the attenuation of explosives in surface soils at military facilities: Sorption-desorption isotherms.* Environmental Toxicology and Chemistry, 2004. **23**(2): p. 306-312.

23. USEPA. *Technical fact sheet - 2,4,6-trinitrotoluene (TNT).* 2014 [4 September 2014]; Available from: http://www2.epa.gov/sites/production/files/2014-03/documents/ffrrofactsheet_contaminant_tnt_january2014_final.pdf.

24. Heitkamp, M.A., et al., *Biodegradation of pra-nitrophenol in an aqueous waste stream by immobilised bacteria.* Applied and Environmental Microbiology, 1990. **56**(10): p. 2967-2973.

25. Yi, S., et al., *Biodegradation of p-nitrophenol by aerobic granules in a sequencing batch reactor.* Environmental Science & Technology, 2006. **40**(7): p. 2396-2401.

26. Zhang, H., et al., *Degradation of 4-nitrophenol in aqueous medium by electro-Fenton method.* Journal of Hazardous Materials, 2007. **145**(1-2): p. 227-232.

27. Li, H. and C. Han, *Sonochemical Synthesis of Cyclodextrin-Coated Quantum Dots for Optical Detection of Pollutant Phenols in Water.* Chemistry of Materials, 2008. **20**(19): p. 6053-6059.

28. Labana, S., et al., *Pot and field studies on bioremediation of p-nitrophenol contaminated soil using Arthrobacter protophormiae RKJ100.* Environmental Science & Technology, 2005. **39**(9): p. 3330-3337.

29. USEPA, *OPPT Chemical Fact Sheets: Nitrobenzene (CAS No. 98-95-3)*, 1995: US. p. 2.

30. Sarasa, J., et al., *Treatment of a wastewater resulting from dyes manufacturing with ozone and chemical coagulation.* Water Research, 1998. **32**(9): p. 2721-2727.

31. Rodriguez, M., et al., *The influence of different irradiation sources on the treatment of nitrobenzene.* Catalysis Today, 2002. **76**(2-4): p. 291-300.

32. Bhatkhande, D.S., V.G. Pangarkar, and A. Beenackers, *Photocatalytic degradation of nitrobenzene using titanium dioxide and concentrated solar radiation: chemical effects and scaleup.* Water Research, 2003. **37**(6): p. 1223-1230.

33. Booth, G. *Ullmann's Encyclopedia of Industrial Chemistry*. Nitro Compounds, Aromatic, 2000. DOI: 10.1002/14356007.a17_411.

34. Zhang, W., et al., *The effect of Fe-0/Fe2+/Fe3+ on nitrobenzene degradation in the anaerobic sludge.* Journal of Hazardous Materials, 2007. **143**(1-2): p. 57-64.

35. Li, Y.-P., et al., *Electrochemical reduction of nitrobenzene at carbon nanotube electrode.* Journal of Hazardous Materials, 2007. **148**(1-2): p. 158-163.

36. Chen, Z., et al., *Electrochemical study of nitrobenzene reduction on galvanically replaced nanoscale Fe/Au particles.* Journal of Hazardous Materials, 2011. **197**: p. 424-429.

37. Al Momani, F., *Impact of photo-oxidation technology on the aqueous solutions of nitrobenzene: Degradation efficiency and biodegradability enhancement.* Journal of Photochemistry and Photobiology a-Chemistry, 2006. **179**(1-2): p. 184-192.

38. Agency, U.S.E.P., *Quality Criteria for Water.* 1986(EPA 440/5-86-239): p. 450.

39. Agency, U.S.E.P., *Toxicology Review of Nitrobenzene*, 2009: Washington. p. 250.

40. Dai, Y., et al., *Nitrobenzene-adsorption capacity of carbon materials released during the combustion of woody biomass.* Journal of Hazardous Materials, 2010. **174**(1-3): p. 776-781.

41. Organic, A. *Safety Data Sheet: Nitrobenzene*. 2014 [31 July 2014]; Available from: http://www.acros.com/DesktopModules/Acros_Search_Results/Acros_Search_Results.aspx?search_type=CatalogSearch&SearchString=nitrobenzene.

42. Pinheiro, H.M., E. Touraud, and O. Thomas, *Aromatic amines from azo dye reduction: status review with emphasis on direct UV spectrophotometric detection in textile industry wastewaters.* Dyes and Pigments, 2004. **61**(2): p. 121-139.

43. Snyderwine, E.G., et al., *Highlights of the Eighth International Conference on Carcinogenic/Mutagenic N-Substituted Aryl Compounds.* Mutation Research-Fundamental and Molecular Mechanisms of Mutagenesis, 2002. **506**: p. 1-8.

44. Casero, I., et al., *Chemical degradation of aromatic amines by Fenton's reagent.* Water Research, 1997. **31**(8): p. 1985-1995.

45. Zhu, L., et al., *High-rate biodegradation and metabolic pathways of 4-chloroaniline by aerobic granules.* Process Biochemistry, 2011. **46**(4): p. 894-899.

46. Gonzalez, A.J., et al., *Biodegradation of p-Chloroaniline and Ammonium Removal in Continuous Biofilm Reactors.* Clean-Soil Air Water, 2014. **42**(4): p. 449-455.

47. IARC. *IARC monographs on the evaluation of carcinogenic risks to humans*. 1993; Available from: http://monographs.iarc.fr/ENG/Monographs/vol57/mono57.pdf.

48. Zhu, L., et al., *Reaction kinetics of the degradation of chloroanilines and aniline by aerobic granule.* Biochemical Engineering Journal, 2012. **68**: p. 215-220.

49. Zhu, L., et al., *A comparative study on the formation and characterization of aerobic 4-chloroaniline-degrading granules in SBR and SABR.* Applied Microbiology and Biotechnology, 2008. **79**(5): p. 867-874.

50. He, C., K. Huang, and J. Huang, *Surface modification on a hyper-cross-linked polymeric adsorbent by multiple phenolic hydroxyl groups to be used as a specific adsorbent for adsorptive removal of p-nitroaniline from aqueous solution.* Journal of Colloid and Interface Science, 2010. **342**(2): p. 462-466.

51. Li, K., et al., *Adsorption of p-nitroaniline from aqueous solutions onto activated carbon fiber prepared from cotton stalk.* Journal of Hazardous Materials, 2009. **166**(2-3): p. 1180-1185.

52. Li, K., Y. Li, and Z. Zheng, *Kinetics and mechanism studies of p-nitroaniline adsorption on activated carbon fibers prepared from cotton stalk by NH4H2PO4 activation and subsequent gasification with steam.* Journal of Hazardous Materials, 2010. **178**(1-3): p. 553-559.

53. Zheng, K., et al., *Enhanced adsorption of p-nitroaniline from water by a carboxylated polymeric adsorbent.* Separation and Purification Technology, 2007. **57**(2): p. 250-256.

54. Wang, Y., et al., *Electrosorptive photocatalytic degradation of highly concentrated p-nitroaniline with TiO2 nanorod-clusters/carbon aerogel electrode under visible light.* Separation and Purification Technology, 2013. **104**: p. 229-237.

55. Naiman, K., et al., *Formation, Persistence, and Identification of DNA Adducts Formed by the Carcinogenic Environmental Pollutant o-Anisidine in Rats.* Toxicological Sciences, 2012. **127**(2): p. 348-359.

56. Stiborova, M., et al., *Identification of a genotoxic mechanism for the carcinogenicity of the environmental pollutant and suspected human carcinogen o-anisidine.* International Journal of Cancer, 2005. **116**(5): p. 667-678.

57. NTP. *12th Report on Carcinogens (RoC)*. 2011 [4 August 2014]; Available from: http://ntp.niehs.nih.gov/ntp/roc/twelfth/profiles/anisidine.pdf.

58. IARC. *IARC Monographs on the Evaluation of Carcinogenic Risks to Humans* 1999 [4 August 2014]; Available from: http://monographs.iarc.fr/ENG/Monographs/vol73/volume73.pdf.

59. USEPA. *o-Anisidine (2-Methoyaniline)*. 2000 [4 August 2014]; Available from: http://www.epa.gov/ttn/atw/hlthef/methoxya.html.

60. Traupe, H., et al., *Higher frequency of atopic dermatitis and decrease in viral warts among children exposed to chemicals liberated in a chemical accident in Frankfurt, Germany.* Dermatology, 1997. **195**(2): p. 112-118.

61. Gu, Z., et al., *Bis-pyridinium dibromides modified organo-bentonite for the removal of aniline from wastewater: A positive role of pi-pi polar interaction.* Applied Surface Science, 2014. **290**: p. 107-115.

62. Han, Y., et al., *Electrochemically enhanced adsorption of aniline on activated carbon fibers.* Separation and Purification Technology, 2006. **50**(3): p. 365-372.

63. An, F., X. Feng, and B. Gao, *Adsorption property and mechanism of composite adsorbent PMAA/SiO2 for aniline.* Journal of Hazardous Materials, 2010. **178**(1-3): p. 499-504.

64. Fessenden, R.J.a.F., J.S, *Organic Chemistry*. 6th Edition ed1998, U.S.: Brooks/Cole Publishing Company. 1170.

65. Lin, X., et al., *Removal of aniline using lignin grafted acrylic acid from aqueous solution.* Chemical Engineering Journal, 2011. **172**(2-3): p. 856-863.

66. Gurten, A.A., et al., *Removal of aniline from aqueous solution by PVC-CDAE ligand-exchanger.* Journal of Hazardous Materials, 2005. **120**(1-3): p. 81-87.

67. USEPA. *Aniline*. 2000 cited 2014 [27 March 2014]; Available from: http://www.epa.gov/ttn/atw/hlthef/aniline.html.

68. Sarasa, J., et al., *Study of the aromatic by-products formed from ozonation of anilines in aqueous solution.* Water Research, 2002. **36**(12): p. 3035-3044.

69. Scientific, F. *Safety Data Sheet: Aniline*. 2012 [6 August 2014]; Available from: https://extranet.fisher.co.uk/chemicalProductData_uk/wercs?itemCode=10263320&lang=EN.

70. Lapworth, D.J., et al., *Emerging organic contaminants in groundwater: A review of sources, fate and occurrence.* Environmental Pollution, 2012. **163**: p. 287-303.

71. Klavarioti, M., D. Mantzavinos, and D. Kassinos, *Removal of residual pharmaceuticals from aqueous systems by advanced oxidation processes.* Environment International, 2009. **35**(2): p. 402-417.

72. Kummerer, K., *Drugs in the environment: emission of drugs, diagnostic aids and disinfectants into wastewater by hospitals in relation to other sources - a review.* Chemosphere, 2001. **45**(6-7): p. 957-969.

73. Bound, J.P. and N. Voulvoulis, *Predicted and measured concentrations for selected pharmaceuticals in UK rivers: Implications for risk assessment.* Water Research, 2006. **40**(15): p. 2885-2892.

74. Quesada-Penate, I., et al., *Degradation of paracetamol by catalytic wet air oxidation and sequential adsorption - Catalytic wet air oxidation on activated carbons.* Journal of Hazardous Materials, 2012. **221**: p. 131-138.
75. Trovo, A.G., et al., *Paracetamol degradation intermediates and toxicity during photo-Fenton treatment using different iron species.* Water Research, 2012. **46**(16): p. 5374-5380.
76. Mohapatra, D.P., et al., *Photocatalytic degradation of carbamazepine in wastewater by using a new class of whey-stabilized nanocrystalline TiO2 and ZnO.* Science of the Total Environment, 2014. **485**: p. 263-269.
77. Rao, Y.F., et al., *Degradation of carbamazepine by Fe(II)-activated persulfate process.* Journal of Hazardous Materials, 2014. **268**: p. 23-32.
78. Jelic, A., et al., *Transformation products and reaction pathways of carbamazepine during photocatalytic and sonophotocatalytic treatment.* Journal of Hazardous Materials, 2013. **263**: p. 177-186.
79. Mohapatra, D.P., et al., *Analysis and advanced oxidation treatment of a persistent pharmaceutical compound in wastewater and wastewater sludge-carbamazepine.* Science of the Total Environment, 2014. **470**: p. 58-75.
80. Sigma-Aldrich. *Safety data sheet - Carbamazepine*. 2014 [27 November 2014]; Available from: http://www.sigmaaldrich.com/MSDS/MSDS/DisplayMSDSPage.do?country=GB&language=en&productNumber=C4024&brand=SIGMA&PageToGoToURL=http%3A%2F%2Fwww.sigmaaldrich.com%2Fcatalog%2Fproduct%2Fsigma%2Fc4024%3Flang%3Den.
81. Real, F.J., et al., *Kinetics of the Chemical Oxidation of the Pharmaceuticals Primidone, Ketoprofen, and Diatrizoate in Ultrapure and Natural Waters.* Industrial & Engineering Chemistry Research, 2009. **48**(7): p. 3380-3388.
82. Sigma-Aldrich. *Safety Data Sheet: Primidone*. 2014 [6 August 2014]; Available from: http://www.sigmaaldrich.com/MSDS/MSDS/DisplayMSDSPage.do?country=GB&language=en&productNumber=P7295&brand=FLUKA&PageToGoToURL=http%3A%2F%2Fwww.sigmaaldrich.com%2Fcatalog%2Fproduct%2Ffluka%2Fp7295%3Flang%3Den.

83. Garavito, R.M., M.G. Malkowski, and D.L. DeWitt, *The structures of prostaglandin endoperoxide H synthases-1 and-2.* Prostaglandins & Other Lipid Mediators, 2002. **68-9**: p. 129-152.

84. Paiga, P., et al., *Pilot monitoring study of ibuprofen in surface waters of north of Portugal.* Environmental science and pollution research international, 2013. **20**(4): p. 2410-20.

85. Buser, H.R., T. Poiger, and M.D. Muller, *Occurrence and environmental behavior of the chiral pharmaceutical drug ibuprofen in surface waters and in wastewater.* Environmental Science & Technology, 1999. **33**(15): p. 2529-2535.

86. Saravanan, M., et al., *Effects of Ibuprofen on hematological, biochemical and enzymological parameters of blood in an Indian major carp, Cirrhinus mrigala.* Environmental Toxicology and Pharmacology, 2012. **34**(1): p. 14-22.

87. Kang, K., et al., *Preparation and characterization of magnetic-core titanium dioxide: Implications for photocatalytic removal of ibuprofen.* Journal of Molecular Catalysis a-Chemical, 2014. **390**: p. 178-186.

88. Kasprzyk-Hordern, B., R.M. Dinsdale, and A.J. Guwy, *The occurrence of pharmaceuticals, personal care products, endocrine disruptors and illicit drugs in surface water in South Wales, UK.* Water Research, 2008. **42**(13): p. 3498-3518.

89. Roberts, P.H. and K.V. Thomas, *The occurrence of selected pharmaceuticals in wastewater effluent and surface waters of the lower Tyne catchment.* Science of the Total Environment, 2006. **356**(1-3): p. 143-153.

90. Bendz, D., et al., *Occurrence and fate of pharmaceutically active compounds in the environment, a case study: Hoje River in Sweden.* Journal of Hazardous Materials, 2005. **122**(3): p. 195-204.

91. Verenitch, S.S., C.J. Lowe, and A. Mazumder, *Determination of acidic drugs and caffeine in municipal wastewaters and receiving waters by gas chromatography-ion trap tandem mass spectrometry.* Journal of Chromatography A, 2006. **1116**(1-2): p. 193-203.

92. Su, C.C., et al., *Degradation of acetaminophen in an aerated Fenton reactor*. Journal of the Taiwan Institute of Chemical Engineers, 2013. **44**(2): p. 310-316.
93. Holme, J.A., et al., *Toxic effects of paracetamol and related structures in V79 chinese-hamster cells*. Mutagenesis, 1988. **3**(1): p. 51-56.
94. Zheng, M., et al., *Electrocatalytical oxidation and sensitive determination of acetaminophen on glassy carbon electrode modified with graphene-chitosan composite*. Materials Science & Engineering C-Materials for Biological Applications, 2013. **33**(3): p. 1514-1520.
95. McMurry, J., *Organic Chemistry*. 7th ed2008, California: Thomson Brooks/Cole. 807.
96. Sebastine, I.M. and R.J. Wakeman, *Consumption and environmental hazards of pharmaceutical substances in the UK*. Process Safety and Environmental Protection, 2003. **81**(B4): p. 229-235.
97. Gros, M., M. Petrovic, and D. Barcelo, *Development of a multi-residue analytical methodology based on liquid chromatography-tandem mass spectrometry (LC-MS/MS) for screening and trace level determination of pharmaceuticals in surface and wastewaters*. Talanta, 2006. **70**(4): p. 678-690.
98. Vulliet, E., C. Cren-Olive, and M.-F. Grenier-Loustalot, *Occurrence of pharmaceuticals and hormones in drinking water treated from surface waters*. Environmental Chemistry Letters, 2011. **9**(1): p. 103-114.
99. Kim, S.D., et al., *Occurrence and removal of pharmaceuticals and endocrine disruptors in South Korean surface, drinking, and waste waters*. Water Research, 2007. **41**(5): p. 1013-1021.
100. Prescott, L.F., *Paracetamol (Acetaminophen), A Critical Bibliographic Review*1996, London: Taylor & Francis. 708.
101. Sigma-Aldrich. *Safety Data Sheet: Acetaminophen*. 2014 [6 August 2014]; Available from: http://www.sigmaaldrich.com/MSDS/MSDS/DisplayMSDSPage.do?country=GB&language=en&productNumber=A7085&brand=SIAL&PageToGoToU

RL=http%3A%2F%2Fwww.sigmaaldrich.com%2Fcatalog%2Fproduct%2Fsial%2Fa7085%3Flang%3Den.

102. Huang, H.H., et al., *Synthesis, characterization, and adsorption behavior of aniline modified polystyrene resin for phenol in hexane and in aqueous solution.* Journal of Colloid and Interface Science, 2008. **317**(2): p. 434-441.

103. Chen, X., et al., *Application of a Novel Semiconductor Catalyst, CT, in Degradation of Aromatic Pollutants in Wastewater: Phenol and Catechol.* Journal of Nanomaterials, 2014.

104. Suresh, S., V.C. Srivastava, and I.M. Mishra, *Adsorption of Hydroquinone in Aqueous Solution by Granulated Activated Carbon.* Journal of Environmental Engineering-Asce, 2011. **137**(12): p. 1145-1157.

105. Ahmaruzzaman, M., *Adsorption of phenolic compounds on low-cost adsorbents: A review.* Advances in Colloid and Interface Science, 2008. **143**(1-2): p. 48-67.

106. Kujawski, W., et al., *Removal of phenol from wastewater by different separation techniques.* Desalination, 2004. **163**(1-3): p. 287-296.

107. Dutta, N.N., S. Borthakur, and R. Baruah, *A novel process for recovery of phenol from alkaline wastewater: laboratory study and predesign cost estimate.* Water Environment Research, 1998. **70**(1): p. 4-9.

108. USEPA. *Phenol.* 2000 [7 August 2014]; Available from: http://www.epa.gov/ttn/atw/hlthef/phenol.html.

109. Moussavi, G., A.A. Aghapour, and K. Yaghmaeian, *The degradation and mineralization of catechol using ozonation catalyzed with MgO/GAC composite in a fluidized bed reactor.* Chemical Engineering Journal, 2014. **249**: p. 302-310.

110. Subramanyam, R. and I.M. Mishra, *Co-degradation of resorcinol and catechol in an UASB reactor.* Bioresource Technology, 2008. **99**(10): p. 4147-4157.

111. Subramanyam, R. and I.M. Mishra, *Biodegradation of catechol (2-hydroxy phenol) bearing wastewater in an UASB reactor.* Chemosphere, 2007. **69**(5): p. 816-824.

112. Schweigert, N., A.J.B. Zehnder, and R.I.L. Eggen, *Chemical properties of catechols and their molecular modes of toxic action in cells, from microorganisms to mammals.* Environmental Microbiology, 2001. **3**(2): p. 81-91.

113. Huang, J., K. Huang, and C. Yan, *Application of an easily water-compatible hypercrosslinked polymeric adsorbent for efficient removal of catechol and resorcinol in aqueous solution.* Journal of Hazardous Materials, 2009. **167**(1-3): p. 69-74.

114. Hudnall, P.M. *Ullmann's Encyclopedia of Industrial Chemistry*. Hydroquinone, 2012. DOI: 10.1002/14356007.a13_499.

115. Sigma-Aldrich. *Safety Data Sheet: Hydroquinone*. 2014 [8 August 2014]; Available from: http://www.sigmaaldrich.com/MSDS/MSDS/DisplayMSDSPage.do?country=GB&language=en&productNumber=H17902&brand=SIAL&PageToGoToURL=http%3A%2F%2Fwww.sigmaaldrich.com%2Fcatalog%2Fsearch%3Finterface%3DAll%26term%3Dhydroquinone%26N%3D0%26mode%3Dmatch%2520partialmax%26focus%3Dproduct%26lang%3Den%26region%3DGB.

116. Li, L., et al., *Adsorbent for hydroquinone removal based on graphene oxide functionalized with magnetic cyclodextrin-chitosan.* International Journal of Biological Macromolecules, 2013. **58**: p. 169-175.

117. USEPA. *Pump-and-treat, Ground-water remediation, A guide for decision makers and practitioners*. 1996 [14 August 2014]; Available from: http://nepis.epa.gov/Adobe/PDF/30004PC8.pdf.

118. Khan, F.I., T. Husain, and R. Hejazi, *An overview and analysis of site remediation technologies.* Journal of Environmental Management, 2004. **71**(2): p. 95-122.

119. Beck, P., *Soil and ground-water remediation techniques.* Geoscience Canada, 1996. **23**(1): p. 22-40.

120. CPEO. *Pump and Treat Technology*. 2010 [11 August 2014]; Available from: http://www.cpeo.org/techtree/ttdescript/pumtre.htm.

121. Dupont, M.H.a.R.R., *Groundwater and soil remediation: Process design and cost estimating of proven technologies*2001, U.S.: ASCE Press. 534.

122. USEPA. *In-situ chemical oxidation*. 2006 [14 August 2014]; Available from: http://www.epa.gov/ada/gw/pdfs/insituchemicaloxidation_engineering_issue.pdf.

123. Brillas, E., J.C. Calpe, and P.L. Cabot, *Degradation of the herbicide 2,4-dichlorophenoxyacetic acid by ozonation catalyzed with Fe2+ and UVA light.* Applied Catalysis B-Environmental, 2003. **46**(2): p. 381-391.

124. Schroeder, E.D., *Water and wastewater treatment*1977, U.S.: McGraw-Hill Book Company. 370.

125. CPEO. *Air sparging*. 2010 [13 August 2014]; Available from: http://www.cpeo.org/techtree/ttdescript/airspa.htm.

126. Bass, D.H., N.A. Hastings, and R.A. Brown, *Performance of air sparging systems: a review of case studies.* Journal of Hazardous Materials, 2000. **72**(2-3): p. 101-119.

127. FRTR. *Remediation technologies screening matrix and reference guide: Air sparging*. 2002 [14 August 2014]; 4th edition:[Available from: http://frtr.gov/matrix2/section4/D01-4-34.html.

128. FRTR. *Disclaimer, Privacy, and Security Notice*. 2014 [17 December 2014]; Available from: http://costperformance.org/privacy/index.htm.

129. Baciocchi, R., M.R. Boni, and L. D'Aprile, *Characterization and performance of granular iron as reactive media for TCE degradation by permeable reactive barriers.* Water Air and Soil Pollution, 2003. **149**(1-4): p. 211-226.

130. USEPA. *A citizen's guide to treatment walls*. 1996 [13 August 2014]; Available from: http://www.epa.gov/tio/download/remed/walls.pdf.

131. USEPA. *Permeable reactive barrier technologies for contaminant remediation*. 1998 [14 august 2014]; Available from: http://nepis.epa.gov/Exe/ZyPDF.cgi?Dockey=30003OIO.PDF.

132. Beltran, F.J., M. Gonzalez, and J.F. Gonzalez, *Industrial wastewater advanced oxidation .1. UV radiation in the presence and absence of hydrogen peroxide.* Water Research, 1997. **31**(10): p. 2405-2414.

133. Comninellis, C., et al., *Advanced oxidation processes for water treatment: advances and trends for R&D.* Journal of Chemical Technology and Biotechnology, 2008. **83**(6): p. 769-776.
134. Rosenfeldt, E.J., et al., *Comparison of the efficiency of center dot OH radical formation during ozonation and the advanced oxidation processes O-3/H2O2 and UV/H2O2.* Water Research, 2006. **40**(20): p. 3695-3704.
135. Vogelpohl, A. and S.M. Kim, *Advanced oxidation processes (AOPs) in wastewater treatment.* Journal of Industrial and Engineering Chemistry, 2004. **10**(1): p. 33-40.
136. Neyens, E. and J. Baeyens, *A review of classic Fenton's peroxidation as an advanced oxidation technique.* Journal of Hazardous Materials, 2003. **98**(1-3): p. 33-50.
137. Huang, C.P., C. Dong, and Z. Tang, *Advanced chemical oxidation: Its present role and potential future in hazardous waste treatment.* Waste Management, 1993. **13**(5-7): p. 361-377.
138. Su, C.-C., et al., *Effect of Electrochemical Oxidation Processes on Acetaminophen Degradation in Various Electro-Fenton Reactors.* Journal of the Electrochemical Society, 2013. **160**(4): p. H207-H212.
139. Walling, C., *Fenton’s Reagent Revisited* Accounts of Chemical Research, 1975. **8**.
140. Lipczynskakochany, E., G. Sprah, and S. Harms, *Influence of some groundwater and surface waters constituents on the degradation of 4-chlorophenol by the Fenton reaction.* Chemosphere, 1995. **30**(1): p. 9-20.
141. Rigg, T., W. Taylor, and J. Weiss, *The rate constant of the reaction between hydrogen peroxide and ferrous ions.* Journal of Chemical Physics, 1954. **22**(4): p. 575-577.
142. Cheves. Walling , A.G., *Mechanism of the ferric ion catalyzed decomposition of hydrogen peroxide. Effect of organic substrates.* Journal of the American Chemical Society, 1973. **95**: p. 2987.
143. de Luna, M.D.G., et al., *Acetaminophen degradation by electro-Fenton and photoelectro-Fenton using a double cathode electrochemical cell.* Journal of Hazardous Materials, 2012. **217**: p. 200-207.

144. Su, C.-C., et al., *Degradation of acetaminophen by Fenton and electro-Fenton processes in aerator reactor.* Separation and Purification Technology, 2012. **99**: p. 8-13.
145. Pera-Titus, M., et al., *Degradation of chlorophenols by means of advanced oxidation processes: a general review.* Applied Catalysis B-Environmental, 2004. **47**(4): p. 219-256.
146. Carlos, L., et al., *Nitration of nitrobenzene in Fenton's processes.* Chemosphere, 2010. **80**(3): p. 340-345.
147. Noubactep, C., *A critical review on the process of contaminant removal in Fe-0-H2O systems.* Environmental Technology, 2008. **29**(8): p. 909-920.
148. Zhang, W.X., *Nanoscale iron particles for environmental remediation: An overview.* Journal of Nanoparticle Research, 2003. **5**(3-4): p. 323-332.
149. Agrawal, A. and P.G. Tratnyek, *Reduction of nitro aromatic compounds by zero-valent iron metal.* Environmental Science & Technology, 1996. **30**(1): p. 153-160.
150. Whitman, G.W., R.P. Russell, and V.J. Altieri, *Effect of hydrogen-ion concentration on the submerged corrosion of steel.* Industrial and Engineering Chemistry, 1924. **16**: p. 665-670.
151. Drazic, D.M. and J.P. Popic, *Anomalous dissolution of metals and chemical corrosion.* Journal of the Serbian Chemical Society, 2005. **70**(3): p. 489-511.
152. Odziemkowski, M.S. and R.P. Simpraga, *Distribution of oxides on iron materials used for emediation of organic groundwater contaminants - Implications for hydrogen evolution reactions.* Canadian Journal of Chemistry-Revue Canadienne De Chimie, 2004. **82**(10): p. 1495-1506.
153. O'Hannesin, S.F. and R.W. Gillham, *Long-term performance of an in situ "iron wall" for remediation of VOCs.* Ground Water, 1998. **36**(1): p. 164-170.
154. Orth, W.S. and R.W. Gillham, *Dechlorination of trichloroethene in aqueous solution using Fe-O.* Environmental Science & Technology, 1996. **30**(1): p. 66-71.
155. Faust, O.M.A.a.S.D., *Adsorption Processes for Water Treatment*1987, United States of America: Butterworth. 509.

156. Jean Rouquerol, F.R., Philip Llewellyn, Guillaume Maurin and Kenneth S.W. Sing *Adsorption by powders and porous solids: Principles, methodology and applications*. Second edition ed2014, San Diego: Elsevier Ltd. 626.
157. H. G. Karge , J.W., *Adsorption and Diffusion*2008, Berlin: Springer. 400.
158. Bhatnagar, A. and M. Sillanpaa, *Utilization of agro-industrial and municipal waste materials as potential adsorbents for water treatment-A review.* Chemical Engineering Journal, 2010. **157**(2-3): p. 277-296.
159. Murugesan, A., et al., *Kinetic Studies and Isotherm Modeling for the Removal of Ni2+ and Pb2+ Ions by Modified Activated Carbon Using Sulfuric Acid.* Environmental Progress & Sustainable Energy, 2014. **33**(3): p. 844-854.
160. Valderrama, C., et al., *Evaluation of polyaromatic hydrocarbon removal from aqueous solutions using activated carbon and hyper-crosslinked polymer (Macronet MN200).* Journal of Chemical Technology and Biotechnology, 2009. **84**(2): p. 236-245.
161. Erto, A., et al., *Experimental and statistical analysis of trichloroethylene adsorption onto activated carbon.* Chemical Engineering Journal, 2010. **156**(2): p. 353-359.
162. Malik, P.K., *Dye removal from wastewater using activated carbon developed from sawdust: adsorption equilibrium and kinetics.* Journal of Hazardous Materials, 2004. **113**(1-3): p. 81-88.
163. Dias, J.M., et al., *Waste materials for activated carbon preparation and its use in aqueous-phase treatment: A review.* Journal of Environmental Management, 2007. **85**(4): p. 833-846.
164. Franz, M., H.A. Arafat, and N.G. Pinto, *Effect of chemical surface heterogeneity on the adsorption mechanism of dissolved aromatics on activated carbon.* Carbon, 2000. **38**(13): p. 1807-1819.
165. Villacanas, F., et al., *Adsorption of simple aromatic compounds on activated carbons.* Journal of Colloid and Interface Science, 2006. **293**(1): p. 128-136.
166. Ku, Y. and K.C. Lee, *Removal of phenols from aqueous solution by XAD-4 resin.* Journal of Hazardous Materials, 2000. **80**(1-3): p. 59-68.

167. Abburi, K., *Adsorption of phenol and p-chlorophenol from their single and bisolute aqueous solutions on Amberlite XAD-16 resin.* Journal of Hazardous Materials, 2003. **105**(1-3): p. 143-156.
168. Lin, S.-H. and R.-S. Juang, *Adsorption of phenol and its derivatives from water using synthetic resins and low-cost natural adsorbents: A review.* Journal of Environmental Management, 2009. **90**(3): p. 1336-1349.
169. Valderrama, C., et al., *Kinetics of polycyclic aromatic hydrocarbons removal using hyper-cross-linked polymeric sorbents Macronet Hypersol MN200.* Reactive & Functional Polymers, 2007. **67**(12): p. 1515-1529.
170. Valderrama, C., et al., *Kinetic evaluation of phenol/aniline mixtures adsorption from aqueous solutions onto activated carbon and hypercrosslinked polymeric resin (MN200).* Reactive & Functional Polymers, 2010. **70**(3): p. 142-150.
171. Moreno-Castilla, C., *Adsorption of organic molecules from aqueous solutions on carbon materials.* Carbon, 2004. **42**(1): p. 83-94.
172. Sinnokrot, M.O. and C.D. Sherrill, *Highly accurate coupled cluster potential energy curves for the benzene dimer: Sandwich, T-shaped, and parallel-displaced configurations.* Journal of Physical Chemistry A, 2004. **108**(46): p. 10200-10207.
173. William H. Brown , C.S.F., Brent L. Iverson , Eric V. Anslyn, *Organic chemistry*. 5th edition ed2009, U.S.: Brooks/Cole Cengage Learning. 1132.
174. Sinnokrot, M.O., E.F. Valeev, and C.D. Sherrill, *Estimates of the ab initio limit for pi-pi interactions: The benzene dimer.* Journal of the American Chemical Society, 2002. **124**(36): p. 10887-10893.
175. Janiak, C., *A critical account on pi-pi stacking in metal complexes with aromatic nitrogen-containing ligands.* Journal of the Chemical Society-Dalton Transactions, 2000(21): p. 3885-3896.
176. Hunter, C.A., et al., *Aromatic interactions.* Journal of the Chemical Society-Perkin Transactions 2, 2001(5): p. 651-669.
177. Wen, Q., et al., *Removal of nitrobenzene from aqueous solution by a novel lipoid adsorption material (LAM).* Journal of Hazardous Materials, 2012. **209**: p. 226-232.

178. Jiang, B.-C., et al., *Inhibiting 1,3-dinitrobenzene formation in Fenton oxidation of nitrobenzene through a controllable reductive pretreatment with zero-valent iron.* Chemical Engineering Journal, 2011. **174**(1): p. 258-265.

179. Luan, F., et al., *Abiotic reduction of nitroaromatic compounds by Fe(II) associated with iron oxides and humic acid.* Chemosphere, 2013. **91**(7): p. 1035-1041.

180. Einschlag, F.S.G., L. Carlos, and A.L. Capparelli, *Competition kinetics using the UV/H2O2 process: a structure reactivity correlation for the rate constants of hydroxyl radicals toward nitroaromatic compounds.* Chemosphere, 2003. **53**(1): p. 1-7.

181. Sacan, M.T., M. Ozkul, and S.S. Erdem, *QSPR analysis of the toxicity of aromatic compounds to the algae (Scenedesmus obliquus).* Chemosphere, 2007. **68**(4): p. 695-702.

182. Goi, A. and M. Trapido, *Hydrogen peroxide photolysis, Fenton reagent and photo-Fenton for the degradation of nitrophenols: a comparative study.* Chemosphere, 2002. **46**(6): p. 913-922.

183. Dong, J., et al., *Effects of geochemical constituents on the zero-valent iron reductive removal of nitrobenzene in groundwater.* Water and Environment Journal, 2013. **27**(1): p. 20-28.

184. Mantha, R., et al., *A continuous system for Fe(0) reduction of nitrobenzene in synthetic wastewater.* Environmental Science & Technology, 2001. **35**(15): p. 3231-3236.

185. Scherer, M.M., et al., *Mass transport effects on the kinetics of nitrobenzene reduction by iron metal.* Environmental Science & Technology, 2001. **35**(13): p. 2804-2811.

186. Mu, Y., et al., *Reductive degradation of nitrobenzene in aqueous solution by zero-valent iron.* Chemosphere, 2004. **54**(7): p. 789-794.

187. Dong, J., et al., *Effects of pH and particle size on kinetics of nitrobenzene reduction by zero-valent iron.* Journal of Environmental Sciences-China, 2010. **22**(11): p. 1741-1747.

188. Yin, W., et al., *Experimental study of zero-valent iron induced nitrobenzene reduction in groundwater: The effects of pH, iron dosage, oxygen and*

common dissolved anions. Chemical Engineering Journal, 2012. **184**: p. 198-204.

189. Liu, H., et al., *Electron efficiency of zero-valent iron for groundwater remediation and wastewater treatment.* Chemical Engineering Journal, 2013. **215**: p. 90-95.
190. Huang, Y.H. and T.C. Zhang, *Effects of low pH on nitrate reduction by iron powder.* Water Research, 2004. **38**(11): p. 2631-2642.
191. Heijman, C.G., et al., *Reduction of nitroaromatic-compounds coupled to microbial iron reduction in laboratory equifer columns.* Environmental Science & Technology, 1995. **29**(3): p. 775-783.
192. Hung, H.M., F.H. Ling, and M.R. Hoffmann, *Kinetics and mechanism of the enhanced reductive degradation of nitrobenzene by elemental iron in the presence of ultrasound.* Environmental Science & Technology, 2000. **34**(9): p. 1758-1763.
193. Hezelova, M., et al., *Effect of chloride ions on the kinetics of nitrobenzene reduction by powdered iron.* Chemical Papers, 2006. **60**(5): p. 360-364.
194. Lin, K., et al., *Study the adsorption of phenol from aqueous solution on hydroxyapatite nanopowders.* Journal of Hazardous Materials, 2009. **161**(1): p. 231-240.
195. Kato, Y., M. Machida, and H. Tatsumoto, *Inhibition of nitrobenzene adsorption by water cluster formation at acidic oxygen functional groups on activated carbon.* Journal of Colloid and Interface Science, 2008. **322**(2): p. 394-398.
196. Rajagopal, C. and J.C. Kapoor, *Development of adsorptive removal process for treatment of explosives contaminated wastewater using activated carbon.* Journal of Hazardous Materials, 2001. **87**(1-3): p. 73-98.
197. Zhang, W., et al., *Selecting activated carbon for water and wastewater treatability studies.* Environmental Progress, 2007. **26**(3): p. 289-298.
198. Rauthula, M.S. and V.C. Srivastava, *Studies on adsorption/desorption of nitrobenzene and humic acid onto/from activated carbon.* Chemical Engineering Journal, 2011. **168**(1): p. 35-43.

199. Derylo-Marczewska, A., et al., *Influence of differences in porous structure within granules of activated carbon on adsorption of aromatics from aqueous solutions.* Carbon, 2004. **42**(2): p. 301-306.

200. Liu, S. and R. Wang, *Modified activated carbon with an enhanced nitrobenzene adsorption capacity.* Journal of Porous Materials, 2011. **18**(1): p. 99-106.

201. Wei, W., et al., *Removal of nitrobenzene from aqueous solution by adsorption on nanocrystalline hydroxyapatite.* Desalination, 2010. **263**(1-3): p. 89-96.

202. Zampori, L., P.G. Stampino, and G. Dotelli, *Adsorption of nitrobenzene and orthochlorophenol on dimethyl ditallowyl montmorillonite: A microstructural and thermodynamic study.* Applied Clay Science, 2009. **42**(3-4): p. 605-610.

203. Dekany, I., et al., *Adsorption of nitrobenzene and n-pentanol from aqueous solution on hydrophilic and hydrophobic clay minerals.* Colloid and Polymer Science, 1996. **274**(10): p. 981-988.

204. Reungoat, J., et al., *Adsorption of nitrobenzene from water onto high silica zeolites and regeneration by ozone.* Separation Science and Technology, 2007. **42**(7): p. 1447-1463.

205. Qin, Q., J. Ma, and K. Liu, *Adsorption of nitrobenzene from aqueous solution by MCM-41.* Journal of Colloid and Interface Science, 2007. **315**(1): p. 80-86.

206. Wang, A.-J., et al., *Efficient Reduction of Nitrobenzene to Aniline with a Biocatalyzed Cathode.* Environmental Science & Technology, 2011. **45**(23): p. 10186-10193.

207. Gupta, V.K., A. Nayak, and S. Agarwal, *Performance evaluation and application of oxygen enriched waste rubber tire adsorbent for the removal of hazardous aniline derivatives from waste water.* Chemical Engineering Journal, 2012. **203**: p. 447-457.

208. El-Safty, S.A., A. Shahat, and M. Ismael, *Mesoporous aluminosilica monoliths for the adsorptive removal of small organic pollutants.* Journal of Hazardous Materials, 2012. **201**: p. 23-32.

209. Anotai, J., M.C. Lu, and P. Chewpreecha, *Kinetics of aniline degradation by Fenton and electro-Fenton processes.* Water Research, 2006. **40**(9): p. 1841-1847.

210. Goncalves, A., et al., *Highly dispersed ceria on activated carbon for the catalyzed ozonation of organic pollutants.* Applied Catalysis B-Environmental, 2012. **113**: p. 308-317.

211. Sanchez, L., J. Peral, and X. Domenech, *Aniline degradation by combined photocatalysis and ozonation.* Applied Catalysis B-Environmental, 1998. **19**(1): p. 59-65.

212. Tang, H., et al., *Photochemical removal of aniline in aqueous solutions: Switching from photocatalytic degradation to photo-enhanced polymerization recovery.* Journal of Hazardous Materials, 2010. **175**(1-3): p. 977-984.

213. Zhang, S., et al., *Performance of enhanced biological SBR process for aniline treatment by mycelial pellet as biomass carrier.* Bioresource Technology, 2011. **102**(6): p. 4360-4365.

214. Chen, S., D. Sun, and J.-S. Chung, *Simultaneous methanogenesis and denitrification of aniline wastewater by using anaerobic-aerobic biofilm system with recirculation.* Journal of Hazardous Materials, 2009. **169**(1-3): p. 575-580.

215. Liu, Q.Y., Y.X. Liu, and X.J. Lu, *Combined Photo-Fenton and Biological Oxidation for the Treatment of Aniline Wastewater*, in *2011 International Conference of Environmental Science and Engineering, Vol 12, Pt A*, M. Ma, Editor 2012. p. 341-348.

216. Sauleda, R. and E. Brillas, *Mineralization of aniline and 4-chlorophenol in acidic solution by ozonation catalyzed with Fe2+ and UVA light.* Applied Catalysis B-Environmental, 2001. **29**(2): p. 135-145.

217. Song, S., Z.Q. He, and J.M. Chen, *US/O-3 combination degradation of aniline in aqueous solution.* Ultrasonics Sonochemistry, 2007. **14**(1): p. 84-88.

218. Garcia, J., et al., *Platinum catalysts supported on MWNT for catalytic wet air oxidation of nitrogen containing compounds.* Catalysis Today, 2005. **102**: p. 101-109.

219. Gomes, H.T., et al., *Catalytic properties of carbon materials for wet oxidation of aniline.* Journal of Hazardous Materials, 2008. **159**(2-3): p. 420-426.

220. Oliviero, L., et al., *Experimental and predictive approach for determining wet air oxidation reaction pathways in synthetic wastewaters.* Chemical Engineering Research & Design, 2003. **81**(A3): p. 384-392.

221. Titus, E., A.K. Kalkar, and V.G. Gaikar, *Adsorption of anilines and cresols on NaX and different cation exchanged zeolites (equilibrium, kinetic, and IR investigations).* Separation Science and Technology, 2002. **37**(1): p. 105-125.

222. Essington, M.E., *Adsorption of aniline and toluidines on montmorillonite.* Soil Science, 1994. **158**(3): p. 181-188.

223. Jianguo, C., et al., *Equilibrium and kinetic studies on the adsorption of aniline compounds from aqueous phase onto bifunctional polymeric adsorbent with sulfonic groups.* Chemosphere, 2005. **61**(4): p. 502-9.

224. Nevskaia, D.M., et al., *Effects of the surface chemistry of carbon materials on the adsorption of phenol-aniline mixtures from water.* Carbon, 2004. **42**(3): p. 653-665.

225. Valderrama, C., et al., *Evaluation of Phenol/Aniline (Single and Binary) Removal from Aqueous Solutions onto Hyper-cross-linked Polymeric Resin (Macronet MN200) and Granular Activated Carbon in Fixed-Bed Column.* Water Air and Soil Pollution, 2011. **215**(1-4): p. 285-297.

226. Tang, B., et al., *Study of aniline/epsilon-caprolactam mixture adsorption from aqueous solution onto granular activated carbon: Kinetics and equilibrium.* Chemical Engineering Journal, 2012. **187**: p. 69-78.

227. Suresh, S., V.C. Srivastava, and I.M. Mishra, *Studies of adsorption kinetics and regeneration of aniline, phenol, 4-chlorophenol and 4-nitrophenol by activated carbon.* Chemical Industry & Chemical Engineering Quarterly, 2013. **19**(2): p. 195-212.

228. Wu, G.Q., et al., *Adsorptive removal of aniline from aqueous solution by oxygen plasma irradiated bamboo based activated carbon.* Chemical Engineering Journal, 2012. **185**: p. 201-210.

229. Al-Johani, H. and M.A. Salam, *Kinetics and thermodynamic study of aniline adsorption by multi-walled carbon nanotubes from aqueous solution.* Journal of Colloid and Interface Science, 2011. **360**(2): p. 760-767.

230. Xiaofeng, X., G. Lian, and S. Jing, *Thermodynamic study on aniline adsorption on chemical modified multi-walled carbon nanotubes.* Colloids and Surfaces a-Physicochemical and Engineering Aspects, 2007. **308**(1-3): p. 54-59.

231. Li, B., et al., *Adsorption of simple aromatics from aqueous solutions on modified activated carbon fibers.* Catalysis Today, 2010. **158**(3-4): p. 515-520.

232. Shao, D., et al., *Polyaniline Multiwalled Carbon Nanotube Magnetic Composite Prepared by Plasma-Induced Graft Technique and Its Application for Removal of Aniline and Phenol.* Journal of Physical Chemistry C, 2010. **114**(49): p. 21524-21530.

233. Li, B., Z. Lei, and Z. Huang, *Surface-Treated Activated Carbon for Removal of Aromatic Compounds from Water.* Chemical Engineering & Technology, 2009. **32**(5): p. 763-770.

234. Yang, X., Q. Guan, and W. Li, *Effect of template in MCM-41 on the adsorption of aniline from aqueous solution.* Journal of Environmental Management, 2011. **92**(11): p. 2939-2943.

235. Cai, J.G., et al., *Adsorption characteristics of aniline and 4-methylaniline onto bifunctional polymeric adsorbent modified by sulfonic groups.* Journal of Hazardous Materials, 2005. **124**(1-3): p. 173-180.

236. Aguinaco, A., et al., *In situ generation of hydrogen peroxide from pharmaceuticals single ozonation: A comparative study of its application on Fenton like systems.* Chemical Engineering Journal, 2014. **235**: p. 46-51.

237. Miranda-Garcia, N., et al., *Photocatalytic degradation of emerging contaminants in municipal wastewater treatment plant effluents using immobilized TiO2 in a solar pilot plant.* Applied Catalysis B-Environmental, 2011. **103**(3-4): p. 294-301.

238. Bernabeu, A., et al., *Solar photo-Fenton at mild conditions to treat a mixture of six emerging pollutants.* Chemical Engineering Journal, 2012. **198**: p. 65-72.

239. Jones, O.A.H., N. Voulvoulis, and J.N. Lester, *The occurrence and removal of selected pharmaceutical compounds in a sewage treatment works utilising activated sludge treatment.* Environmental Pollution, 2007. **145**(3): p. 738-744.

240. Shariati, F.P., et al., *Membrane bioreactor for treatment of pharmaceutical wastewater containing acetaminophen.* Desalination, 2010. **250**(2): p. 798-800.

241. De Gusseme, B., et al., *Degradation of acetaminophen by Delftia tsuruhatensis and Pseudomonas aeruginosa in a membrane bioreactor.* Water Research, 2011. **45**(4): p. 1829-1837.

242. Tambosi, J.L., et al., *Removal of pharmaceutical compounds in membrane bioreactors (MBR) applying submerged membranes.* Desalination, 2010. **261**(1-2): p. 148-156.

243. Ruiz, B., et al., *Surface heterogeneity effects of activated carbons on the kinetics of paracetamol removal from aqueous solution.* Applied Surface Science, 2010. **256**(17): p. 5171-5175.

244. Terzyk, A.P., *Molecular properties and intermolecular forces - factors balancing the effect of carbon surface chemistry in adsorption of organics from dilute aqueous solutions.* Journal of Colloid and Interface Science, 2004. **275**(1): p. 9-29.

245. Cotoruelo, L.M., et al., *Adsorption of oxygen-containing aromatics used in petrochemical, pharmaceutical and food industries by means of lignin based active carbons.* Adsorption-Journal of the International Adsorption Society, 2011. **17**(3): p. 539-550.

246. Trovo, A.G., et al., *Paracetamol degradation intermediates and toxicity during photo-Fenton treatment using different iron species.* Water Research, 2012. **46**(16): p. 5374-5380.

247. Carra, I., et al., *Study of iron sources and hydrogen peroxide supply in the photo-Fenton process using acetaminophen as model contaminant.* Journal of Chemical Technology and Biotechnology, 2013. **88**(4): p. 636-643.

248. de Luna, M.D.G., et al., *Kinetics of acetaminophen degradation by Fenton oxidation in a fluidized-bed reactor.* Chemosphere, 2013. **90**(4): p. 1444-1448.

249. Choi, J., et al., *Heterogeneous photocatalytic treatment of pharmaceutical micropollutants: Effects of wastewater effluent matrix and catalyst modifications.* Applied Catalysis B-Environmental, 2014. **147**: p. 8-16.

250. Bernabeu, A., et al., *Solar photocatalysis as a tertiary treatment to remove emerging pollutants from wastewater treatment plant effluents.* Catalysis Today, 2011. **161**(1): p. 235-240.

251. Jagannathan, M., F. Grieser, and M. Ashokkumar, *Sonophotocatalytic degradation of paracetamol using TiO2 and Fe3+.* Separation and Purification Technology, 2013. **103**: p. 114-118.

252. Beninati, S., D. Semeraro, and M. Mastragostino, *Adsorption of Paracetamol and Acetylsalicylic Acid onto Commercial Activated Carbons.* Adsorption Science & Technology, 2008. **26**(9): p. 721-734.

253. Terzyk, A.P. and G. Rychlicki, *The influence of activated carbon surface chemical composition on the adsorption of acetaminophen (paracetamol) in vitro - The temperature dependence of adsorption at the neutral pH.* Colloids and Surfaces a-Physicochemical and Engineering Aspects, 2000. **163**(2-3): p. 135-150.

254. Terzyk, A.P., *The influence of activated carbon surface chemical composition on the adsorption of acetaminophen (paracetamol) in vitro Part II. TG, FTIR, and XPS analysis of carbons and the temperature dependence of adsorption kinetics at the neutral pH.* Colloids and Surfaces a-Physicochemical and Engineering Aspects, 2001. **177**(1): p. 23-45.

255. Terzyk, A.P., *Adsorption of biologically active compounds from aqueous solutions on to commercial unmodified activated carbons. Part III. Theoretical description of paracetamol adsorption data at neutral pH.* Adsorption Science & Technology, 2002. **20**(1): p. 63-81.

256. Terzyk, A.P., *Adsorption of biologically active compounds from aqueous solutions on to commercial unmodified activated carbons. Part IV. Do the properties of amphoteric carbon surface layers influence the adsorption of paracetamol at acidic pH levels?* Adsorption Science & Technology, 2003. **21**(1): p. 93-123.

257. Mestre, A.S., et al., *Activated carbons from sisal waste by chemical activation with K2CO3: Kinetics of paracetamol and ibuprofen removal from aqueous solution.* Bioresource Technology, 2011. **102**(17): p. 8253-8260.

258. Villaescusa, I., et al., *Mechanism of paracetamol removal by vegetable wastes: The contribution of pi-pi interactions, hydrogen bonding and hydrophobic effect.* Desalination, 2011. **270**(1-3): p. 135-142.

259. Ruppert, G., et al., *Mineralization of cyclic organic-water contaminants by the photo-Fenton reaction - influence of structure and substituents.* Chemosphere, 1993. **27**(8): p. 1339-1347.

260. Ksibi, M., A. Zemzemi, and R. Boukchina, *Photocatalytic degradability of substituted phenols over UV irradiated TiO2.* Journal of Photochemistry and Photobiology a-Chemistry, 2003. **159**(1): p. 61-70.

261. Wang, J., et al., *Photolytic and photocatalytic degradation of micro pollutants in a tubular reactor and the reaction kinetic models.* Separation and Purification Technology, 2014. **122**: p. 105-111.

262. Melian, J.A.H., et al., *Comparative study of phenolics degradation between biological and photocatalytic systems.* Journal of Solar Energy Engineering-Transactions of the Asme, 2008. **130**(4).

263. Gong, Y.-W., X.-N. Cheng, and H.-X. Zhang, *Photocatalytic degradation of acrylic acid, acrolein and hydroquinone using TiO2 under simulated solar irradiation*, in *Advances in Chemical Engineering Iii, Pts 1-4*, L. Yu, et al., Editors. 2013. p. 2129-2132.

264. Yao, R.-S., et al., *Degradation of phenolic compounds with hydrogen peroxide catalyzed by enzyme from Serratia marcescens AB 90027.* Water Research, 2006. **40**(16): p. 3091-3098.

265. Tudorache, M., et al., *Biocatalytic microreactor incorporating HRP anchored on micro-/nano-lithographic patterns for flow oxidation of phenols.* Journal of Molecular Catalysis B-Enzymatic, 2011. **69**(3-4): p. 133-139.

266. Mohamed, F.S., W.A. Khater, and M.R. Mostafa, *Characterization and phenols sorptive properties of carbons activated by sulphuric acid.* Chemical Engineering Journal, 2006. **116**(1): p. 47-52.

267. Yildiz, N., et al., *Adsorption of benzoic acid and hydroquinone by organically modified bentonites.* Colloids and Surfaces a-Physicochemical and Engineering Aspects, 2005. **260**(1-3): p. 87-94.

268. Fu, J.W., et al., *Comparative study of phenol compounds adsorption on mesoporous sieves with different degrees of modification.* Colloids and Surfaces a-Physicochemical and Engineering Aspects, 2011. **375**(1-3): p. 136-140.

269. Ayranci, E. and O. Duman, *Adsorption behaviors of some phenolic compounds onto high specific area activated carbon cloth.* Journal of Hazardous Materials, 2005. **124**(1-3): p. 125-132.

270. Zhu, Z., et al., *Adsorption behaviors of hydroquinone onto porous adsorbents*, in *Progress in Environmental Science and Engineering, Pts 1-4*, Q.J. Xu, Y.H. Ju, and H.H. Ge, Editors. 2013. p. 1971-1974.

271. Goertzen, S.L., et al., *Standardization of the Boehm titration. Part I. CO2 expulsion and endpoint determination.* Carbon, 2010. **48**(4): p. 1252-1261.

272. Yu, Y. and L.S. Wu, *Analysis of endocrine disrupting compounds, pharmaceuticals and personal care products in sewage sludge by gas chromatography-mass spectrometry.* Talanta, 2012. **89**: p. 258-263.

273. Brunauer, S., P.H. Emmett, and E. Teller, *Adsorption of gases in multimolecular layers.* Journal of the American Chemical Society, 1938. **60**: p. 309-319.

274. Sing, K.S.W., et al., *Reporting physisorption data for gas solid systems with special reference to the determination of surface-area and porosity (Recommendations 1984).* Pure and Applied Chemistry, 1985. **57**(4): p. 603-619.

275. Atkins Peter, J.D.P., *Atkins' Physical Chemistry*2002, United State: Oxford University Press. 958.

276. Brunauer, S., et al., *On a theory of the van der Waals adsorption of gases.* Journal of the American Chemical Society, 1940. **62**: p. 1723-1732.

277. Christian, G.D., *Analytical Chemistry*1994, Canada: John Wiley & Sons, Inc. 812.

278. Harold M. McNair, J.M.M., *Basic Gas Chromatography*. Second edition ed2009, Canada: John Wiley & Sons, Inc. 239.

279. Kemp, W., *Organic spectroscopy*. Third edition ed1991, New York: Palgrave. 393.

280. PerkinElmer. *FTIR spectrosccopy: Attenuated total reflectance*. 2005 [29 September 2014]; Available from: http://www.perkinelmer.co.uk/CMSResources/Images/44-74844TCH_FTIRATR.pdf.

281. Boyd, G.E., A.W. Adamson, and L.S. Myers, *The exchange adsorption of ions from aqueous solutions by organic zeolites .2.* Journal of the American Chemical Society, 1947. **69**(11): p. 2836-2848.

282. Tao, B. and A.J. Fletcher, *Metaldehyde removal from aqueous solution by adsorption and ion exchange mechanisms onto activated carbon and polymeric sorbents.* Journal of Hazardous Materials, 2013. **244**: p. 240-250.

283. Wang, X., et al., *Aniline modified hypercrosslinked polystyrene resins and their adsorption equilibriums, kinetics and dynamics towards salicylic acid from aqueous solutions.* Chemical Engineering Journal, 2013. **233**: p. 124-131.

284. Ho, Y.S. and G. McKay, *The kinetics of sorption of basic dyes from aqueous solution by sphagnum moss peat.* Canadian Journal of Chemical Engineering, 1998. **76**(4): p. 822-827.

285. Aksakal, O. and H. Ucun, *Equilibrium, kinetic and thermodynamic studies of the biosorption of textile dye (Reactive Red 195) onto Pinus sylvestris L.* Journal of Hazardous Materials, 2010. **181**(1-3): p. 666-672.

286. Hamdaoui, O., *Batch study of liquid-phase adsorption of methylene blue using cedar sawdust and crushed brick.* Journal of Hazardous Materials, 2006. **135**(1-3): p. 264-273.

287. Plazinski, W., W. Rudzinski, and A. Plazinska, *Theoretical models of sorption kinetics including a surface reaction mechanism: A review.* Advances in Colloid and Interface Science, 2009. **152**(1-2): p. 2-13.

288. Langmuir, I., *THE ADSORPTION OF GASES ON PLANE SURFACES OF GLASS, MICA AND PLATINUM.* Journal of the American Chemical Society, 1918. **40**: p. 1361-1403.

289. Do, D.D., *Adsorption analysis: Equilibria and kinetics*. Vol. Volume 2. 1998, London: Imperial College Press. 892.

290. Chen, H., et al., *Isotherm, thermodynamic, kinetics and adsorption mechanism studies of methyl orange by surfactant modified silkworm exuviae.* Journal of Hazardous Materials, 2011. **192**(1): p. 246-254.

291. Freundlich, H., *Concerning adsorption in solutions.* Zeitschrift Fur Physikalische Chemie--Stochiometrie Und Verwandtschaftslehre, 1906. **57**(4): p. 385-470.

292. Gary D. Christian , P.K.D., Kevin A. Schug, *Analytical chemistry*. Seventh edition ed2014, United States of America: John Wiley & Sons, Inc. 826.

293. Oickle, A.M., et al., *Standardization of the Boehm titration: Part II. Method of agitation, effect of filtering and dilute titrant.* Carbon, 2010. **48**(12): p. 3313-3322.

294. Valderrama, C., et al., *Evaluation of hyper-cross-linked polymeric sorbents (Macronet MN200 and MN300) on dye (Acid red 14) removal process.* Reactive & Functional Polymers, 2008. **68**(3): p. 679-691.

295. Erno Pretsch , P.B., Martin Badertscher, *Structure determination of organic compounds*. 4th edition ed2009, Berlin: Springer. 433.

296. Sun, H., et al., *A novel integrated active capping technique for the remediation of nitrobenzene-contaminated sediment.* Journal of Hazardous Materials, 2010. **182**(1-3): p. 184-190.

297. Wenying, X.U., L.I. Ping, and F.A.N. Jinhong, *Reduction of nitrobenzene by the catalyzed Fe/Cu process.* Journal of Environmental Sciences, 2008. **20**(8): p. 915-921.

298. Lavine, B.K., G. Auslander, and J. Ritter, *Polarographic studies of zero valent iron as a reductant for remediation of nitroaromatics in the environment.* Microchemical Journal, 2001. **70**(2): p. 69-83.

299. Tong, M., et al., *Reduction of nitrobenzene in groundwater by iron nanoparticles immobilized in PEG/nylon membrane.* Journal of Contaminant Hydrology, 2011. **122**(1-4): p. 16-25.

300. Valderrama, C., et al., *Sorption kinetics of polycyclic aromatic hydrocarbons removal using granular activated carbon: Intraparticle diffusion coefficients.* Journal of Hazardous Materials, 2008. **157**(2-3): p. 386-396.

301. Dabrowski, A., et al., *Adsorption of phenolic compounds by activated carbon - a critical review.* Chemosphere, 2005. **58**(8): p. 1049-1070.

302. Terzyk, A.P., et al., *Impact of the interaction with the positive charge in adsorption of benzene and other organic compounds from aqueous solutions on carbons.* Applied Surface Science, 2007. **253**(8): p. 4006-4009.

APPENDICES

Appendix A

To calculate total capacities of carboxylic and lactonic functionalities (Na_2CO_3) of GAC:

Based on stoichiometry (for neutralisation), the number of moles of acid is equal to the number of moles of base, hence,

$$m_1 = m_2$$

$$(V_a \cdot X_1) + (V_b \cdot X_2) = (V_c \cdot X_3)$$

$$(0.01 \text{ L} \cdot X_1) + (0.0238 \text{ L} \cdot 0.053 \text{ mol L}^{-1}) = (0.03 \text{ L} \cdot 0.05 \text{ mol L}^{-1})$$

$$(0.01 \text{ L} \cdot X_1) + (1.26 \times 10^{-3} \text{ mol}) = 1.5 \times 10^{-3} \text{ mol}$$

$$(0.01 \text{ L} \cdot X_1) = 2.4 \times 10^{-4} \text{ mol}$$

$$X_1 = \underline{0.024 \text{ mol L}^{-1}}$$

The total number of moles of carboxylic/lactonic functionalities can be determined from the number of moles of base that has been reacted after 24 hours (the difference between the initial number of moles of base and the number of moles of base after 24 hours)

$$\text{Total moles of carboxylic/lactonic groups} = (0.05 \text{ L} \cdot 0.05 \text{ mol L}^{-1}) - (0.05 \text{ L} \cdot 0.024 \text{ mol L}^{-1})$$

= (2.5 x 10^{-3} mol) – (1.2 x 10^{-3} mol)

= <u>1.3 x 10^{-3} mol</u>

Total capacity of acidic groups, mol g^{-1} = 1.3 x 10^{-3} mol / 1.5 g

= <u>0.867 mmol g^{-1}</u>

Since 2 mol of OH^- reacted with 1 mol of H^+ for Na_2CO_3, hence, the total capacity of lactonic and carboxylic groups is half of the total capacity of acidic groups

= 0.867 mmol g^{-1} / 2

= 0.434 mmol g^{-1}

Appendix B

To calculate the capacity of carboxylic functionalities ($NaHCO_3$) of GAC:

Based on stoichiometry (for neutralisation), the number of moles of acid is equal to the number of moles of base, hence,

$$m_1 = m_2$$

$$(V_a \cdot X_1) + (V_b \cdot X_2) = (V_c \cdot X_3)$$

$$(0.01\ \mathrm{L} \cdot X_1) + (0.0124\ \mathrm{L} \cdot 0.05\ \mathrm{mol\ L^{-1}}) = (0.02\ \mathrm{L} \cdot 0.05\ \mathrm{mol\ L^{-1}})$$

$$(0.01\ \mathrm{L} \cdot X_1) + (6.2 \times 10^{-4}\ \mathrm{mol}) = 1.0 \times 10^{-3}\ \mathrm{mol}$$

$$(0.01\ \mathrm{L} \cdot X_1) = 3.8 \times 10^{-4}\ \mathrm{mol}$$

$$X_1 = \underline{0.038\ \mathrm{mol\ L^{-1}}}$$

The number of moles of carboxylic functionalities can be determined from the number of moles of base that has been reacted after 24 hours (the difference between the initial number of moles of base and the number of moles of base after 24 hours)

$$\begin{aligned} \text{Moles of carboxylic functionalities} &= (0.05\ \mathrm{L} \cdot 0.05\ \mathrm{mol\ L^{-1}}) - \\ &\quad (0.05\ \mathrm{L} \cdot 0.038\ \mathrm{mol\ L^{-1}}) \\ &= (2.5 \times 10^{-3}\ \mathrm{mol}) - (1.9 \times 10^{-3}\ \mathrm{mol}) \\ &= \underline{6 \times 10^{-4}\ \mathrm{mol}} \end{aligned}$$

Total capacity of carboxylic functionalities, mol g^{-1} $= 6.4 \times 10^{-4}$ mol / 1.5 g

$=$ <u>0.4 mmol g^{-1}</u>

Since the capacity of carboxylic functionalities is 0.4 mmol g^{-1}:

Capacity of lactonic functionalities of GAC = 0.434 mmol g^{-1} – 0.4 mmol g^{-1}

= 0.034 mmol g^{-1}

Capacity of phenolic functionalities of GAC = 0.75 mmol g^{-1} – 0.434 mmol g^{-1}

= 0.316 mmol g^{-1}

Appendix D

To calculate the capacity of sulfonic functionalities of MN500:

Based on stoichiometry (for neutralisation), the number of moles of acid is equal to the number of moles of base, hence,

$m_1 = m_2$

$(V_a \text{ x } X_1) + (V_b \text{ x } X_2) = (V_c \text{ x } X_3)$

$(0.01 \text{ L}\cdot X_1) + (0.011 \text{ L}\cdot 0.05 \text{ mol L}^{-1}) = (0.02 \text{ L}\cdot 0.05 \text{ mol L}^{-1})$

$(0.01 \text{ L}\cdot X_1) + (5.5 \times 10^{-4} \text{ mol}) = 1 \times 10^{-3} \text{ mol}$

$(0.01 \text{ L}\cdot X_1) = 4.5 \times 10^{-4} \text{ mol}$

$X_1 = \underline{0.045 \text{ mol L}^{-1}}$

The number of moles of sulfonic functionalities can be determined from the number of moles of base that has been reacted after 24 hours (the difference between the initial number of moles of base and the number of moles of base after 24 hours)

Moles of sulfonic functionalities $= (0.05 \text{ L}\cdot 0.05 \text{ mol L}^{-1}) – (0.05 \text{ L}\cdot 0.045 \text{ mol L}^{-1})$

$= (2.5 \times 10^{-3} \text{ mol}) – (2.25 \times 10^{-3} \text{ mol})$

$= \underline{2.5 \times 10^{-4} \text{ mol}}$

Capacity of sulfonic functionalities, mol $g^{-1} = 2.5 \times 10^{-4}$ mol / 0.1 g

$= \underline{2.5 \text{ mmol g}^{-1}}$

Appendix E

To calculate the total capacities of sulfonic and phosphonic functionalities of S957:

Based on stoichiometry (for neutralisation), the number of moles of acid is equal to the number of moles of base, hence,

$m_1 = m_2$

$(V_a \cdot X_1) + (V_b \cdot X_2) = (V_c \cdot X_3)$

$(0.01\ \mathrm{L} \cdot X_1) + (0.0136\ \mathrm{L} \cdot 0.05\ \mathrm{mol\ L^{-1}}) = (0.02\ \mathrm{L} \cdot 0.05\ \mathrm{mol\ L^{-1}})$

$(0.01\ \mathrm{L} \cdot X_1) + (6.8 \text{ x } 10^{-4}\ \mathrm{mol}) = 1 \times 10^{-3}\ \mathrm{mol}$

$(0.01\ \mathrm{L} \cdot X_1) = 3.2 \times 10^{-4}\ \mathrm{mol}$

$X_1 = \underline{0.032\ \mathrm{mol\ L^{-1}}}$

The number of moles of total sulfonic and phosphonic functionalities can be determined from the number of moles of base that has been reacted after 24 hours (the difference between initial number of moles of base and the number of moles of base after 24 hours)

Moles of sulfonic functionalities $= (0.05\ \mathrm{L} \cdot 0.05\ \mathrm{mol\ L^{-1}}) - (0.05\ \mathrm{L} \cdot 0.032\ \mathrm{mol\ L^{-1}})$

$= (2.5 \times 10^{-3}\ \mathrm{mol}) - (1.6 \times 10^{-3}\ \mathrm{mol})$

$= \underline{9 \text{ x } 10^{-4}\ \mathrm{mol}}$

Capacity of sulfonic functionalities, mol g^{-1} = 9×10^{-4} mol / 0.1 g

= $\underline{9 \text{ mmol } g^{-1}}$

Appendix F

Chromatogram of NB (retention time: 5.8 min), AN (retention time: 4.3) and dimethyl phthalate (retention time: 9.8 min)